

Advanced Vibration Controlling Techniques

Sanjiv Kumar Sharma



@Seismicisolation Alpha Science

About the pagination of this eBook

Due to the unique page numbering scheme of this book, the electronic pagination of the eBook does not match the pagination of the printed version. To navigate the text, please use the electronic Table of Contents that appears alongside the eBook or the Search function.

For citation purposes, use the page numbers that appear in the text.

Advanced Vibration Controlling Techniques

@Seismicisolation

@Seismicisolation

Advanced Vibration Controlling Techniques

Sanjiv Kumar Sharma



Alpha Science International Ltd.
Oxford, U.K.

@Seismicisolation

Advanced Vibration Controlling Techniques
216 pgs.

Sanjiv Kumar Sharma
Department of Mechanical Engineering
Baba Bande Singh Bahadur Engineering College
Fatehgarh Sahib
Punjab

Copyright © 2018

ALPHA SCIENCE INTERNATIONAL LTD.

7200 The Quorum, Oxford Business Park North
Garsington Road, Oxford OX4 2JZ, U.K.

www.alphasci.com

ISBN 978-1-78332-389-0

E-ISBN 978-1-78332-424-8

Printed from the camera-ready copy provided by the Author.

All rights reserved. No part of this publication may be reproduced, stored in a retrieval system, or transmitted in any form or by any means, electronic, mechanical, photocopying, recording or otherwise, without prior written permission of the publisher.

@Seismicisolation

To my dearest Mother

@Seismicisolation

@Seismicisolation

Preface

In the past few decades, effective progress has been made in the field of vibration analysis, prompted by advances in technology. The requirement for the analysis of increasingly complex systems has been instrumental in the development of powerful computational techniques whilst the development of fast digital computers has provided the means of numerical implementation of these techniques. Undoubtedly, one of the most significant advances in recent years is in the field of finite element methods, a method which is developed originally for the analysis of complex structures. The method has proved to be much more versatile than conceived originally, finding applications in areas such as fluid mechanics, refrigeration and air-conditioning and heat transfer. Progressively, a significant improvement was being made in linear system theory, permitting efficient derivation of the response of large-order systems. Advanced Vibration Controlling Techniques was written in recognition of these advances.

This book is different from other books in several aspects. In the first place, the appeal of the first few chapters has been framed with the inclusion of numerous methods of killing vibrations in structures. This book will serve as a reference for post graduate students, research scholars, practicing engineers, researchers, academicians and professionals in the field of vibrations. It offers a study of analytical techniques in vibration reduction by Finite Element Methods (FEM) and results are shown with the help of SIMULINK a simulation toolbox in MATLAB. The book contains adequate theoretical mathematics in the form of differential equations of motion for a sufficient understanding of the frame work of the topics discussed.

Organization of the Book

Chapter 1 is a general introduction of advanced control systems e.g. Active Vibration Control, Adaptive control systems, Control algorithms etc.

Chapter 2 offers an elaborated discussion on Active vibration control of the structures and their experimental setup.

Chapter 3 throws some light on modelling and performance analysis of PCLD treated beams using FEM and energy based analytical methods.

Chapter 4 deals with active vibration control of beams using combined Pre-stressed layer damping (PSLD) and ACLD treatments.

Chapter 5 discusses about FEM based design and experimental vibration analysis of Enhanced ACLD (EACLD) treatment using Stand-off Layer (SOL layer).

Chapter 6 explains about analysis of rotating beams with combined ACLD and Stressed layer damping (SLD) treatments.

Chapter 7 tells about the vibration analysis of rotating beams with ACLD treatment using Stand- off layer (SOL layer).

Chapter 8 spells out efficient active vibration control of smart structures with modified positive position feedback control using pattern search methods in the presence of instrumentation phase lead and lag.

The reader may refer other books or monographs or research papers for more detailed information on these topics. No numerical problem has been solved in this book as the range of the subject is very wide and each chapter is a subject by itself, requiring a debate of wide variety of problems.

No one is perfect in this world whilst every human effort has been done to enhance the knowledge of readers about the subject. Readers can also write me at sanjiv.kumar@bbsbec.ac.in, or sanjivsharma2001@gmail.com if any errors and significant omissions are noticed. I will appreciate constructive criticism, comments and suggestions for the improvement of this book. It is also presumed that the reader has the basic knowledge in the field of vibrations.

Notations and Units

SI systems of units have been used thought the book.

Sanjiv Kumar Sharma

Acknowledgements

I am grateful to all those who have remained as a direct or indirect impact of this book. Many people working in the general area of design, dynamics, analysis and simulation of vibrations have influenced the structure and format of this book. In addition, I greatly owe my indebtedness too all the authors of the articles listed in the bibliography of this book. I would also like to thank the reviewers for their efforts and for the comments and suggestions, which have well served to compile the formation of such a book that will create a deep impact and footprints on the minds of our honourable audience. Finally, I appreciate and acknowledge the encouragement, patience and continuous support by my family members: my mother Smt. Abhilash Devi, my father Sh. Narain Dutt, my wife Bindu and my lovely son Anurag who have also shared the pain, frustration and fun of producing this manuscript. I would also like to appreciate my colleague Dr. Sanjeev Bhandari for his moral support provided by him. Above all, I express my deep and cordial gratitude to my elder brother Dr. Rajiv Kumar Vashisht who guided me as noble guide about the subject and its importance in our daily life from time to time. He is my ideal person of life and I see him as my father.

I would appreciate for being informed of errors, comments and compliments about the book to authors working address or sending an email on sanjiv.kumar@bbsbec.ac.in and (or) sanjivsharma2001@gmail.com

Sanjiv Kumar Sharma

@Seismicisolation

Contents

1. Introduction	1.1-1.12
1.1 Adaptive control system	1.1
1.2 Overview of system identification and control system design	1.2
1.2.1 Vibration control	1.2
1.2.2 Smart materials as sensors and actuators	1.3
1.2.3 Mathematical modeling and system identification	1.3
1.2.3.1 Mathematical modeling by FEMs	1.3
1.2.3.2 System identification by experimental data	1.3
1.2.3.2.1 System categorization based on time	1.4
1.2.3.2.2 System categorization based on I/O relationship	1.4
1.2.3.2.3 System categorization based on number of I/Os	1.4
1.2.3.2.4 System categorization based on continuity	1.4
1.2.3.2.5 System categorization based on structural parameters	1.4
1.2.3.2.6 System categorization based on feedback	1.5
1.2.4 System classification and Neural Networks	1.6
1.2.5 Controller design	1.6
1.2.5.1 Linear quadratic gaussian control	1.7
1.2.5.2 Adaptive control	1.7
1.2.5.3 Control software and hardware	1.7
1.3 Vibration control of LTI structures	1.8
1.3.1 Vibration control of stationary and rotating LTI structures using passive constrained layer damping (PCLD) treatment	1.8
1.3.2 Vibration control of stationary and rotating LTI structures using active constrained layer damping (ACLD) treatment	1.8
1.3.2 Vibration control of stationary and rotating LTI structures using Piezoelectric Materials	1.8
1.4 Briefing of this book	1.8
1.5 Objectives of present research study	1.9
1.5.1 Primary objectives	1.9
1.5.2 Secondary objectives	1.10
1.5.3 Theoretical work	1.10
1.5.4 Experimental work	1.10
1.6 Objectives of this book	1.10
1.7 Outline of the book	1.11
2. Active Vibration Control Structure	2.1-2.6
2.1 Experimental setup	2.2
2.2 Equipment characteristics	2.3
2.2.1 Software ‘MATLAB-Simulink’	2.3
2.2.2 Simultaneous I/O data acquisition card (DAQ 6062 E)	2.4

2.2.2.1	Analog input FIFO	2.4
2.2.2.2	Analog output	2.4
2.2.2.3	DAQ-STC system	2.4
2.2.2.4	Multifunction DAQ software NI-DAQ	2.5
2.2.2.5	Sampling rate	2.5
2.2.3	Amplifiers	2.5
2.2.4	Pre-filter	2.5
2.2.5	Real time engine	2.5
2.2.6	Host PC (Pentium 4)	2.6
2.2.7	Cathode ray oscilloscope	2.6
2.2.8	PZT patches as sensors/actuators	2.6
3. Modeling and Analysis of Beams		3.1-3.22
3.1	Derivation of Lagrange's equation from Hamilton's principle	3.1
3.2	Deriving stiffness and mass matrices for beam element	3.2
3.3	Deriving stiffness and mass matrices for rod element	3.5
3.4	PCLD system description and modeling	3.6
3.4.1	Basic relationships	3.7
3.4.2	Finite element modeling	3.8
3.4.2.1	The shape functions	3.8
3.4.2.2	Energies of the beam with PCLD treatment	3.9
3.4.2.2.1	Kinetic energies	3.9
3.4.2.2.1.1	Passive constraining layer	3.9
3.4.2.2.1.2	Base beam	3.10
3.4.2.2.1.3	VEM layer	3.10
3.4.2.2.2	Potential energies	3.10
3.4.2.2.2.1	Passive constraining layer	3.10
3.4.2.2.2.2	VEM layer	3.11
3.4.2.2.2.3	Base beam	3.11
3.4.2.3	Pure beam elements	3.11
3.4.2.4	Equations of motion	3.12
3.4.3	Analytical modeling	3.12
3.4.3.1	Assumed mode method	3.12
3.4.3.2	Energies of the PCLD system	3.13
3.4.3.2.1	Kinetic energies	3.13
3.4.3.2.2	Potential energies	3.13
3.4.3.2.2.1	Passive constraining layer	3.13
3.4.3.2.2.2	VEM layers	3.14
3.4.3.2.2.3	Base beam	3.14
3.4.3.3	Selection of admissible functions	3.14
3.4.3.4	Lagrange's equations of motion	3.14
3.5	Results and discussion	3.15
3.5.1	Results for different boundary conditions and different thicknesses of VEM and constraining layers	3.15
3.5.1.1	Simply supported beams	3.15
3.5.1.2	Free-free beams	3.17

3.5.1.3	Fixed-fixed beams	3.18
3.5.1.4	Cantilever beams	3.20
4.	Vibration Control with Active and Passive Techniques	4.1-4.23
4.1	System description and finite element modeling	4.2
4.1.1	Basic relationships	4.2
4.1.2	The shape functions	4.5
4.1.3	Energies of the ACLD treatment augmented with SLD treatment	4.6
4.1.3.1	Kinetic energies	4.6
4.1.3.1.1	Active constraining layer	4.6
4.1.3.1.2	Base beam	4.6
4.1.3.1.3	PVC layers	4.6
4.1.3.1.4	Passive constraining layer (Sensor layer)	4.6
4.1.3.2	Potential energies	4.6
4.1.3.2.1	Active constraining layer	4.7
4.1.3.2.2	PVC layers	4.7
4.1.3.2.3	Base beam	4.7
4.1.3.2.4	Passive constraining layer (Sensor Layer)	4.7
4.1.3.2.5	Effect of initial stress in PVC layer	4.7
4.1.4	Work done	4.8
4.1.5	Equations of motion	4.8
4.1.5.1	Open loop conditions	4.9
4.1.5.2	Closed loop conditions	4.9
4.2	Results and discussion	4.10
4.2.1	Performance using SLD (i.e. TeLD or CoLD) treatment only	4.10
4.2.2	Performance of PCLD treatment augmented with CoLD treatment	4.12
4.2.3	Performance of ACLD treatment augmented with CoLD treatment	4.14
4.3	Experimental validation	4.16
4.3.1	Experimental setup	4.16
4.3.2	Experimental system identification	4.17
4.3.3	Experimental determination of frequency dependent young's modulus, shear modulus and corresponding loss factors for PVC layer	4.18
4.3.3.1	Young's modulus and corresponding loss factor	4.18
4.3.3.2	Shear modulus and corresponding loss factor	4.19
4.3.4	Experimental implementation of digital controller	4.20
5.	Vibration Control with Advanced methods	5.1-5.23
5.1	System description and modeling	5.2
5.1.1	Basic relationships	5.2
5.1.2	The shape functions	5.4
5.1.3	Energies of the enhanced ACLD treatment using SOL system	5.5
5.1.3.1	Kinetic energies	5.6

5.1.3.1.1	Active constraining layer	5.6
5.1.3.1.2	Base beam	5.6
5.1.3.1.3	VEM layer	5.6
5.1.3.1.4	Stand-off layer	5.7
5.1.3.1.5	Sensor layer	5.7
5.1.3.2	Potential energies	5.7
5.1.3.2.1	Active constraining layer	5.7
5.1.3.2.2	Base beam	5.7
5.1.3.2.3	VEM layer	5.8
5.1.3.2.4	Stand-off layer	5.8
5.1.3.2.5	Sensor layer	5.8
5.1.3.2.6	Edge elements or springs	5.8
5.1.4	Work done	5.8
5.1.5	Pure beam elements	5.9
5.1.6	Equations of motion	5.9
5.1.6.1	Open loop conditions	5.9
5.1.6.2	Closed loop conditions	5.9
5.2	Results and discussion	5.10
5.2.1	Comparison with previous study results	5.10
5.2.2	Performance with simple passive constraining layer damping treatment	5.11
5.2.3	Performance with the addition of SOL layer to passive constraining layer damping treatment	5.12
5.2.4	Performance with simple active constraining layer damping treatment	5.14
5.2.5	Performance with the addition of SOL layer to active constraining layer damping treatment	5.16
5.3	Experimental validation	5.21
5.3.1	Experimental setup	5.21
6.	Vibration Control of Rotating Structures with Advanced Methods	6.1-6.24
6.1	System description and finite element modeling	6.2
6.1.1	Basic relationships	6.2
6.1.2	The shape functions	6.4
6.1.3	Energies of the ACLD treatment combined with SLD treatment	6.5
6.1.3.1	Kinetic energies	6.5
6.1.3.2	Potential energies	6.5
6.1.3.2.1	Constraining layer	6.6
6.1.3.2.2	PVC layer	6.6
6.1.3.2.3	Base beam	6.6
6.1.3.2.4	Sensor layer	6.6
6.1.3.2.5	Centrifugal stiffening effect	6.7
6.1.3.2.6	Effect of initial stress in PVC layers	6.7
6.1.4	Work done	6.7
6.1.5	Pure beam elements	6.8
6.1.6	Equations of motion	6.8
6.1.6.1	Open loop Conditions	6.9
6.1.6.2	Closed loop Conditions	6.10
6.2	Results and discussion	6.11

6.2.1	Comparisons with results in literature	6.11
6.2.2	Performance with SLD treatment	6.12
6.2.3	Performance combined with PCLD and SLD treatment	6.14
6.2.4	Performance combined with ACLD and SLD treatment	6.17
6.3	Experimental validation	6.22
6.3.1	Experimental setup	6.22
7.	Vibration Control of Rotating Structures using a Unique Layer	7.1-7.15
7.1	System description and finite element modeling	7.1
7.1.1	Basic relationships	7.1
7.1.2	The shape functions	7.3
7.1.3	Energies of the ACLD system with SOL treatment	7.3
7.1.3.1	Kinetic energies	7.3
7.1.3.2	Potential energies	7.4
7.1.3.2.1	Constraining layer	7.4
7.1.3.2.2	VEM layer	7.4
7.1.3.2.3	SOL layer	7.4
7.1.3.2.4	Base beam	7.5
7.1.3.2.5	Sensor layer	7.5
7.1.3.2.6	Centrifugal stiffening effect	7.5
7.1.4	Work done	7.5
7.1.5	Pure beam elements	7.6
7.1.6	Equations of motion	7.6
7.1.6.1	Open loop conditions	7.8
7.1.6.2	Closed loop conditions	7.8
7.2	Results and discussion	7.9
7.2.1	Comparison with results from Previous Researches	7.9
7.2.2	Performance with full PCLD treatment using SOL layer	7.9
7.2.3	Performance with ACLD treatment using SOL layer	7.11
7.2.3.1	Full treatment	7.11
7.2.3.2	Partial treatment	7.12
7.3	Experimental validation	7.13
7.3.1	Experimental setup	7.13
8.	Controlling Vibrations by Various Controllers	8.1-8.26
8.1	Modeling of the flexible beam	8.2
8.2	Grey box subspace system identification	8.5
8.3	Design of efficient positive position feedback control	8.7
8.3.1	Standard stability criterion	8.8
8.3.2	Stability considerations using H_2 norm or H_∞ norm calculations	8.9
8.3.3	Efficient positive position feedback controller design using pattern search algorithm	8.10
8.3.3.1	Terminology and working of pattern search algorithm	8.10
8.3.3.2	Controller design based on pattern search algorithm	8.11
8.4	Results with positive position feedback control	8.15
8.4.1	Frequency domain results using efficient positive position feedback control	8.15
8.4.1.1	Effect of phase lead (effect of high pass filter)	8.15
8.4.1.2	Effect of phase lag (effect of time delay)	8.17

8.4.2	Time domain results using efficient positive position feedback control	8.20
8.5	Experimental validation and results	8.21
8.5.1	Experimental setup	8.22
8.5.1.1	Software Lab-View	8.22
8.5.1.2	Simultaneous I/O Data acquisition card (DAQ 6062 E)	8.22
8.5.1.2.1	Analog input FIFO	8.23
8.5.1.2.2	Analog output	8.23
8.5.1.2.3	DAQ-STC system	8.23
8.5.1.2.4	Multifunction DAQ software NI-DAQ	8.23
8.5.1.2.5	Sampling rate	8.23
8.5.1.3	Amplifiers	8.24
8.5.1.4	High pass and low pass filter	8.24
8.5.1.5	Host PC (Core 2 Duo)	8.24
8.5.1.6	Cathode ray oscilloscope	8.24
8.5.1.7	PZT patches as sensors/actuators	8.24
8.5.2	Experimental results	8.24
<i>Glossary of Terms</i>		G1-G19
<i>Glossary of Symbols</i>		G20-G21
<i>Glossary of Abbreviations</i>		G22-G24
<i>Bibliography</i>		B1-B4
<i>Index</i>		I1-I5

LIST OF FIGURES

Fig. No.	Title	Page No.
1.1	Adaptive control system	1.2
1.2	ACLD treatment of a stationary beam with SOL layer sandwiched between base beam and VEM layer	1.9
1.3	ACLD treatment of a rotating beam with SOL layer sandwiched between base beam and VEM layer	1.9
1.4	ACLD treatment of a rotating beam with SLD treatment combined with constrained layer damping treatment	1.10
1.5	Flow chart for the present work	1.12
2.1	Schematic view of a rotating beam with ACLD treatment	2.3
3.1	Beam element	3.2
3.2	Rod element	3.5
3.3	(a) Schematics of the structure with PCLD treatment (b) Undeformed geometry of the beam with PCLD treatment	3.7 3.7
3.4	Nodal displacement of a treated beam element	3.8
3.5	Percentage errors in loss factors (taking FEM as base) as a function of constraining layer thickness at various thicknesses of VEM layer for simply supported beam	3.16
3.6	Closer view of percentage error in loss factor of first mode (taking FEM as base) as a function of constraining layer thickness at various thicknesses of VEM layer for a simply supported beam.	3.16
3.7	Percentage errors in natural frequencies (taking FEM as base) as a function of constraining layer thickness at various thicknesses of VEM layer for a simply supported beam	3.17
3.8	Percentage errors in loss factors (taking FEM as base) as a function of constraining layer thickness at various thicknesses of VEM layer for a free-free beam	3.17
3.9	Closer view of percentage errors in loss factors (taking FEM as base) as a function of constraining layer thickness at various thicknesses of VEM layer for free-free beam.	3.18

xviii List of Figures

3.10	Percentage errors in natural frequencies (taking FEM as base) as a function of constraining layer thickness at various thicknesses of VEM layer for free-free beam.	3.19
3.11	Percentage errors in loss factors (taking FEM as base) as a function of constraining layer thickness at various thicknesses of VEM layer for fixed-fixed beam	3.19
3.12	Closer view of percentage errors in loss factors (taking FEM as base) as a function of constraining layer thickness at various thicknesses of VEM layer for fixed-fixed beam	3.20
3.13	Percentage errors in natural frequencies (taking FEM as base) as a function of constraining layer thickness at various thicknesses of VEM layer for fixed-fixed beam.	3.20
3.14	Percentage errors in loss factors (taking FEM as base) as a function of constraining layer thickness at various thicknesses of VEM layer for cantilever beam.	3.21
3.15	Closer views of percentage errors in loss factors (taking FEM as base) as a function of constraining layer thickness at various thicknesses of VEM layer for cantilever beam.	3.21
3.16	Percentage errors in natural frequencies (taking FEM as base) as a function of constraining layer thickness at various thicknesses of VEM layer for simply supported beam	3.22
4.1	Schematics of structure with ACLD using SLD treatment	4.2
4.2	(a) Cross-section of the undeformed beam. (b) Beam with ACLD treatment augmented with SLD treatment	4.3 4.3
4.3	(a) Deformation of the beam with constrained layer damping (b) Degrees of freedom of an element	4.4 4.4
4.4	Comparison of loss factors by positive and negative strain to base beam (partial and full treatment)	4.11
4.5	Comparison of natural frequencies by positive and negative strain to base beam (partial treatment)	4.12
4.6	Comparison of loss factors by PCLD + CoLD treatment and only CoLD treatment (partial) at different location of the patch	4.12
4.7	Comparison of natural frequencies by (PCLD + CoLD) treatment and only CoLD treatment (partial)	4.13
4.8	Comparison of loss factors by PCLD + CoLD treatment and only CoLD treatment (partial) at other different location of the patch.	4.14

4.9	Comparison of loss factors by (ACLD + CoLD) treatment with displacement feedback gain of 10 and (PCLD + CoLD) treatment (partial) at different location of the patch.	4.15
4.10	Comparison of loss factors by (ACLD + CoLD) treatment and only CoLD treatment at four other locations i.e. at 40 mm, 60 mm, 80 mm and 100 mm.	4.16
4.11	Schematics of the experimental setup (for identification and control)	4.16
4.12	Young's and shear modulus with corresponding loss factor as a function of frequency	4.19
4.13	Comparison of experimental and theoretical vibration characteristics of the beam system using (ACLD + CoLD) treatment	4.21
4.14	Time domain system responses (simulations and experimentations)	4.22
4.15	Frequency domain system responses (simulations and experimentations)	4.23
5.1	Schematics of structure EACLDSOL treatment	5.2
5.2	Cross-section of beam with EACLDSOL treatment	5.3
5.3	Nodal displacement of a treated beam element	5.4
5.4	Various modal loss factors as a function of modulus of rigidity of SOL layer (thickness of SOL=2 mm)	5.12
5.5	Various modal frequencies as a function modulus of rigidity of SOL layer	5.12
5.6	Various modal loss factors as a function of modulus of rigidity of SOL layer at different thicknesses of SOL layer.	5.13
5.7	Various loss factors as a function of modulus of rigidity of SOL layer at different stiffness's of anchors.	5.14
5.8	Various modal loss factors as a function of feedback gain Kp at different stiffness's of anchors with 20 % coverage	5.15
5.9	Various modal loss factors as a function of position of ACLD patch at different stiffness's of anchors with 33 % coverage.	5.16
5.10	Comparison of active and passive loss factors for first mode as a function of position of ACLD patch (with and w/o SOL layer) at different stiffness's of anchors with 33 % coverage and Kp =20	5.17

xx List of Figures

5.11	Comparison of active and passive loss factors for second mode as a function of position of ACLD patch (with and w/o SOL layer) at different stiffness's of anchors with 33 % coverage and Kp =20	5.18
5.12	Comparison of active and passive loss factors for third mode as a function of position of ACLD patch (with and w/o SOL layer) at different stiffness's of anchors with 33 % coverage and Kp =20	5.18
5.13	Comparison of active and passive loss factors for fourth mode as a function of position of ACLD patch (with and w/o SOL layer) at different stiffness's of anchors with 33 % coverage and Kp =20	5.19
5.14	First and second modal loss function as a function of position of ACLD patch (with SOL layer thickness as 4 mm) at different stiffness's of anchors at different feedback gain Kp with 33 % coverage	5.20
5.15	Third and fourth modal loss function as a function of position of ACLD patch (with SOL layer thickness as 4 mm) at different stiffness's of anchors at different feedback gain Kp with 33 % coverage	5.21
5.16	Schematics of the experimental setup	5.22
6.1	Schematics of structure with (ACLD + CoLD/ TeLD) treatment	6.3
6.2	Cross-section of beam with ACLD combined with CoLD treatment (both sides)	6.3
6.3	Effect of initial compressive strain and loss factor of poly vinyl chloride (PVC) layer on the damping ratios	6.13
6.4	Effect of initial compressive strain and loss factor of PVC layer on the natural frequencies	6.13
6.5	Effect of initial strain on the damping ratios using SLD treatment at different speeds (RPM) of the beam with PVC patch located at a distance of 20 mm from the fixed end	6.14
6.6	Effect of initial strain on the damping ratios using PCLD + SLD treatment at 1000 RPM of the beam with PVC patch located at a distance of 20 mm from the fixed end.	6.15
6.7	Effect of speed (RPM) of the beam on the damping ratios at 1% strain in PVC layer with SLD treatment	6.16
6.8	Comparison of damping ratios of PCD Treatment with PCLD + SLD treatment with 1% strain in PVC layer at different RPM of the beam.	6.17
6.9	Effect of speed (RPM) of the beam on damping ratios at different locations of PVC patch by using PCLD+SLD treatment.	6.17

6.10	Effect of speed (RPM) of the beam on damping ratios of the first mode at different locations of PVC patch by using PCLD+SLD treatment.	6.18
6.11	Comparison of ACLD and PCLD treatment combined with SLD treatment at various speeds (RPM's) of the beam.	6.18
6.12	Effect of speed (RPM) of the beam on the damping ratios of the ACLD+SLD treatment at different locations of the PVC patch at $K_p = 20$.	6.19
6.13	Effect of speed (RPM) of the beam on the natural frequencies of the ACLD+SLD treatment at different locations of the PVC patch at $K_p = 20$.	6.20
6.14	Damping effectiveness of the PCLD and ACLD treatments combined with CoLD treatment at different thickness of the constraining layer.	6.21
6.15	Comparison of damping ratios by different techniques as a function of initial strain in PVC patch lying at a distance of 20 mm from the fixed end at 1000 RPM.	6.21
6.16	Comparison of damping ratios using CoLD and TeLD treatment as a function of initial strain in the PVC patches lying at a distance of 20 mm from the fixed end at 1000 RPM.	6.22
6.17	Schematic experimental setup of the rotating beam	6.23
7.1	Cross-section of beam with ACLD treatment using stand-off layer (SOL)	7.2
7.2	Damping ratios of the rotating PCLD beam system (with SOL layer) as a function of RPM at different thicknesses of SOL layer [thickness of VEM layer = 0.25 mm, $G_s = (0.2615e9)*(1+0.38 \times i)$]	7.9
7.3	Natural frequencies of the rotating PCLD beam system (with SOL layer) as a function of RPM at different thicknesses of SOL layer [thickness of VEM layer = 0.25 mm, $G_s = (0.2615e9)*(1+0.38 \times i)$]	7.10
7.4	Comparison of damping ratios of the rotating PCLD beam system (with SOL layer) and ACLD (without SOL) as a function of RPM at different thicknesses of SOL layer [thickness of VEM layer = 0.25 mm, $G_s = (0.2615e9)*(1+0.38 \times i)$]	7.10
7.5	Comparison of active and passive portion of damping ratios of the rotating ACLD beam system (with SOL layer) as a function of RPM at different thicknesses of SOL layer (thickness of VEM layer = 0.25 mm, $G_s = (0.2615e9)*(1+0.38 \times i)$) with $K_p = 20$	7.11
7.6	Damping ratios of the rotating PCLD beam system as a function of RPM at different location of patch (SOL layer thickness = 1.5 mm, VEM layer thickness = 0.25 mm, $G_s = (0.2615e9)*(1+0.38 \times i)$) ACLD	7.12

7.7	Damping ratios of the rotating beam system as a function of RPM at different location of patch (SOL layer thickness = 1.5mm, VEM layer thickness = 0.25 mm, $K_p = 15$, $G_s = (0.2615e9)*(1+0.38 \times i)$)	7.13
7.8	Schematic of the rotating beam along with control hardware	7.14
8.1	(a) Geometry of the flexible beam with PZT actuator and PVDF sensor (b) Effect of feed through term on the FRF of the flexible beam (c) Schematic for experimental setup for system identification	8.3 8.4 8.4
8.2	Comparison of ‘FEM’ and ‘Experimental’ results	8.7
8.3	(a) Block diagram of simple PPF control (b) Block diagram of efficient PPF control	8.8 8.8
8.4	Block diagram of Lead / Lag compensator circuit	8.12
8.5	(a) Flow chart for efficient PPF controller design (compact) (b) Flow chart for efficient PPF controller design (detailed)	8.13 8.14
8.6	Frequency response function of the system with GA based optimal PPF controller (Type-I and Type-II)	8.15
8.7	Frequency response functions of the implemented low pass (LP) and high pass (HP) filters	8.16
8.8	Frequency response functions of the open loop system with filters	8.16
8.9	Frequency response function of the system (with LP and HP filters) using PS based optimal PPF controllers designed without considering the filters in the loop (Type-I and Type-II)	8.17
8.10	Effect of system delay on the open loop system (with filters)	8.18
8.11	Quantification of system delay using Pade’s approximation	8.18
8.12	Effect of considering the filters and system delay in the design of PS based optimal PPF controllers	8.18
8.13	Frequency response function of the open and closed loop system using various types of PS based optimal PPF controllers along with compensator (with filters and system delay in the system)	8.19
8.14	Effect of system delay from 1 ms to 10 ms on the closed loop system with PS based optimal controller [Type-II]	8.19

8.15	Effect of system delay from 1 ms to 10 ms on the closed loop system with PS based optimal controller [Type-II] (close up for the second mode)	8.20
8.16	Transfer function for compensation circuits for various types PPF controllers	8.21
8.17	Open and closed loop response using PPF control with $H\infty$ norm minimization	8.21
8.18	Schematic of experimental setup	8.22
8.19	Experimental time domain response of the open and closed loop system with digitized PS based optimal PPF controller [Type-II], digitized at 1.3 kHz (with and without compensator).	8.25
8.20	Experimental time domain response of the open and closed loop system with digitized PS based optimal PPF controller [Type-II], digitized at 1.3 kHz for a random force applied at the free end (with and without compensator)	8.25
8.20	Experimental frequency domain response of the open and closed loop system with digitized PS based optimal PPF controller [Type-II], digitized at 1.3 kHz for a random force applied at the free end (with and without compensator)	8.26

@Seismicisolation

LIST OF TABLES

Table No.	Title	Page No.
2.1	Geometrical parameters and mechanical properties of the stationary beam	2.2
2.2	Geometrical parameters and mechanical properties of the rotating beam	2.2
2.3	Electrical properties of PZT material	2.2
3.1	Geometrical parameters of beams under different boundary conditions	3.15
4.1	Geometrical parameters and mechanical properties of the structure used under analysis	4.10
4.2	Electrical properties of PZT	4.10
5.1	Comparison between results from previous studies and present method for frequencies and modal loss factors	5.11
5.2	Electrical properties of the sensor and actuator materials	5.14
5.3	Comparison of experimental and theoretical frequency response of the beam system using PCLD with SOL treatment	5.23
5.4	Comparison of experimental and theoretical frequency response of the beam system using ACLD with SOL treatment with feedback gain $K_p=4$	5.23
6.1	Geometrical parameters and mechanical properties of Base beam, VEM layer and Constraining layers	6.11
6.2	Natural frequencies of the PCLD beam under different boundary conditions at 1000 RPM	6.11
6.3	Geometrical parameters and mechanical properties of structure used under analysis	6.12
6.4	Electrical properties of the piezoelectric materials	6.19
6.5	Comparison of experimental and theoretical frequency response of the beam using ACLD + CoLD treatment at $k_p=10$	6.24

xxvi List of Tables

7.1	Comparison of experimental and theoretical frequency response of the beam	7.15
8.1	Electrical properties of PZT	8.5

LIST OF PHOTOGRAPHS

Photo. No.	Title	Page No.
4.1	Picture of the flexible beam with CoLD treatment	4.18
5.1	Picture of the experimental beam	5.23
6.1	Apparatus for PTLD treatment (a) Tensioning of the base beam at Universal Testing Machine (b) PVC layers attached to base beam	6.22
6.2	Closer view of the beam treated with (ACLD+ PTLD + CoLD) treatment	6.24
7.1	Beam treated with PCLD (with SOL layer) treatment	7.13
7.2	Experimental setup of the rotating beam mounted on milling M/C bed	7.14

@Seismicisolation

CHAPTER – 1

INTRODUCTION

Usually satellites and other space structures have low flexural rigidity and are lightly damped due to the presence of small structural damping. Besides, it is difficult to provide other forms of damping, such as air damping, in space. Therefore, vibrations once produced grow to large amplitudes and take a lot of time to decay. This may lead to instability and failure of these structures.

Passive dampers, due to their heavy weight and fixed parameters, are not suitable for these applications. Also, for large space structures mathematical modeling is difficult and differs from on-orbit behavior. Corrosion and other environmental factors result in the change of structural characteristics at a slow rate. In certain cases the quick change in parameters can also occur due to sensor/actuator failure causing the long range of change in frequencies where the designer has to deal with lot of uncertainty. Thus online identification and adaptive control is desirable in these situations. Use of high loss factor viscoelastic materials is an important damping technique. However, these are effective only in small frequency range and are not adaptive to intelligent control. In active control, piezoelectric materials have been given special attention due to their high stiffness, low weight and wide frequency range of applications.

Automated adaptive controllers provide control signals to a structure in an attempt to cause the structure to exhibit a desired behavior. Together, the structure, the controller, and their interconnection comprise the system. The design of controllers is complicated by system instability which results in an improper system operation, and possibly, significant damage to equipment and/or injury to people. Fortunately, a properly designed controller prevents the system from operating in a dangerous, unstable mode.

It is, therefore, imperative that the controller be engineered with stable operation as a primary goal; performance is a secondary design consideration to be pursued only after stability is assured. Using online identification and adaptive control, a good control function can be maintained, confirming stability as well as optimal performance.

It is desired that once the vibration is induced, it should be damped out as quickly as possible. This task can be easily accomplished using higher control voltages. Since the control voltage that can be applied at the actuators is limited in amplitude and hence limited control energy is available for functioning of these controllers. Therefore, there is need to develop a controller which requires minimum control effort and provides minimum settling time to the system.

1.1 ADAPTIVE CONTROL SYSTEM

Figure 1.1 shows the basic components of a typical adaptive control system. The structure, represented by system matrices \mathbf{A} , \mathbf{B} and \mathbf{C} , is the device to be controlled. A controller, \mathbf{K} , produces the control signal, \mathbf{u} , which is used to modify the behavior

of the plant. The plant output, y mimics an external, time-varying, input signal called the reference or excitation input, u_x . Performance is measured by the error signal, e , which is the difference between the reference signal and the plant output: $e = u_x - y$.

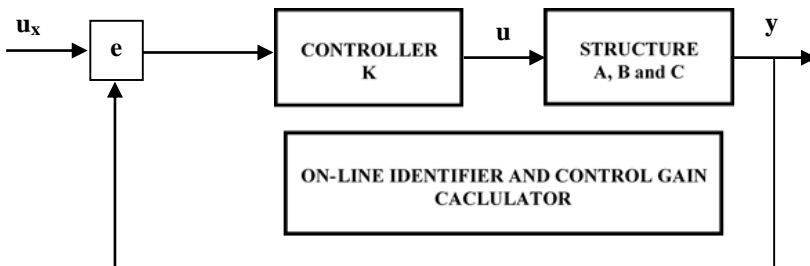


Fig. 1.1 Adaptive control system

The vast majority of research in control theory is dedicated to systems which are linear time-invariant (LTI). The simple mathematics of LTI systems enables the application of the mature and extensive body of linear systems theory. Consequently, the design of stable controllers is straightforward. With the passage of time, as the system parameters A, B and C are changing, the online identifier calculates these system matrices and calculates the control gains K for optimal performance of the system.

1.2 OVERVIEW OF SYSTEM IDENTIFICATION AND CONTROL SYSTEM DESIGN

A significant amount of the current research activity in the field of structural mechanics has focused on the study of smart, intelligent or adaptive structures. Specific studies have considered definition, analysis and synthesis of smart structures. The long term objective of the design of a smart and intelligent structure is to develop a structural system that can execute selected functions like an intelligent person. The near time objective, however, is to be able to design a structural system that can be described as adaptive structure. These adaptive structures have their own sensors, detection circuits, controllers and actuators. The sensors and actuators are made of a class of materials known as ‘smart materials’. Piezoceramic materials, Polyvinylene Difluoride (PVDF) films, shape memory alloys, electro rheological fluids, fiber optic devices and electro restrictive devices can be considered in the class of smart materials.

1.2.1 Vibration Control

To reduce the amplitude of vibrating structures, two types of control strategies are possible:

1. By using dampers or shock absorbers; the vibration amplitude can be reduced, in a short span of time.
2. By using the layers of viscoelastic materials, the same effect can be produced. Composite materials made by sandwiching the layers of viscoelastic materials between the layers of parent material, are quite common. Reducing the vibration amplitude by this technique is called Passive control (PC).

The second type of control is obtained by using the structure mounted with smart materials. Due to the vibrations, the strain is developed in smart sensors fixed on the surface of the structure. This strain produces electrical voltage in these materials. This voltage is used as sensor signal. Using the information of the sensor voltage, suitable

feedback electrical voltage is applied to the actuators made of smart materials. The applied actuator voltage produces strain in opposite direction and reduces the vibration amplitude. This type of vibration control is called Active Control (AC).

Due to the heavy weights of the passive controllers and their fixed parameter nature, these are not suitable for lightweight structures. Active vibration control finds extensive usage for these types of light weight structures. Applications of adaptive structures using AC have been in the fields of vibration control of flexible structures, optical surfaces maintenance, flaw detection and control and improvement in performance of systems such as aircrafts, helicopters and space vehicles by changing the shape and configuration.

1.2.2 Smart Materials as Sensors and Actuators

Smart materials play a main role in above mentioned applications. Piezoceramic materials are less costly and have higher electromechanical coupling, therefore, these are widely used as smart distributed sensors and actuators. Piezoelectricity offers many advantages for active vibration excitation and isolation over a wide frequency range, especially for small amplitudes. Most conventional piezoelectric materials such as Barium Titanium Oxide, Lead Zirconium Oxide and Quartz are, however, brittle and difficult to fabricate in complex shapes. This has limited their applications up to some extent. Polyvinylidene fluoride (PVDF) is a piezopolymer with unique properties that make it attractive for active vibration control applications. PVDF is tough, pliant and can be easily formed in sheets and complex shapes. Lead Zirconated Titanate (PZT) is another ceramic with favorable mechanical and electrical properties.

1.2.3 Mathematical Modeling and System Identification

To study the effectiveness of control algorithms, accurate modeling of electro-elastic interactions of piezoelectric sensors and actuators with substrate is necessary and is discussed in the following sub-sections.

1.2.3.1 Mathematical Modeling by Finite Element Methods

Exact closed form solution of these dynamic problems is limited to extremely simple structures. Very simple cases of geometry and boundary conditions can be accommodated in this method. Finite Element Methods (FEM) can be used for analyzing the static and dynamic performance of intelligent structures. FEM analysis is normally based on first order shear deformation theory. However, such models suffer from the problem of spurious shear stiffness, which need special consideration. Thus there is a need for improved FE approximation techniques for analyzing ‘Intelligent’ structures of general configurations. When ordinary FEA techniques are used for laminated composite plates with piezoelectric layers acting as sensors and actuators, the theoretical results deviate from experimental results. Also a lot of computational effort and time is needed in modeling these structures. Due to manufacturing inaccuracies, non-linearity, non-isotropy and structure degradation, the theoretical results given by FE analysis deviate from experimental results. In case of adaptive systems where system parameters are changing with the passage of time, application of FEM is not possible.

1.2.3.2 System Identification by Experimental Data

In the cases discussed above, the online estimation of system parameters is needed. In such applications, system parameter identification from experimental input – output data is preferable. This forms the basis of experimental system identification

techniques. To properly understand the system identification theory, different system models must be studied. Various system forms, normally used in system identification and control theory are discussed below:

1.2.3.2.1 System categorization based on time

Depending upon the relationship between time and system parameters, following two categories are possible:

- (i) **Time Varying Systems:** These are the systems whose parameters vary with the passage of time.
- (ii) **Time In-varying Systems:** These are the systems whose parameters do not vary with the passage of time.

1.2.3.2.2 System categorization based on input-output relationships

Depending upon the relationships between input and output, following two categories are made:

- (i) **Linear Systems:** Outputs are linear function of inputs
- (ii) **Non-linear Systems:** Outputs are related with inputs by non-linear relationships.

To deal with different sub-categories of the system, respective mathematical treatments are developed. In normal practice, the linear and time invariant systems are encountered. These are combined together to form a class of systems called Linearly Time Invariant (**LTI**) systems.

1.2.3.2.3 System categorization based on number of input/outputs

Depending upon the number of inputs and outputs, following categories are made.

- (i) **SISO:** i.e. Single Input Single Output Systems
- (ii) **SIMO:** i.e. Single Input Multiple Output Systems
- (iii) **MISO:** i.e. Multiple Input Single Output Systems
- (iv) **MIMO:** i.e. Multiple Input Multiple Output Systems. These systems are also called Multivariable Systems.

1.2.3.2.4 System categorization based on number of input/outputs

Based on the form of data available, following two categories are made:

- (i) **Continuous Systems:** The data is continuously available from the sensors regardless of the sampling frequency. This means that at each instant of time t , the signal is available.
- (ii) **Discrete Systems:** Using the modern digital computers it is easy to handle the system in discrete form. Even if it is available in continuous form, it is possible to convert it into discrete form. In this case the signal is available at certain discrete steps of time i.e. at $t_k = t_{k-1} + \Delta t$, where Δt is the sampling interval. Discrete system is easy to handle and a lot of mathematical background is available

1.2.3.2.5 System categorization based on structural parameters

Depending on the structure of system parameters and the relationship with each other, following two categories are made:

- (i) **Transfer Function Form:** The dynamic SISO LTI system in continuous form can also be presented in transfer function form. These transfer functions are presented as the ratio of two polynomials. In mathematical form:

$$H(s, P) = \frac{N(s, P)}{D(s, P)} = \frac{\sum_{k=0}^n \alpha_k s^k}{\sum_{k=0}^n \beta_k s^k} = \frac{\alpha_0 s^0 + \alpha_1 s^1 + \dots + \alpha_n s^n}{\beta_0 s^0 + \beta_1 s^1 + \dots + \beta_d s^d}$$

where s is the Laplace complex number; α and β are the coefficients of system outputs and inputs respectively. This forms the part of classical control theory. Various control techniques like pole zero placement, root locus method etc., can be used for control implementations of the system in this form. However, using certain transformations, these continuous systems can be presented in discrete form given as below:

$$H(z, P) = \frac{N(z, P)}{D(z, P)} = \frac{\sum_{k=0}^n \alpha_k z^k}{\sum_{k=0}^n \beta_k z^k} = \frac{\alpha_0 z^0 + \alpha_1 z^1 + \dots + \alpha_n z^n}{\beta_0 z^0 + \beta_1 z^1 + \dots + \beta_d z^d}$$

where z is a shift forward operator.

For MIMO systems, these polynomials form the part of a matrix. This type of matrix is called polynomial transfer function matrix. But as the number of inputs and outputs are increased, it becomes quite difficult to handle the system in this form. To avoid this problem for MIMO systems, state space models are quite useful and are presented below:

- (ii) **State-Space Form:** Any continuous, LTI system can be written in the following form:

$$\begin{aligned} \mathbf{X}(k+1) &= \mathbf{A} \mathbf{X}(k) + \mathbf{B} \mathbf{u}(k) \\ \mathbf{y}(k) &= \mathbf{C} \mathbf{X}(k) \end{aligned}$$

Where $\mathbf{X}(k)$, $\mathbf{u}(k)$ and $\mathbf{y}(k)$ are the state vector, input vector and output vector at k^{th} instant of time respectively. \mathbf{A} , \mathbf{B} and \mathbf{C} are called state coupling matrix, input coupling matrix and output coupling matrix respectively. Using the standard methods, it is easy to transform these methods to discrete form.

- (iii) **Difference Equation Form:** Although state space models are best suited for control applications, the identification in this form is comparatively complex. Complexity increases tremendously as the system order is increased. Difference equations are the best form, in which identification can be carried out from experimental data. Certain methods are available in literature which can be used to transform the system from state-space form to difference equation form and vice versa. Thus, it is desirable to identify the system in difference equation form and then convert it into state-space form. The difference equation form can be written as:

$$\mathbf{Iy}(t) + \mathbf{A}_1 \mathbf{y}(t-1) + \dots + \mathbf{A}_n \mathbf{y}(t-n) = \mathbf{B}_0 \mathbf{u}(t) + \mathbf{B}_1 \mathbf{u}(t-1) + \dots + \mathbf{B}_n \mathbf{u}(t-n)$$

The matrices $\mathbf{A}_0, \mathbf{A}_1, \mathbf{A}_2, \dots, \mathbf{A}_n$ are the coefficient matrices of the output vectors and $\mathbf{B}_0, \mathbf{B}_1, \mathbf{B}_2, \dots, \mathbf{B}_n$ are coefficient matrices of the input vectors.

1.2.3.2.6 System categorization based on feedback

Depending upon the presence or absence of the control signal, following two categories are made:

- (i) **Open-Loop Systems and Identification:** Any natural system can be presented in terms of input output relationships. These parameters represent the system in parametric form. This form is quite useful in control applications. Since the free

excitation of the system is normally possible, the flexible structures can be excited with specially designed input signals for system identification of these structures. The only condition for free excitation is that the system should not turn to be unstable. Thus, for open-loop identification, system stability is the first requirement. Stable systems are those systems which turn to their equilibrium position after excitation. From the output data thus obtained, parametric identification can be made. This is called open-loop identification or off-line identification.

- (ii) ***Closed-Loop Systems and Identification:*** Sometimes the systems are not stable i.e. if they are disturbed from their equilibrium position, they never return to their original position. So these systems are always run under feedback conditions. Using specially designed excitation signal along with feedback signal, system parameters can be identified from input-output data by using various techniques in closed-loop conditions. Sometimes system parameters are time varying. In these situations, it becomes necessary to identify the changed parameters in the presence of the control action. This type of identification is called closed-loop identification or on-line identification.

1.2.4 System Classification and Neural Networks

There are systems where the parameters are changing so quickly with time that parameter identification techniques fail to compensate for these changes. Flexible robotic manipulator is an example of such type of systems. In all the types of robotic configurations, system parameters change abruptly. The controller designed for one configuration is almost useless for the other configuration. For these situations, accurate and extremely fast methods of identification are required. This task requires methods which are computationally fast and give adequately accurate identification results. One of the approaches could be to identify a large system of system parameters off-line for various link configurations and grouping them into different classes based on certain criteria. This process is called system classification. Depending upon the situation, a particular class of the system is identified from a large collection of classes. This method is extremely fast and quite accurate results are obtained, which is a prerequisite for identification of parameters for control applications. **Learning Vector Quantization Neural Networks (LVQNN)** is best suited for this classification. Using this strategy, classification can be done based on natural frequencies of the system. These natural frequencies are available from spectrum analyzer. LVQNN is trained offline. For online identification of system parameters, this trained neural network is used. The computational requirement of this type of LVQNN is very small, as only few additions and multiplications are needed for this purpose. Dynamic systems changing at fast rates can be identified accurately and in very small periods of time.

1.2.5 Controller Design

Using the tools of classical control theory, the controller can be designed. Laplace transformations are used to convert system descriptions in terms of integral-differential equations to equivalent algebraic relations involving rational functions. These can be easily used to transform the system into transfer functions form. Root locus method can be used to design the controller. Following controller design strategies may be used.

1.2.5.1 Linear Quadratic Gaussian Control

Using state-space approach, controller can be easily designed for MIMO systems meeting any desired performance index. In a state-space feedback control, the states of the system must be fed back to the system to generate the future control signals. The observers are used for this purpose. Observers estimate the states of the system from input–output data. Deterministic as well as stochastic observers can be used, based on signal-to-noise (S/N) ratio. For lower S/N ratio, stochastic observers like Kalman Filter are beneficial. Although these require more computational effort as compared to deterministic observers, the resulting accuracy overcomes the demands of higher computational complexity. For higher S/N ratio, deterministic observers, like Leunberger Observer, are sufficient. In Linear Quadratic Gaussian (LQG), a Linear Quadratic Regulator (LQR) is used in combination with Kalman Filter. LQR is designed by solving the Riccati equation. System matrices **A**, **B** and **C** are used along with weighing matrices to design the gain matrix.

1.2.5.2 Adaptive Control

When the system parameters are varying with time, adaptive system identification is necessary. The controller is designed for a particular set of system parameters. As the system parameters are changed, the performance of the control system degrades. Re-identifying the system parameters and then redesigning the controller based on these new set of system parameters can maintain the controller performance at a near optimum level. To achieve this goal, various identification strategies can be applied. If the system is changing at a slow rate, closed-loop identification gives adequate results. From input/output data, the open-loop transfer function can be calculated in polynomial matrix form. These are basically difference equations in multivariable form. Based on certain transformations, these can be converted into state-space form. The control gain matrix can now be calculated based on these new system matrices. But if the system parameters are changing at a fast rate, enough time is not available for system identification tasks. System classification technique using LVQNN is applied in that case to identify a particular class of the system. The specified class gives system matrices and control gain matrix.

1.2.5.3 Control Software and Hardware

Proper experimental validation is required to authenticate, any theoretically designed control system. Digital control systems require that signal samples be collected from sensors mounted on flexible structure. After certain digital calculations on the sensor signal, control signals to be applied to the actuators are calculated. Most often the sensors and actuators are analog devices, so analog-to-digital (A/D) and digital-to-analog (D/A) conversion is necessary. Data acquisition is the digital conversion of a set of analog sensor signals and the transmission of their samples to a digital processor. The high-level languages deal with more abstract instructions and divorce the programmer from underlying machine code. Using an environment of high-level languages like, graphical programming language ‘Lab VIEW’, the experimental validations can be done easily.

Various types of sensors like Linear Variable Differential Transformer (LVDT), accelerometers and piezoceramic sensors can be used. National Instruments’ data acquisition card is used for data collection, A/D and D/A conversion. Amplifiers are used to magnify the signal applied to actuators. Since the control signal generated by the computer lies in the range -10 to +10 volt, and here the use of amplifiers is needed. Using the amplifiers, the signal is amplified 10 to 15 times to obtain the optimal results.

The sampling rate is maintained by a periodic signal called the step clock that informs the processor each time a new set of measurements.

Several advanced applications, such as those in jet fighters, automobiles and spacecraft's, require structures that are highly strong, lightweight and possess high structural damping property. Reduction in weight, however, results in low rigidity and consequently poor vibration characteristics. Unless the vibration is effectively controlled, it may destabilize the system and may very often result in the failure of the system. Therefore, there is a need to design and use structures that are equipped with suitable vibration control features. Smart structure technology may provide a solution to this problem.

Smart structures use piezoelectric materials, electro-rheological (ER) fluids, magneto-rheological (MR) fluids and shape memory alloys as sensors and actuators. This provides real-time control capabilities to these structures. Results of several investigations are available on the use of such materials for vibration control. The literature on vibration control of structures, in general, may broadly be divided into two main categories, on-line identification of adaptive vibration control and on-line identification of non-adaptive vibration control of **Linear Time Invariant (LTI)** systems using piezoelectric materials. The former may be studied separately under the sub-titles, on-line identification of flexible structures and adaptive vibration control. A brief survey of literature falling under these categories is presented below.

1.3 VIBRATION CONTROL OF LTI STRUCTURES

The work done on vibration control of LTI structures is very vast and is broadly classified and discussed under the following three sections:

- 1.3.1 Vibration Control of Stationary and Rotating LTI Structures Using Passive Constrained Layer Damping (PCLD) treatment.**
- 1.3.2 Vibration Control of Stationary and Rotating LTI Structures Using Active Constrained Layer Damping (ACLD) Treatment.**
- 1.3.3 Vibration Control of Stationary and Rotating LTI Structures using Piezoelectric Materials**

1.4 BRIEFING OF THE BOOK

The book has been briefed as below:

- ❖ Many of the books have been published on the adaptive vibration control using gain scheduling, self-tuning regulators and LMS algorithms but further investigations using piezoelectric materials as sensors/actuators for intelligent adaptive controls are desired to be published and are done in this book.
- ❖ Although the use of frequency domain methods are quite popular in control system design, but very less number of books are available about the use of these methods for vibration control of lightweight structures and the readers will find all this stuff in the book. Frequency domain methods are quite attractive as they require less computation power and are robust towards sensor noise.
- ❖ There is a need to carry out the work on the improved and fast methods of parametric and non-parametric estimation of transfer function. This book would fulfill this need.

- ❖ Very less or no book is available for the implementation of Viscoelastic Layers and Stand-off Layers in identification and control of structural vibrations. There is a need to carry out further research to include Multi-Input Multi-Output (MIMO) systems. This would be the first book to study Viscoelastic Layers and Stand-off Layers in identification and control of structural vibrations
- ❖ All the books available till now, deal with the work on stationary cantilever beams or plates, which are one of the easier configurations for control effectiveness measurements. This book carries all the details of the work done on rotating cantilever beams and on built up structures. Present work is being undertaken for studying control of built up structures, consisting of both rotating and stationary beams to control their vibrations with different treatments.

1.5 OBJECTIVES OF THIS BOOK

1.5.1 Primary Objectives

- To compare the accuracy of the analytical and FEM based methods for constrained layer damping techniques.
- To combine the various techniques of constrained layer damping treatment to obtain maximum efficiency.
- To develop an active-passive treatment for stationary beams in which SOL layer is sandwiched between base beam and VEM layer. (Figure 1.2)
- To develop an active-passive treatment for rotating beams in which SOL layer is sandwiched between base beam and VEM layer. (Figure 1.3)
- To develop an active/passive treatment for rotating beams in which SLD treatment is combined with Constrained Layer Damping treatment. (Figure 1.4)

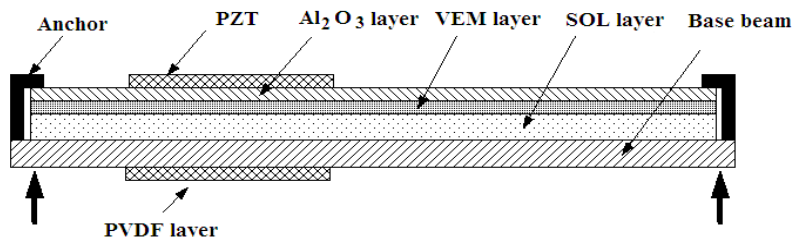


Fig. 1.2 ACLD treatment of a stationary beam with SOL layer sandwiched between the base beam and VEM layer.

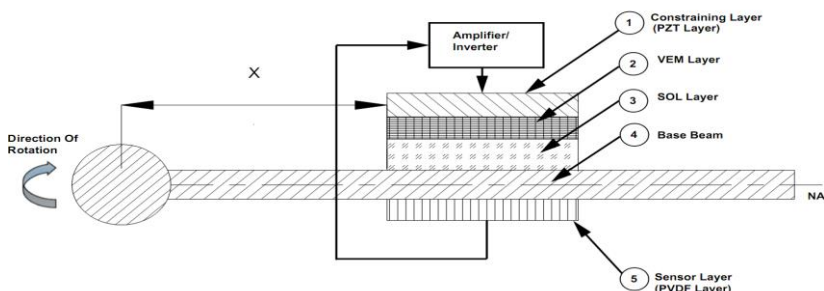


Fig. 1.3 ACLD treatment of a rotating beam with SOL layer, sandwiched between the base beam and VEM layer.

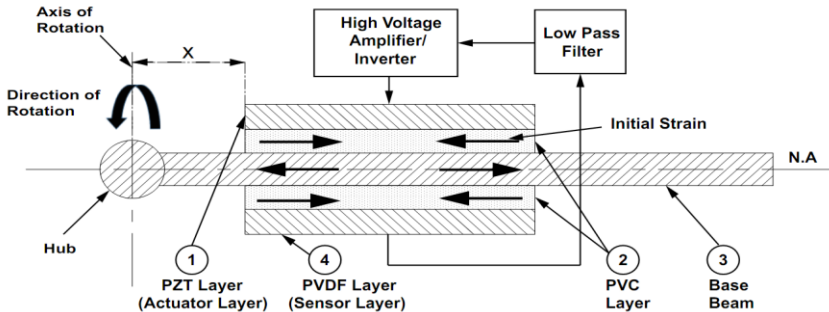


Fig. 1.4 ACCLD treatment of a rotating beam with SLD treatment combined with constrained layer damping treatment.

1.5.2 Secondary Objectives

To develop an experimental setup for validating the above theoretical work for rotating beams. The present work is composed of the following theoretical as well as practical components.

1.5.3 Theoretical work

Theoretical work comprises the following:

- Mathematical Modeling:** For carrying out the mathematical analysis the beam structure is chosen. The structure (stationary as well as rotating) is assumed to be made up of small segments with embedded piezoelectric patches along with VEM layers, SOL layers and stresses PVC layers. FEM technique is applied to find the natural frequencies and loss factors of the structure.
- Controller Design:** Position feedback, velocity feedback and combined position and velocity feedback controller is implemented for active control applications.
- Comparison with existing literature:** The results obtained by the FEM technique are compared with existing literature to validate the code developed.

1.5.4 Experimental Work

For testing of the theoretical results experimentally, the same beam structure equipped with piezoelectric patches as actuators and sensors is used.

1.6 OBJECTIVES OF THIS BOOK

In an effort to achieve the primary goal the following methodology is adopted:

- First of all, the constrained layer damping technique is modeled by FEM techniques and the results are compared with that obtained from analytical model.
- Afterwards, better method of the above two models is used to model the Passive Constrained Layer Damping Treatment using SOL layer for stationary beams.
- Active Constrained Layer Damping Treatment is modeled by using SOL layer for stationary beams.
- Passive Constrained Layer Damping Treatment is modeled by using SOL layer for rotating beams.
- Active Constrained Layer Damping Treatment is modeled by using SOL layer for rotating beams.

6. Passive Constrained Layer Damping Treatment is combined with stressed layer damping treatment for rotating beams.
7. Active Constrained Layer Damping Treatment is combined with stressed layer damping treatment for rotating beams.
8. Validating some of the results experimentally.

1.7 OUTLINE OF THE BOOK

The flow chart given in Figure 1.5 shows the schematic progress of the present work. The chapter wise division of the work is as follows:

Chapter 1: gives the introduction to active and passive vibration control techniques, and problem details of the present work done. An introduction to various topics of system identification and control is also presented.

Chapter 2: describes the geometrical modeling of the structure (rotating beam) used for Active Vibration Control (AVC) and its experimental setup.

Chapter 3: analyzes the performance of finite element modeling of Pre-Compressed Layer Damping (PCLD) treated beam which is related with Energy Based Analytical Methods.

Chapter 4: explains the active vibration control of beams with combined effect of active constrained layer damping (ACLD) and pre-compressed layer damping (PCLD) treatment theoretically and experimentally.

Chapter 5: describes the finite element modeling and design of the beam with enhanced active constrained layer damping (EACLD) using Stand-off Layer (SOL). Experimental damping treatment and vibration analysis is also discussed.

Chapter 6: presents the comparison of theoretical and experimental vibration analysis of a rotating beam with combined effect of active constrained layer damping (ACLD) and stressed (Compressed/Tensed) layer damping (SLD) treatment.

Chapter 7: gives the comparison of theoretical and experimental vibration analysis of a rotating beam with active constrained layer damping (ACLD) and stand-off layer (SOL) damping treatment.

Chapter 8: presents a new technique of efficient vibration control of smart structures with modified positive position feedback (PPF) control using Pattern Search Method in the presence of Instrumentation Phase Lead and Lag.

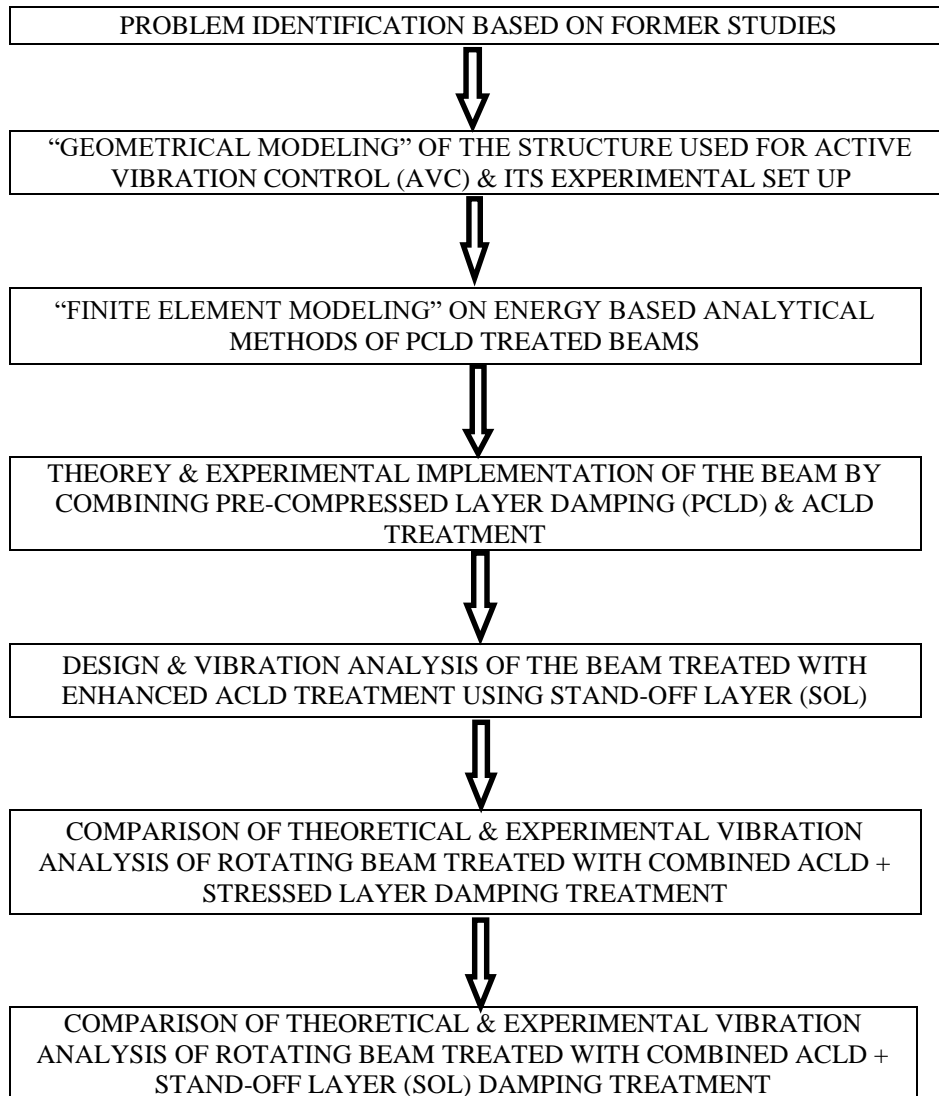


Fig. 1.5 Book Flow chart

CHAPTER – 2

ACTIVE VIBRATION CONTROL STRUCTURE

Active vibration control is comparatively a new field. For controlling the systems with higher frequency modes, the high sampling rate is normally required. At these high-sampling rates the processors has to be fast, so as to generate control inputs within the sampling intervals. For this purpose, in the present work, the MATLAB was used which delivers deterministic real-time performance. The complete MATLAB can be downloaded to the ‘Real Time Engine’ and can be run at very high speed with this dedicated processor. These types of hardware and software combinations are a must for real time active vibration control. Thus, with embedded automation, it is possible to generate digitally processed control signals for vibration control applications, which were not possible few years back.

Using different types of distributed sensors and actuators based on piezoceramics, with higher electromechanical coupling, sensing and control has become practically feasible for large and complex shaped flexible structures. With these developments in the control hardware, Active vibration control (AVC) has now become a practical reality. A lot of practical applications of AVC are emerging day by day.

This chapter deals with the experimental setup for the control of vibrations of the rotating/stationary beam with distributed sensors/actuators. The rotating/stationary beam is chosen since it is a simple extension of a one dimensional beam to a two-dimensional structure. The practical applications of this structure are included in our everyday industrial operations and machine tools. For example, all the machines like drilling, milling, rolling, grinding etc. are representative of a rotating beam structure. In the subsequent chapters of this book, this structure with the geometrical parameters and mechanical properties given in Table 2.1 with stationary beam, in Table 2.2 with rotating beam and the properties of PZT material in Table 2.3, has been used for all theoretical and experimental analysis.

Since under various payloads and changing configurations of the respective arms, the modal parameters of the flexible manipulators (in the present case it is stationary or rotating beam) keep on changing with time. As the quality of any machine depends upon the accurate positioning of all of its parts, the vibrations once produced should be damped as quickly as possible. The active vibration controller is designed on the basis of system parameters, which are based on the modal parameters of the structure.

In the present work, it is assumed that the other parameters remain constant except the payload (tip load) at the free end. The controller once designed for a particular system, becomes ineffective and even in some cases unstable, when system’s modal parameters are changed with changing tip load or payload.

Table 2.1: Geometrical parameters and mechanical properties of the stationary beam

Parameter/Property	Base Beam	VEM/PVC layer	Constraining layer
Length (mm)	300	100	100
Width (mm)	14	14	14
Thickness (mm)	1.0	1.5	0.5
Young's Modulus (N/m ²)	3.21×10^{10}	2×10^7	7.037×10^{10}
Density (Kg/m ³)	4972	1390	7500
Loss Factor	0.008	0.5	0
Shear Modulus (N/M ²)	-	7.69×10^6	-

Table 2.2: Geometrical parameters and mechanical properties of rotating beam

Parameter/Property	Base beam	VEM layer	Constraining Layer
Length (mm)	300	300	300
Width (mm)	12.7	12.7	12.7
Thickness (mm)	2.286	0.25	0.762
Young's Modulus (N/m ²)	7.1×10^{10}	2.98×10^7	6.49×10^{10}
Density (Kg/m ³)	2700	1250	7600
Loss factor	-	0.38	-
Shear Modulus (N/m ²)	-	0.2615×10^6	-

Table 2.3: Electrical properties of PZT material

Material Property	Symbol	PZT
Piezoelectric charge constant (m V ⁻¹)	d ₃₁	171×10^{-12}
Electromechanical coupling factor	k ₃₁	0.12
Piezoelectric voltage constant (V m V ⁻¹)	g ₃₁	216×10^{-3}
Dielectric constant	k _{3t}	12

Under these circumstances, the system needs re-identification. With the updated values of system parameters, the new controller is designed. Active control requires very accurate models for controller design. Non-collocated sensors and actuators have inherently small stability margins. A lot of work has been done in the past for the development of accurate dynamic models. In practice it is difficult to obtain sufficiently accurate model parameters by FEM techniques. Especially when the system parameters are changing, there emerges the need to identify the changing dynamics of the system with change in system parameters. For example, changing speed and changing configurations of any machine can destabilize the fixed gain controller, based on original configuration of the system. Thus there is a need to develop on-line methods of system identification so that changing dynamics can be estimated.

2.1 EXPERIMENTAL SETUP

The schematic diagram of the experimental setup with active constrained layer damping treatment is shown in Figure 2.1. This shows the rotating beam on a milling machine bed. The rotating beam is equipped with 2 PZT patches. One of these is being used as a sensor and the other one is used as an actuator. The strain developed due to

vibrations is converted into electrical voltages, and is measured at the output sensors. The observed signal is in the range of $-10V$ to $+10V$. This does not need amplification. To remove the effect of higher modes the signals are pre-filtered. Then the signal goes to data acquisition card. Analog-to-digital (A/D) conversion of the signal is done in this card. Based on these digitized, input signals, control signals are calculated by the real time engine. These signals are in the range of $-10V$ to $+10V$. After digital-to-analog (D/A) conversion in the data acquisition card, control signal goes to the amplifier where it is amplified 10 to 15 times, so that the voltage after amplification is in the range $-150V$ to $+150V$. This high voltage signal is then sent to the PZT actuators. This voltage develops the strain in the structure such that the vibration damping is achieved.

PZT patches are used as sensors as well as actuators. Both input data and output data are fed to spectrum analyzer to get the Fast Fourier Transform of the data. A digital ‘low pass filter’ is used to remove the effect of higher modes of vibration. The circuit virtually consists of two parts i.e. adaptive part and fixed part. In adaptive part, the system contains ‘system matrices’ & ‘control gains’ and fixed part consists of all the above for initial control. In the pre-filter, data with frequency more than the second mode is filtered out. A/D and D/A conversions are done inside the data acquisition card. The amplifier/filter unit is capable of amplifying the input/output signal. The digital filters in this filter unit are capable of acting as High Pass filter, Low Pass filter and Band Pass filter for the incoming signal.

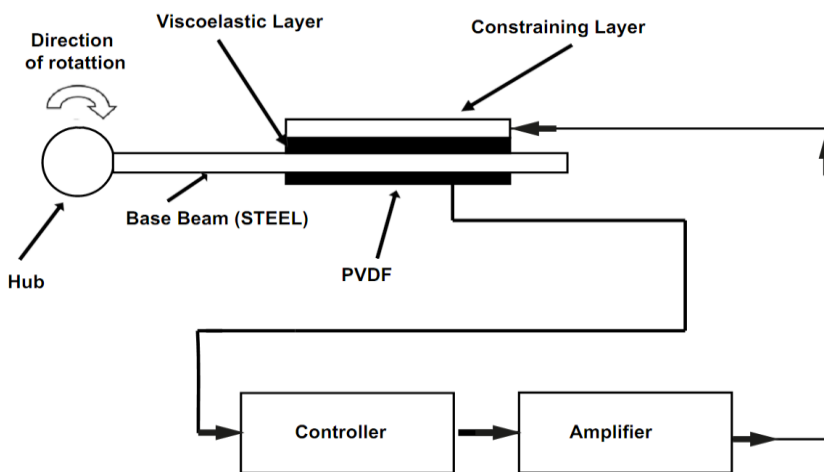


Fig. 2.1: Schematic view of a rotating beam with ACLD treatment

2.2 EQUIPMENT CHARACTERISTICS

The characteristics of the different hardware and software components of the experimental setups are discussed in the following subsections: -

2.2.1 Software ‘MATLAB-Simulink’

The ‘MATLAB’ is a highly productive graphical development environment for building data acquisition, instrumentation and control systems. With ‘MATLAB’ it is easy to create interfaces that give interactive control of software system. The tight integration of ‘MATLAB’ with measurement hardware facilities, rapid development of data acquisition and control is possible. This software contains powerful built-in

measurement analysis and a graphical compiler for optimum performance. For applications that require real time performance, there is special system called ‘MATLAB-Simulink’. This downloads standard ‘MATLAB’ codes to a dedicated hardware target running a real-time operating system independent of the operating system.

2.2.2 Simultaneous I/O Data Acquisition Card (DAQ 6062 E)

National Instrument’s ‘E-Series’ technology is a complete data acquisition (DAQ) hardware architecture that takes advantage of the latest in electronics and technological innovations and advances the capabilities of PC-based DAQ solutions. ‘E-Series’ is a standard architecture in instrumentation class, for multichannel data acquisition. This architecture includes the followings:

- NI-PGIA (Programmable Gain Instrumentation Amplifier) gain independent, fast settling time amplifier
- RTSI (Real time System Integration) multiboard/multifunction synchronization bus
- DAQ-STC (System Time Counter) counter/timer
- MITE PCI bus master interface
- Shielded, latching metal connectors

Following are some of the important features of the E series data acquisition system:

2.2.2.1 Analog Input FIFO

The ‘E series’ devices perform both single and multiple Analog to Digital (A/D) conversion of a dynamic signal made of infinite number of samples. A large FIFO buffer holds the data during the A/D conversion so that no data is lost. Multiple A/D conversions can be handled with programmed input-output, interrupts, or direct memory access (DMA). Total 16 no. of channels can be handled. The maximum input voltage range is –10 Volts to +10 Volts. It produces 12-bit resolution which means that full-scale accuracy is 1.443 mV

2.2.2.2 Analog Output

The ‘E series’ devices also perform both single and multiple ‘Digital-to-Analog (D/A) conversion’ from a fixed number of data points to infinite number of samples. Multiple D/A conversions can be handled with programmed input-output, interrupts, or direct memory access (DMA). Total 2 numbers of channels can be handled. The maximum input voltage range is –10 V to +10 V. It provides 12 bit resolution with a full scale accuracy of 1.443 mV. Large FIFO DAC buffers for high-speed analog output updates are available to accommodate varying bus latencies and to ensure no data loss.

2.2.2.3 DAQ-STC System

The ‘E Series’ devices use the National Instruments DAQ-STC for counting and timing related functions. The DAQ-STC is specially designed with functions for A/D and D/A timing with random logic associated with routing timing I/O signals between I/O connector and the RTSI bus. The DAQ-STC derives its internal timing from a 20 MHz source. External clocking options are available for all counter/timing sections. Each group can be configured independently with timing resolution down to 50 ‘ns’. The general-purpose counter/timers are capable of DMA data transfers and fast processing. This capability is important for relative time stamping of signals with varying frequency, synchronization with analog conversions. The DAQ-STC provides a flexible timing I/O interconnection that consists of 10 programmable inputs (PFI).

2.2.2.4 *Multifunction DAQ Software NI-DAQ*

'NI-DAQ driver software' bundled with 'E-series' multifunction DAQ device, provides access to the features of the DAQ hardware.

2.2.2.5 *Sampling Rate*

Sampling rates up to 500 kHz can be handled. But even with real time engine there is limit to computational speed. For each loop in control implementation, states of the system are calculated from input output data using FEM applications and control signals are generated using the gain matrices. Each computation requires some computational effort. Thus there is a limit to sampling frequency, which can be handled using the real time engine. Control signals must be calculated form input-output data, in a time interval, less than the sampling period. Hence based on the capability of the processor, one cannot go beyond a certain sampling rate.

Exact closed form solution of these dynamic problems is limited to extremely simple structures. Very simple cases of geometry and boundary conditions can be accommodated in this method. Finite Element Methods (FEM) can be used for analyzing the static and dynamic performance of intelligent structures. FEM analysis is normally based on first order shear deformation theory. However, such models suffer from the problem of spurious shear stiffness, which need special consideration. Thus there is a need for improved FE approximation techniques for analyzing 'Intelligent' structures of general configurations. When ordinary FEA techniques are used for laminated composite plates with piezoelectric layers acting as sensors and actuators, the theoretical results deviate from experimental results. Also a lot of computational effort and time is needed in modeling these structures. Due to manufacturing inaccuracies, non-linearity, non-isotropy and structure degradation; theoretical results given by FE analysis deviate from experimental results. In case of adaptive systems where system parameters are changing with the passage of time, application of FEM is not possible.

2.2.3 *Amplifiers*

The control signals generated from the computer via data acquisition card are in the range -10 volt to +10 volt. Since for getting lesser and lesser settling times, the control voltage has to be increased. This job is done by the amplifiers. These amplifiers are capable of increasing the control signal voltage up to 200 volt, without any phase change.

2.2.4 *Pre-Filter*

Any vibrating flexible structure contains infinite number of modes of vibration. However, for practical purposes only few modes are of importance. The dynamics of these structures can be modeled mathematically, using finite number of modes using modal analysis. For better sensing the signal obtained from these vibrating structures, higher modes need to be eliminated. This is achieved by higher order low pass filters. They pre-filter the input signal, to remove the high frequency signals and hence are also called 'pre-filters'.

2.2.5 *Real Time Engine*

At the core of the real time engine is the real time operating system. One of the main differences between real time operating system and general-purpose operating system is the ability to guarantee worst-case latency. Operating systems have varying latencies and do not guarantee worst-case latency. With a general purpose operating system, an external interrupt could be put into a queue and then serviced later after the operating

system has finished its current operation and any other interrupts in the queue. On the other hand, a real time operating system can halt its current process to handle an interrupt immediately. In essence, the real time operating system guarantees event response within a certain time interval. Using National Instrument's Lab VIEW Real Time engine, the programs from main host PC can be downloaded to a dedicated processor running a real time operating system. These types of environments had made the active control a practical reality.

2.2.6 Host PC (Pentium 4)

For control applications, the real time processor was used. But for offline identification and other offline purposes Pentium 4 was used as computational machine. The RAM is 2GB with a clock speed of 1.2 GHz.

2.2.7 Cathode Ray Oscilloscope

Agilent 56020 Cathode Ray Oscilloscopes (CRO) was used. For getting the instant value of the dynamic signals CRO are quite helpful, even in the presence of data acquisition card, since it affects the efficiency of control to get every state back on the host PC.

2.2.8 PZT Patches as Sensors/Actuators

“Piezoelectric (PE)” materials are those materials which when subjected to electric field get deformed and vice-versa. This change in configuration may be used to nullify the effect of vibrations induced by external disturbances. These are made by the combination of three elements i.e. lead, zirconium and titanium. The geometrical and mechanical properties of these materials are discussed earlier.

CHAPTER – 3

MODELING AND ANALYSIS OF BEAMS

For active/passive vibration control applications, low order models of flexible structures are always preferable. Mathematical models of passive constrained layer damping (PCLD)/active constrained layer damping (ACLD) treatment generated by energy based analytical methods (EBAM) are of much smaller orders as compared to finite element methods (FEM). Using these analytical methods, one can get rid of complex model reduction techniques but unfortunately these model reduction techniques are subjected to errors if applied directly to PCLD or ACLD systems. However, analytical techniques cannot be applied blindly to any PCLD system. There is significant error in loss factor prediction for certain boundary conditions. This error is also dependent on the relative thicknesses of viscoelastic material (VEM) layer, constraining layer and base beam. For certain combination of the above thicknesses and under certain boundary conditions, the models generated are useless for controller design purposes. On the other hand, FEM are highly robust and can be applied easily to any set of boundary conditions with guaranteed accuracy. Also, results predicted by this method are of high accuracy for any combinations of thicknesses of different layers. The only disadvantage of this technique is the high order of the developed model. In this chapter detailed performance comparison of both the techniques to predict the modal parameters of the PCLD treated beam is presented.

The work presented in this book is an effort to show that the results given using Energy Based Analytical Methods are not always correct. Only under certain boundary conditions and combination of VEM layer and constraining layer thicknesses, the results obtained by these analytical methods are accurate and can replace FEM techniques.

3.1 DERIVATION OF LAGRANGE'S EQUATION FROM HAMILTON'S PRINCIPLE

According to Hamilton's principle:

$$\delta \int_{t_1}^{t_2} \int_0^L [U - T - W] dx dt = 0 \quad (3.1)$$

Let q represents the generalized coordinate, and then the above equation becomes:

$$\delta \int_{t_1}^{t_2} \int_0^L [U(q) - T(q, \dot{q}) - W] dx dt = 0 \quad (3.2)$$

Let 'F' be the distributed force so that:

$$W = F q$$

$$\delta U = \frac{\partial U}{\partial q} \delta q$$

$$\delta T = \frac{\partial T}{\partial \dot{q}} \delta \dot{q} + \frac{\partial T}{\partial q} \delta q$$

$$\delta W = F \delta q \quad (3.3)$$

Putting the value of eqn. (3.2) into (3.1):

$$\int_{t_1}^{t_2} \int_0^L \left[\frac{\partial U}{\partial q} \delta q - \left(\frac{\partial T}{\partial \dot{q}} \delta \dot{q} + \frac{\partial T}{\partial q} \delta q \right) - F \delta q \right] dx dt = 0 \quad (3.4)$$

Integrating \dot{q} term by parts with respect to time:

$$\begin{aligned} \int_{t_1}^{t_2} \frac{\partial T}{\partial \dot{q}} \delta q dt &= \left[\frac{\partial T}{\partial \dot{q}} \delta q \right] - \int_{t_1}^{t_2} \frac{d}{dt} \frac{\partial T}{\partial \dot{q}} \delta q dt \\ \int_{t_1}^{t_2} \frac{d}{dt} \frac{\partial T}{\partial \dot{q}} \delta q dt & \end{aligned} \quad (3.5)$$

Putting the value of eqn. (3.5) into (3.4):

$$\int_{t_1}^{t_2} \int_0^L \left[\frac{\partial U}{\partial q} + \frac{d}{dt} \left(\frac{\partial T}{\partial \dot{q}} \right) - \frac{\partial T}{\partial q} - F \right] \delta q dx dt = 0$$

This reduces to the Lagrange's equation as under:

$$\left[\frac{\partial U}{\partial q} + \frac{d}{dt} \left(\frac{\partial T}{\partial \dot{q}} \right) - \frac{\partial T}{\partial q} - F \right] = 0 \quad (3.6)$$

3.2 DERIVING STIFFNESS AND MASS MATRICES FOR BEAM ELEMENT

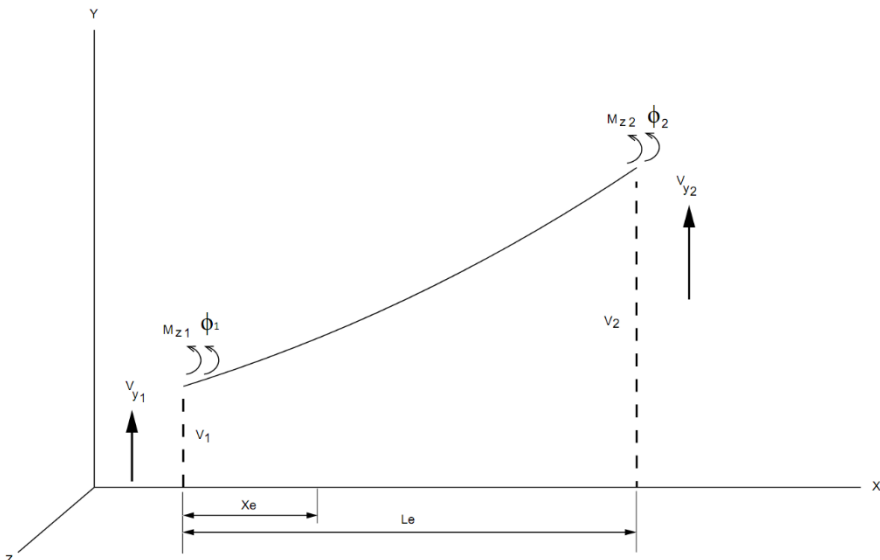


Fig. 3.1: Beam Element

The nodal deflections are v_1 and v_2 . While the nodal slopes are Φ_1 and Φ_2 that are positive in direction y and in anti-clockwise direction.

Defining the shape functions as:

$$\hat{v}(\hat{x}) = a_1 \hat{x}^3 + a_2 \hat{x}^2 + a_3 \hat{x} + a_4 \quad (3.7)$$

With the help of boundary conditions of the element at the two nodes we have:

$$\left. \begin{aligned} \hat{v}(0) &= \hat{v}_1 = a_4 \\ \frac{d \hat{v}(0)}{dx} &= \hat{\theta}_1 = a_3 \\ \hat{v}(L) &= \hat{v}_2 = a_1 L^3 + a_2 L^2 + a_3 L + a_4 \\ \frac{d \hat{v}(L)}{dx} &= \hat{\theta}_2 = 3 a_1 L^2 + 2 a_2 L + a_3 \end{aligned} \right\} \quad (3.8)$$

Solving for the four constants of 'a' and substituting in eqn. (3.7), we get.

$$\hat{v}(x) = \left[\frac{2}{L^3} (\hat{v}_1 - \hat{v}_2) + \frac{1}{L^2} (\hat{\theta}_1 - \hat{\theta}_2) \right] \hat{x}^3 - \left[\frac{3}{L^3} (\hat{v}_1 - \hat{v}_2) + \frac{1}{L} (2 \hat{\theta}_1 + \hat{\theta}_2) \right] \hat{x}^2 + \hat{\theta}_1 \hat{x} + \hat{v}_1 \quad (3.9)$$

$$\hat{v}(x) = [N] \{ \hat{d} \} \quad (3.10)$$

Where

$$\left. \begin{aligned} [N] &= [N_1 \ N_2 \ N_3 \ N_4] \\ N_1 &= \frac{1}{L^3} (2 \hat{x}^3 - 3 \hat{x}^2 L + L^3) \\ N_2 &= \frac{1}{L^3} (\hat{x}^3 L - 2 \hat{x}^2 L^2 + \hat{x} L^3) \\ N_3 &= \frac{1}{L^3} (-2 \hat{x}^3 + 3 \hat{x}^2 L) \\ N_4 &= \frac{1}{L^3} (\hat{x}^3 L - \hat{x}^2 L^2) \end{aligned} \right\} \quad (3.11)$$

Bending moment displacement relation yields that:

$$\hat{M}(x) = EI_{zz} \cdot \frac{d^2 \hat{v}}{d \hat{x}^2} \quad (3.12)$$

Using eqn. (3.11)

$$\hat{M}(x) = EI_{zz} [B] \{ \hat{d} \} \quad (3.13)$$

Where

$$[B] = \left[\frac{\partial^2 N_1}{\partial \hat{x}^2} \ \frac{\partial^2 N_2}{\partial \hat{x}^2} \ \frac{\partial^2 N_3}{\partial \hat{x}^2} \ \frac{\partial^2 N_4}{\partial \hat{x}^2} \right] \quad (3.14)$$

The values of $N_1 \ N_2 \ N_3 \ N_4$ can be taken from eqn. 3.11

$$\frac{\partial^2 N_1}{\partial x^2} = \frac{1}{L^3} (12\hat{x} - 6L)$$

$$\frac{\partial^2 N_2}{\partial \hat{x}^2} = \frac{1}{L^3} (6\hat{x}L - 4L^2)$$

$$\frac{\partial^2 N_3}{\partial \hat{x}^2} = \frac{1}{L^3} (-12\hat{x} + 6L)$$

$$\frac{\partial^2 N_4}{\partial \hat{x}^2} = \frac{1}{L^3} (6\hat{x}L - 2L^2)$$

and

$$\{d\} = \begin{bmatrix} \hat{v}_1 \\ \hat{\theta}_1 \\ \hat{v}_2 \\ \hat{\theta}_2 \end{bmatrix} \quad (3.15)$$

The strain energy of the element will be:

$$V = \frac{1}{2} EI_{zz} \int_0^L \left(\frac{d^2 v}{dx^2} \right) dx$$

$$V = \frac{1}{2} EI_{zz} \{d\}^T \int_0^L [\hat{B}]^T [\hat{B}] \{d\} dx \quad (3.16)$$

From Lagrange equation, considering the potential energy term only:

$$\frac{\partial V}{\partial \{d\}} = \frac{1}{2} EI_{zz} \int_0^L [\hat{B}]^T [\hat{B}] \{d\} dx \quad (3.17)$$

The above equation can be written as:

$$[\hat{K}] \{d\} = F \quad (3.18)$$

$$[\hat{K}] = EI_{zz} \int_0^L \begin{bmatrix} \frac{\partial^2 N_1}{\partial x^2} \\ \frac{\partial^2 N_2}{\partial x^2} \\ \frac{\partial^2 N_3}{\partial x^2} \\ \frac{\partial^2 N_4}{\partial x^2} \end{bmatrix} \begin{bmatrix} \frac{\partial^2 N_1}{\partial x^2} & \frac{\partial^2 N_2}{\partial x^2} & \frac{\partial^2 N_3}{\partial x^2} & \frac{\partial^2 N_4}{\partial x^2} \end{bmatrix} dx \quad (3.19)$$

After substitution the elemental stiffness matrix becomes:

$$[\hat{K}]_e = \frac{EI_{zz}}{L^3} \begin{bmatrix} 12 & 6L & -12 & 6L \\ 6L & 4L^2 & -6L & 2L^2 \\ -12 & -6L & 12 & -6L \\ 6 & 2L^2 & -6L & 4L^2 \end{bmatrix} \quad (3.20)$$

Now, we have to derive the elemental mass matrix

The kinetic energy of the beam element is:

$$T = \frac{1}{2} \rho A \int_0^L \hat{v}^2 dx \quad (3.21)$$

Considering equation (3.6)

$$\left[\frac{\partial V}{\partial q} + \frac{d}{dt} \left(\frac{\partial T}{\partial \dot{q}} \right) - \frac{\partial T}{\partial q} \right] = F$$

Considering the K.E term alone

$$\frac{d}{dt} \left(\frac{\partial T}{\partial \{\dot{V}\}} \right) = \{F\} \quad (3.22)$$

Writing

$$\dot{V} = [N]\{\dot{d}\}$$

$$T = \frac{1}{2} \rho A \{\dot{d}\}^T \int_0^L [N]^T [N] \{\dot{d}\} dx \quad (3.23)$$

$$\frac{d}{dt} \left(\frac{\partial T}{\partial \{\dot{V}\}} \right) = \rho A \int_0^L [N]^T [N] \{\ddot{d}\} dx \quad (3.24)$$

$$\rho A \int_0^L [N]^T [N] \{\ddot{d}\} dx = \{F\} \quad (3.25)$$

$$M\{\ddot{d}\} = F$$

Where

$$M = \rho A \int_0^L [N]^T [N] dx \quad (3.26)$$

Therefore the elemental mass matrix becomes:

$$[\bar{M}]_e = \frac{1}{420} \rho A L \begin{bmatrix} 156 & 22L & 54 & -13L \\ 22L & 4L^2 & 13L & -3L^2 \\ 54 & 13L & 156 & -22L^2 \\ -13L & -3L^2 & -22L & 4L^2 \end{bmatrix} \quad (3.27)$$

From eq. (3.18) and (3.25)

$$M\{\ddot{d}\} + K\{d\} = \{F\} \quad (3.28)$$

3.3 DERIVING STIFFNESS AND MASS MATRICES FOR ROD ELEMENT

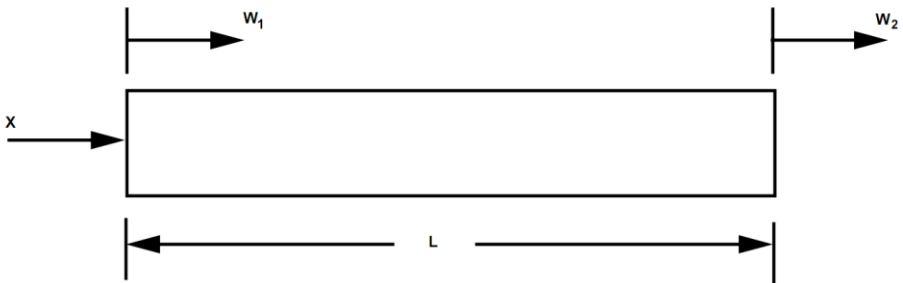


Fig. 3.2: Rod Element

A one dimensional rod element of length L is shown in the Figure 3.2. The element has 2-degrees of freedom denoted by w_1 , the displacement of the left end of the element and w_2 the displacement of the right end of the element. We define x as the local coordinate x, $0 \leq x \leq L$ along the axis of the element.

The simplest displacement function for the element can be written as:

$$u(x, t) = w_1 + \frac{1}{L} (w_2 - w_1) x \quad (3.29)$$

The kinetic energy of the element, assuming uniform properties is given by:

$$T = \frac{1}{2} \int_0^L \rho A \left(\frac{\partial u}{\partial t} \right)^2 dx \quad (3.30)$$

$$= \frac{1}{2} \int_0^L \rho A \left[\frac{1}{L} (\dot{w}_2 - \dot{w}_1)x + \dot{w}_1 \right]^2 dx \quad (3.31)$$

This becomes

$$= \frac{1}{2} \frac{\rho A L}{3} (\dot{w}_1^2 + \dot{w}_1 \dot{w}_2 + \dot{w}_2^2) \quad (3.32)$$

This can be written in quadratic form as:

$$T = \frac{1}{2} \frac{\rho A L}{6} [\dot{w}_1 \ \dot{w}_2] \begin{bmatrix} 2 & 1 \\ 1 & 2 \end{bmatrix} \begin{bmatrix} \dot{w}_1 \\ \dot{w}_2 \end{bmatrix} \quad (3.33)$$

Thus the element mass matrix is given by:

$$[M]_e = \frac{\rho A L}{6} \begin{bmatrix} 2 & 1 \\ 1 & 2 \end{bmatrix} \quad (3.34)$$

The potential energy of the element, assuming uniform properties is given by:

$$T = \frac{1}{2} \int_0^L EA \left(\frac{\partial u}{\partial x} \right)^2 dx \quad (3.35)$$

$$= \frac{1}{2} \int_0^L EA \left[\frac{1}{L} (w_2 - w_1) \right]^2 dx \\ = \frac{1}{2} \frac{EA}{L} (w_2^2 - 2 w_1 w_2 + w_1^2) \quad (3.36)$$

The potential energy can be written in quadratic form as:

$$V = \frac{1}{2} \frac{EA}{L} [w_1 \ w_2] \begin{bmatrix} 1 & -1 \\ -1 & 1 \end{bmatrix} \begin{bmatrix} w_1 \\ w_2 \end{bmatrix} \quad (3.37)$$

From which the element stiffness matrix is determined as:

$$[K]_e = \frac{EA}{L} \begin{bmatrix} 1 & -1 \\ -1 & 1 \end{bmatrix} \quad (3.38)$$

3.4 PCLD SYSTEM DESCRIPTION AND MODELING

The complete system description and modeling is described in the following sub-sections:

3.4.1 Basic Relationships

The schematic of the base beam with PCLD treatment is shown in Figure 3.3 (a). The upper part of host structure or the base beam is attached with a VEM layer. VEM layer in turn is constrained by a passive material layer. This layer is termed as constraining layer.

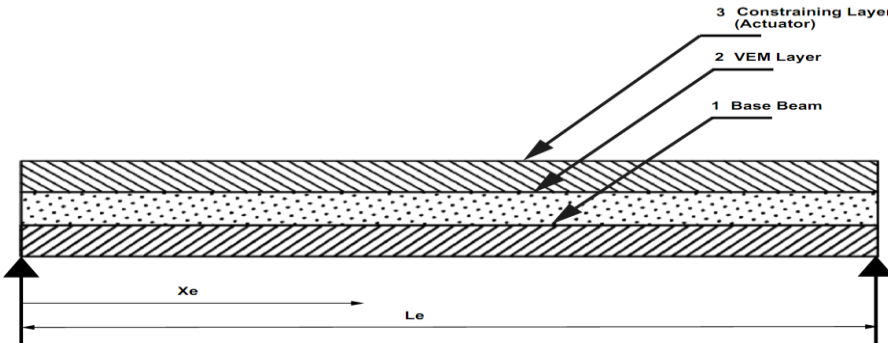


Fig. 3.3 (a): Schematics of the structure with PCLD Treatment

For simplicity, the constrained layer is numbered as 1, VEM layer as no. 2 and the base beam as no. 3. Figure 3.3(b) shows the cross-section of the beam with PCLD treatment

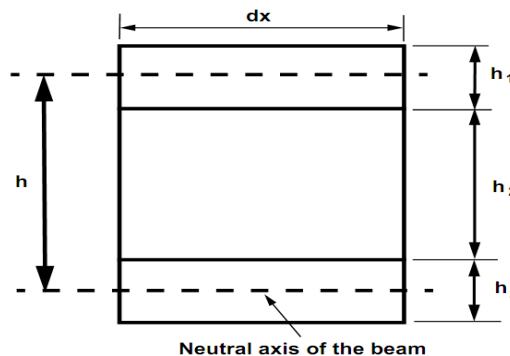


Fig. 3.3 (b): Undeformed geometry of the beam with PCLD treatment

The base beam and constraining layer can be modeled as Euler-Bernoulli beams. For the continuity of displacements at the interface between the layers, the relation between shear angle (strain) and various displacements is as:

$$\left. \begin{aligned} \varepsilon_1 &= \frac{\partial u_1}{\partial x} = \frac{\partial u_{1m}}{\partial x} - z_1 \frac{\partial^2 w}{\partial x^2} \\ \varepsilon_2 &= \frac{\partial u_2}{\partial x} = \frac{\partial u_{2m}}{\partial x} - z_2 \frac{\partial^2 w}{\partial x^2} \\ \varepsilon_3 &= \frac{\partial u_3}{\partial x} = \frac{\partial u_{3m}}{\partial x} - z_3 \frac{\partial^2 w}{\partial x^2} \end{aligned} \right\} \quad (3.39)\{a, b, c\}$$

$$\gamma_2 = \frac{u_{1m} - u_{3m}}{h_2} + \frac{h}{h_2} \theta \quad (3.40)$$

$$\text{Where } h = h_2 + \frac{(h_1+h_3)}{2}$$

and θ denotes the slope. u and w denote the longitudinal and transverse displacements respectively. u_m represents the corresponding displacements at neutral axis of the beam. h_1 , h_2 and h_3 denote the thickness of constraining layer, VEM layer and base beam respectively. ε 's are corresponding strains. The shear stress developed in VEM layers is denoted by τ_2 . The shear strain of the VEM layers is represented by γ_2 . u_1 , u_2 and u_3 are the longitudinal displacement of the constraining layer, VEM layers and the base beam respectively and w is the transverse displacement of all the layers. The shear stress in VEM layer is given as:

$$\tau_2 = G_2 \gamma_2 \quad (3.41)$$

3.4.2 Finite Element Modeling

FEM technique is implemented for modeling the beam with PCLD treatment and is discussed below:

3.4.2.1 The Shape Functions

Figure 3.2 shows a treated beam element. Nodal displacements are given as:

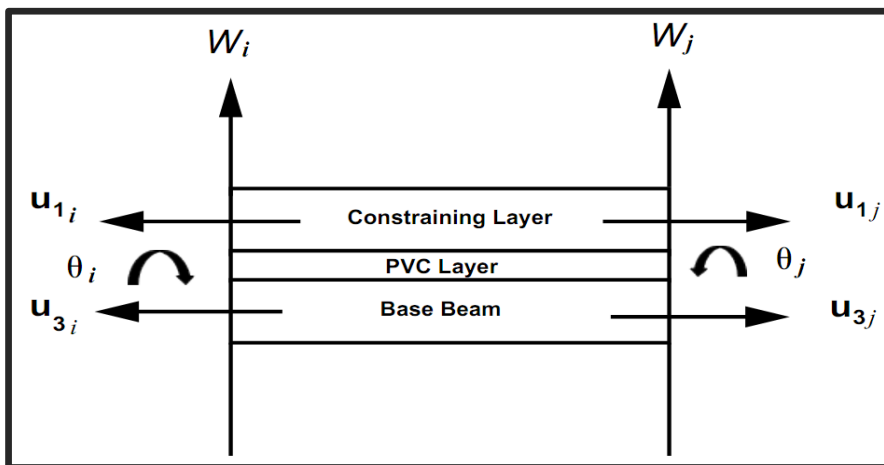


Fig. 3.4: Nodal displacement of a treated beam element

$$\{U\}_e = \{ w_i \ \theta_i \ u_{bi} \ u_{ci} \ w_j \ \theta_j \ u_{bj} \ u_{cj} \}^T \quad (3.42)$$

The transverse displacement w , the rotation θ and the axial displacements of the respective layers are expressed in terms of nodal displacements by finite element shape functions as:

$$w = [N_w] \{U\}_e, \theta = [N_\theta] \{U\}_e, u_1 = [N_{u1}] \{U\}_e, u_2 = [N_{u2}] \{U\}_e, u_3 = [N_{u3}] \{U\}_e \\ \gamma_2 = [N_{\gamma_2}] \{U\}_e \quad (3.43) \{a, b, c, d, e, f\}$$

Where the shape functions are given as:

$$[N_w] = \begin{bmatrix} 1 - 3\left(\frac{x}{L_e}\right)^2 + 2\left(\frac{x}{L_e}\right)^3 \\ x - 2\left(\frac{x^2}{L_e}\right) + \left(\frac{x^3}{L_e^2}\right) \\ 0 \\ 0 \\ 3\left(\frac{x}{L_e}\right)^2 - 2\left(\frac{x}{L_e}\right)^3 \\ -\left(\frac{x^2}{L_e}\right) + \left(\frac{x^3}{L_e^2}\right) \\ 0 \\ 0 \end{bmatrix}^T, \quad [N_\theta] = \begin{bmatrix} -6\left(\frac{x}{L_e^2}\right) + 6\left(\frac{x^2}{L_e^3}\right) \\ 1 - 4\left(\frac{x}{L_e}\right) + 3\left(\frac{x}{L_e}\right)^2 \\ 0 \\ 0 \\ 6\left(\frac{x}{L_e^2}\right) - 6\left(\frac{x^2}{L_e^3}\right) \\ -2\left(\frac{x}{L_e}\right) + 3\left(\frac{x}{L_e}\right)^2 \\ 0 \\ 0 \end{bmatrix}$$

$$[N_{u3}] = \begin{bmatrix} 0 & 0 & 1 - \frac{x}{L_e} & 0 & 0 & 0 & \frac{x}{L_e} & 0 \end{bmatrix}$$

$$[N_{u1}] = \begin{bmatrix} 0 & 0 & 0 & 1 - \frac{x}{L_e} & 0 & 0 & 0 & \frac{x}{L_e} \end{bmatrix}$$

$$[N_{u2}] = [N_{u3}] - \left(\frac{h_1 + h_3}{2}\right) [N_\theta]$$

$$[N_{\gamma 2}] = \left[\frac{1}{h_2} ([N_{u1}] - [N_{u3}]) + \frac{h}{h_2} [N_\theta] \right]$$

Where L_e represents the elemental length of the system and x is displacement (axial or transverse).

3.4.2.2 Energies of the Beam with PCLD Treatment

For simplicity, all the energies are given for a single element. The total energy can be obtained by the combination of all the elements. Kinetic energy (T_e) and strain energy (V_e) are discussed below:

3.4.2.2.1 Kinetic energies

The total kinetic energy (T_e) of the complete system comprises the kinetic energies of the constraining layer (T_1+T_2), base beam (T_3+T_4) and VEM layers (T_5+T_6) i.e. $T_e = T_1 + T_2 + T_3 + T_4 + T_5 + T_6$. For each individual part it is given below:

3.4.2.2.1.1 Passive constraining layer

The kinetic energy of the passive constraining layer due to axial displacement for a single element is:

$$T_1 = \frac{1}{2} \rho_1 h_1 b \int_0^{L_e} \left(\frac{\partial u_1}{\partial t} \right)^2 dx = \frac{1}{2} \{ \dot{U} \}_e^T [M_{1u}]_e \{ \dot{U} \}_e \quad (3.44)$$

Where

$$[M_{1u}]_e = \rho_1 h_1 b \int_0^{L_e} [N_{u1}]^T [N_{u1}] dx$$

The kinetic energy of the passive constraining layer due to transverse displacement is:

$$T_2 = \frac{1}{2} \rho_1 h_1 b \int_0^{L_e} \left(\frac{\partial w}{\partial t} \right)^2 dx = \frac{1}{2} \{ \dot{U} \}_e^T [M_{1w}]_e \{ \dot{U} \}_e \quad (3.45)$$

Where

$$[M_{1w}]_e = \rho_1 h_1 b \int_0^{L_e} [N_w]^T [N_w] dx$$

3.4.2.2.1.2 Base beam

The kinetic energy of the base beam due to axial displacement is:

$$\mathbf{T}_3 = \frac{1}{2} \rho_3 h_3 b \int_0^{L_e} \left(\frac{\partial u_3}{\partial t} \right)^2 dx = \frac{1}{2} \{ \dot{U} \}_e^T [M_{3u}]_e \{ \dot{U} \}_e \quad (3.46)$$

Where

$$[M_{3u}]_e = \rho_3 h_3 b \int_0^{L_e} [N_{u3}]^T [N_{u3}] dx$$

The kinetic energy of the base beam due to transverse displacement is:

$$\mathbf{T}_4 = \frac{1}{2} \rho_3 h_3 b \int_0^{L_e} \left(\frac{\partial w}{\partial t} \right)^2 dx = \frac{1}{2} \{ \dot{U} \}_e^T [M_{3w}]_e \{ \dot{U} \}_e \quad (3.47)$$

Where

$$[M_{3w}]_e = \rho_3 h_3 b \int_0^{L_e} [N_w]^T [N_w] dx$$

3.4.2.2.1.3 VEM layer

The kinetic energy of the VEM layer due to axial displacement is:

$$\mathbf{T}_5 = \frac{1}{2} \rho_2(h_2) b \int_0^{L_e} \left(\frac{\partial u_2}{\partial t} \right)^2 dx = \frac{1}{2} \{ \dot{U} \}_e^T [M_{2u}]_e \{ \dot{U} \}_e \quad (3.48)$$

Where

$$[M_{2u}]_e = \rho_2(h_2) b \int_0^{L_e} [N_{u2}]^T [N_{u2}] dx$$

The kinetic energy of the VEM layer due to transverse displacement is:

$$\mathbf{T}_6 = \frac{1}{2} \rho_2(h_2) b \int_0^{L_e} \left(\frac{\partial w}{\partial t} \right)^2 dx = \frac{1}{2} \{ \dot{U} \}_e^T [M_{2w}]_e \{ \dot{U} \}_e \quad (3.49)$$

Where

$$[M_{2w}]_e = \rho_2(h_2) b \int_0^{L_e} [N_w]^T [N_w] dx$$

Where ρ is the density, h is the beam thickness and b is the width of the layer.

3.4.2.2.2 Potential energies

The total potential energy V_e of the complete system comprises the strain energies of constraining layer ($\mathbf{V}_1, \mathbf{V}_2$), VEM layer ($\mathbf{V}_3-\mathbf{V}_5$) and base beam ($\mathbf{V}_6, \mathbf{V}_7$) and i.e

$\mathbf{V}_e = \mathbf{V}_1 + \mathbf{V}_2 + \mathbf{V}_3 + \mathbf{V}_4 + \mathbf{V}_5 + \mathbf{V}_6 + \mathbf{V}_7$. For each individual part it is given below:

3.4.2.2.2.1 Passive constraining layer

The potential energy of the passive constraining layer due to axial displacement is:

$$\mathbf{V}_1 = \frac{1}{2} E_1 h_1 b \int_0^{L_e} \left(\frac{\partial u_1}{\partial x} \right)^2 dx = \frac{1}{2} \{ U \}_e^T [K_{1u}] \{ U \}_e \quad (3.50)$$

Where

$$[K_{1u}] = E_1 h_1 b \int_0^{L_e} \left[\frac{\partial N_{u1}}{\partial x} \right]^T \left[\frac{\partial N_{u1}}{\partial x} \right] dx$$

The potential energy of the passive constraining layer due to transverse displacement is:

$$\mathbf{V}_2 = \frac{1}{2} E_1 I_1 \int_0^{L_e} \left(\frac{\partial^2 w}{\partial x^2} \right)^2 dx = \frac{1}{2} \{ U \}_e^T [K_{1w}] \{ U \}_e \quad (3.51)$$

Where

$$[K_{1w}] = E_1 I_1 \int_0^{L_e} \left[\frac{\partial^2 N_w}{\partial x^2} \right]^T \left[\frac{\partial^2 N_w}{\partial x^2} \right] dx$$

3.4.2.2.2.2 VEM layer

The potential energy of the VEM layer due to axial displacement is:

$$V_3 = \frac{1}{2} E_2 (h_2) b \int_0^{L_e} \frac{\partial u_2}{\partial x} dx = \frac{1}{2} \{U\}_e^T [K_{2u}] \{U\}_e \quad (3.52)$$

Where

$$[K_{2u}] = E_2 (h_2) b \int_0^{L_e} \left[\frac{\partial N_{u2}}{\partial x} \right]^T \left[\frac{\partial N_{u2}}{\partial x} \right] dx$$

The potential energy of the PVC layers due to transverse displacement is:

$$V_4 = \frac{1}{2} E_2 I_2 \int_0^{L_e} \left(\frac{\partial^2 w}{\partial x^2} \right)^2 dx = \frac{1}{2} \{U\}_e^T [K_{2w}] \{U\}_e \quad (3.53)$$

where

$$[K_{2w}] = E_2 I_2 \int_0^{L_e} \left[\frac{\partial^2 N_w}{\partial x^2} \right]^T \left[\frac{\partial^2 N_w}{\partial x^2} \right] dx$$

The potential energy of the VEM layer due to shearing:

$$V_5 = \frac{1}{2} G_2 (h_2) b \int_0^{L_e} \gamma_2^2 dx = \frac{1}{2} \{U\}_e^T [K_{2\gamma}] \{U\}_e \quad (3.54)$$

Where

$$[K_{2\gamma}] = G_2 (h_2) b \int_0^{L_e} [N_{\gamma 2}]^T [N_{\gamma 2}] dx$$

3.4.2.2.2.3 Base beam

The potential energy of the base beam due to axial displacement is:

$$V_6 = \frac{1}{2} E_3 h_3 b \int_0^{L_e} \left(\frac{\partial u_3}{\partial x} \right)^2 dx = \frac{1}{2} \{U\}_e^T [K_{3u}] \{U\}_e \quad (3.55)$$

Where

$$[K_{3u}] = E_3 h_3 b \int_0^{L_e} \left[\frac{\partial N_{u3}}{\partial x} \right]^T \left[\frac{\partial N_{u3}}{\partial x} \right] dx$$

The potential energy of the base beam due to transverse displacement is:

$$V_7 = \frac{1}{2} E_3 I_3 \int_0^{L_e} \left(\frac{\partial^2 w}{\partial x^2} \right)^2 dx = \frac{1}{2} \{U\}_e^T [K_{3w}] \{U\}_e \quad (3.56)$$

Where

$$[K_{3w}] = E_3 h_3 b \int_0^{L_e} \left[\frac{\partial^2 N_w}{\partial x^2} \right]^T \left[\frac{\partial^2 N_w}{\partial x^2} \right] dx$$

3.4.2.3 Pure Beam Elements

The stiffness and mass matrices of pure beam elements have dimensions of 6x6, and are similar to those given by eq. (3.45).

3.4.2.4 Equations of Motion

Using Hamilton's principle, the equations of motion for a PCLD element can be written as:

$$\int_{t_1}^{t_2} \delta (T_e - V_e) dt + \int_{t_1}^{t_2} \delta (w_e) dt = 0 \quad (3.57)$$

After using Hamilton's Principle, the equations of motion at the element level without any external work done can be written as:

$$[M]_e \{\ddot{U}\}_e + \left[[K]_e + [K_{2\gamma}]_e \right] \{U\}_e = \{0\}_e \quad (3.58)\{a\}$$

$$[M]_e = ([M_{3u}]_e + [M_{3w}]_e) + ([M_{1u}]_e + [M_{1w}]_e) + ([M_{2u}]_e + [M_{2w}]_e) \quad (3.58)\{b\}$$

$$[K]_e = ([K_{3u}]_e + [K_{3w}]_e) + ([K_{1u}]_e + [K_{1w}]_e) + ([K_{2u}]_e + [K_{2w}]_e) \quad (3.58)\{c\}$$

It can also be written as:

$$[M]_e \{\ddot{U}\}_e + [K]_e \{U\}_e = \{0\}_e \quad (3.58)\{d\}$$

Where

$$[M]_e = [M]_e$$

$$[K]_e = [[K]_e + [K_{2\gamma}]_e]$$

For a beam with distributed elements, through standard FEM assembling procedure with appropriate boundary conditions, the following global dynamic equation can be derived as:

$$[M]\{\ddot{U}\} + [K]\{U\} = \{0\} \quad (3.58)\{e\}$$

The above equation without subscript 'e' denotes the global form of corresponding elemental co-efficient matrices. The eigen value problem associated with eq. (3.58) {e} is

$$\{[M]\omega^{*2} + [K]\}\{U\} = \{0\} \quad (3.59)$$

The eigen frequencies will be complex since there is a complex shear modulus in VEM layer. After the complex eigen frequencies have been found, the modal frequencies and the loss factors of the system can be calculated as follows:

$$\omega = \sqrt{Re(\omega^*)^2}$$

$$\eta = \frac{Im[(\omega^*)^2]}{Re[(\omega^*)^2]} \quad (3.60) \{a, b\}$$

3.4.3 Analytical Modeling

The analytical modeling of the system is described in the following sub-sections:

3.4.3.1 Assumed Mode Method

The analytical treatment used here is based on assumed mode method. Assumed modes, which are in generalized coordinates, are used for expanding the unknown

parameters in the equations 3.50 to 3.56. There are basically three unknown variables i.e. w , u_1 and u_3 . From the kinematics as shown in eq. (3.40), γ_2 can be represented as:

$$\gamma_2 = \frac{u_1 - u_3}{h_2} + \frac{h}{h_2} \left(\frac{\partial w}{\partial x} \right) \quad (3.61)$$

The transverse and longitudinal displacement variables are expanded as:

$$\left. \begin{aligned} w(x, t) &= \sum_{i=1}^{n_w} w_i(x) \eta_i(t) = w^T \eta \\ u_1(x, t) &= \sum_{i=1}^{n_{\eta_1}} v_{1i}(x) \zeta_{1i}(t) = v_1^T \xi_1 \\ u_3(x, t) &= \sum_{i=1}^{n_{\eta_3}} v_{3i}(x) \zeta_{3i}(t) = v_3^T \xi_3 \end{aligned} \right\} \quad (3.62)\{a, b, c\}$$

Where w are the assumed mode shapes of the beam in transverse direction. u_1 and u_3 are longitudinal mode shapes of the base beam and constraining layer respectively. η , ξ_1 and ξ_3 are modal displacements of the corresponding layers.

3.4.3.2 Energies of the PCLD System

For simplicity, all the energies are given for a single element. The total energy can be obtained by the combination of all the elements. Kinetic energy (T_e) and strain energy (V_e) are discussed as below:

3.4.3.2.1 Kinetic energies

The total kinetic energy T_e of the complete system comprises the kinetic energies of the constraining layer, base beam and VEM layers. Only the energy due to vertical displacement is counted. The total kinetic energy is given as:

$$T = \frac{1}{2} (\rho_1 h_1 + \rho_2 h_2 + \rho_3 h_3) b \int_0^L \left(\frac{\partial w}{\partial t} \right)^2 dx = \frac{1}{2} \{ \dot{\eta} \}^T [M] \{ \dot{\eta} \} \quad (3.63)\{a, b\}$$

Where

$$[M] = (\rho_1 h_1 + \rho_2 h_2 + \rho_3 h_3) b \int_0^L [w]^T [w] dx$$

3.4.3.2.2 Potential energies

The total potential energy (V_e) of the complete system comprises the strain energies of constraining layer, base beam and VEM. For each individual part it is given as below:

3.4.3.2.2.1 Passive constraining layer

$$V_1 = \frac{1}{2} \{ \xi_1 \}^T [K_1^{-1}] \{ \xi_1 \} + \frac{1}{2} \{ \eta \}^T [K_2^{-1}] \{ \eta \} \quad (3.64)$$

Where

$$[K_1^{-1}] = E_1 h_1 b \int_0^L \left[\frac{\partial v_1}{\partial x} \right] \left[\frac{\partial v_1}{\partial x} \right]^T dx$$

and

$$[K_2^{-1}] = E_1 I_1 \int_0^L \left[\frac{\partial^2 w}{\partial x^2} \right] \left[\frac{\partial^2 w}{\partial x^2} \right]^T dx$$

3.4.3.2.2.2 VEM layers

$$\begin{aligned} \mathbf{V}_2 = & \frac{1}{2} \{\xi_1\}^T [\mathbf{K}_1^2] \{\xi_1\} - \{\xi_1\}^T [\mathbf{K}_2^2] \{\xi_3\} + \frac{1}{2} \{\xi_2\}^T [\mathbf{K}_3^2] \{\xi_2\} + \{\xi_1\}^T [\mathbf{K}_4^2] \{\eta\} \\ & - \{\xi_2\}^T [\mathbf{K}_5^2] \{\eta\} + \frac{1}{2} \{\eta\}^T [\mathbf{K}_6^2] \{\eta\} \end{aligned} \quad (3.65)$$

Where $[\mathbf{K}_1^2] = C \int_0^L \mathbf{v}_1 \mathbf{v}_1^T dx$

$$C = \frac{G_2 b}{h_2}$$

$$[\mathbf{K}_2^2] = C \int_0^L \mathbf{v}_1 \mathbf{v}_3^T dx$$

$$[\mathbf{K}_3^2] = C \int_0^L \mathbf{v}_3 \mathbf{v}_3^T dx$$

$$[\mathbf{K}_4^2] = hC \int_0^L \mathbf{v}_1 \left[\frac{\partial w}{\partial x} \right]^T dx$$

$$[\mathbf{K}_5^2] = hC \int_0^L \mathbf{v}_3 \left[\frac{\partial w}{\partial x} \right]^T dx$$

$$[\mathbf{K}_6^2] = h^2 C \int_0^L \left[\frac{\partial w}{\partial x} \right] \left[\frac{\partial w}{\partial x} \right]^T dx$$

3.4.3.2.2.3 Base beam

$$\mathbf{V}_3 = \frac{1}{2} \{\xi_3\}^T [\mathbf{K}_1^3] \{\xi_3\} + \frac{1}{2} \{\eta\}^T [\mathbf{K}_2^3] \{\eta\} \quad (3.66)$$

Where

$$[\mathbf{K}_1^3] = E_3 h_3 b \int_0^L \left[\frac{\partial v_3}{\partial x} \right] \left[\frac{\partial v_3}{\partial x} \right]^T dx$$

and

$$[\mathbf{K}_2^3] = E_3 I_3 \int_0^L \left[\frac{\partial^2 w}{\partial x^2} \right] \left[\frac{\partial^2 w}{\partial x^2} \right]^T dx$$

3.4.3.3 Selection of Admissible Functions

The transverse and longitudinal mode shape functions of the base beam and the constraining layer can be chosen from any standard textbook giving due consideration to the boundary conditions. The longitudinal mode shapes of the constraining layer depend upon various other factors. For example, for a simply supported base beam with full length treatment, the longitudinal mode shape of the constraining layer is chosen as of free-free beam. For other boundary conditions this will not be the case. However, for partial treatment, the longitudinal mode shape of the constraining layer is always chosen as of free-free beam.

3.4.3.4 Lagrange's Equations of Motion

The Lagrange's equation of motion is used to derive the equations of motion. It is given as:

$$\frac{\partial}{\partial t} \left(\frac{\partial L}{\partial \dot{q}_i} \right) - \left(\frac{\partial L}{\partial q_i} \right) = 0 \quad (3.67)$$

Where $L = T - V$ – (Work done), q_i is the respective generalized co-ordinate. L represents Lagrangian. In expanded form in the absence of external work is written as:

$$\mathbf{L} = \mathbf{T} - (\mathbf{V}_1 + \mathbf{V}_2 + \mathbf{V}_3) \quad (3.68)$$

Applying Lagrange equation and taking the partial derivatives of the equations of kinetic and potential energies w.r.t. respective generalized co-ordinates, we get the following equations:

$$\begin{bmatrix} M & 0 & 0 \\ 0 & 0 & 0 \\ 0 & 0 & 0 \end{bmatrix} \begin{Bmatrix} \ddot{\eta} \\ \ddot{\xi}_3 \\ \ddot{\xi}_1 \end{Bmatrix} + \begin{bmatrix} K_2^3 + K_2^1 + K_6^2 & -K_5^2 & K_4^2 \\ -K_5^2 & K_1^3 + K_3^2 & -K_2^2 \\ K_4^2 & -K_2^2 & K_1^1 + K_1^2 \end{bmatrix} \begin{Bmatrix} \eta \\ \xi_3 \\ \xi_1 \end{Bmatrix} = \begin{Bmatrix} 0 \\ 0 \\ 0 \end{Bmatrix} \quad (3.69)$$

The eigenvalue problem associated with this is given as:

$$([\mathbf{K}] - \omega^2 [\mathbf{M}]) \begin{Bmatrix} \eta \\ \xi_3 \\ \xi_1 \end{Bmatrix} = \begin{Bmatrix} 0 \\ 0 \\ 0 \end{Bmatrix} \quad (3.70)$$

The eigen frequencies will be complex since there is a complex shear modulus in VEM layer. After the complex eigen frequencies have been found, the modal frequencies and the loss factors of the system can be calculated using equation (3.60 and 3.69) by doing simulation with the help of a MATLAB tool box called SIMULINK.

3.5 RESULTS AND DISCUSSION

3.5.1 Results for Different Boundary Conditions and Different Thicknesses of VEM and Constraining Layers

Based on the above discussion, it is obvious that different boundary conditions and different thicknesses of constraining layer and VEM layer produce different results. The geometrical parameters for the beam with different boundary conditions assumed are presented in Table 3.1.

Table 3.1: Geometrical parameters for beams under different boundary conditions

Parameter	Symbol	Boundary Conditions			
		Simply Supported	Free-Free	Fixed-Fixed	Cantilever
Length (mm)	L	300	177.7	177.7	177.7
Width (mm)	B	30	12.7	12.7	12.7

Based on the above boundary conditions, following four cases are thoroughly investigated:

3.5.1.1 Simply Supported Beams

First, the results are obtained for a simply supported beam of length 300 mm. The width and thickness of the base beam is 30 mm and 1.5 mm respectively. The thickness of the constraining layer is varied from 0.4 mm to 1.8 mm in steps of 0.2 mm. The thickness of the VEM layer is varied from 0.1 mm to 1.5 mm in steps with values as 0.1 mm, 0.2 mm, 0.6 mm, 0.8 mm, 1 mm, 1.2 mm and 1.5 mm. Percentage error by taking FEM based results as the basic results is shown for the first four modes. Error in prediction of loss factors is less than 0.5 percent for all the modes except the first mode. For first mode there is large variation in results. The error is maximum when minimum thickness of VEM layer is used. As thickness of the VEM layer increases the error decreases. Similarly, the percentage error decreases as the constraining layer

thickness increases. The error is less than 0.8 % when thickness of the VEM and constraining layer is equal to the base beam i.e. 1.5 mm. Figure 3.6 shows the closer view of Figure 3.5 for the first mode. Figure 3.7 shows the percentage error in the prediction of natural frequencies using EBAM. The error is less than 1% for all the frequencies.

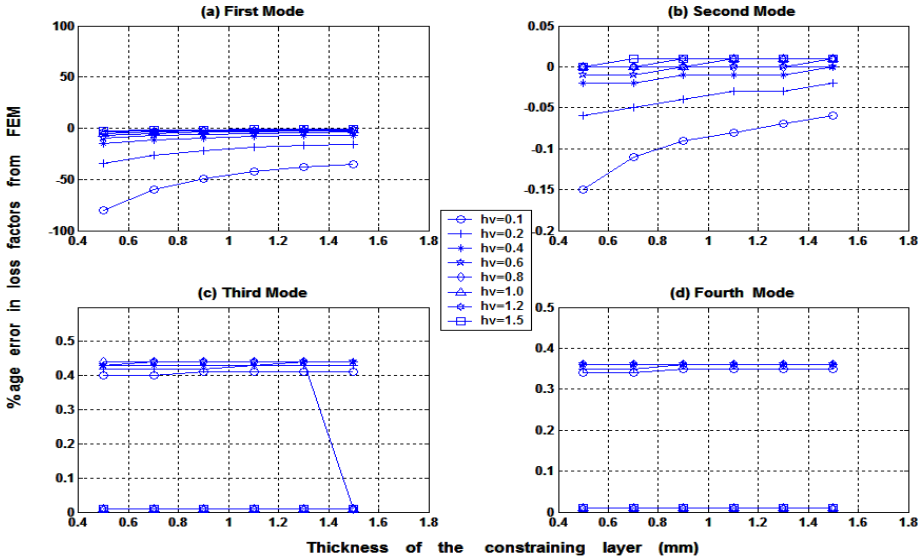


Fig. 3.5: Percentage errors in loss factors (taking FEM as base) as a function of constraining layer thickness at various thicknesses of VEM layer for simply supported beam

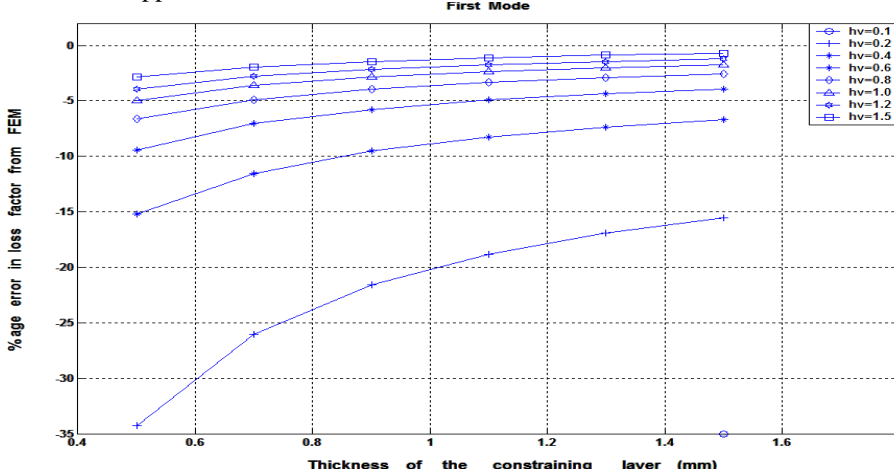


Fig. 3.6: Closer view of percentage error in loss factor of first mode (taking FEM as base) as a function of constraining layer thickness at various thicknesses of VEM layer for simply supported beam.

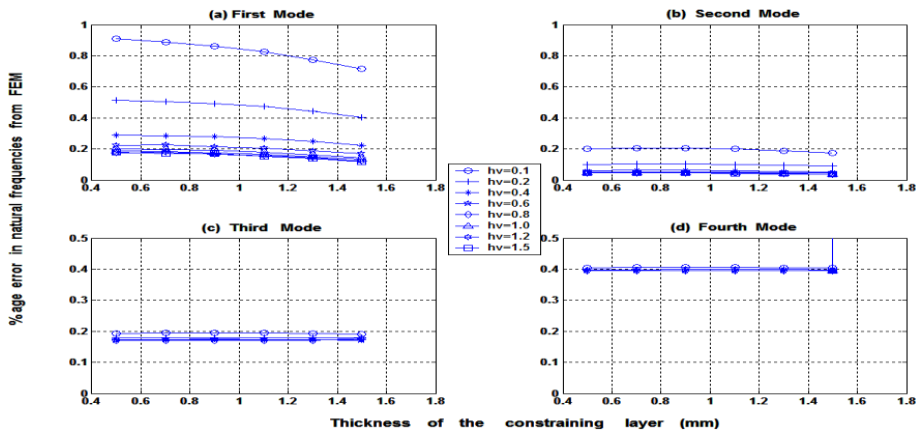


Fig. 3.7: Percentage errors in natural frequencies (taking FEM as base) as a function of constraining layer thickness at various thicknesses of VEM layer for simply supported beam

3.5.1.2 Free-Free Beams

The constraining layer thickness is also varied in steps with values as 0.1 mm, 0.3 mm, 0.7 mm, 0.9 mm and 1.52 mm for the beam with free-free boundary conditions. The VEM layer thickness is varied as in steps with values as 0.127 mm, 0.5 mm, 1 mm and 1.52 mm. The error in prediction of loss factors is maximum when the thickness of the VEM layer is least (i.e. 0.127 mm) as shown in Figure 3.8.

Also the error is smallest when constraining layer thickness is largest. Figure 3.9 shows the closer view. The error is smallest when the thickness of the VEM layer is maximum i.e. 1.52 mm (i.e. equal to the base beam thickness of 1.5 mm). The same is true for the constraining layer. The best results with minimum error are obtained if the thickness of the constraining layer is equal to the thickness of the base beam. Figure 3.10 shows the error in prediction of natural frequencies. For all the modes, error is less than 0.5 % which is perfectly acceptable.

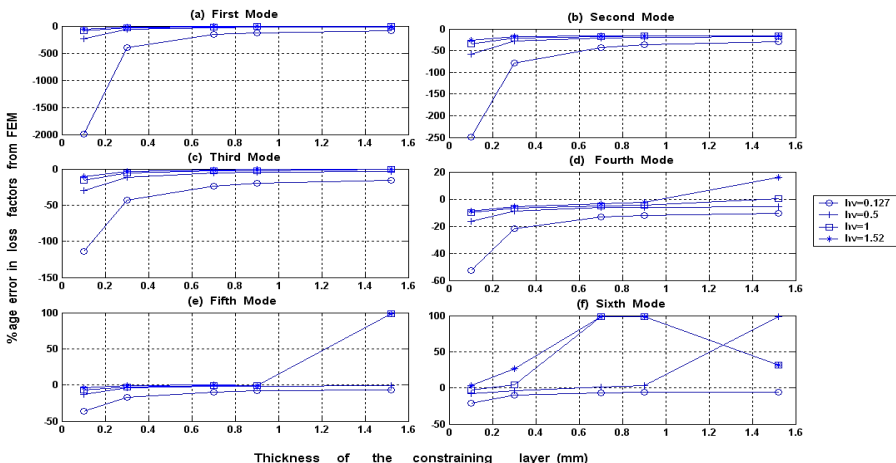


Fig. 3.8: Percentage errors in loss factors (taking FEM as base) as a function of constraining layer thickness at various thicknesses of VEM layer for a free-free beam

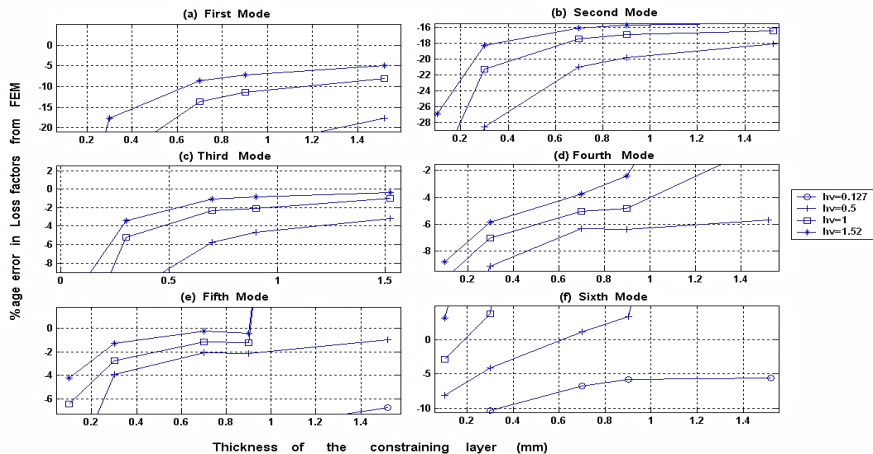


Fig. 3.9: Closer view of percentage errors in loss factors (taking FEM as base) as a function of constraining layer thickness at various thicknesses of VEM layer for free-free beam

3.5.1.3 Fixed-Fixed Beams

The constraining layer thickness is varied in steps with values as 0.1 mm, 0.3 mm, 0.7 mm, 0.9 mm and 1.52 mm. The VEM layer thickness is varied in steps with thickness as 0.127 mm, 0.5 mm, 1 mm and 1.52 mm. Figure 3.11 shows the error in prediction of loss factors for the first five modes. Figure 3.12 shows the close-up view. The error is maximum as shown in Figure 3.11 when the thickness of the VEM layer is smallest (i.e. 0.127 mm). Also the error is smallest when constraining layer thickness is largest. For VEM layer and constraining layer thickness of 1.52 mm (i.e. nearly equal to the base beam thickness) the error is less than 2 % for all the modes. Figure 3.13 shows the error in natural frequencies. The error is less than 0.8 % for all the first five modes which is perfectly acceptable.

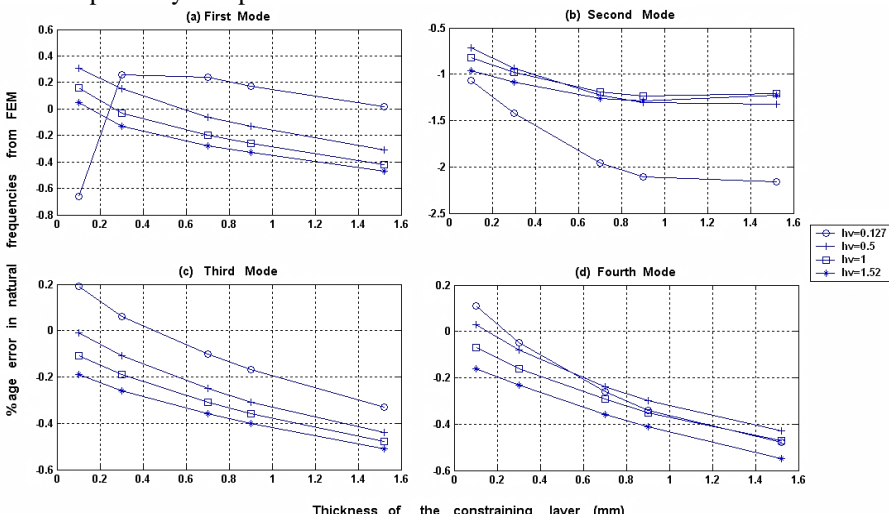


Fig. 3.10: Percentage errors in natural frequencies (taking FEM as base) as a function of constraining layer thickness at various thicknesses of VEM layer for free-free beam.

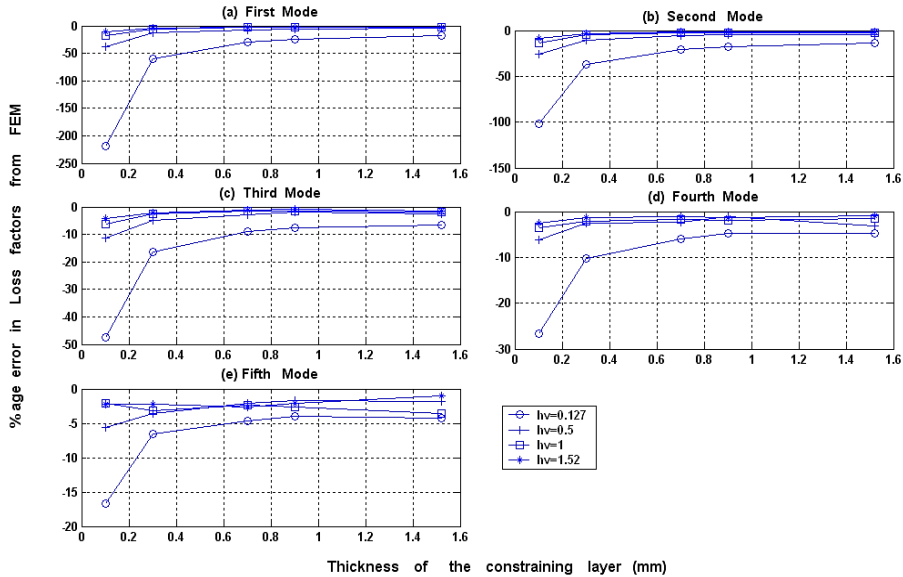


Fig. 3.11: Percentage errors in loss factors (taking FEM as base) as a function of constraining layer thickness at various thicknesses of VEM layer for fixed-fixed beam

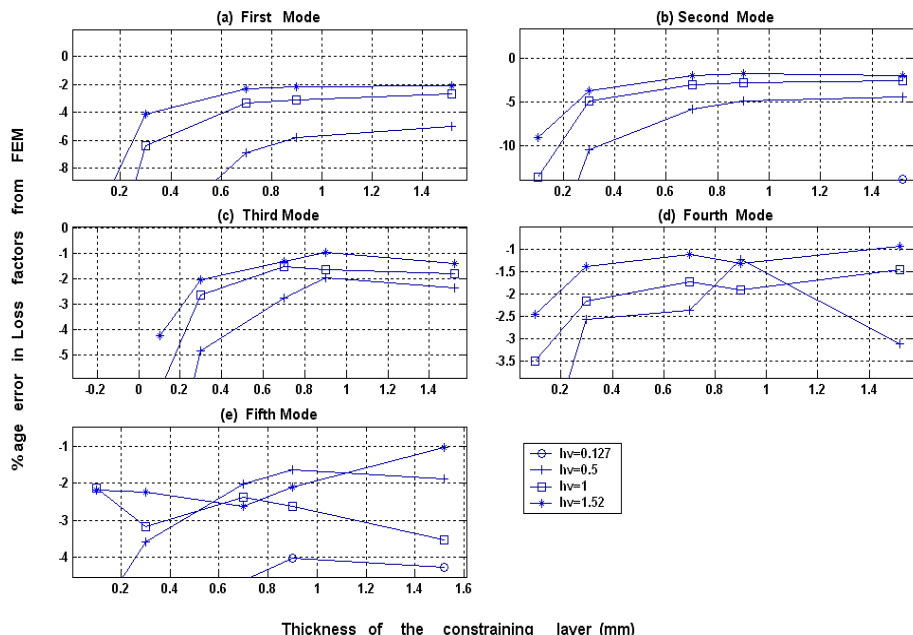


Fig. 3.12: Closer view of percentage errors in loss factors (taking FEM as base) as a function of constraining layer thickness at various thicknesses of VEM layer for fixed-fixed beam.

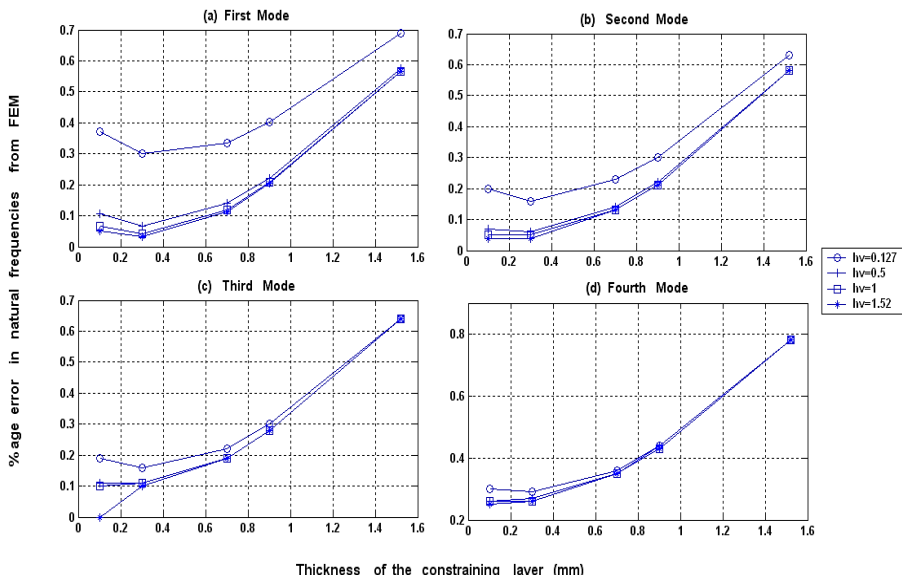


Fig. 3.13: Percentage errors in natural frequencies (taking FEM as base) as a function of constraining layer thickness at various thicknesses of VEM layer for fixed-fixed beam.

3.5.1.4 Cantilever Beams

The error in loss factors prediction by EBAM had been frustrating for this set of boundary conditions. So, the models generated by EBAM are useless for this set of boundary conditions. The VEM layer thickness is varied as in steps with thickness as 0.127 mm, 0.25 mm, 0.5 mm, 1 mm and 1.52 mm. Other parameters are same as for free-free and fixed-fixed beams. Figure 3.14 shows the percentage errors in loss factors. The error is highest when the thickness of the VEM layer is smallest (i.e. 0.127 mm). Also the error is smallest when constraining layer thickness is largest i.e. 1.52 mm. (i.e. equal to the base beam thickness of 1.5 mm). Figure 3.15 shows the closer views of percentage errors in loss factors. The errors are highest for the first two modes (i.e. near 20%). As the mode number increases the percentage error decreases. With the VEM layer thickness equal to constraining layer thickness i.e. 1.52 mm comparatively better results are obtained. Except for the first two modes, percentage error is less than 4%. There is no error in the code developed as the percentage error in natural frequencies is very less (i.e. 0.6%) for first to fourth mode. Loss factor and natural frequencies are related to each other. If there is an error in the developed code, the natural frequencies calculated would have also been wrong. However, the difference in natural frequencies calculated by EBAM and FEM is very small (Figure 3.16).

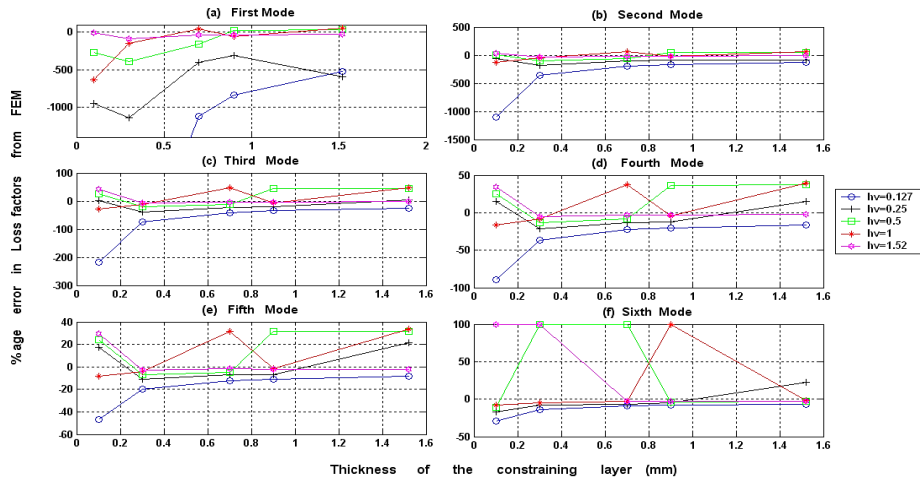


Fig. 3.14: Percentage errors in loss factors (taking FEM as base) as a function of constraining layer thickness at various thicknesses of VEM layer for cantilever beam

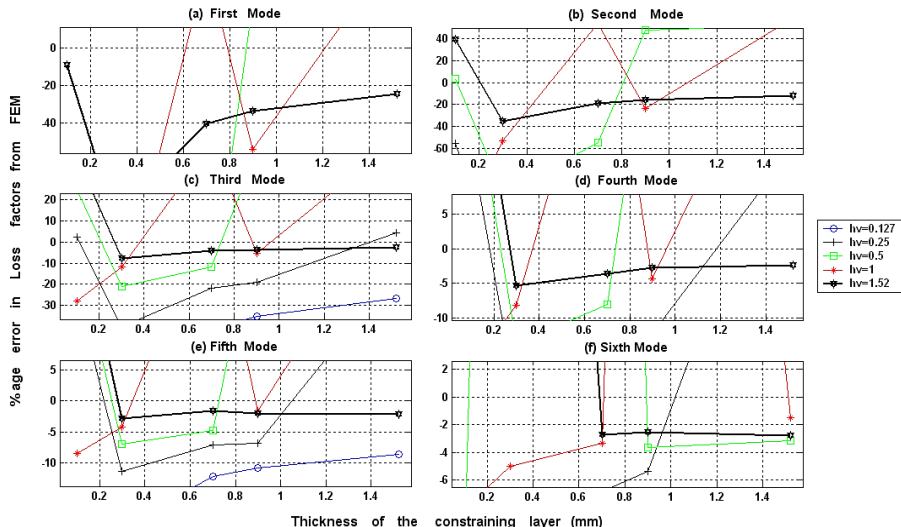


Fig. 3.15: Closer views of percentage errors in loss factors (taking FEM as base) as a function of constraining layer thickness at various thicknesses of VEM layer for cantilever beam

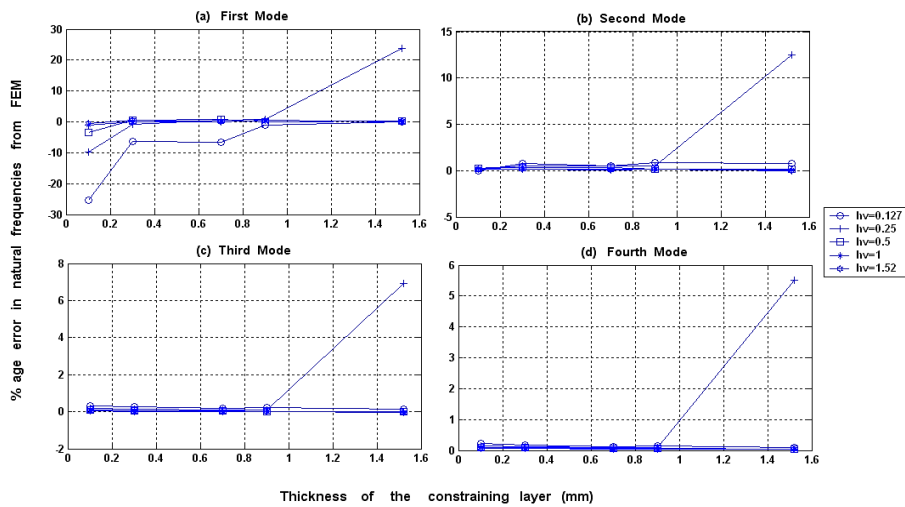


Fig. 3.16: Percentage errors in natural frequencies (taking FEM as base) as a function of constraining layer thickness at various thicknesses of VEM layer for cantilever beam

CHAPTER – 4

VIBRATION CONTROL WITH ACTIVE AND PASSIVE TECHNIQUES

The widely used smart materials for vibration control in structures are piezoelectric materials since they have desirable characteristics. Based on these characteristics, piezoelectric materials are being used as sensors and actuators. Apart from active control techniques, passive damping techniques are robust, effective and reliable. Passive constrained layer damping (PCLD) is an old technique to suppress vibrations. In combination with active control techniques, PCLD treatment can be made even more effective. This technique is called active constrained layer damping (ACLD) treatment. Present work is based on the development of newer passive techniques, which can be used in combination with active techniques to enhance the damping performance of the overall system.

By attaching initially stressed poly vinyl chloride (PVC) layers on the flexible structures, necessary passive damping can be provided. Using passive constrained layers on these PVC layers, the efficiency can be made even better than ordinary PCLD treatment. By using stressed PVC layers, a rich performance in case of circuit failure conditions is always available. An active constraining layer further enhances the damping performance of this passive technique. In this unit, pre-compressed layer damping treatment augmented with ACLD treatment has been suggested, which has many desirable features as compared to existing pre-tensed layer damping treatment. Such enhancement in damping performance is not possible by conventional ACLD as well as PCLD techniques. The effect of initial strain (compressive or tensile) and other parameters of the PVC layers on the vibration characteristics of flexible structure have been investigated. Hamilton Principle in conjunction with finite element method is used to derive the differential equations of motion. Using proportional feedback controllers, the complex closed loop eigen value problem is developed and solved numerically. The effectiveness of the proposed technique has been validated experimentally using digital Linear Quadratic Gaussian controller. Present work investigates the vibration behavior and control of simply supported flexible beam with partially covered ACLD treatment augmented with stressed PVC layers instead of VEM layers. The stress-strain relationship for the PVC layer is described by complex modulus. Instead of applying pre-tensed PVC layers, pre-compressed PVC layers are provided (glued) on the base beam forming pre-compressed layer damping (CoLD) treatment. The damping ratios of all the modes increase uniformly with stress in proposed CoLD treatment, removing the first limitation of the PTLD treatment. For the purpose of uniformity this treatment is termed as Tensed Layer Damping (TeLD) treatment. The second limitation is removed by combining the ordinary CoLD treatment with conventional PCLD and ACLD treatment. The first mode damping

ratio slightly decreased with the application of constraining layers on the PVC layers but the damping ratios of all other modes improved dramatically.

There are a large number of techniques for modeling of piezoelectric-structure coupling like FEM, Boundary Element Methods and analytical methods etc. Due to the compatibility of FEM for partial treatment, it has been chosen for the present work. Hamilton principle in conjunction with Finite Element Method (FEM) is used to derive the equations of motion. Proportional feedback controller is designed for piezosensor and piezoactuator system. The closed loop (CL) equation of motion for the system is derived and complex eigenvalue problem is solved numerically. The effect of thickness of PVC layers, loss factor of PVC layers and initial compressive or tensile strain in PVC layers have been investigated. The effect of each parameter on the damping ratios and damped natural frequencies is also studied.

The main contribution of the present work is divided into following parts:

- a) *Finite Element Method is employed in the present work, so that partial treatment can be accommodated easily for Stressed Layer Damping (SLD) techniques; this is not easily possible by analytical methods.*
- b) *Effect of initial strain in PVC layers attached to base beam is investigated with combination of PCLD and ACLD treatment which is never considered earlier in literature.*
- c) *The pre-tensing of base beam which causes compressive stresses in PVC layers (equivalent to applying pre-compressed PVC layers) is primarily analyzed for the first time. This has certain desirable features w.r.t. the pre-tensed PVC layer technique as discussed in the earlier paragraph.*

It is confirmed by the present study that partially treated beam using TeLD technique has certain undesirable properties which can be eliminated by using CoLD technique. To validate the theoretical results, experimental analysis was performed. A digital Linear Quadratic Gaussian (LQG) controller has been used in the experimental study. The study will also be useful for rotating structures like rotorcraft blades, helicopter wings and robotic systems with certain modifications.

4.1 SYSTEM DESCRIPTION AND FINITE ELEMENT MODELING

4.1.1 Basic Relationships

The schematic of the simply supported beam with ACLD treatment combined with SLD treatment is shown in Figure 4.1.

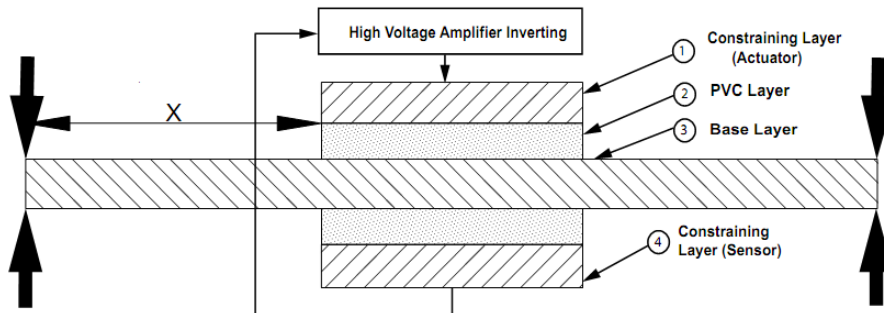


Fig. 4.1: Schematics of structure with ACLD using SLD treatment

The upper and lower surface of host structure or the base beam is attached with PVC Layer. Each of the PVC layer in turn is constrained by an active piezoelectric material PZT (Lead Zirconated Titrate). It acts as a constraining layer, a sensor and an actuator. For simplicity, the constrained layer (i.e. PZT patch on one side) is numbered as 1, PVC layer as no. 2, the base beam as no. 3 and sensor layer (i.e. PZT patch on the opposite side of the base beam) as no. 4. Figure 4.2 shows the cross-section of the beam with ACLD treatment with stressed PVC layers. For a Timoshenko beam theory rotation angle is not the derivative of deflection, hence relations become slightly complicated. Thus, the base beam and constraining layer has been modeled as **Euler-Bernoulli beams** without much variation in results for metallic beams.

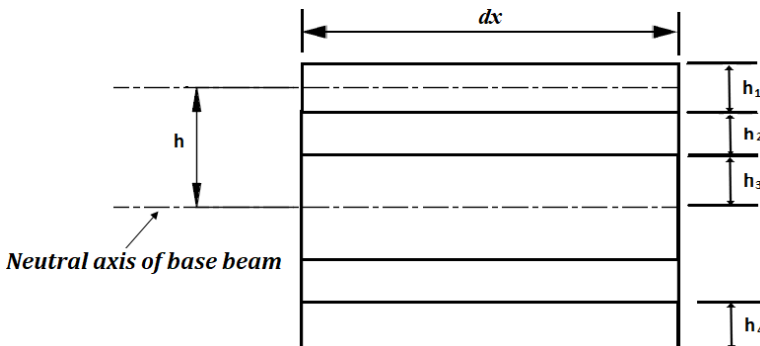


Fig. 4.2 (a): Cross-section of undeformed beam

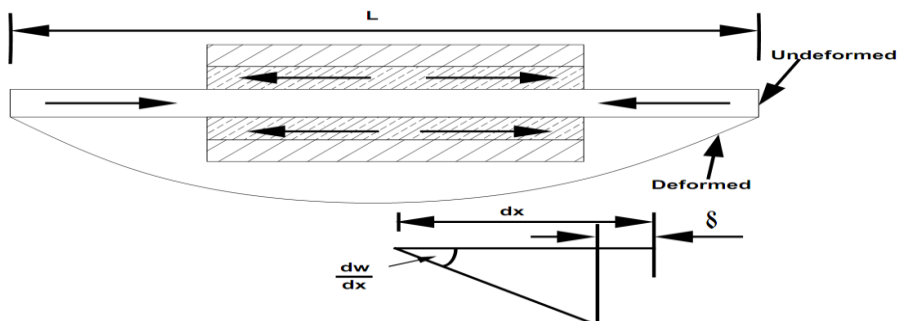


Fig. 4.2 (b): Beam with ACLD treatment augmented with SLD treatment

For the continuity of displacements at the interface between the layers, the relation between shear angle (strain) and various displacements is as given by:

$$\left. \begin{aligned} \varepsilon_1 &= \frac{\partial u_1}{\partial x} = \frac{\partial u_{1m}}{\partial x} - z_1 \frac{\partial^2 w}{\partial x^2} \\ \varepsilon_2 &= \frac{\partial u_2}{\partial x} = \frac{\partial u_{2m}}{\partial x} - z_2 \frac{\partial^2 w}{\partial x^2} \\ \varepsilon_3 &= \frac{\partial u_3}{\partial x} = \frac{\partial u_{3m}}{\partial x} - z_3 \frac{\partial^2 w}{\partial x^2} \\ \varepsilon_4 &= \frac{\partial u_4}{\partial x} = \frac{\partial u_{4m}}{\partial x} - z_4 \frac{\partial^2 w}{\partial x^2} \end{aligned} \right\} \quad (4.1) \{a, b, c, d\}$$

Figure 4.3 shows the constrained layer damping treated beam.

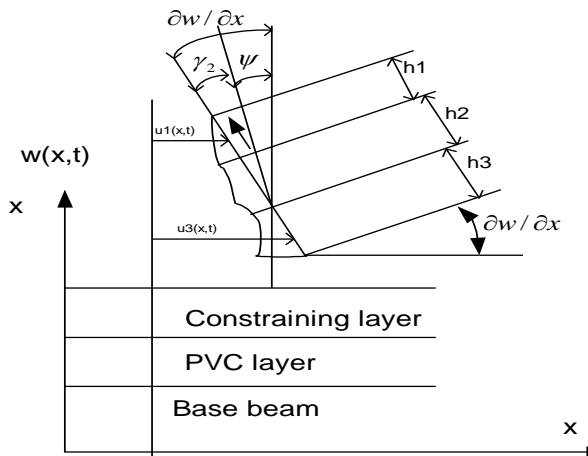


Fig. 4.3 (a): Deformation of the beam with constrained layer damping

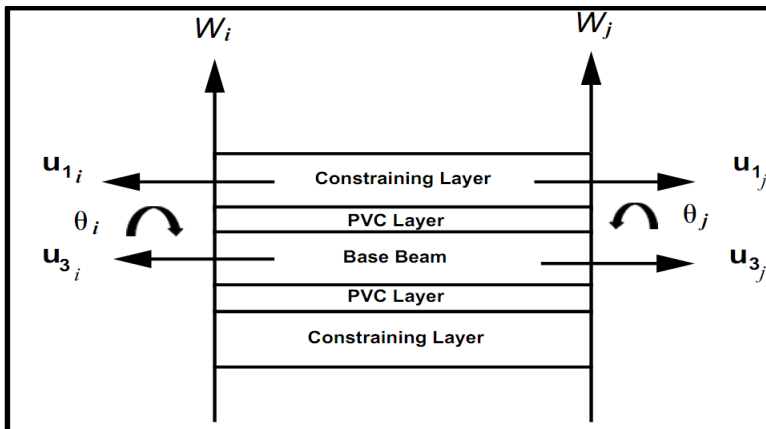


Fig. 4.3 (b): Degrees of freedom of an element

As shown in Figure 4.3(a) the shear strain in the viscoelastic material (i.e. PVC here) is given as:

$$\gamma_2 = \left(\frac{\partial w}{\partial x} \right) - \psi \quad 4.1(e)$$

where ψ is the shear angle of the PVC or VEM layer. The axial displacement of PVC layer is given in terms of axial displacement of the base beam, rotation and shear strain in PVC material as:

$$u_2 = u_3 - \frac{h_3}{2} \frac{\partial w}{\partial x} - \frac{h_2}{2} \psi \quad 4.1(f)$$

Hence shear strain in the PVC material is given as:

$$\gamma_2 = \frac{u_1 - u_3}{h_2} + \frac{h}{h_2} \frac{\partial w}{\partial x} \quad 4.2$$

$$h = h_2 + \frac{(h_1 + h_3)}{2}$$

and θ denotes the slope. u and w denote the longitudinal and transverse displacements respectively. u_m represent the corresponding displacements from neutral axis of the beam and z represents the distance from the neutral axis of the corresponding layers. h_1, h_2, h_3 and h_4 denote the thickness of constraining layer, PVC layer, base beam and sensor layer respectively. ε 's are the corresponding strains. The shear stress developed in PVC layers is denoted by τ_2 . The shear strain of the PVC layers is represented by γ_2 . u_1, u_2, u_3 and u_4 are the longitudinal displacements of the constraining layer, PVC layers, the base beam and sensor layer respectively and w is the transverse displacement of all the layers. The shear stress in PVC layers is given as:

$$\tau_2 = G_2 \gamma_2 \quad (4.3)$$

The PVC layers are initially stressed (tensile or compressive) to a magnitude of β_2 to cause stress of corresponding sign in the base beam.

4.1.2 The Shape Functions

Figure 4.3 shows a treated beam element. Nodal displacements are given as:

$$\{U\}_e = \{w_i \ \theta_i \ u_{3i} \ u_{1i} \ w_j \ \theta_j \ u_{3j} \ u_{1j}\}^T \quad (4.4)$$

The transverse displacement w , the rotation θ and the axial displacements of the respective layers are expressed in terms of nodal displacements by finite element shape functions as:

$$\begin{aligned} w &= [N_w] \{U\}_e, \theta = [N_\theta] \{U\}_e, u_1 = [N_{u1}] \{U\}_e, u_2 = [N_{u2}] \{U\}_e, u_3 = [N_{u3}] \{U\}_e \\ u_4 &= [N_{u4}] \{U\}_e \quad \gamma_2 = [N_{\gamma2}] \{U\}_e \end{aligned} \quad (4.5)\{a, b, c, d, e, f, g\}$$

Using these shape functions, the newly constructed shape functions are as:

$$[N_w] = \begin{bmatrix} 1 - 3\left(\frac{x}{L_e}\right)^2 + 2\left(\frac{x}{L_e}\right)^3 \\ x - 2\left(\frac{x^2}{L_e}\right) + \left(\frac{x^3}{L_e^2}\right) \\ 0 \\ 0 \\ 3\left(\frac{x}{L_e}\right)^2 - 2\left(\frac{x}{L_e}\right)^3 \\ -\left(\frac{x^2}{L_e}\right) + \left(\frac{x^3}{L_e^2}\right) \\ 0 \\ 0 \end{bmatrix}, \quad [N_\theta] = \begin{bmatrix} -6\left(\frac{x}{L_e^2}\right) + 6\left(\frac{x^2}{L_e^3}\right) \\ 1 - 4\left(\frac{x}{L_e}\right) + 3\left(\frac{x}{L_e}\right)^2 \\ 0 \\ 0 \\ 6\left(\frac{x}{L_e^2}\right) - 6\left(\frac{x^2}{L_e^3}\right) \\ -2\left(\frac{x}{L_e}\right) + 3\left(\frac{x}{L_e}\right)^2 \\ 0 \\ 0 \end{bmatrix}$$

$$[N_{u3}] = \begin{bmatrix} 0 & 0 & 1 - \frac{x}{L_e} & 0 & 0 & 0 & \frac{x}{L_e} & 0 \end{bmatrix}$$

$$[N_{u1}] = \begin{bmatrix} 0 & 0 & 0 & 1 - \frac{x}{L_e} & 0 & 0 & 0 & \frac{x}{L_e} \end{bmatrix}$$

$$[N_{u2}] = [N_{u3}] - \left(\frac{h_1 + h_3}{2}\right) [N_\theta]$$

$$[N_{\gamma2}] = \left[\frac{1}{h_2} ([N_{u1}] - [N_{u3}]) + \frac{h}{h_2} [N_\theta] \right]$$

4.1.3 Energies of the ACLD Treatment augmented with SLD Treatment

For simplicity, all the energies are given for a single element. The total energy can be obtained by the combination of all the elements. Kinetic energy (T_e), strain energy (V_e) and as well as the work done (W_e) by external transverse load, piezoelectric forces and moments are discussed as below:

4.1.3.1 Kinetic Energies

The total kinetic energy (T_e) of the complete system comprises the kinetic energies of the constraining layer (T_1+T_2), base beam (T_3+T_4) and PVC layers (T_5+T_6) and sensor layer ($T_7 + T_8$) i.e. $T_e = T_1+T_2+T_3+T_4+T_5+T_6+T_7+T_8$. For each individual part it is given below:

4.1.3.1.1 Active constraining layer

The kinetic energy of the active constraining layer due to axial displacement for a single element is:

$$T_1 = \frac{1}{2} \rho_1 h_1 b \int_0^{L_e} \left(\frac{\partial u_1}{\partial t} \right)^2 dx \quad (4.6)$$

The kinetic energy of the active constraining layer due to transverse displacement is:

$$T_2 = \frac{1}{2} \rho_1 h_1 b \int_0^{L_e} \left(\frac{\partial w}{\partial t} \right)^2 dx \quad (4.7)$$

4.1.3.1.2 Base beam

The kinetic energy of the base beam due to axial displacement is:

$$T_3 = \frac{1}{2} \rho_3 h_3 b \int_0^{L_e} \left(\frac{\partial u_3}{\partial t} \right)^2 dx \quad (4.8)$$

The kinetic energy of the base beam due to transverse displacement is:

$$T_4 = \frac{1}{2} \rho_3 h_3 b \int_0^{L_e} \left(\frac{\partial w}{\partial t} \right)^2 dx \quad (4.9)$$

4.1.3.1.3 PVC layers

The kinetic energy of the PVC layers due to axial displacement is:

$$T_5 = \frac{1}{2} \rho_2 (2h_2) b \int_0^{L_e} \left(\frac{\partial u_2}{\partial t} \right)^2 dx \quad (4.10)$$

The kinetic energy of the PVC layers due to transverse displacement is:

$$T_6 = \frac{1}{2} \rho_2 (2h_2) b \int_0^{L_e} \left(\frac{\partial w}{\partial t} \right)^2 dx \quad (4.11)$$

4.1.3.1.4 Passive constraining layer (Sensor Layer)

The kinetic energy of the sensor layer due to axial displacement is:

$$T_7 = \frac{1}{2} \rho_4 h_4 b \int_0^{L_e} \left(\frac{\partial u_4}{\partial t} \right)^2 dx \quad (4.12)$$

The kinetic energy of the sensor layer due to transverse displacement is:

$$T_8 = \frac{1}{2} \rho_4 h_4 b \int_0^{L_e} \left(\frac{\partial w}{\partial t} \right)^2 dx \quad (4.13)$$

where ρ is the density, h is the beam thickness and b is the width of the layer.

4.1.3.2 Potential Energies

The total potential energy V_e of the complete system comprises the strain energies of constraining layer (V_1+V_2), PVC layer ($V_3+V_4+V_5$) and base beam (V_6+V_7), Sensor layer (V_8+V_9) and effect of initial stress in PVC layer (V_{10}) i.e. $V_e = (V_1+V_2+V_3+V_4+V_5+V_6+V_7+V_8+V_9+V_{10})$. For each individual part it is given below:

4.1.3.2.1 Active constraining layer

The potential energy of the active constraining layer due to axial displacement is:

$$V_1 = \frac{1}{2} E_1 h_1 b \int_0^{L_e} \left(\frac{\partial u_1}{\partial x} \right)^2 dx \quad (4.14)$$

The potential energy of the active constraining layer due to transverse displacement is:

$$V_2 = \frac{1}{2} E_1 I_1 \int_0^{L_e} \left(\frac{\partial^2 w}{\partial x^2} \right)^2 dx \quad (4.15)$$

4.1.3.2.2 PVC layers

The potential energy of the PVC layers due to axial displacement is:

$$V_3 = \frac{1}{2} E_2 (2h_2) b \int_0^{L_e} \left(\frac{\partial u_2}{\partial x} \right)^2 dx \quad (4.16)$$

The potential energy of the PVC layers due to transverse displacement is:

$$V_4 = \frac{1}{2} E_2 (2I_2) \int_0^{L_e} \left(\frac{\partial^2 w}{\partial x^2} \right)^2 dx \quad (4.17)$$

The potential energy of the PVC layers due to shearing:

$$V_5 = \frac{1}{2} G_2 (2h_2) b \int_0^{L_e} \gamma_2^2 dx \quad (4.18)$$

It is worth mentioning that in some of the above equations the h_2 and I_2 are multiplied by 2 to consider the contribution of both the PVC layers attached to both the sides of the base beam.

4.1.3.2.3 Base beam

The potential energy of the base beam due to axial displacement is:

$$V_6 = \frac{1}{2} E_3 h_3 b \int_0^{L_e} \left(\frac{\partial u_3}{\partial x} \right)^2 dx \quad (4.19)$$

The potential energy of the base beam due to transverse displacement is:

$$V_7 = \frac{1}{2} E_3 I_3 \int_0^{L_e} \left(\frac{\partial^2 w}{\partial x^2} \right)^2 dx \quad (4.20)$$

4.1.3.2.4 Passive constraining layer (Sensor Layer)

The potential energy of the sensor layer due to axial displacement is:

$$V_8 = \frac{1}{2} E_4 h_4 b \int_0^{L_e} \left(\frac{\partial u_4}{\partial x} \right)^2 dx \quad (4.21)$$

The potential energy of the sensor layer due to transverse displacement is:

$$V_9 = \frac{1}{2} E_4 I_4 \int_0^{L_e} \left(\frac{\partial^2 w}{\partial x^2} \right)^2 dx \quad (4.22)$$

4.1.3.2.5 Effect of initial stress in PVC layer

Let Q be the axial compressive force and Δ be the inward movement of the beam element of length dx (Figure 4.2 (b)). Then δ , due to its slope $\frac{\partial y}{\partial x}$ is:

$$\delta = \left\{ 1 - \cos \left(\frac{\partial y}{\partial x} \right) \right\} dx \cong \frac{1}{2} \left(\frac{\partial y}{\partial x} \right)^2 dx \quad (4.23)\{a\}$$

Hence, the potential energy due to initial stresses (i.e. compressive or tensile) is given by:

$$V_{10} = \pm \frac{1}{2} \int_0^{L_e} Q \left(\frac{\partial y}{\partial x} \right)^2 dx \quad (4.23)\{b\}$$

Where $Q = \beta_2 b (2h_2)$

In eq. 4.23 (b), the positive sign is for tensile stress and negative sign for compressive stress in the base beam. This corresponds to CoLD and TeLD treatment respectively.

4.1.4 Work Done

For one dimensional structure with uni-axial loading, the constitutive equations of PZT material can be written as:

$$[\boldsymbol{\varepsilon}_D] = \begin{bmatrix} S^E_{11} & d_{31} \\ d_{31} & \varepsilon^T_{33} \end{bmatrix} [\boldsymbol{\sigma}_E] \quad (4.24, 4.25)$$

where \boldsymbol{D} is the electrical displacement, \boldsymbol{E} is the electric field, $\boldsymbol{\varepsilon}$ is the mechanical strain in x direction and $\boldsymbol{\sigma}$ is the mechanical stress in x direction. S^E_{11} is the elastic compliance constant, ε^T_{33} is the dielectric constant, and d_{31} is the piezoelectric constant. Forces exerted on the system are:

- a) The externally applied mechanical force.
- b) The piezoelectric force developed by the PZT patch.

The work done W_1 by the external transverse load \boldsymbol{F}_d acting on the beam/ACLD system is given as:

$$W_1 = \int_0^{L_e} F_d w(x, t) dx \quad (4.26)$$

The work done W_2 by the piezoelectric control forces and moments are given as:-

$$W_2 = E_1 A_1 \int_0^{L_e} \left[\varepsilon_{piezo} \left(\frac{\partial u_1}{\partial x} \right) + h \varepsilon_{piezo} \left(\frac{\partial^2 w}{\partial x^2} \right) \right] dx \quad (4.27)$$

Where ε_{piezo} denotes the strain introduced by the piezoelectric effect and is given as:

$$\varepsilon_{piezo} = \frac{d_{31} v_a \|_e}{h_1}$$

Here v_a is the applied voltage to the piezoelectric actuator. However $v_a \|_e$ represents corresponding elemental voltage although both are same in magnitude. This representation has significance in CL conditions. The work done can now be written as:

$$W_2 = E_1 d_{31} b v_a \|_e \int_0^{L_e} \left(\frac{\partial u_1}{\partial x} \right) dx + h E_1 d_{31} b v_a \|_e \int_0^{L_e} \left(\frac{\partial^2 w}{\partial x^2} \right) dx \quad (4.28)$$

The total work done is given by $W_e = W_1 + W_2$

4.1.5 Equations of Motion

Using Hamilton's principle:

$$\int_{t_1}^{t_2} \delta (T_e - V_e) dt + \int_{t_1}^{t_2} \delta (W_e) dt = 0 \quad (4.29)$$

Let $\{F_p\}_e$ represents the generalized forces developed due to piezoelectric effect (i.e. by considering the forces and moments generated by piezoelectric actuation). The equations of motion for an ACLD element can be written as:

$$[M]_e \{\ddot{U}\}_e + ([K]_e + [K_{pre-stress}]_e + [K_\gamma]_e) \{U\}_e = \{F_d\}_e + \{F_p\}_e \quad (4.30)\{a\}$$

Where $[M]_e$ and $[K]_e$ are elemental mass and stiffness matrix without the contribution of viscoelastic effect and pre-stress in PVC layers. The elemental matrix $[K_{pre-stress}]_e$ gives the contribution of pre-stress in PVC layers. Similarly, the

elemental matrix $[K_\gamma]_e$ corresponds to the contribution due to viscoelastic effect. For a simply supported beam using distributed elements, through standard FEM assembling procedure with appropriate boundary conditions, the following global dynamic equation can be derived as:

$$[M]\{\ddot{U}\} + \left([K] + [K_{pre-stress}](\omega) + [K_\gamma](\omega) \right)\{U\} = \{F_d\} + \{F_p\} \quad (4.30)\{b\}$$

The equation without subscript e denotes the global form of corresponding elemental co-efficient matrices. Since Young's modulus and Shear modulus of VEM are function of frequency, hence matrices $[K_{pre-stress}]$ and $[K_\gamma]$ have been represented as $[K_{pre-stress}](\omega)$ and $[K_\gamma](\omega)$ respectively.

4.1.5.1 Open loop conditions

The voltage developed v_s for a uniform sensor of length L_e (i.e. length of one element) is obtained from the following formula as:

$$V_s \parallel_e = -\frac{k^2_{31} D_d b}{g_{31} C} \int_0^{L_e} \frac{\partial^2 w}{\partial x^2} dx \quad (4.31)\{a\}$$

Where k_{31} is the electromechanical coupling factor, D_d is the distance from the neutral axis to sensor surface, g_{31} is piezoelectric voltage constant. The capacitance C of the sensor is given as:

$$C = \frac{8.854 \times 10^{-12} A_s k_{3t}}{h_b} \quad (4.31)\{b\}$$

Where A_s is the sensor area and k_{3t} is the dielectric constant.

Thus the voltage developed is given as:

$$\nu_s \parallel_e = [K_{sensor}]_e^T \{U\}_e \quad (4.31)\{c\}$$

Where

$$[K_{sensor}]_e = -\frac{k^2_{31} D_d b}{g_{31} C} \int_0^{L_e} \frac{\partial^2 N_w}{\partial x^2} dx$$

4.1.5.2 Closed loop conditions

With Proportional Derivative (PD) controller, the relationship between actuator voltage $\nu_a \parallel_e$ and sensor voltage $\nu_s \parallel_e$ is given as:

$$\nu_a \parallel_e = -K_p \nu_s \parallel_e - K_d \frac{d \nu_s \parallel_e}{dt} \quad (4.32)$$

Where K_p and K_d are proportional and derivative control gains, respectively. By considering the proportional gain K_p only and using Eqns. 4.31-4.33 one can easily find out the expressions for generated forces using piezoelectric actuator. Representing these in terms of $\{U\}$ and using standard FEM assembling procedure, with appropriate boundary conditions, the following equations can be derived as:

$$[M]\{\ddot{U}\} + ([K] + [K_{pre-stress}] + [K_\gamma] + [G_p])\{U\} = \{0\} \quad (4.33)\{a\}$$

Where $[G_p]$ represents the contribution of PD controller. For the purpose of theoretical simulations, frequency dependence of $[K]_{pre-stress}(\omega)$ and $[K_\gamma](\omega)$ can be neglected at the moment (i.e. taking Young's modulus and shear modulus as independent of frequency). Hence, the eigenvalue problem associated with eq. (4.33a) is:

$$\{[M]\omega^2 + ([K] + [K_{pre-stress}] + [K_\gamma] + [G_p])\}\{U\} = \{0\} \quad (4.33)\{b\}$$

The eigen frequencies will be complex since there is a complex shear modulus in PVC layers. After the complex eigen frequencies have been found, the modal frequencies and the loss factors of the system can be calculated as:

$$\omega = \sqrt{Re(\omega^2)}, \quad \eta = \frac{Im[(\omega^2)]}{Re[(\omega^2)]} \quad (4.34)\{a,b\}$$

4.2 RESULTS AND DISCUSSION

4.2.1 Performance using SLD (i.e. TeLD or CoLD) Treatment Only

Table 4.1 given below represents properties of the base beam, PVC layers and piezoelectric patches and Table 4.2 represents the electrical properties of the PZT materials. To analyze the effectiveness of the SLD treatment, the PVC layers of full length (i.e. with same length as of the base beam) are first attached on both the sides of the base beam under two different conditions of the pre-stress (i.e. tensile and compression).

Table 4.1: Geometrical parameters and mechanical properties of the structure used under analysis

Parameter/Property	Base beam	PVC layer	Constraining Layer
Length (mm)	300	100	100
Width (mm)	14	14	14
Thickness (mm)	1.0	1.5	0.5
Young's Modulus (N/m ²)	3.21×10^{10}	2×10^7	70.37×10^9
Density (Kg/m ³)	4972	1390	7500
Loss factor	0.008	0.5	0
Shear Modulus (N/m ²)	-	7.69×10^6	-

Table 4.2: Electrical properties of PZT

Property	Symbol	Value
Piezoelectric charge constant (m V ⁻¹)	d ₃₁	171×10^{-12}
Electromechanical Coupling factor	k ₃₁	0.12
Piezoelectric voltage constant (VmN ⁻¹)	g ₃₁	216×10^{-3}
Dielectric constant	k _{3t}	12

The initial strain developed was measured by the digital height gauge. The length of the beam before and after the treatment was measured accurately for the strain calculations. The first column of Figure 4.4 shows the loss factors of full length TeLD and CoLD treatment. The biggest disadvantage of TeLD technique presented by various researchers is that, except for the first mode, the loss factors decrease initially with the strain and afterwards there is a rise in loss factors with pre-tensioned in PVC layers. Further, the maximum allowable value of pre-strain in PVC materials is 1% due to creep limitations. If due to certain reasons this value of strain is not maintained, there can be a serious fall in the loss factors of higher modes. Due to weight and ease of attachment considerations, full treatment is not recommended.

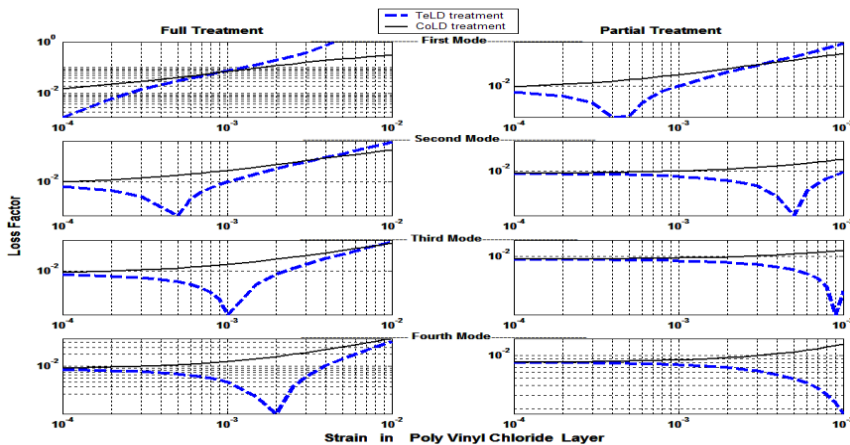


Fig. 4.4: Comparison of loss factors by positive and negative strain to base beam (Partial and Full treatment)

Hence, partial treatment is also included in the analysis. For partial treatment, analytical method as studied by various researchers is not suitable. Hence, FEM method has been applied here.

The second column of Figure 4.4 shows the loss factors for a partial treatment. The length of the treatment was 60 mm (i.e. 20% of full length of base beam) and the edge of PVC layers was at a distance of 30 mm from the simply supported edge of the base beam for this particular Figure. *The problem of fall in loss factors due to decrease in strain level in PVC layers is more severe here.* A small decrease in strain level drastically reduces the loss factors for partial treatment case. Even the first mode is not spared completely for partial treatment. Third and fourth modal loss factors are at much lower values at 1% strain. Thus, partial SLD treatment is not a suitable remedy for higher modes.

Afterwards, the proposed technique i.e. CoLD treatment is explored. Here the base beam is under tension and PVC layers are under compression. There is a uniform rise in all the loss factors, with increasing initial strain in the PVC layers or base beam. For full length treatment, performance of CoLD treatment is slightly inferior for the first and second mode at very high value of initial strain. For the third and fourth mode, performance of CoLD treatment is much better for small to moderate initial strains. For partial treatment, almost similar performance was observed by using both the techniques for the first mode. For all other modes, much better performance was obtained with CoLD treatment as compared with TeLD treatment (Figure 4.4, column two) as shown above. *The basic limitation of TeLD treatment has been removed by using CoLD treatment.*

Figure 4.5, shows the natural frequencies of the fully treated beam. Due to tension in base beam in CoLD treatment, the natural frequencies tend to increase with initial strain. However, reverse results were observed in the TeLD treatment. Hence, from here onwards in the present study, CoLD treatment only will be used and analyzed in details. *Since the thicknesses of the PVC layers and the base beam are of equal order, such a large shift in natural frequencies is there at high values of initial stresses in the PVC layers.*

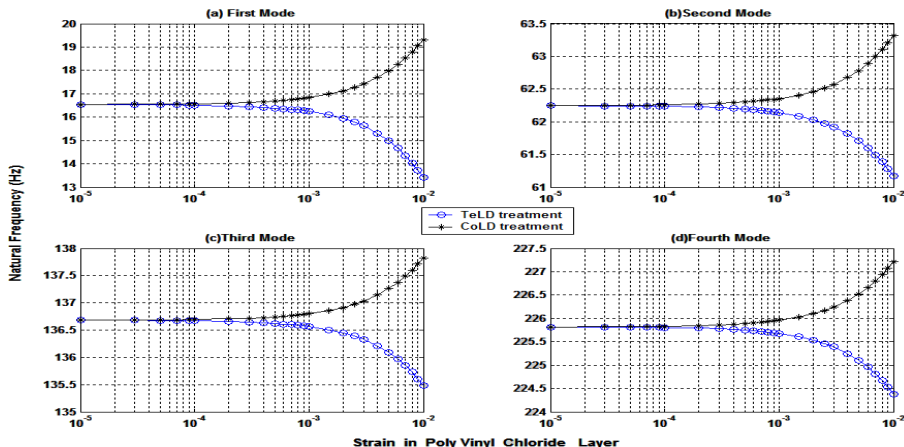


Fig. 4.5: Comparison of natural frequencies by positive and negative strain to base beam (Partial treatment)

4.2.2 Performance of PCLD Treatment Augmented with CoLD Treatment

To increase the efficiency of the SLD treatment, constraining layers were attached on the PVC layers. These constraining layers are made of piezoelectric (PZT) material. When current is applied to the PZT layers, these act as active constraining layers (i.e. ACLD treatment) otherwise passive constraining layers (i.e. PCLD treatment). Figure 4.6 shows the results of PCLD treatment augmented with CoLD treatment.

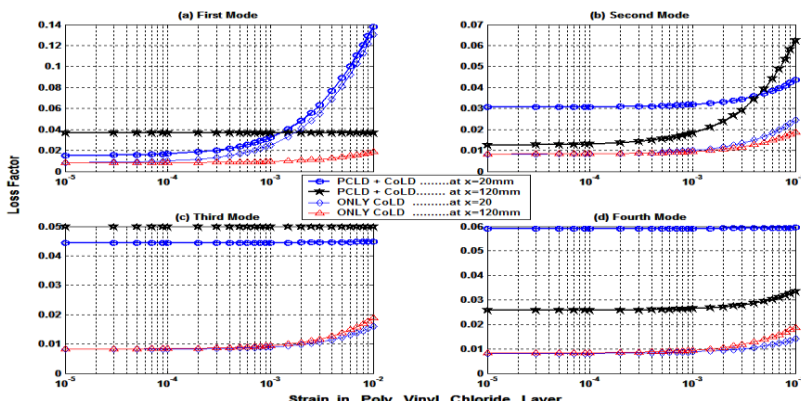


Fig. 4.6: Comparison of loss factors by (PCLD + CoLD) treatment and only CoLD treatment (Partial) at different location of the patch

For brevity this type of treatment is written as (PCLD +CoLD) treatment in the figures and in the remaining text of the manuscript. This partial treatment was done at certain particular locations. The results for two different locations were taken. In the first case, the treatment was done at a distance of 20 mm from the simply supported end of the base beam. Here 20 mm is the distance between the first edge of the PVC layer and the simply supported edge of the base beam. For the second case, treatment was done at a distance of 120 mm from the same simply supported edge.

For the first location of treatment, PCLD + CoLD treatment produces much more damping effectiveness as compared to CoLD treatment alone for all the modes except the first mode. For first mode, PCLD + CoLD treatment produces only slightly better results as compared to CoLD treatment. However, performance enhancement by 7 times was observed as compared to the case if no initial strain was present as is clear from the above Figure 4.6.

For the second mode, using CoLD treatment alone, damping effectiveness *increases by a factor of 1.5* as compared to the conditions in which no initial strain is present. The corresponding factor is 2.5 if PCLD + CoLD treatment was used. However, PCLD + CoLD treatment is much better than CoLD treatment even at zero initial strain. The natural frequencies of the overall system are reduced with (PCLD + CoLD) treatment as compared to CoLD treatment as shown in Figure 4.7.

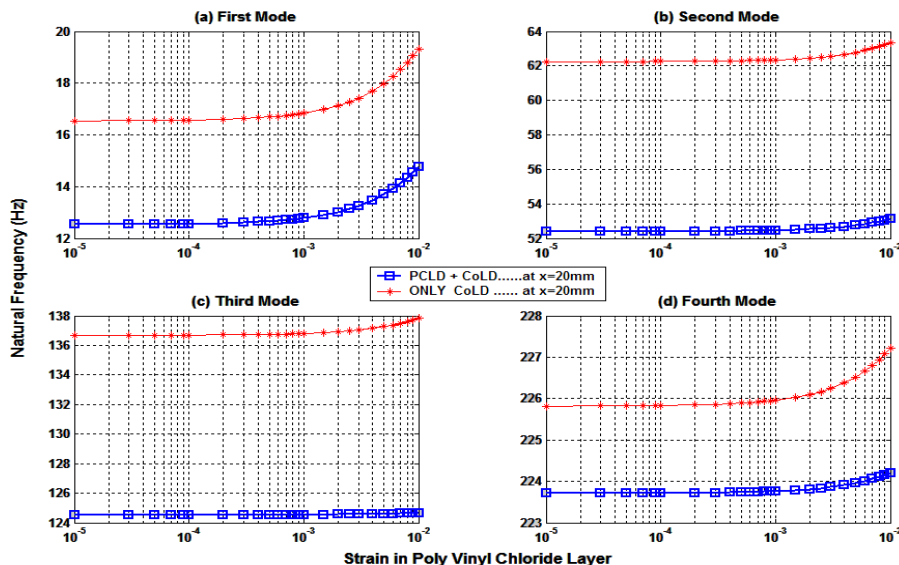


Fig. 4.7: Comparison of natural frequencies by (PCLD + CoLD) treatment and only CoLD treatment (Partial)

The damping efficiency improves to *double* for third and fourth mode if CoLD treatment is used alone. However, with PCLD + CoLD treatment, third mode loss factor increases by a factor of 4.5 and for the fourth mode by a factor of 6. Using constrained layers, the efficiency of higher modes can be improved which is not possible with CoLD treatment if used alone.

For the second location of the treatment, second and third mode damping performance enhancement is maximum when PCLD + CoLD treatment is used. For the second mode, damping effectiveness increases by a factor of 6.15 as compared to the case when no initial strain was present. Similar improvement was observed (by a factor of 3.1) as compared to the case when CoLD treatment was used alone. However, for the first and fourth mode, damping enhancement is comparatively less. First mode damping performance is independent of the initial strain at this particular location of treatment. Hence, *different locations of treatment affect the modal loss factors in a different way*.

Application of constraining layers, decrease all the modal frequencies which is good as tensing the base beam tries to increase the natural frequencies. To check the damping performance at some other locations of the treatment, Figure 4.8 was constructed. The treatment at distances of

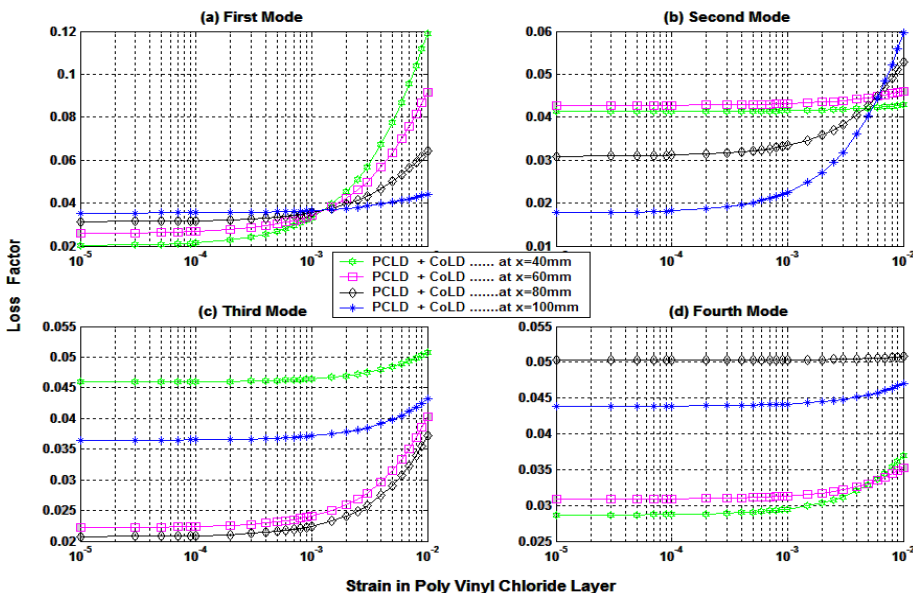


Fig. 4.8: Comparison of loss factors by PCLD + CoLD treatment and only CoLD treatment Partial) at other different location of the patch

40 mm, 60 mm, 80 mm and 100 mm was also done. It was observed that $x = 40$ mm is the best among other locations for first mode. This modal loss factor was increased by 6 times at 1% initial strain as compared to a situation when no strain was present. Second modal loss factor was maximum at $x=100$ mm. This modal loss factor was increased by 3 times at 1% initial strain as compared to a situation when no strain was present. Third modal loss factor was maximum again at $x=40$ mm. At this location contribution of pre-strain is comparatively less as compared to other locations; but this location itself is best for improving the damping of third modal loss factor. The fourth modal loss factor was maximum when treatment was done at $x = 80$ mm. Although the contribution of initial strain is again very less for this location of treatment, but this location itself is best for improving the damping of fourth modal loss factor. In this way, it is concluded that contribution of initial strain to the damping performance is different for different modes and it is highly dependent on the location of the treatment. *This fact can be explained on the basis of mode shapes of the simply supported beam. The maximal modal loss factor is obtained when the treatment is done at a point where modal amplitude is minimum (i.e. slope is maximum).*

4.2.3 Performance of ACLD Treatment augmented with CoLD Treatment

In this subsection, an ACLD treatment augmented with CoLD treatment is investigated. For brevity this type of treatment is written as (ACLD +CoLD) treatment in Figures and the texts of the manuscript. Comparison of this treatment is done with PCLD + CoLD treatment. If, instead of using PVC layers, VEM layers (of same shear

modulus and loss factor but no initial strain) are attached, damping performance varies. This is termed as conventional ACLD and conventional PCLD treatment and is shown in Figure 4.9.

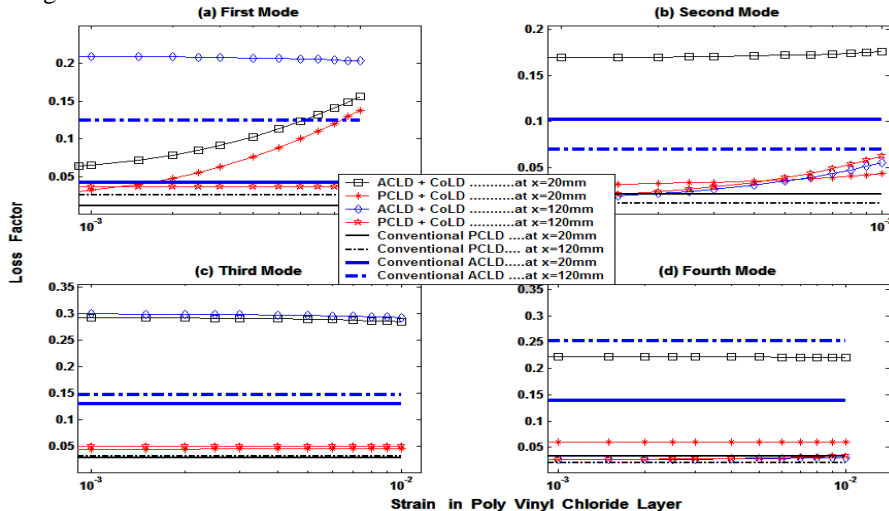


Fig. 4.9: Comparison of loss factors by (ACLD + CoLD) treatment with displacement feedback gain of 10 and (PCLD + CoLD) treatment (partial) at different location of the patch

The treatment is again done at two different locations. First location is at a distance of 20mm from the simply supported end and the second is at a distance of 120 mm from the same end. For the first location, ACLD + CoLD treatment and PCLD + CoLD treatment improves the first mode loss factor with the initial strain. For the first mode, the performance increases roughly by a factor of 3 using both types of treatments. Certain good amount of performance enhancement is available at second mode also. The performance enhancement of ACLD + CoLD treatment is much more as compared to that with PCLD treatment only. Loss factors of other higher modes are independent of initial strain in CoLD treatment. It is natural to compare this proposed technique with conventional ACLD and conventional PCLD treatment. Displacement feedback gain of 10 is used here. Loss factors for all the modes are much better with conventional ACLD system than conventional PCLD system. Since performance is dependent on stress, in case of SLD treatment, the ACLD + CoLD treatment is much better as compared to conventional ACLD treatment with VEM layer.

For the second location, damping performance with ACLD + CoLD treatment is much better as compared to other cases for the first and third mode. However, for the second and fourth mode, this location is not advantageous. At this location, the damping performance of the fourth mode is best using conventional ACLD treatment.

To check the efficiency of the ACLD + CoLD treatment at certain other locations, data was generated which is shown in Figure 4.10.

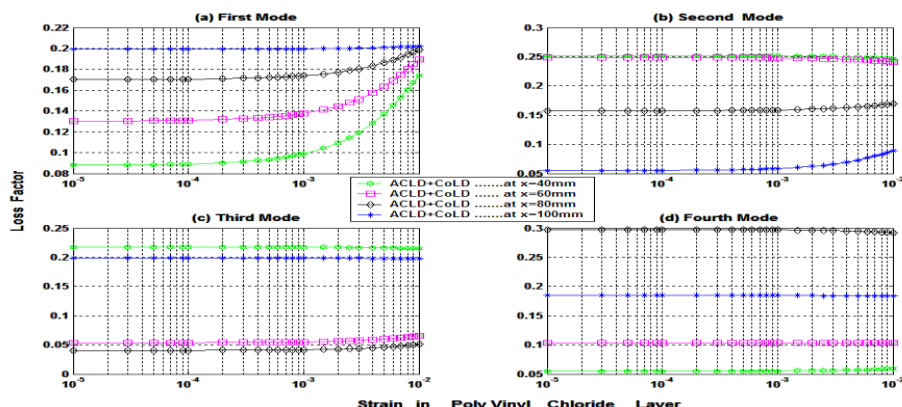


Fig. 4.10: Comparison of Loss Factors by (ACLD + CoLD) treatment and only CoLD treatment at four other locations i.e. at 40 mm, 60 mm, 80 mm and 100 mm considered.

First mode damping performance was best when treatment was done at 100 mm (i.e. when the center of the treatment or center of the PZT patch coincides with the center of the base beam). At this location the vibration amplitude is maximum. For the best effectiveness of the treatment, PZT patch (i.e. active constraining layer) should be at a location where modal amplitude is highest. This situation is different from PCLD + CoLD system where the performance was best at a location of treatment of 40 mm. For the second mode, the amplitude of vibration is maximum at a distance $\frac{1}{4}$ th and $\frac{3}{4}$ th of L from the simply supported edge. ‘L’ is the length of the base beam. Hence, second mode damping performance (with ACLD treatment) was best when the treatment was done at a distance of 40 mm from the simply supported edge. Fourth mode damping performance was best when the treatment was done at a distance of 80 mm (Figure 4.10). This can also be explained on the basis of mode shapes of the simply supported beam.

4.3 EXPERIMENTAL VALIDATION

4.3.1 Experimental Setup

To check the authenticity of the theoretical results experimental setup was generated as shown in Figure 4.11.

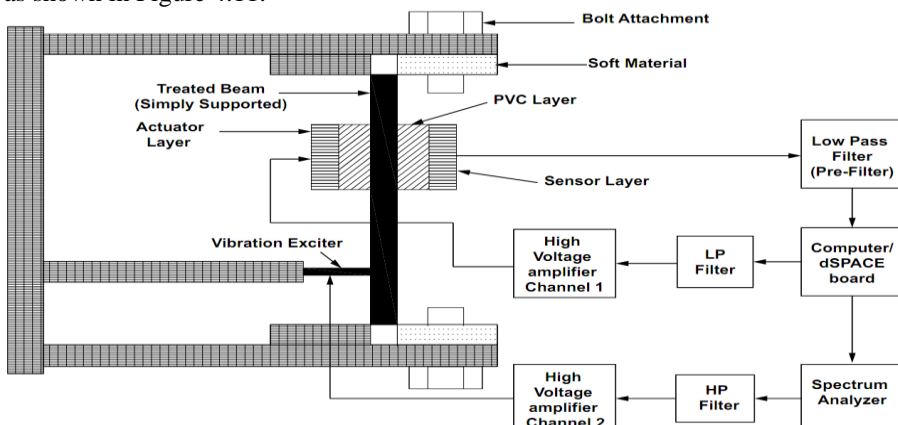
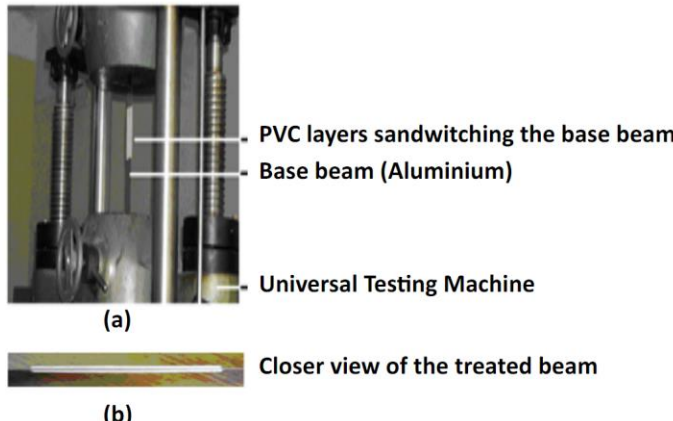


Fig. 4.11: Schematics of the experimental setup (for identification and control)

However, before starting the experimental implementation of the controller designed experimental system identification must be carried out. Photograph of the flexible beam with CoLD treatment has been shown in Photograph 4.1. The controller was implemented using a dSPACE DS1103 rapid prototyping Controller board together with MATLAB and SIMULINK environment. The sampling frequency was set as 600 Hz, while the cut-off frequency of both the low pass filters was set at 300 Hz. A high voltage amplifier MA – 17 from Apex Technologies was capable of driving highly capacitive loads and was used to supply necessary voltage for actuating the piezoelectric patch.



Photograph 4.1: Picture of the flexible beam with CoLD treatment

4.3.2 Experimental System Identification

For an accurate identification, any arbitrary signal may not be suitable. The input data supplied to the system for system identification should be informative. Both for open loop (OL) and closed loop (CL) operations, ‘informative’ means that the input should be persistently exciting of a certain order; i.e. it contains sufficiently many distinct frequencies. For the identification of linear systems, there are three basic facts that govern the choices:

- (1) The asymptotic properties of the estimate (bias and variance) depend only on the input spectrum and not the actual waveform of the input.
- (2) The input must have limited amplitude.
- (3) Periodic inputs may have certain advantages. Based on several factors, the classification of the input signal can be done into following categories;
 - a) Filtered Gaussian White Noise
 - b) Random Binary Signal
 - c) Pseudo – Random Binary Signal
 - d) Chirp Signals or Swept Sinusoids

The desired property of the waveform, to be used as input signal, is defined in terms of **crest factor** C_r :

$$C_r^2 = \frac{\max_t u_{x_k}^2(t)}{\lim_{L \rightarrow \infty} \frac{1}{L} \sum_{t=1}^L u_{x_k}^2(t)} \quad (4.35)$$

Where $u_{x_k}(t)$ is the sequence of the applied excitation signal at the actuator. A good signal waveform is the one that has a smallest crest factor. In the present case, to excite the system in OL conditions, the multisine wave with minimum crest factor and magnitude of the excitation signal 20 volt was used. The duration of the excitation signal was chosen to be 10 seconds. The frequency content of the signal was 0-300 Hz. To minimize the measurement noise the experiment was repeated several times.

4.3.3 Experimental Determination of Frequency Dependent Young's Modulus, Shear Modulus and Corresponding Loss Factors for PVC Layer

The GHM (Golla –Hughes – McTavish) method has been used to tackle the problem. It uses a second order physical co-ordinate system. Frequency dependent Young's modulus, shear modulus and the corresponding loss factors can be easily accommodated using this method. GHM method requires the representation of material modulus function as a series of damped "mini-oscillator" terms or internal variables. This method was developed for direct incorporation into finite element method. The material complex modulus can be written in Laplace domain in the form as:

$$E(s) = E_0 \left(1 + h(s) \right) = E_0 \left(1 + \sum_{n=1}^k \hat{\alpha}_n \frac{s^2 + 2\hat{\xi}_n \hat{\omega}_n s}{s^2 + 2\hat{\xi}_n \hat{\omega}_n s + \hat{\omega}_n^2} \right) \quad (4.36)$$

Where E_0 is the equilibrium value of the modulus, and s is the Laplace operator. The capped terms are free variables for curve fitting to the complex data for a particular material at a given temperature. The number of expansion terms, k , may be modified to represent the high or low frequency dependence of the complex terms. The expansion $h(s)$ represents the material modulus as a series of mini oscillator terms.

4.3.3.1 Young's modulus and corresponding loss factor

To determine the frequency dependent Young's modulus of elasticity and the corresponding loss function the parameters $\hat{\alpha}_n$, $\hat{\xi}_n$ and $\hat{\omega}_n$ have to be determined. The equation of motion of transverse vibration of a viscoelastic beam may be presented by a GHM finite element method with one mini-oscillator term as:

$$[M_e]\{\ddot{q}\} + [D_e]\{\dot{q}\} + [K_e]\{q\} = \{f_e\} \quad (4.37)$$

Where the finite element matrices are given by:-

$$[M_e] = \begin{bmatrix} [M_e] & [0] \\ [0] & (\hat{\alpha}/\hat{\omega}^2)E_0[\Lambda_e] \end{bmatrix}$$

$$[D_e] = \begin{bmatrix} [0] & [0] \\ [0] & (2\hat{\alpha}\hat{\xi}/\hat{\omega})E_0[\Lambda_e] \end{bmatrix}$$

$$[K_e] = \begin{bmatrix} [K_e]E_0(1 + \hat{\alpha}) & -\hat{\alpha}E_0\{R_e\}[\Lambda_e] \\ -\hat{\alpha}E_0[\Lambda_e]\{R^T_e\} & \hat{\alpha}E_0[\Lambda_e] \end{bmatrix}$$

With $\{f_e\}$ as an element force vector. The co-ordinate vector is represented by $\{q\} = [\{x\} \{z\}]^T$ with an element displacement vector $\{x\} = [w_1 \theta_1 w_2 \theta_2]^T$. $\{z\}$ being the additional co-ordinates and depend upon the nature of material and the number of mini-oscillatory terms. The sub matrix $[\Lambda_e]$ is a diagonal matrix of non-zero

eigenvalues of matrix $[K_e]$ and $[R_e]$ is the corresponding ortho normalized eigen vectors. *FRF is obtained using vibration exciter as actuator and PZT patch as sensor.* The parameters $\hat{\alpha}_n$, $\hat{\xi}_n$, and $\hat{\omega}_n$ can be determined from experimental FRF by curve fitting techniques. A simply supported PVC beam of 600 mm length, 50 mm width and 3 mm thickness was used for determination of FRF of the flexible beam system. After the determination of parameters $\hat{\alpha}_n$, $\hat{\xi}_n$ and $\hat{\omega}_n$ from the experimental FRF, by curve fitting technique, Young's modulus of elasticity and corresponding loss factors were plotted as a function frequency. A single mini-oscillator term was used for curve fitting technique. It was found that $\hat{\alpha} = 1.2$, $\hat{\xi} = 3$, $E_0 = 1.7 \times 10^7 \text{ N/m}^2$ and $\hat{\omega} = 20000$ gives satisfactory results. Using these parameters frequency dependent Young's modulus and the corresponding loss factor can be plotted as shown in Figure 4.12.

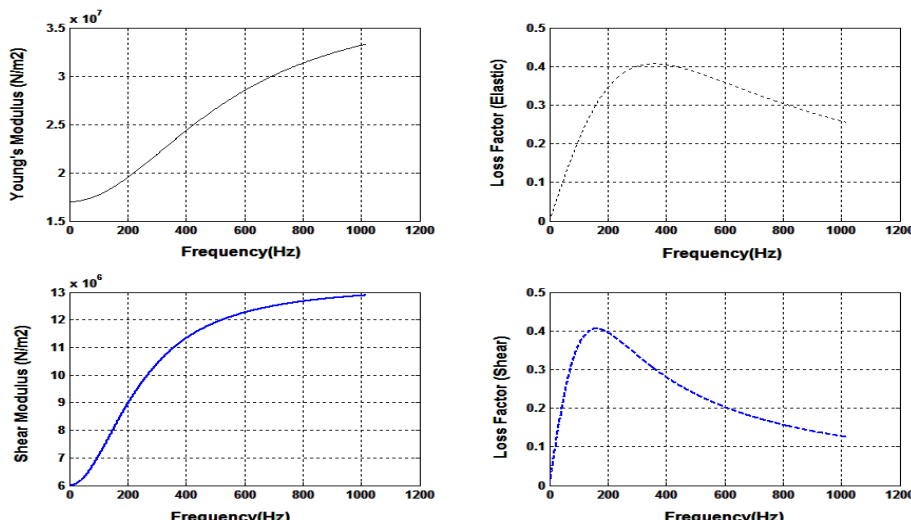


Fig. 4.12: Young's and shear modulus with corresponding loss factor as a function of Frequency

4.3.3.2 Shear modulus and corresponding loss factor

For measuring the frequency dependent shear modulus, ACLD treated beam with PVC layers (with no initial stress in these layers) was used instead of standard VEM layers. The length of the treatment is chosen as 100 mm with 33% coverage. Correspondingly 300 mm long base beam was selected for equivalent coverage. Aluminum alloy is the material of the base beam. Other geometrical and material properties are specified in Table 1. To find the shear modulus and the corresponding loss factor, no pre- stress was applied to the base beam as well as PVC layers. Considering a single term GHM expression, the equations of motion are given as:-

$$[M_e]\{\ddot{Q}_e\} + [D_e]\{\dot{Q}\} + [K_e]\{Q\} = \{F_e\} \quad (4.38)$$

Where

$$\{Q\} = [\{U\} \{Z\}]^T$$

$$[M_e] = \begin{bmatrix} [M_e] & [0] \\ [0] & (\hat{\alpha}/\hat{\omega}^2)E_0[\Lambda_e] \end{bmatrix}$$

$$[D_e] = \begin{bmatrix} [0] & [0] \\ [0] & (2\hat{\alpha}\hat{\xi}/\hat{\omega})[\Lambda_e] \end{bmatrix} 0.10$$

$$[K_e] = \begin{bmatrix} [K_e] + [K_{ey}] & (1 + \hat{\alpha}) & -\hat{\alpha}[R_e] \\ -\hat{\alpha}[R_e]^T & \hat{\alpha}[\Lambda_e] \end{bmatrix}$$

Where

$$\{Z\}_e = [\hat{R}]^T \{\hat{Z}\}_e, [R] = [\hat{R}][\Lambda], [\Lambda] = G^\infty [\hat{\Lambda}], [K_{ey}] = G^\infty [\hat{K}_{ey}], [\hat{K}_{ey}] = [\hat{R}][\hat{\Lambda}][\hat{R}]^T$$

and $[\hat{\Lambda}]$ is a diagonal matrix of the non-zero (necessarily positive) eigen values of matrix $[\hat{R}]$. A single mini-oscillator term was used for curve fitting technique. It was found that $\alpha = 1.2$, $\xi = 5$, $G^\infty = 6 \times 10^6 \text{ N/m}^2$ and $\hat{\omega} = 15000 \text{ rad/s}$ gives satisfactory results. Using these parameters, frequency dependent shear modulus and the corresponding loss factor were plotted as shown in Figure 4.12 above.

4.3.4 Experimental Implementation of Digital Controller

System identification is a very complex process in which parameter estimation is one step. A primary and very important choice is that of the class of models to be considered. System identification basically consists of two steps (i) Model structure estimation (ii) Model parameter estimation. Based on the previous knowledge about the system or FRF of the system, the order of the system can be selected. After obtaining the order of the system, the parameter estimation process is discussed as follows:

The system can be represented in the state form as:

$$\begin{aligned} \dot{x}(t) &= Ax(t) + Bu(t) \\ &= \begin{pmatrix} 0 & 1 \\ -\Omega & -\Lambda \end{pmatrix} x(t) + \begin{pmatrix} 0 \\ B_2 \end{pmatrix} u(t) \end{aligned} \quad (4.39)\{a\}$$

$$y(t) = Cx(t) = (B^T \quad 0) x(t) \quad (4.39)\{b\}$$

Where Ω and $\Lambda \in \mathbf{R}^{n \times m}$ and $B_2 \in \mathbf{R}^{n \times m}$ has to be estimated if inputs and outputs are collocated, which is there in our present work. Here m represents the number of inputs of the system. For a single input single output (SISO) system, with single mode consideration, the above model can be written as:-

$$\begin{aligned} \dot{x}(t) &= \begin{pmatrix} 0 & 1 \\ -\omega^2 & -2\xi\omega \end{pmatrix} x(t) + \begin{pmatrix} 0 \\ \phi_{12} \end{pmatrix} u(t) \\ y(t) &= (1 \quad 0) x(t) \end{aligned} \quad (4.40)$$

Where ω , ξ and ϕ are the natural frequency, damping ratio and mode shape (of the considered mode) of the structure respectively. ϕ_{12} is obtained by multiplying the mass normalized mode shapes at the sensor and actuator location. By considering the various modes of interest, the model above can be extended to multi-mode case easily. The Figure 4.13 shows the comparison of results in frequency domain using FEM and experimentally generated FRF.

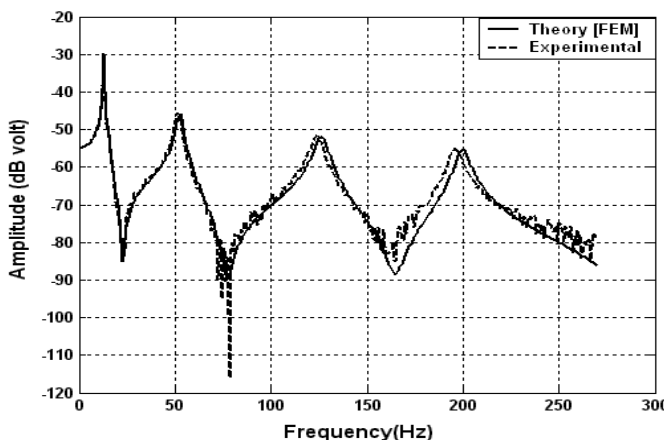


Fig. 4.13: Comparison of experimental and theoretical vibration characteristics of the beam system using (ACLD + CoLD) treatment.

Frequency dependent Young's modulus and shear modulus has been used to construct the FRF from the FEM model using equation 4.31. The experimental results are closely related to theoretical results due to this factor. The significant difference lies at higher frequencies only. This figure shows the open loop FRF of the treated beam by proposed technique, from PZT actuator to PZT sensor voltage. The variation between the results is attributed to the reasons that the strain developed in the base beam varies due to lose adhesive bond of the gluing adhesives and the variation in the properties of the PVC and PZT material.

Figure 4.11 above shows the schematics of experimental setup for control purpose also. To provide pre-compression in PVC layers indirect method was employed. *The base beam was tensed on the 'Universal Testing Machine' and the PVC layers were attached.* Afterwards the tension on the base beam was removed so that base is under tension and PVC layers under compression (refer Photograph 4.1). Now two PZT layers were glued on the PVC layers, one forming the actuator and one forming the sensor. *The simply supported beam was clamped with soft rubber like materials on a frame for supporting the beam, so that vertical displacement only was restrained.* The beam is capable of deformation in terms of slope at the edges. A low pass filter was also used to remove the effect of out of range modes. The voltage from sensor PZT patch was passed to a high voltage amplifier MA-17. After amplification from the first channel of the amplifier, the voltage was directed to the actuator PZT patch. The spectrum analyzer from HP technologies was used to create signals of various frequencies. This signal was amplified from the second channel of the amplifier.

Digital Linear Quadratic Regulator (LQR) has been used in the present work to compare the experimental results with the simulations. Equations 4.39 and 4.40 are used to calculate matrices **A** and **B**. From analog domain the system is discretized to digital domain at 600 Hz (sampling frequency). By combining the LQR with Kalman Filter (required for state estimation), Linear Quadratic Gaussian (LQG) controller is constructed. Due to various uncertainties, the system dynamics may not constant. LQG control is an *excellent control system design methodology and has been extensively used in the past.* The system to be controlled is given by equation 4.42. Using the gain matrix **K** control inputs are calculated by the following equation:

$$u(t) = -KX(t) \quad (4.41)$$

The system matrices **A** and **B** and the weighting matrices **R** and **Q** are used to calculate the gain matrix **K**. The systematic procedure to choose **R** and **Q**. The relative amplitude of the elements of these matrices determines the amplitude of the control signal vector **u** (t). Before designing the controller, the observability and controllability must be checked by calculating the observability and controllability Gramians. Normally input – output data is available from experimental setup. Due to the presence of ‘Measurement Noise’ and ‘Process noise’ the system state and output equations of the stochastic system have the following form:

$$\begin{aligned} \dot{X}(t) &= A X(t) + B u(t) + w(t) \\ y(t) &= C X(t) + D u(t) + v(t) \end{aligned} \quad (4.42)$$

Where $v(t)$ is the measurement noise vector and $w(t)$ is the process noise vector respectively. As assumed $w(t)$ and $v(t)$ are each zero-mean, white noise sequences in vector form, with known covariance and uncorrelated with each other. Using the inputs $u(t)$ and outputs $y(t)$, the future state vector $X(t)$ can be estimated accurately by using Kalman Filter. MATLAB commands ‘dlqr’ and ‘dkalman’ can be used to design the LQG controller. To implement the LQG controller, the states of the system and noise characteristics, must be known accurately. As discussed earlier, two types of noises are considered viz. measurement noise and process noise. The measurement and process noise have been considered with zero mean. The noise free part of the signal is obtained by repeating the experiment several times by using a particular input sequence and observing the average of the corresponding output sequences.

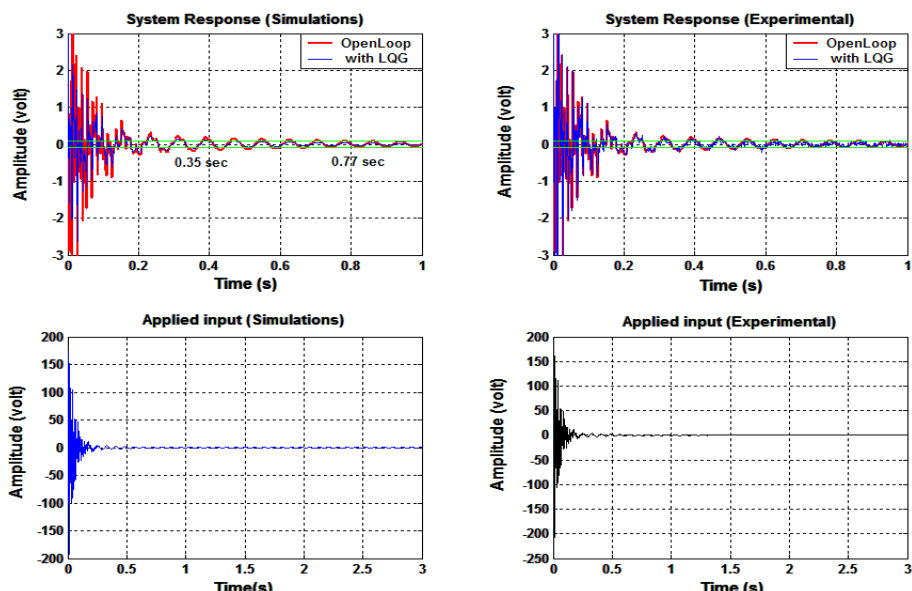


Fig. 4.14: Time domain system response (Simulations and Experimental)

The comparison of experimental data with the simulations in time domain has been shown in Figure 4.14 above. To quantify the controller effectiveness concept of settling time has been used. Settling time has been taken as the time period in which the final amplitude of the vibration signal becomes equal to 1% of the initial amplitude.

As the system is excited and the controller is applied, it can be seen that CL settling time (0.35 sec) is much less than the OL settling time (0.77 sec). Due to the presence of measurement noise, there is performance degradation of the CL system.

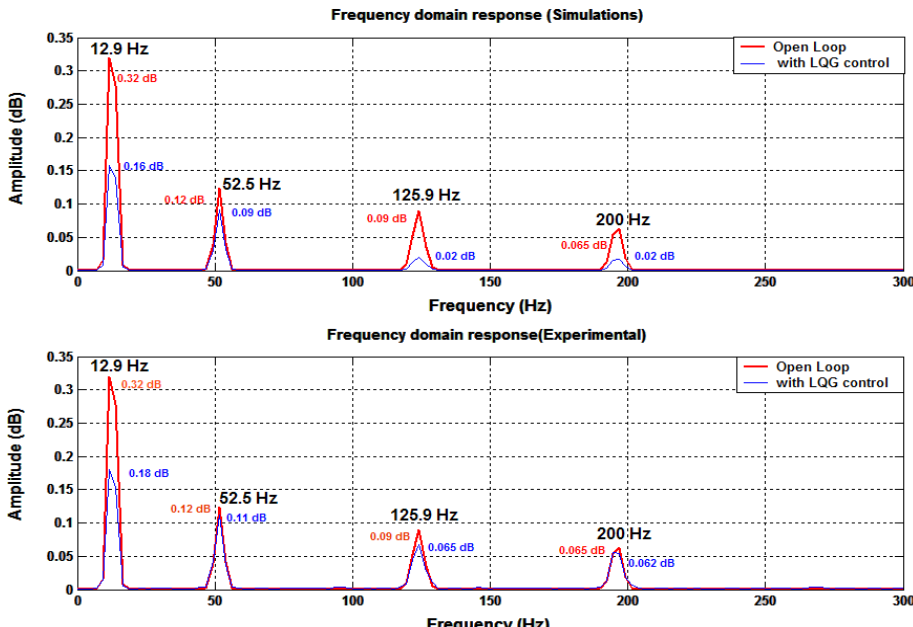


Fig. 4.15: Frequency domain system responses (Simulations and Experimental)

The comparison of OL and CL system in frequency domain is clearly visualized from the above Figure 4.15. In OL (Open Loop) condition, the amplitude of first four modes was 0.32 dB, 0.12 dB, 0.09 dB and 0.065 dB respectively. The first four natural frequencies are 12.9 Hz, 52.5 Hz, 125.9 Hz and 200 Hz. With the application of the controller, the amplitude was reduced to 0.16 dB, 0.09 dB, 0.02 dB and 0.02 dB respectively for the first four modes. The lower part of this figure shows the OL and CL amplitude of the system in frequency domain obtained from experimental data. The deterioration of the performance due to experimental noise is clearly visible. Higher modes, at which vibration amplitude is less, are more prone to performance degradation. However, for the first mode, the vibration amplitude is more; hence there is a very marginal difference in experimental and simulated results.

@Seismicisolation

CHAPTER – 5

VIBRATION CONTROL WITH ADVANCED METHODS

The potential and suitability of using smart composite structures for active suppression of vibration in aerospace industry is a widely investigated topic of research. The widely used smart materials for vibration control in structures are piezoelectric materials since they have desirable characteristics. PCLD is an old technique to suppress vibrations. By combining PCLD treatment with active control techniques, desirable results can be obtained. This technique is called ACLD treatment. Present work is based on the development of newer passive techniques, which can enhance the damping performance of PCLD and ACLD systems.

The main disadvantage of active constrained layer damping treatment is the reduced transmissibility of active forces. This problem can be solved up to certain extent by using edge anchors. These edge anchors or stiffeners increase the transmissivity of forces only at very high feedback gains but decrease the effectiveness of passive constrained layer damping (PCLD) treatment. The efficiency of the passive constrained layer damping treatment can be improved drastically by adding the stand-off-layer (SOL) between the viscoelastic layer and the base beam. This technique has additional advantages as well. Firstly, it increases the viscoelastic strain so that more energy is dissipated via viscoelastic layer. Secondly, it enhances the effect of active forces and moments even without using edge anchors because the shear modulus of the SOL is in the range 10^8 to 10^9 N/m 2 . Hamilton's principle in conjunction of finite element method is used to derive the equations of motion. The complex eigen value is developed and solved numerically by using simple proportional feedback control strategy. Results are compared with ordinary active constrained layer damping (ACLD) treatment in order to highlight the effectiveness of the proposed technique. Validity of the proposed treatment has also been verified experimentally.

The ACLD treatment is usually a three layer composite consisting of a viscoelastic material (VEM) damping layer sandwiched between a piezoelectric layer (constraining layer) and the basic structure. The applicability of the longitudinal displacement relationship between base beam and constraining layer is presented in this chapter. A third admissible function representing the longitudinal displacement of the constraining layer is also considered here.

From the detailed survey, it has been concluded that FEM version of the treatment in which SOL layer and VEM layer are used together, is still missing in literature even for PCLD treatment. The effectiveness of this technique for ACLD treatment, too, needs an investigation. The present work has been undertaken after considering these factors:

The main contribution of the present work is divided into following parts:

1. A Finite Element Method based on energy methods (which have certain advantages as discussed above) has been employed in the present work, so that partial treatment can be accommodated easily.
2. Effect of SOL layer is investigated for ACLD treatment which has never been considered earlier in literature.
3. The edge elements increase the damping performance of the ACLD system at very high values of feedback gains. This high value of gain means working at very high voltages which causes additional problems. Anchors also decrease the effectiveness of the PCLD system in case of failure of active system. Hence, the use of edge anchors has also been investigated for the proposed technique.

5.1 SYSTEM DESCRIPTION AND MODELING

5.1.1 Basic Relationships

The enhanced ACLD treatment with SOL layer is termed as EACLDSOL for convenience. The schematic of EACLDSOL is shown in Figure 5.1.

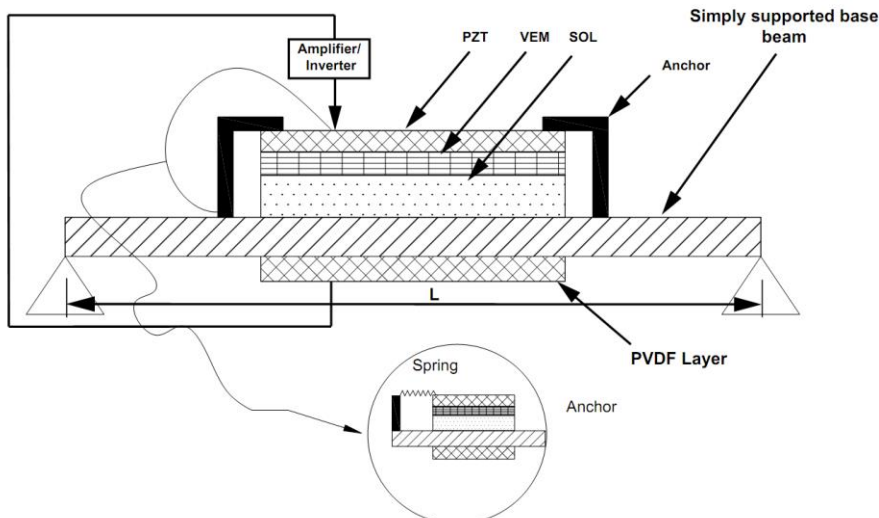


Fig. 5.1: Schematics of structure EACLDSOL treatment

The new thing here is that the additional SOL layer has been sandwiched. The upper surface of host structure or the beam is attached with a SOL and VEM layer. This layer in turn is constrained by an active piezoelectric material like Lead Zirconated Titinate (PZT). This layer acts as an actuator layer. A Polyvinilidene Di Fluoride (PVDF) layer acts as sensor. A pair of edge elements mounted at both ends of the constraining sheet to connect the constraining layer directly to the host structure (Figure 5.1). These edge elements are modeled as springs. These are also called anchors. The purpose of these elements is to increase the transmissibility of the active control action. Figure 5.2 below shows the cross-section of the beam with EACLDSOL system.

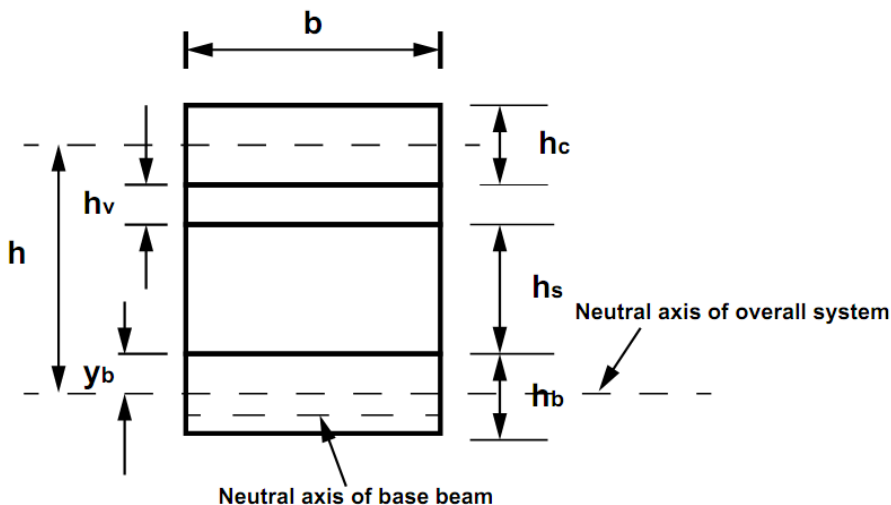


Fig. 5.2: Cross-section of beam with EACLDSOL treatment

For the continuity of displacements at the interface between the layers the relation between shear angle (strain) and various displacements given by:

$$\left. \begin{aligned} u_s &= u_b - \frac{h_b + h_c}{2} \theta \\ u_v &= \frac{h_b + h_c}{2} + \frac{(h_c - 2h_s - h_b)}{4} \theta \end{aligned} \right\} \quad (5.1)\{a, b\}$$

$$\gamma_s = \left[\frac{u_c - u_b}{h_s} + \frac{1}{2} \left(1 + \frac{h_c + 2h_v + y_b}{2h_s} \right) \theta \right] - \left(\frac{h_v}{h_s} \right) \gamma_v \quad (5.1)\{c\}$$

Where $h = y_b + h_v + h_s + h_c/2$, θ denotes the slope and u and w denote the longitudinal and transverse displacements respectively. For VEM layer and SOL layer, u is denoted by u_v and u_s respectively. Transverse displacement of all the layers is assumed to be same and hence denoted by w for all the layers. h_c , h_b , h_v and h_s denote the thickness of constraining layer, base beam, VEM layer and SOL layer. The distance between the top surface of the base beam and the neutral axis of the overall system is denoted by y_b . The shear stress developed in VEM layer is denoted by τ_v . The shear strain of the VEM layer is represented by γ_v . Similarly, shear stress developed in SOL layer is denoted by τ_s . The shear strain of the SOL layer is represented by γ_s . u_c and u_b are the longitudinal displacement of the constraining layer and the base beam respectively and w is the transverse displacement of the constraining layer as well as of the base beam. Slope θ is the derivative of w with respect to x . The edge stiffeners are modeled as springs of certain stiffness. The shear stress in both the layers is given as:

$$\tau_s = G_s \gamma_s \text{ and } \tau_v = G_v \gamma_v \quad (5.2)\{a,b\}$$

Since equal stress is developed in both the layers, hence

$$\tau_s = \tau_v \quad (5.3)$$

Relation (5.2) and (5.3) show that:-

$$\gamma_s = \left(\frac{G_v}{G_s} \right) \gamma_v \quad (5.4)$$

Solution of equations (5.1) and (5.2-5.4), provides:

$$\gamma_s = \left[\frac{u_c - u_b}{h_s} + \left(1 + \frac{h_c + 2h_v + 2y_b}{2h_s} \right) \frac{\partial w}{\partial x} \right] \left(\frac{G_v}{G_s} \right) / \left(\frac{h_v}{h_s} + \frac{G_v}{G_s} \right) \quad (5.5)\{a\}$$

$$\gamma_v = \left[\frac{u_c - u_b}{h_s} + \left(1 + \frac{h_c + 2h_v + 2y_b}{2h_s} \right) \frac{\partial w}{\partial x} \right] \left(\frac{G_v}{G_s} \right) / \left(\frac{h_v}{h_s} + \frac{G_v}{G_s} \right) \quad (5.5)\{b\}$$

The deformations in the edge element springs are given as:

- Left spring element:

$$\Delta x_L = u_c(x_L) - u_b(x_L) + h \frac{\partial w(x_L)}{\partial x} \quad (5.6)\{a\}$$

- Right spring element:

$$\Delta x_R = u_c(x_R) - u_b(x_R) + h \frac{\partial w(x_R)}{\partial x} \quad (5.6)\{b\}$$

5.1.2 The Shape Functions

Figure 5.3 shows a treated beam element.

Nodal displacements are given as:

$$\{U\}_e = \{w_i \ \theta_i \ u_{bi} \ u_{ci} \ w_j \ \theta_j \ u_{bj} \ u_{cj}\} \quad (5.7)$$

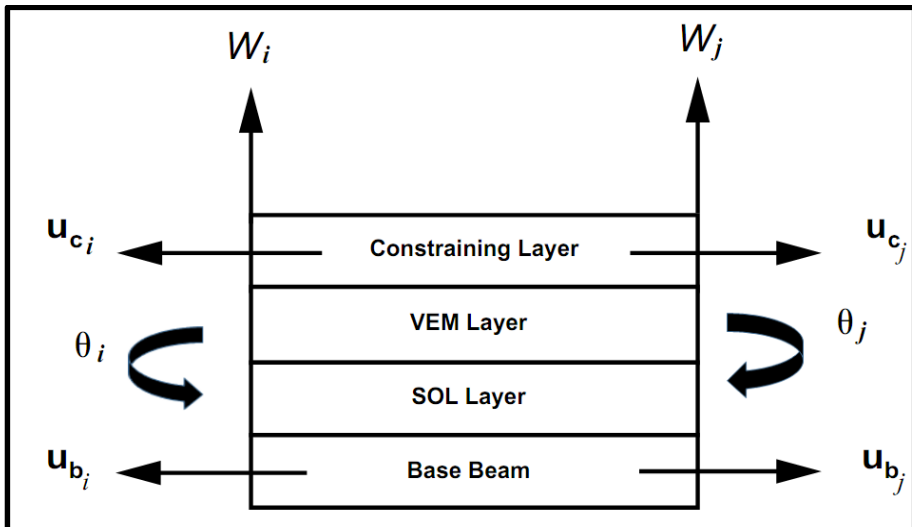


Fig. 5.3: Nodal displacement of a treated beam element

The transverse displacement w , the rotation θ , the axial displacement of the base beam u_b and the axial displacement of the constraining layer u_c are expressed in the nodal displacements by finite element shape functions as:

$$w = [N_w] \{U\}_e, \theta = [N_\theta] \{U\}_e, u_b = [N_{ub}] \{U\}_e, u_c = [N_{uc}] \{U\}_e \quad (5.8)\{a, b, c, d\}$$

Where the shape functions are given as:

$$[N_w] = \begin{bmatrix} 1 - 3\left(\frac{x}{L_e}\right)^2 + 2\left(\frac{x}{L_e}\right)^3 \\ x - 2\left(\frac{x^2}{L_e}\right) + \left(\frac{x^3}{L_e^2}\right) \\ 0 \\ 0 \\ 3\left(\frac{x}{L_e}\right)^2 - 2\left(\frac{x}{L_e}\right)^3 \\ -\left(\frac{x^2}{L_e}\right) + \left(\frac{x^3}{L_e^2}\right) \\ 0 \\ 0 \end{bmatrix}^T, \quad [N_\theta] = \begin{bmatrix} -6\left(\frac{x}{L_e^2}\right) + 6\left(\frac{x^2}{L_e^3}\right) \\ 1 - 4\left(\frac{x}{L_e}\right) + 3\left(\frac{x}{L_e}\right)^2 \\ 0 \\ 0 \\ 6\left(\frac{x}{L_e^2}\right) - 6\left(\frac{x^2}{L_e^3}\right) \\ -2\left(\frac{x}{L_e}\right) + 3\left(\frac{x}{L_e}\right)^2 \\ 0 \\ 0 \end{bmatrix}^T$$

$$[N_{ub}] = \begin{bmatrix} 0 & 0 & 1 - \frac{x}{L_e} & 0 & 0 & 0 & \frac{x}{L_e} & 0 \end{bmatrix}$$

$$[N_{uc}] = \begin{bmatrix} 0 & 0 & 0 & 1 - \frac{x}{L_e} & 0 & 0 & 0 & \frac{x}{L_e} \end{bmatrix}$$

From eq. (5.1-5.6), u_s , u_v , γ_s , γ_v , Δx_L , and Δx_R can be expressed in the nodal displacement as follows:

$$\left. \begin{aligned} u_s &= [N_{us}] \{U\}_e, \quad u_v = [N_{uv}] \{U\}_e \\ \gamma_s &= [N_{\gamma s}] \{U\}_e, \quad \gamma_v = [N_{\gamma v}] \{U\}_e \\ \Delta x_L &= [N_{L Spring}] \{U\}_e \quad \text{and} \quad \Delta x_R = [N_{R Spring}] \{U\}_e \end{aligned} \right\} \quad (5.9) \{a, b, c, d, e, f\}$$

Where

$$\begin{aligned} [N_{us}] &= [N_{ub}] - \left(\frac{h_b + h_s}{2}\right) [N_\theta] \\ [N_{uv}] &= \frac{1}{2}([N_{uc}] + [N_{ub}]) + \left(\frac{h_c - 2h_s - h_b}{4}\right) [N_\theta] \\ [N_{\gamma s}] &= \left[\frac{1}{h_s} ([N_{uc}] - [N_{ub}]) + \left(\frac{h_c + 2h_s + 2h_v + h_b}{4}\right) [N_\theta] \right] \left(\frac{G_v/G_s}{h_v/h_s + G_v/G_s} \right) \end{aligned}$$

$$[N_{\gamma v}] = \left[\frac{1}{h_s} ([N_{uc}] - [N_{ub}]) + \left(\frac{h_c + 2h_s + 2h_v + h_b}{4}\right) [N_\theta] \right] \left(\frac{1}{h_v/h_s + G_v/G_s} \right)$$

$$[N_{L Spring}] = [N_{uc}]_{x=0} - [N_{ub}]_{x=0} + h [N_\theta]_{x=0}$$

$$[N_{R Spring}] = [N_{uc}]_{x=L} - [N_{ub}]_{x=L} + h [N_\theta]_{x=L}$$

In all the above expressions, y_b is replaced by $hb/2$ with almost no loss of accuracy.

5.1.3 Energies of the enhanced ACLD treatment using SOL System

Kinetic energy (T), strain energy (V) and as well as the work done (W) by external transverse load, piezoelectric forces and moments are discussed below:

5.1.3.1 Kinetic Energies

The total kinetic energy of the complete system comprises the kinetic energies of constraining layer, base beam, VEM layer, the SOL layer, sensor layer and the edge elements. For each individual part it is given below:

5.1.3.1.1 Active constraining layer

For one dimensional structure with uni-axial loading, the constitutive equations of PZT material can be written as:

$$\begin{bmatrix} \boldsymbol{\varepsilon} \\ \mathbf{D} \end{bmatrix} = \begin{bmatrix} S^E_{11} & d_{31} \\ d_{31} & \varepsilon^\tau_{33} \end{bmatrix} \begin{bmatrix} \boldsymbol{\sigma} \\ \mathbf{E} \end{bmatrix} \quad (5.10)$$

Where \mathbf{D} is the electrical displacement, \mathbf{E} is the electric field, $\boldsymbol{\varepsilon}$ is the mechanical strain in x direction, and $\boldsymbol{\sigma}$ is the mechanical stress in x direction. S^E_{11} is the elastic compliance constant, ε^τ_{33} is the dielectric constant, and d_{31} is the piezoelectric constant.

The kinetic energy of the constraining layer due to axial displacement for a single element is:

$$\mathbf{T}_{c1} = \frac{1}{2} \rho_c h_c b \int_0^{L_e} \left(\frac{\partial u_c}{\partial t} \right)^2 dx = \frac{1}{2} \{ \dot{U} \}_e^T [M_{cu}]_e \{ \dot{U} \}_e \quad (5.11)\{a, b\}$$

$$\text{Where } [M_{cu}]_e = \rho_c h_c b \int_0^{L_e} [N_{uc}]^T [N_{uc}] dx$$

The kinetic energy of the constraining layer due to transverse displacement is:

$$\mathbf{T}_{c2} = \frac{1}{2} \rho_c h_c b \int_0^{L_e} \left(\frac{\partial w}{\partial t} \right)^2 dx = \frac{1}{2} \{ \dot{U} \}_e^T [M_w]_e \{ \dot{U} \}_e \quad (5.12)\{a, b\}$$

$$\text{Where } [M_{cw}]_e = \rho_c h_c b \int_0^{L_e} [N_w]^T [N_w] dx$$

5.1.3.1.2 Base beam

The kinetic energy of the base beam due to axial displacement is:

$$\mathbf{T}_{b1} = \frac{1}{2} \rho_b h_b b \int_0^{L_e} \left(\frac{\partial u_b}{\partial t} \right)^2 dx = \frac{1}{2} \{ \dot{U} \}_e^T [M_{bu}]_e \{ \dot{U} \}_e \quad (5.13)\{a, b\}$$

$$\text{Where } [M_{bu}]_e = \rho_b h_b b \int_0^{L_e} [N_{ub}]^T [N_{ub}] dx$$

The kinetic energy of the constraining layer due to transverse displacement is:

$$\mathbf{T}_{b2} = \frac{1}{2} \rho_b h_b b \int_0^{L_e} \left(\frac{\partial w}{\partial t} \right)^2 dx = \frac{1}{2} \{ \dot{U} \}_e^T [M_w]_e \{ \dot{U} \}_e \quad (5.14)\{a, b\}$$

$$\text{Where } [M_{bw}]_e = \rho_b h_b b \int_0^{L_e} [N_w]^T [N_w] dx$$

5.1.3.1.3 VEM layer

The kinetic energy of the VEM layer due to axial displacement is:

$$\mathbf{T}_{v1} = \frac{1}{2} \rho_v h_v b \int_0^{L_e} \left(\frac{\partial u_v}{\partial t} \right)^2 dx = \frac{1}{2} \{ \dot{U} \}_e^T [M_{vu}]_e \{ \dot{U} \}_e \quad (5.15)\{a, b\}$$

$$\text{Where } [M_{vu}]_e = \rho_v h_v b \int_0^{L_e} [N_{uv}]^T [N_{uv}] dx$$

The kinetic energy of the VEM layer due to transverse displacement is:

$$\mathbf{T}_{v2} = \frac{1}{2} \rho_v h_v b \int_0^{L_e} \left(\frac{\partial w}{\partial t} \right)^2 dx = \frac{1}{2} \{ \dot{U} \}_e^T [M_{vw}]_e \{ \dot{U} \}_e \quad (5.16)\{a, b\}$$

$$\text{Where } [M_{vw}]_e = \rho_v h_v b \int_0^{L_e} [N_w]^T [N_w] dx$$

5.1.3.1.4 Stand-off layer

The kinetic energy of the SOL layer due to axial displacement is:

$$\mathbf{T}_{s1} = \frac{1}{2} \rho_s h_s b \int_0^{L_e} \left(\frac{\partial u_s}{\partial t} \right)^2 dx = \frac{1}{2} \{ \dot{U} \}_e^T [M_{su}]_e \{ \dot{U} \}_e \quad (5.17)\{a,b\}$$

$$\text{Where } [M_{su}]_e = \rho_s h_s b \int_0^{L_e} [N_{us}]^T [N_{us}] dx$$

The kinetic energy of the SOL layer due to transverse displacement is:

$$\mathbf{T}_{s2} = \frac{1}{2} \rho_s h_s b \int_0^{L_e} \left(\frac{\partial w}{\partial t} \right)^2 dx = \frac{1}{2} \{ \dot{U} \}_e^T [M_{sw}]_e \{ \dot{U} \}_e \quad (5.18)\{a,b\}$$

$$\text{Where } [M_{sw}]_e = \rho_s h_s b \int_0^{L_e} [N_w]^T [N_w] dx$$

5.1.3.1.5 Sensor layer

The kinetic energy of the sensor layer due to axial displacement is:

$$\mathbf{T}_{PV1} = \frac{1}{2} \rho_{PV} h_{PV} b \int_0^{L_e} \left(\frac{\partial u_b}{\partial t} \right)^2 dx = \frac{1}{2} \{ \dot{U} \}_e^T [M_{PVu}]_e \{ \dot{U} \}_e \quad (5.19)\{a,b\}$$

$$\text{Where } [M_{PVu}]_e = \rho_{PV} h_{PV} b \int_0^{L_e} [N_{ub}]^T [N_{ub}] dx$$

The kinetic energy of the sensor layer due to transverse displacement is:

$$\mathbf{T}_{PV2} = \frac{1}{2} \rho_{PV} h_{PV} b \int_0^{L_e} \left(\frac{\partial w}{\partial t} \right)^2 dx = \frac{1}{2} \{ \dot{U} \}_e^T [M_{PVw}]_e \{ \dot{U} \}_e \quad (5.20)\{a,b\}$$

$$\text{Where } [M_{PVw}]_e = \rho_{PV} h_{PV} b \int_0^{L_e} [N_w]^T [N_w] dx$$

Where ρ is the density, h is the beam thickness and b is the width of the layer.

5.1.3.2 Potential Energies

The total potential energy of the complete system comprises the strain energies of constraining layer, base beam, VEM layer, SOL layer, sensor layer and springs (i.e. anchors or edge elements). For each individual part it is given as below:

5.1.3.2.1 Active constraining layer

The potential energy of the constraining layer due to axial displacement is:

$$\mathbf{V}_{c1} = \frac{1}{2} E_c h_c b \int_0^{L_e} \left(\frac{\partial u_c}{\partial x} \right)^2 dx = \frac{1}{2} \{ U \}_e^T [K_{cu}]_e \{ U \}_e \quad (5.21)\{a, b\}$$

$$\text{Where } [K_{cu}]_e = E_c h_c b \int_0^{L_e} [N_{uc}]'^T [N_{uc}]' dx$$

The potential energy of the constraining layer due to transverse displacement is:

$$\mathbf{V}_{c2} = \frac{1}{2} E_c I_c \int_0^{L_e} \left(\frac{\partial^2 w}{\partial x^2} \right)^2 dx = \frac{1}{2} \{ U \}_e^T [K_{cw}]_e \{ U \}_e \quad (5.22)\{a, b\}$$

$$\text{Where } [K_{cw}]_e = E_c I_c \int_0^{L_e} [N_w]''^T [N_w]'' dx$$

5.1.3.2.2 Base beam

The potential energy of the base beam due to axial displacement is:

$$\mathbf{V}_{b1} = \frac{1}{2} E_b h_b b \int_0^{L_e} \left(\frac{\partial u_b}{\partial x} \right)^2 dx = \frac{1}{2} \{ U \}_e^T [K_{bu}]_e \{ U \}_e \quad (5.23)\{a, b\}$$

$$\text{Where } [K_{bu}]_e = E_b h_b b \int_0^{L_e} [N_{ub}]'^T [N_{ub}]' dx$$

The potential energy of the base beam due to transverse displacement is:

$$\mathbf{V}_{b2} = \frac{1}{2} E_b I_b \int_0^{L_e} \left(\frac{\partial^2 w}{\partial x^2} \right)^2 dx = \frac{1}{2} \{ U \}_e^T [K_{bw}]_e \{ U \}_e \quad (5.24)\{a,b\}$$

$$\text{Where } [K_{bw}]_e = E_b I_b \int_0^{L_e} [N_w]''^T [N_w]'' dx$$

5.1.3.2.3 VEM layer

The potential energy of the VEM layer is:

$$\mathbf{V}_v = \frac{1}{2} G_v h_v b \int_0^{L_e} \gamma_v^2 v \, dx = \frac{1}{2} \{\mathbf{U}\}_e^T [\mathbf{K}_{vv}] \{\mathbf{U}\}_e \quad (5.25)\{a, b\}$$

Where $[\mathbf{K}_{vv}]_e = G_v h_v b \int_0^{L_e} [N_{vv}]^T [N_{vv}] \, dx$

5.1.3.2.4 Stand-off layer

The potential energy of the SOL layer is:

$$\mathbf{V}_s = \frac{1}{2} G_s h_s b \int_0^{L_e} \gamma_s^2 s \, dx = \frac{1}{2} \{\mathbf{U}\}_e^T [\mathbf{K}_{ss}] \{\mathbf{U}\}_e \quad (5.26)\{a, b\}$$

Where $[\mathbf{K}_{ss}]_e = G_s h_s b \int_0^{L_e} [N_{ss}]^T [N_{ss}] \, dx$

5.1.3.2.5 Sensor layer

The potential energy of the sensor due to axial displacement is:

$$\mathbf{V}_{PV1} = \frac{1}{2} E_{PV} h_{PV} b \int_0^{L_e} \left(\frac{\partial u_p}{\partial x} \right)^2 dx = \frac{1}{2} \{\mathbf{U}\}_e^T [\mathbf{K}_{PVu}]_e \{\mathbf{U}\}_e \quad (5.27)\{a,b\}$$

Where $[\mathbf{K}_{PVu}]_e = E_{PV} h_{PV} b \int_0^{L_e} [N_{ub}]'^T [N_{ub}]' dx$

The potential energy of the sensor layer due to transverse displacement is:

$$\mathbf{V}_{PV2} = \frac{1}{2} E_{PV} I_{PV} \int_0^{L_e} \left(\frac{\partial^2 w}{\partial x^2} \right)^2 dx = \frac{1}{2} \{\mathbf{U}\}_e^T [\mathbf{K}_{PVw}]_e \{\mathbf{U}\}_e \quad (5.28)\{a,b\}$$

Where $[\mathbf{K}_{PVw}]_e = E_{PV} I_{PV} \int_0^{L_e} [N_w]''^T [N_w]'' dx$

5.1.3.2.6 Edge elements or springs

The deformations in edge elements are given by Eqn. 5.6.

The potential or strain energy stored in the springs is given as:

$$V_k = \frac{1}{2} k_L (\Delta x_L)^2 + \frac{1}{2} k_R (\Delta x_R)^2 = \frac{1}{2} \{\mathbf{U}\}_e^T [\mathbf{k}_{L\ spring}]_e \{\mathbf{U}\}_e + \frac{1}{2} \{\mathbf{U}\}_e^T [\mathbf{k}_{R\ spring}]_e \{\mathbf{U}\}_e \quad (5.29)\{a,b\}$$

Where $[\mathbf{k}_{L\ spring}]_e = k_L \int_0^{L_e} [N_{L\ spring}]^T [N_{L\ spring}] \, dx$

and $[\mathbf{k}_{R\ spring}]_e = k_R \int_0^{L_e} [N_{R\ spring}]^T [N_{R\ spring}] \, dx$

5.1.4 Work Done

Forces exerted on the system are:

a) The externally applied mechanical force.

b) The piezoelectric force developed by the PZT patch.

The work done \mathbf{W}_1 by the external transverse load f_d acting on the beam/ACLD system for a single element is given as:

$$W_1 = \int_0^{L_e} f_d w(x, t) \, dx = \{\mathbf{U}\}_e^T f_d$$

Where $f_d = f \int_0^{L_e} [N_w]^T$ (5.30)\{a, b\}

The work done \mathbf{W}_2 by the piezoelectric control forces and moments are given as:

$$W_2 = E_c A_c \int_0^{L_e} \left[\varepsilon_{piezo} \left(\frac{\partial u_c(x, t)}{\partial x} \right) + h \varepsilon_{piezo} \left(\frac{\partial^2 w(x, t)}{\partial x^2} \right) \right] dx \quad (5.30)\{c\}$$

Where ε_{piezo} denotes the strain introduced by the piezoelectric effect and is given as:

$$\varepsilon_{piezo} = \frac{d_{31} v_a \|_e}{h_c}$$

Here $v_a \parallel_e$ is the applied voltage to the piezoelectric actuator. The work done can now be written as:

$$\begin{aligned} W_2 &= E_c d_{31b} v_a \parallel_e \int_0^{L_e} \left(\frac{\partial u_c}{\partial x} \right) dx + h E_c d_{31b} v_a \parallel_e \int_0^{L_e} \left(\frac{\partial^2 w(x)}{\partial x^2} \right) dx \\ &= E_c d_{31b} v_a \parallel_e \int_0^{L_e} [N_{uc}]^T dx \{U\}_e^T + h E_c d_{31b} v_a \parallel_e \int_0^{L_e} [N_w]^T dx \{U\}_e^T \\ &= (\{f_{c1}\}_e + \{f_{c2}\}_e) \{U\}_e^T \end{aligned} \quad (5.31) \{a\}$$

Where $\{f_{c1}\}_e = E_c d_{31b} v_a \parallel_e \int_0^{L_e} [N_{uc}]^T dx = E_c d_{31b} v_a \parallel_e [0 \ 0 \ 0 \ -1 \ 0 \ 0 \ 0 \ 1]^T$
and $\{f_{c2}\}_e = h E_c d_{31b} v_a \parallel_e \int_0^{L_e} [N_w]^T dx = h E_c d_{31b} v_a \parallel_e [0 \ -1 \ 0 \ 0 \ 0 \ 1 \ 0 \ 0]^T$

5.1.5 Pure Beam Elements

The stiffness and mass matrices of pure beam elements have dimensions of 6x6, and are similar to those given by Eqn. 5.9.

5.1.6 Equations of Motion

Using Hamilton's principle, the equations of motion for an EACLDSOL element can be written as discussed in the following sub-sections:

5.1.6.1 Open Loop Conditions

$$\begin{aligned} [M]_e \{\ddot{U}\}_e + [K]_e \{U\}_e + [K_{vy} + K_{sy}]_e \{U\}_e &= \{f_d\}_e + \{f_{c1}\}_e + \{f_{c2}\}_e \quad (5.32) \{a\} \\ [M]_e &= ([M_{bu}]_e + [M_{bw}]_e) + [M_{cu}]_e + [M_{cw}]_e \dots \dots \\ &\quad = ([M_{su}]_e + [M_{sw}]_e) + [M_{vu}]_e + [M_{vw}]_e + [M_{PVu}]_e + [M_{PVw}]_e \quad \underbrace{\qquad}_{(5.32)\{b, c\}} \\ [K]_e &= ([K_{bu}]_e + [K_{bw}]_e) + [K_{cu}]_e + [K_{cw}]_e \dots \dots \\ &\quad = ([K_{su}]_e + [K_{sw}]_e) + [K_{vu}]_e + [K_{vw}]_e + [K_{PVu}]_e + [K_{PVw}]_e \quad \underbrace{\qquad}_{(5.32)\{b, c\}} \end{aligned}$$

For a simply supported beam with distributed EACLDSOL elements, through standard FEM assembling procedure with appropriate boundary conditions, the following global dynamic equation can be derived:

$$[M]\{\ddot{U}\} + [K]\{U\}_e = \{F_d + F_{c1} + F_{c2}\} \quad (5.32)\{d\}$$

5.1.6.2 Closed Loop Conditions

With proportional derivative controller, the relationship between actuator voltage (v_a) and sensor voltage (v_s) is given as:

$$v_a(t) = -K_p v_s(t) - K_d \frac{dv_s(t)}{dt} \quad (5.33)$$

Where K_p and K_d are proportional and derivative control gains, respectively. v_s for a uniform sensor is obtained from the following formula:

$$v_s = -\frac{k_{31}^2 D_d b}{g_{31} C} \int_0^{L_e} \frac{\partial^2 w}{\partial x^2} dx \quad (5.34)$$

Where k_{31} is the electromechanical coupling factor, D_d is the distance from the neutral axis to sensor surface. g_{31} is piezoelectric voltage constant. The capacitance C of the sensor is given by:

$$C = \frac{8.854 \times 10^{-12} A_s k_{3t}}{h_b} \quad (5.35)$$

Where A_s is the sensor area and k_{3t} is the dielectric constant. Substitution of Eqs. 5.36-5.38 into Eq. 5.32 gives:

$$\{f_{c1}\}_e = k_p [0 \ 0 \ 0 - 1 \ 0 \ 0 \ 0 \ 1]^T \begin{bmatrix} 0 & -\frac{g}{2} & 0 & 0 & 0 & \frac{g}{2} & 0 & 0 \end{bmatrix} \{U\}_e \quad (5.36)\{a\}$$

$$\{f_{c2}\}_e = k_p [0 \ -1 \ 0 \ 0 \ 0 \ 1 \ 0 \ 0]^T \begin{bmatrix} 0 & -\frac{gh}{2} & 0 & 0 & 0 & \frac{gh}{2} & 0 & 0 \end{bmatrix} \{U\}_e \quad (5.36)\{b\}$$

Where g is defined as:

$$g = \frac{E_c b^2 d_{31} k^2_{31} D_d}{g_{31} C}$$

Expressing $\{f_{c1}\}_e$ and $\{f_{c2}\}_e$ in terms of displacement feedback gain matrix $[G_p]_e$ yields:

$$\{f_{c1}\}_e + \{f_{c2}\}_e = -[G_p]_e \{U\}_e \quad (5.37)\{a\}$$

$$\text{Where } [G_p]_e = -K_p(C_1 + C_2)$$

Where constants C_1 and C_2 are given by following relations:

$$C_1 = [0 \ 0 \ 0 \ -1 \ 0 \ 0 \ 0 \ 1]^T \begin{bmatrix} 0 & -\frac{g}{2} & 0 & 0 & 0 & \frac{g}{2} & 0 & 0 \end{bmatrix}$$

and

$$C_2 = [0 \ -1 \ 0 \ 0 \ 0 \ 1 \ 0 \ 0]^T \begin{bmatrix} 0 & -\frac{gh}{2} & 0 & 0 & 0 & \frac{gh}{2} & 0 & 0 \end{bmatrix}$$

Substituting the global form of Eqn. 5.37 into Eqn. 5.32, the closed loop equation of motion for the system becomes:

$$[M]\{\ddot{U}\} + [K + G_p]\{U\} = \{0\} \quad (5.38)$$

The eigen value problem associated with Eqn. 5.38 is:

$$\{[M] \omega^{*2} + [K + G_p]\} = \{0\} \quad (5.39)$$

The Eigen frequencies will be complex since there is a complex shear modulus in VEM and SOL layer material. After the complex Eigen frequencies have been found, the modal frequencies and the loss factors of the system can be calculated as follows:

$$\omega = \sqrt{Re(\omega^{*2})}$$

$$\eta = \frac{Im[(\omega^{*2})]}{Re[(\omega^{*2})]} \quad (5.40)\{a, b\}$$

5.2 RESULTS AND DISCUSSION

5.2.1 Comparisons with previous study results

Table 5.1 shows the comparison between results from previous studies and present method for frequencies and modal loss factors. There is quite a close map between the results showing the correctness of the code developed and accuracy of the FEM technique w.r.t. other methods.

Table 5.1: Comparison between results from previous studies and present method for frequencies and modal loss factors

Mode No.	Frequencies (rad/s)		Loss factors	
	Results from previous studies	Results from Present method	Results from previous studies	Results from Present method
1	65.02	65.01	0.0816	0.0818
2	299.66	299.59	0.072	0.0723
3	750.34	750.26	0.0462	0.0464
4	1405.55	1406.09	0.0267	0.0268
5	2280.98	2283.78	0.0173	0.0172
6	3379.28	3386.27	0.0118	0.0117
7	4715.02	4723.24	0.0086	0.0084
8	6243.78	6303.95	0.0065	0.0063

To validate the results of present PCLD treatment, one example given by previous researchers has been taken in this study. A uniform symmetrical three-layer damped sandwich beam with clamped – free boundary conditions is taken. Many authors have analyzed this sandwich beam by using various methods. The material for the base beam and the covering layer is the same with Young's Modulus of elasticity as 7.037×10^{10} N/m² and Poisson's ratio as 0.3. Density of both the layers is 2770 Kg/m³. Thickness of base and constraining layer is 1.52 mm. Shear modulus and loss factor of the core material is 7.037×10^5 N/m² and 0.3 respectively. Density and thickness of the core material is 970 Kg/m³ and 0.127 mm respectively. The length and width of the beam is taken as 177.8 mm and 12.7 mm respectively.

5.2.2 Performance with Simple Passive Constraining Layer Damping Treatment

Modal loss factors of the beam are a function of thickness of VEM and thicknesses of the constraining layer. As the thickness increases, the first modal loss factor increases, while the other modal loss factors decrease. For the purpose of brevity the results are not shown here. But after analyzing the first modal loss factor minutely, it was clear that there is a marginal increase in loss factor beyond 0.5 mm thick VEM layer at higher thicknesses of constraining layer. Thus, it is advisable to take VEM layer of very small thickness. The thickness of the constraining layer also plays an important role. At higher thickness loss factor becomes higher, but the natural frequencies are changed to a larger extent by increasing the thickness of the constraining layer. The optimal value of the thickness should be chosen by considering both the factors.

It has been found that all the loss factors are dependent on the shear modulus of the VEM layer. As this shear modulus increases, the loss factors are dramatically increased up to a critical value. Beyond that it starts decreasing. Thus, the VEM having comparatively higher values of shear modulus are of much importance. The modal frequencies are changed by a large value at high shear modulus of VEM layer and modulus of elasticity of constraining layer (results are not shown). These effects are tolerable if the shear modulus of VEM layer is less than 1×10^7 N/m², which is usually the case in normal practice.

5.2.3 Performance with the Addition of SOL Layer to Passive Constraining Layer Damping Treatment

Figure 5.4 shows the effect of SOL layer shear modulus on the modal loss factors. In the present work, a SOL layer is added on the base beam and after that the VEM layer is pasted on it. The constraining layer is then glued on the VEM layer. If the material of the SOL layer is same as of VEM layer, it will increase the thickness of VEM layer. It will decrease all modal loss factors except the first mode. The improvement for this mode is only up to certain limit and after that damping performance decreases. It is not desirable. But, by increasing the modulus of rigidity (shear modulus) of the SOL layer, damping performance is enhanced dramatically.

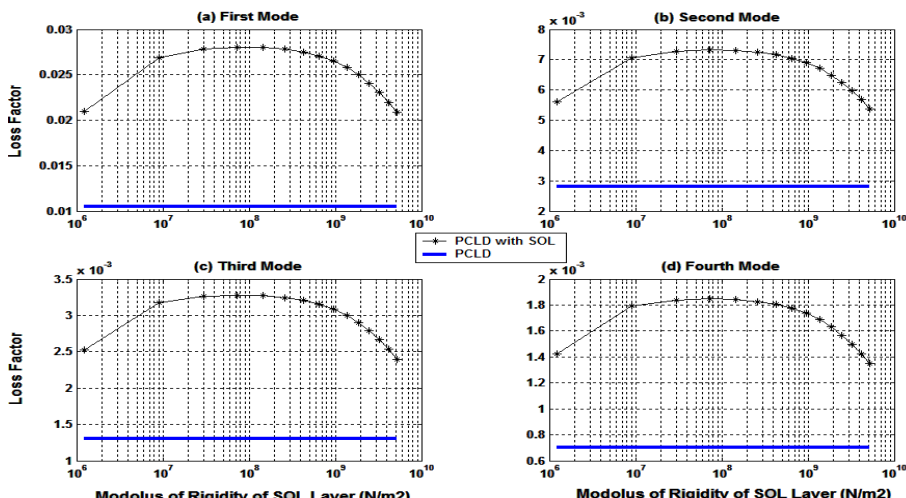


Fig. 5.4: Various modal loss factors as a function of modulus of rigidity of SOL layer (thickness of SOL=2 mm)

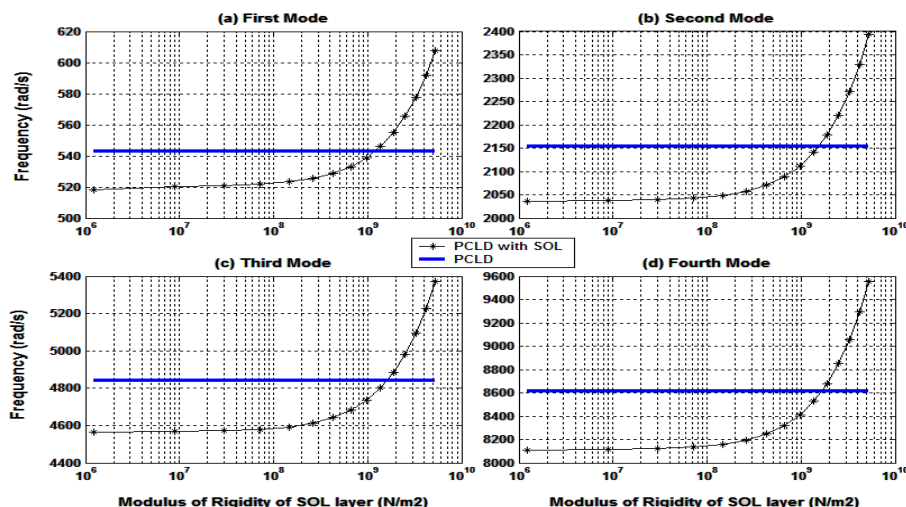


Fig. 5.5: Various modal frequencies as a function modulus of rigidity of SOL layer

The corresponding effect on the modal frequencies is shown in above Figure 5.5. The thickness of SOL layer in this particular case was selected as 2 mm. The modulus of rigidity of VEM layer was chosen to be $0.896 \times 10^5 \text{ N/m}^2$. It is clear from the figure that optimal results are obtained if the modulus of rigidity of SOL layer is 1000 times that of VEM layer (Figure 5.6). An increase in loss factor by 280%, 250%, 246% and 264% for first, second, third and fourth mode respectively was obtained.

All the modal frequencies increase with increase in the shear modulus of SOL layer. These values match with ordinary PCLD treatment when the value of shear modulus of SOL layer is in the range 0.8×10^9 to $1.1 \times 10^9 \text{ N/m}^2$. Afterwards, the effect of the shear modulus of VEM layer was investigated. By increasing shear modulus of VEM layer, damping performance was enhanced (not shown due to brevity). The thickness of the SOL layer was set to be 1mm for this set of readings. With shear modulus of VEM layer as $1 \times 10^7 \text{ N/m}^2$ maximum performances were achieved. But, the modal frequencies shoot up from their previous values. With shear modulus of VEM layer as $1 \times 10^6 \text{ N/m}^2$ the modal frequencies do not vary much and hence is the optimal choice.

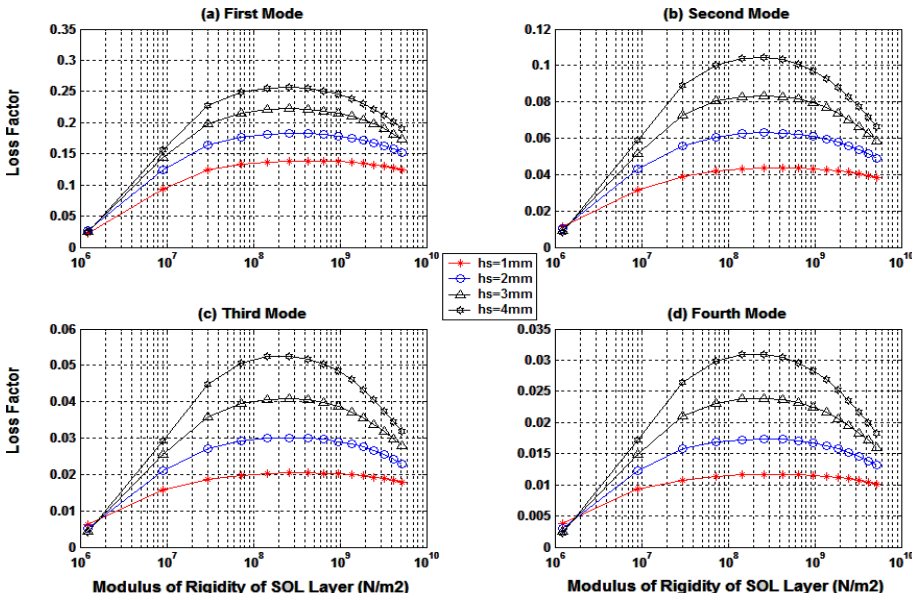


Fig. 5.6: Various modal loss factors as a function of Modulus of Rigidity of SOL layer at different thicknesses of SOL Layer

It is also fortunate that as the shear modulus of SOL layer increases, the effect of thickness of SOL layer on the natural frequencies becomes minimum (results not plotted due to brevity) except for the first mode. Edge stiffeners decrease the modal loss factor (Figure 5.7) of the PCLD system.

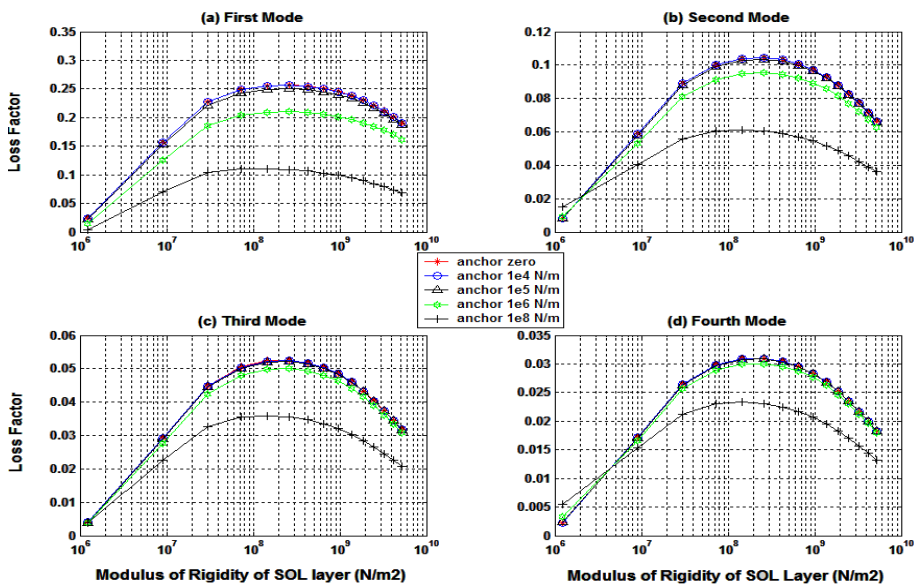


Fig. 5.7: Various loss factors as a function of modulus of rigidity of SOL layer at different stiffnesses of anchors

On the other hand, the natural frequencies were increased by using anchors. This is because of the reason that in the presence of anchors, it becomes difficult to deform the VEM and SOL layers. The beam system becomes stiffer and the natural frequencies increase. At this time, it will be felt that anchors are useless. Only at very high values of feedback gains, when active control action comes into picture their role will become obvious.

5.2.4 Performance with Simple Active Constraining Layer Damping Treatment

In this section the performance of the system with ACLD treatment is checked. First of all the ACLD system without SOL layer is investigated. Table 5.2 shows the electrical properties of the PZT and PVDF materials. PVDF layer of 0.06mm is attached on the lower side of the base beam as shown in Figure 5.1. Effect of this layer on the damping performance of the beam/PCLD system is negligible. Anchors with stiffness 1×10^6 N/m² give optimal results. By the action of active control by PZT material, the passive control action can be enhanced. It is practically difficult to employ a constraining layer of PZT of full length as of the base beam due to brittle nature of the piezo ceramics.

Table 5.2: Electrical properties of the sensor and actuator materials

Property	Symbol	Value	
		PZT	PVDF
Piezoelectric charge constant (m V ⁻¹)	d ₃₁	171×10^{-12}	22×10^{-12}
Electromechanical Coupling factor	k ₃₁	-	0.12
Piezoelectric voltage constant (VmN ⁻¹)	g ₃₁	-	216×10^{-3}
Dielectric constant	k _{3t}	-	12

Partial treatment is an attractive solution. A PZT layer of 60 mm is attached (i.e. 20% coverage) starting from simply supported edge of the base beam on the VEM layer. The modal loss factors are increased with increasing feedback gain factor K_p as shown in Figure 5.8.

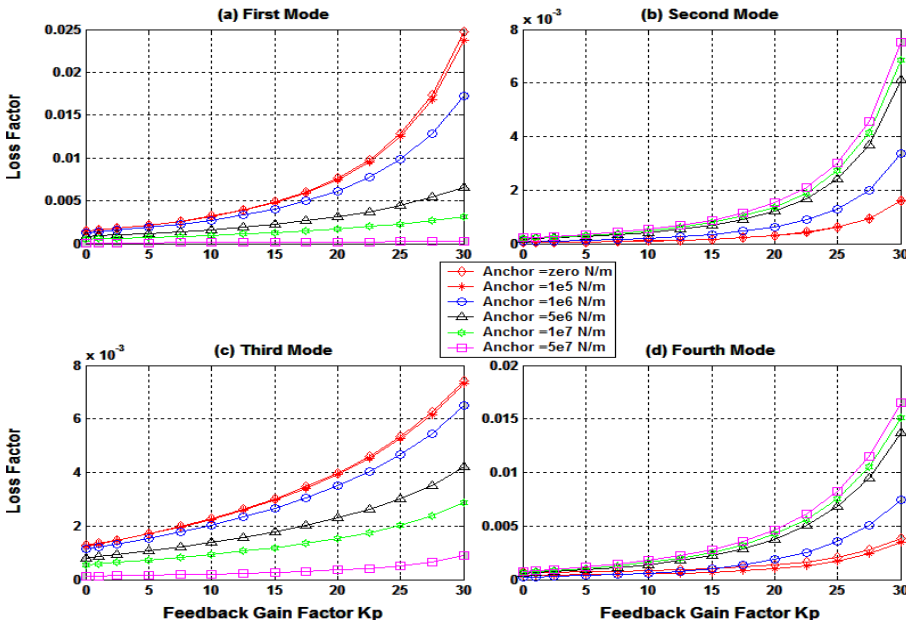


Fig. 5.8: Various modal loss factors as a function of feedback gain K_p at different stiffness of anchors with 20 % coverage

Passive loss factors are much less than for full coverage but with active action (i.e. ACLD beam); loss factors are improved a lot. A VEM layer with $0.896 \times 10^6 \text{ N/m}^2$ shear modulus is chosen for this particular task. The stiffness of the anchors plays a complex role. By increasing the anchor stiffness, only second and fourth modal loss factors are increased. On the other hand, first and third modal loss factor decrease with anchor stiffness. This is not the case with other locations where the PZT layer is glued. Various coverages (i.e. 30% or 40% etc.), locations, and anchor stiffness simultaneously govern the values of various modal losses factors

For a feedback gain factor of 20 (i.e. $K_p=20$) and 100mm long constraining layer (i.e. 33% coverage) the loss factors at various values of anchor stiffness is shown in Figure 5.9. The X-axis of the figure shows the distance of the first edge of the treatment from the simply supported end of the base beam. First and second modal loss factor is maximum without the use of anchors, whereas third and fourth modal loss factor are enhanced at high values of anchor stiffness. Here, it has been observed that at lower feedback gains anchors decrease the modal loss factor of first two modes although third and fourth modal loss factor improves. Thus, very careful use of anchors should be made. Also, depending upon the particular mode of interest, the combination of location and edge stiffness of the anchors should be chosen.

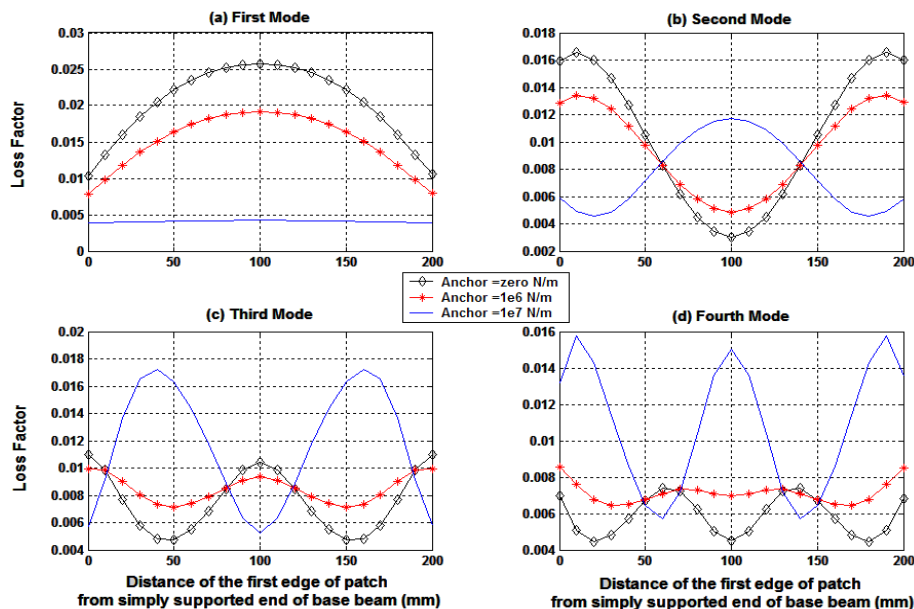


Fig. 5.9: Various modal loss factors as a function of position of ACLD patch at different stiffnesses of anchors with 33 % coverage

5.2.5 Performance with the Addition of SOL Layer to Active Constraining Layer Damping Treatment

To better understand the results, in this case the total loss factor is divided into two parts. First is the active portion and second is the passive portion. The active part of the control action is due to the application of voltage to the PZT patch and is obtained by subtracting the loss factor of the PCLD system from that of ACLD system. To understand the effect of location of the ACLD patch on the damping performance, the location of nodal points (where the modal amplitude is zero) and the points where the modal amplitude is maximum must be analyzed thoroughly. The first mode has no node but maxima at a distance of 150 mm from simply supported end. Second mode has a node at 150 mm and maximum's at 75 mm and 225 mm. Third mode has nodes at 100 mm and 200 mm, but maximum's at 50 mm, 150 mm and 250 mm. The fourth mode has nodes at 75 mm, 150 mm and 225 mm but maximum's at 37.5 mm, 112.5 mm and 187.5 mm. The exact location of these nodes and antinodes is marked on the lower left sub-figure of each main figure from 5.10 to 5.13. On these figures the distance of the first edge of the ACLD patch from the simply supported end of the base beam has been marked. Accordingly, the position of the nodes is changed by 50 mm on all these Figures 5.10- 5.13.

First of all, the ACLD patch without SOL layer is considered as in Figure 5.10. That gives the first modal loss factors as a function of location of the ACLD patch (with and without SOL layer) at different edge stiffnesses. For the first mode, without SOL layer, the passive loss factor as well as active loss factors is maximum at the location where the centre of the patch coincides with the center of the base beam. However, for ACLD patch with SOL layer, the passive loss factor follows the reverse trend i.e. the loss factor becomes minimum as the centre of the patch goes near the center of the base beam.

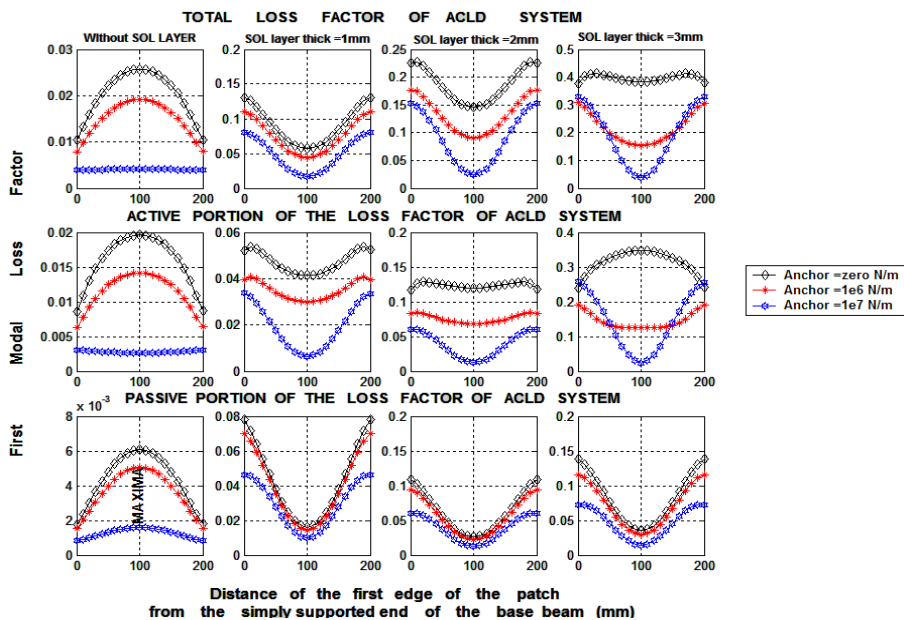


Fig. 5.10: Comparison of active and passive loss factors for first mode as a function of position of ACLD patch (with and w/o SOL layer) at different stiffnesses of anchors with 33% coverage and $K_p = 20$

For the ACLD treatment without SOL layer, the total system follows the same trend as a plain beam. But, as the SOL layer is used, this correlation is lost due to the increased contribution of weight and stiffness of the SOL layer. The active part of the modal loss factor follows the same trend as passive loss factor. At high thickness of SOL, the trend of active portion of the loss factor matches with that of without SOL layer. However, the passive loss factor shows no change in trend as thickness of SOL layer varies. With increase in thickness, the passive as well as active modal loss factor increases. The anchors play a negative role for the first modal loss factor. Hence various factors collectively predict the trend of modal loss factors.

For the second mode (Figure 5.11), the passive loss factor is minimum for a patch without SOL at the nodal point where vibration amplitude is zero. Trend of passive loss factor with and without SOL layer is totally reversing at all the anchor stiffnesses. By the use of SOL layer, the loss factor is maximum when patch is located at the nodal point. Trend of active modal loss factors is also confusing. At lower values of SOL layer thickness, anchors enhance the active portion of the loss factor at certain locations of the patch. But, at higher thickness of SOL layer, anchors play a negative role for all the locations of the patch.

For the third mode (Figure 5.12), without SOL layer, the passive loss factor is minimum at nodal points with small anchor stiffness. Trend of passive loss factor reverses at higher values of stiffness of the anchors.

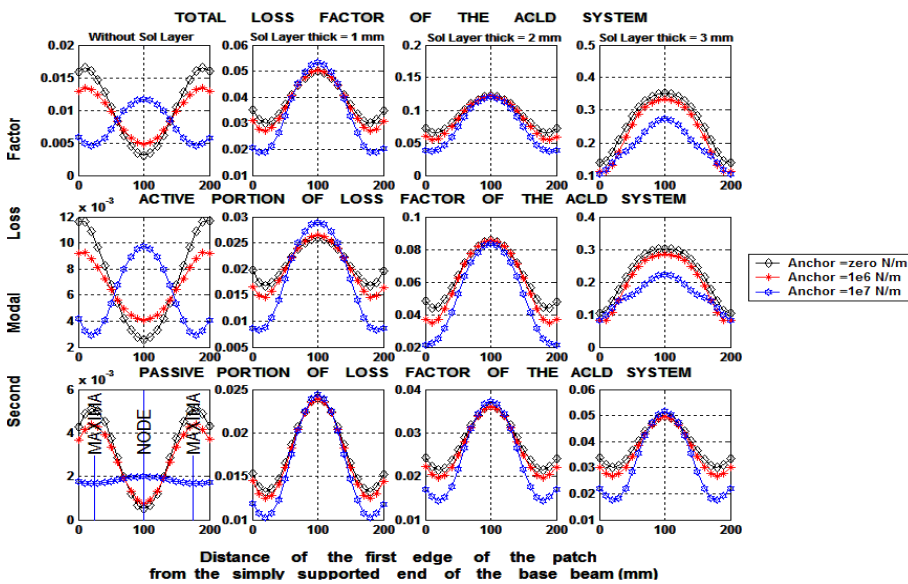


Fig. 5.11: Comparison of active and passive loss factors for second mode as a function of position of ACLD patch (with and w/o SOL layer) at different stiffnesses of anchors with 33% coverage and $K_p = 20$

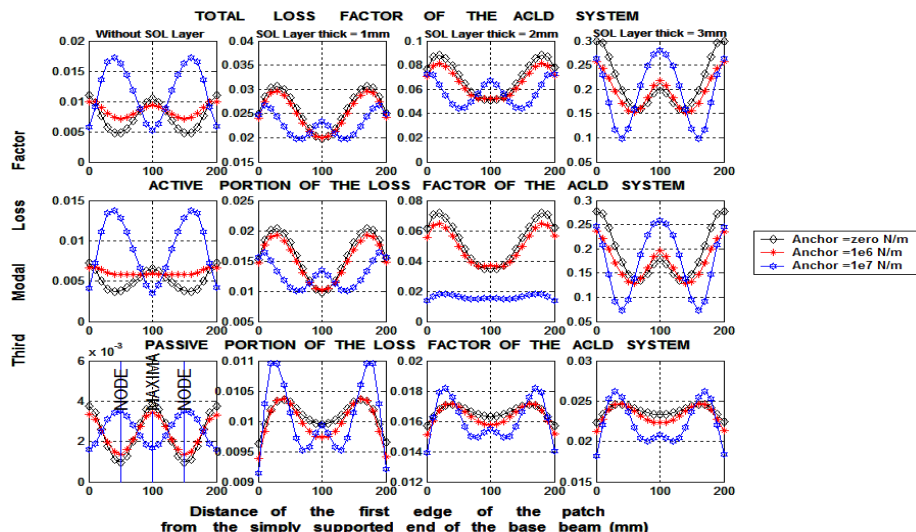


Fig. 5.12: Comparison of active and passive loss factors for third mode as a function of position of ACLD patch (with and w/o SOL layer) at different stiffnesses of anchors with 33% coverage and $K_p = 20$

Active portion of the loss factor is direct function of anchor stiffness. By using a SOL layer, the trend is totally reversed for passive loss factor as compared to the situation when SOL layer and anchors are not used. Same thing happens with active modal loss factor. Both portions of the total loss factor are maximum for a situation when center of the patch lies at the nodal points of the base beam. The application of anchors

reduces the damping performance of the ACLD treatment with SOL layer at certain locations and enhances at certain other locations. For the fourth mode (Figure 5.13), passive loss factor is maximum when the patch without SOL layer is near the nodal point of the base beam with using highly stiff anchors.

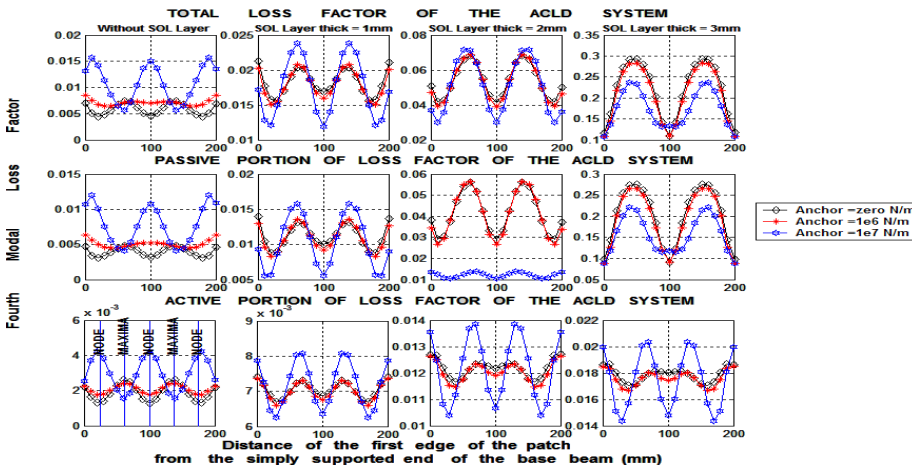


Fig. 5.13: Comparison of active and passive loss factors for fourth mode as a function of position of ACLD patch (with and w/o SOL layer) at different stiffnesses of anchors with 33% coverage and $K_p = 20$

By not using the anchors, the trend reverses. This trend remains the same for the patch with SOL layer. Similarly, the active modal loss factor follows the same trend. Use of anchors, reduce the active as well as passive damping performance at larger thickness of the SOL layer. The overall damping performance reduces at high thickness of the SOL layer using anchors. Although for a simple ACLD system without SOL layer, the third and fourth modal loss factors improve by using anchors, same is not true for a system with SOL layer. Generally, at high values of anchor stiffness, the shear strain (and hence the strain energy) produced decreases. Hence lesser vibration energy is dissipated in shearing process (through VEM and SOL layers), and lesser overall loss factor is achieved. These anchors are useful for the active case (at high values of feedback gain K_p) as these anchors increase the transmissivity of control forces from PZT layers to base beam. The loss factors of the overall flexible system are obtained from Eqn. 5.38. These are the equations of motion of the overall system and are obtained by considering the effect of strain energy stored in the anchors as shown in Eqn. 5.29. At lower values of anchor stiffness, the effect on shear strain is less and hence more energy is dissipated in shearing process (through VEM and SOL layers). Thus, the overall loss factor is less affected.

To decrease the overall loss factor, a comparable value of anchor stiffness should be there. This is the reason that only high values of anchor stiffness affect the overall loss factor of the system significantly.

Ordinarily one may think that as thickness increases the active action will decrease due to less transmissibility of control forces through the viscoelastic layers. However, the modulus of rigidity of SOL layer is almost 10^3 times more than that of VEM layer, so the ACLD system with SOL layer can transmit the control forces effectively. Secondly, the bending moment generated by the PZT layer is a direct function of the

distance between the neutral axis of the PZT layer and the base beam. This distance is quite increased due to the presence of SOL layer. The total active action which is the sum of control forces generated by PZT layer and the control bending moment generated by PZT layer, increases largely due to the increased bending moment generated. Thus, better results can be obtained by the presence of SOL layer and that too without using anchors for beams with SOL layer based ACLD treatment. All the readings are with a feedback gain of 20. As the thickness of SOL layer increases, all the modal loss factors increase by about 300% w.r.t. its previous value. However, at this feedback gain, the ACLD system with SOL layer of 4 mm loses stability (only in numerical calculations). The third and fourth mode gets unstable. Hence maximum value of the feedback gain should not exceed above 16 for this thickness of the SOL layer.

Further, the modal frequencies as a function of location of PCLD patch, anchor stiffness and the thickness of the constraining layer are discussed. The first modal frequency is a function of various parameters. When the center of the ACLD patch reaches near the mid of the base beam the first natural frequency is minimum. Use of anchors increases the stiffness of the beam and hence there is rise in natural frequency. By the addition of the SOL layer, the natural frequency increases and it is minimum when the patch is located at the mid of the beam. When the PCLD patch acts as ACLD beam the corresponding frequency decreases. Similar is the case with other modal frequencies (results are not plotted due to brevity).

It is preferable to have small changes in the natural frequencies with the application of constrained layer damping techniques. With the application of SOL layer, this change is significant for a passive constraining layer. Fortunately, by using active constrained layer, this difference can be minimized at least for lower modes.

Feedback gain has marked effect on modal loss factors. By varying the feedback gain from 4 to 16, modal loss factor increases by a factor of 200%, 300%, 370% and 480% for first, second, third and fourth mode respectively (Figures 5.14 and 5.15).

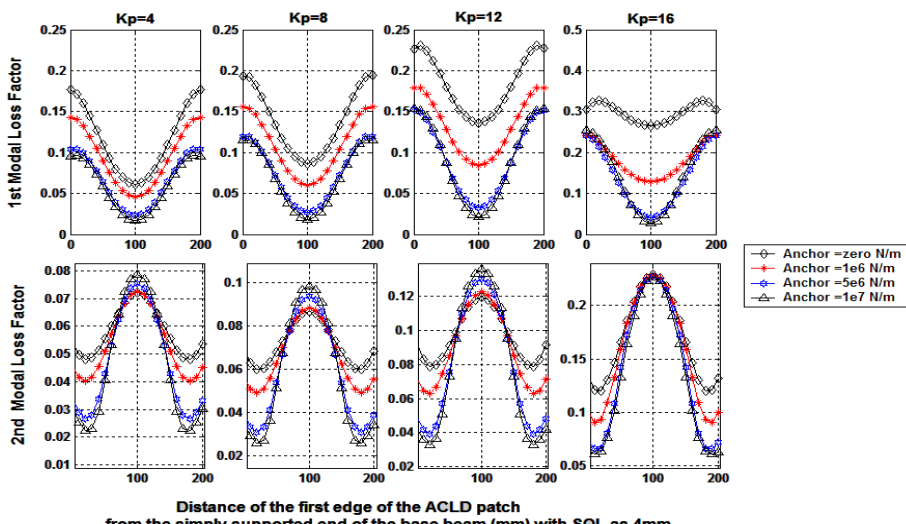


Fig. 5.14: First and Second modal loss function as a function of position of ACLD patch (with SOL layer thickness as 4 mm) at different stiffnesses of anchors at different feedback gain K_p with 33 % coverage

A feedback gain of 20, results in instability of the numerical calculations. In this case, the thickness of the SOL layer was taken as 4mm. First and third mode loss factors were maximum for zero stiffness of the anchors. However, second and fourth modal loss factor were maximum at highest values of anchor stiffness (Figures 5.14 and 5.15).

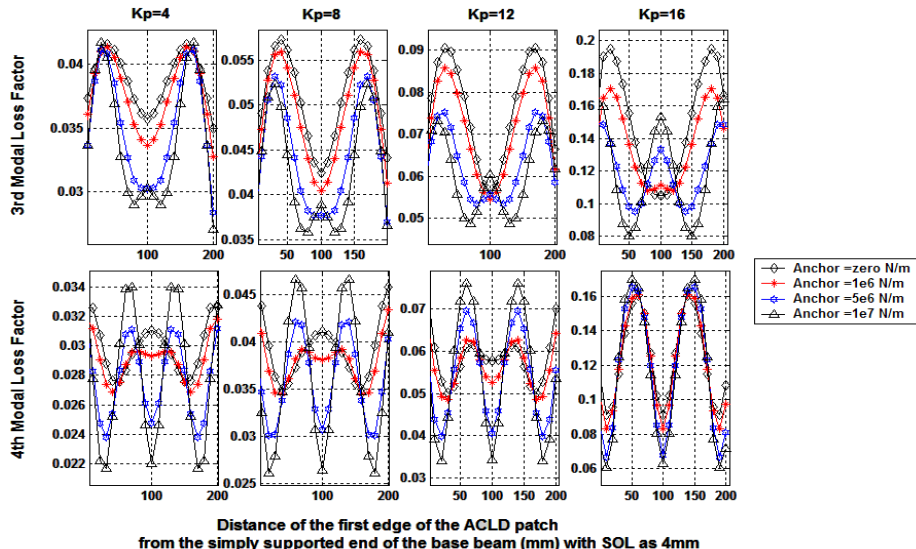


Fig. 5.15: Third and Fourth modal loss function as a function of position of ACLD patch (with SOL layer thickness as 4 mm) at different stiffnesses of anchors at different feedback gain K_p with 33% coverage.

5.3 EXPERIMENTAL VALIDATION

5.3.1 Experimental Setup

To check the authenticity of the theoretical results experimental setup was generated. Figure 5.16 shows the schematics of experimental setup when the validation of the experimentation was done. Photograph 5.1 is also shown on the next page that shows the picture of experimental treated beam. Length of the beam is 300 mm. The other dimensions of various layers are shown in the photograph. However, the PVDF and PZT layer are not shown in the photograph. A passive constraining layer of aluminium of 0.1 mm thickness is shown in the photograph. Length of the treated portion is 60 mm and the treatment is done at the middle of the beam. DYAD 606 and ISD 112 are the professional material names for SOL and VEM layer respectively. For ACLD treatment, a PZT patch of 0.2 mm was attached on the aluminium constraining layer and a PVDF layer of 0.08 mm was attached on the other side of the base beam. The simply

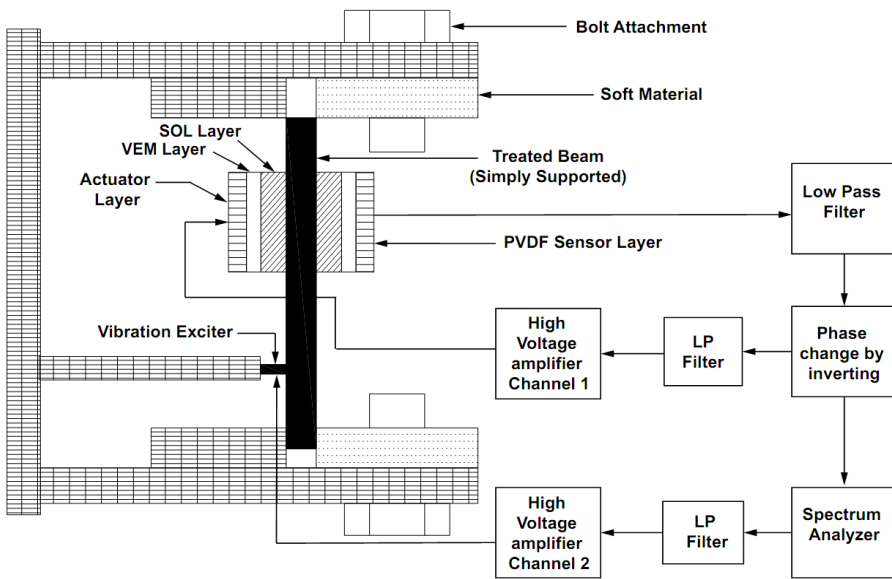
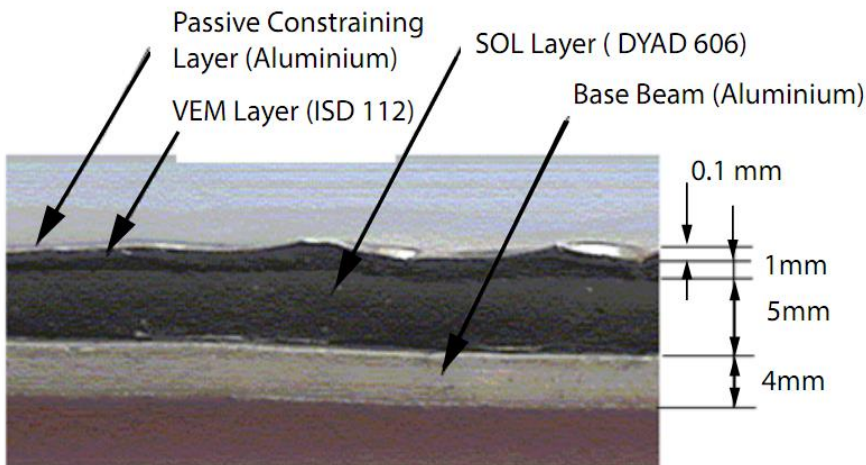


Fig. 5.16: Schematics of the experimental setup

supported beam was clamped with soft rubber like materials on a frame for supporting the beam, so that vertical displacement was restrained only. The beam is capable of deformation in terms of slope at the edges. The voltage from sensor PZT patch was passed to a high voltage amplifier MA-17. A low pass filter with cut-off frequency equal to just above the third resonance frequency of the vibrating structure was applied to remove the influence of higher modes.



Photograph 5.1: Picture of the experimental beam

After inversion and amplification from the first channel of the amplifier, the voltage was directed to the actuator PZT patch. A spectrum analyzer was used to create signals of various frequencies. This signal was amplified from the second channel of the amplifier and was used to actuate the shaker (in the form of point actuator). The modulus of rigidity and density of the base beam for this material is $70 \times 10^9 \text{ N/m}^2$

and 2710 Kg/m^3 respectively. The thickness of the SOL layer and VEM layer was 5 mm and 1 mm respectively. Practically the shear modulus of DYAD 606 (SOL layer material) is 100-300 times that of ISD 112 (VEM layer). Table 5.3 shows the comparison of theoretical and experimental response.

Table 5.3: Comparison of experimental and theoretical frequency response of the beam system using PCLD with SOL treatment

Vibration Characteristics	Mode No.	Theoretical	Experimental	% age Error
Frequencies (Hz)	Mode 1	93.29	91.93	1.46
	Mode 2	455.29	453.9	0.31
	Mode 3	872.51	864.78	0.89
Damping ratios	Mode 1	0.0128	0.012	6.25
	Mode 2	0.0518	0.053	-2.32
	Mode 3	0.012	0.014	-16.67

The experimental results are sufficiently close to theoretical results. The variation between the results is attributed to the reasons that the strain developed in the base beam varies due to lose adhesive bond of the gluing adhesives and the variation in the properties of the PZT, aluminium, VEM, SOL layer material parameters and compressional damping factor which needs addition of separate transverse displacement for the constraining layer. For calculations, the loss factor and shear modulus of the VEM and SOL layer were taken to be constant for small frequency range covering first three modes. This can cause certain deviation of theoretical results from experimental data. Table (5.4) shows the vibration parameters for a proportional feedback gain of 4. For the second mode, the difference between loss factor of the PCLD and ACLD treatment is very less.

This is due to the reason that, the treatment is done at the center of the beam i.e. at the point where the amplitude of vibration is zero for the second mode (node). For this mode, the maximum amplitude of vibration (anti-node) is at a distance of $1/4^{\text{th}}$ of the length of the beam from the simply supported end. The change in slope is minimum (since amplitude is zero) in that region where the patch with SOL layer is located on the base beam. Hence there is minimum effect of active control for this mode (i.e. second mode). Due to this reason the difference between loss factors for PCLD and ACLD treatment is very less.

Table 5.4: Comparison of experimental and theoretical frequency response of the beam system using ACLD with SOL treatment with feedback gain $K_p=4$

Vibration characteristics	Mode No.	Theoretical	Experimental	% age Error
Frequencies (Hz)	Mode 1	88.85	87	2.08
	Mode 2	454.08	451.12	0.65
	Mode 3	841.02	835.1	0.70
Damping ratios	Mode 1	0.0184	0.0181	1.63
	Mode 2	0.0536	0.054	-0.75
	Mode 3	0.0152	0.0161	-5.92

@Seismicisolation

CHAPTER – 6

VIBRATION CONTROL OF ROTATING STRUCTURES WITH ADVANCED METHODS

The widely used smart materials for vibration control in structures are piezoelectric materials since they have desirable characteristics. Based on these characteristics, the previous research on active vibration control presented in earlier chapters of this book was based on the application of piezoelectric materials various researchers to flexible structures. Not fully satisfied with purely active control techniques, this research study has now been directed towards the combination of active and passive techniques. Passive constrained layer damping (PCLD) is an old technique to suppress vibrations. In combination with active control techniques, PCLD treatment can be made even more effective. This technique is called active constrained layer damping (ACLD) treatment.

Active constrained layer damping (ACLD) treatment increases the efficiency of passive constrained layer damping (PCLD) treatment, but in case of circuit failure, only the decreased efficiency of PCLD treatment is available. By adding a stressed poly vinyl chloride (PVC) layer on the base beam, necessary damping can also be provided. Using passive constrained layers on the PVC layers, the efficiency can be made even better than ordinary PCLD treatment. Using an active constraining layer, maximum damping performance can be obtained. Based on this philosophy, theoretical/experimental investigations are carried for rotating beams. Hamilton Principle in conjunction with finite element method is used to derive the non-linear differential equations of motion. Using proportional feedback controllers, the complex closed loop eigen value problem is developed and is solved numerically. The effect of rotational speed of the beam, initial strain and other parameters of the PVC layer is investigated. Present study will be useful for improving the active as well as passive damping performance of rotating structures like helicopter blades, rotorcraft blades and flexible robotic systems. To prove the effectiveness of the new technique, experimental investigations have also been carried out. Present work is based on the development of newer passive techniques, which can enhance the damping performance of PCLD and ACLD systems. PVC layer has certain value of loss factors which can enhance the energy losses of the overall system in the form of damping. This treatment can be named as stressed layer damping as the PVC layer attached was always under stress. Experiments were performed on a cantilever beam. With increase in the initial stress in PVC layers the damping performance was found to increase for the first mode. However, for the rest of modes, the damping performance was found to decrease initially. After certain critical value, the damping ratios of these modes were observed to increase exponentially.

The basic limitation of this treatment is that it can be applied to thin walled structures. For higher thickness structures, more and more value of initial stress is required. This

could be possible at high values of initial strain in PVC layers. Maximum strain up to 1% was tolerable in these materials due to creep limitations. Although the first and second modal damping was enhanced by several times with this technique, the damping ratios of higher modes were very less as compared to ordinary PCLD treatment. This limitation has been removed in the present work by combining the Stressed Layer Damping (SLD) with PCLD and ACLD treatment. The first mode damping ratio decreased slightly with the application of constraining layers but the damping ratio of all other modes improved dramatically. Present work investigates the vibration behavior and control of axial deformation and chord wise bending of a clamped-free rotating flexible beam with partially covered ACLD treatment with stressed PVC layers instead of viscoelastic material (VEM) layers. Since the beam taken is rotating in horizontal plane, gravitational effect and rotary inertia are neglected. The stress strain relationship for the PVC layer is described by complex modulus. Hamilton principle in conjunction with Finite Element Method (FEM) is used to derive the equation of motion. The effect of centrifugal stiffening due to rotation is also considered. Proportional feedback controller is designed for piezo sensor and actuator. The closed loop equation of motion for the system is derived and complex eigen value problem is solved numerically. The effects of different rotating speeds, thickness of PVC layer, and loss factor of PVC layers, initial compressive and tensile strain in PVC layers are studied. The effect of each parameter on the damping ratios and damped natural frequencies is investigated.

The main contribution of the present work is divided into following parts:

1. A Finite Element Method is employed in the present work, so that partial treatment can be accommodated easily for SLD technique which is not easily possible for analytical methods.
2. Effect of initial strain in PVC layers attached to base beam is investigated with combination of PCLD and ACLD treatment which is never considered earlier in literature.
3. Normally, active control increases efficiency of the PCLD system, but it has been investigated that only by using passive techniques (i.e. SLD Treatment) similar increase in efficiency of PCLD system can be made. However, active constrained layer further enhances the damping performance of the overall system.
4. In the work done by a researcher namely Mostafa in 2006, the pre-tensed PVC layers which cause tensile stress in PVC layers are used, here pre-tensioning of base beam which causes compressive stresses in PVC layers is also analyzed which has certain desirable properties w.r.t. the former technique.

6.1 SYSTEM DESCRIPTION AND MODELING

6.1.1 Basic Relationships

The schematic of the rotating beam with ACLD treatment combined with SLD treatment is shown in Figure 6.1.

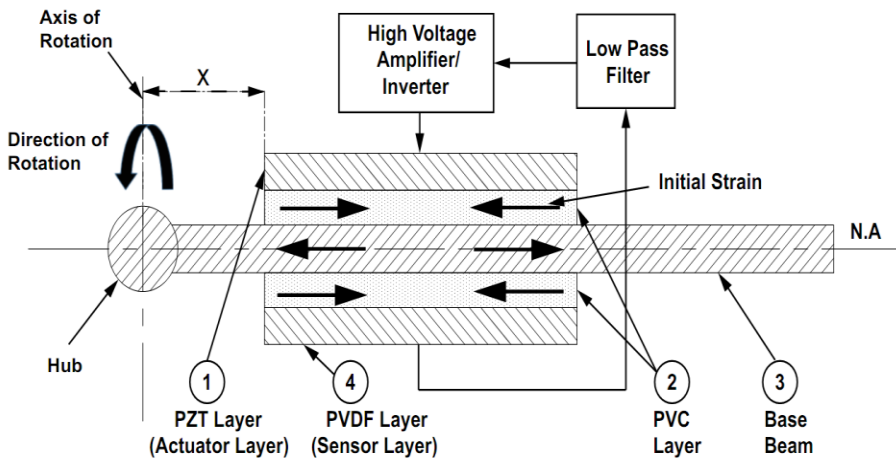


Fig. 6.1: Schematics of structure with ACLD + CoLD/TeLD treatment

The upper and lower surface of host structure or the base beam is attached with a Poly Vinyl Chloride (PVC) layer. Each of the PVC layer in turn is constrained by an active piezoelectric material PZT (Lead Zirconated Titinate). It acts as a constraining layer, a sensor and an actuator. For simplicity, the constrained layer (i.e. PZT patch on one side) is numbered as 1, PVC layer as no. 2, the base beam as no. 3 and sensor layer (i.e. PZT patch on the opposite side of the base beam) as no. 4. Figure 6.2 shows the cross-section of the beam with ACLD treatment combined with SLD treatment.

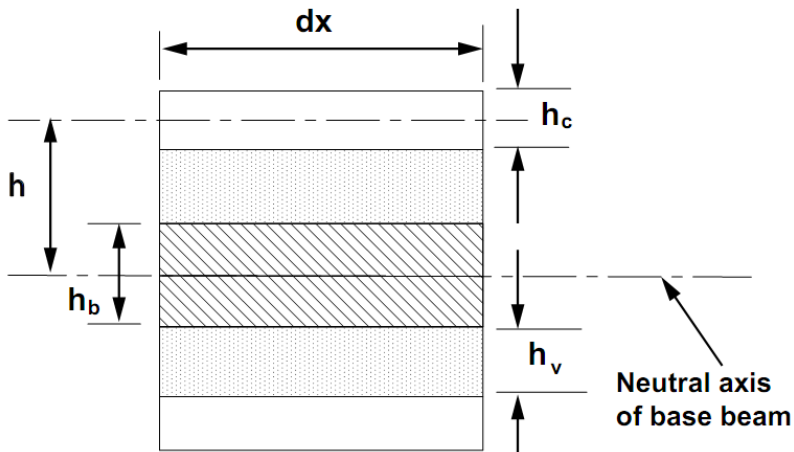


Fig. 6.2: Cross-section of beam with ACLD combined with CoLD treatment (both sides)

The following assumptions are made in deriving the model:

- Face-layers i.e. constraining layers and base beam are purely elastic and suffer no shear deformation normal to the layer faces.
- Inertial effects of transverse flexural motion are dominant while in plane inertia effects are negligible i.e. rotary and axial inertia are negligible.
- Longitudinal displacement u is different for all the layers.

- Transverse displacement w is same for all the layers
- The shear strain in base material and PZT layers is negligible.
- The Poisson's ratio for the PVC layer is taken as zero for analysis purpose.
- Interfaces are perfect i.e. no slip occurs between layers.
- Applied voltage is assumed to be uniform along the PZT.
- Linear theories of elasticity, viscoelasticity and piezoelectricity are valid.

The base beam and constraining layer can be modeled as Euler-Bernoulli beams using first two conditions. For the continuity of displacements at the interface between the layers, the relation between shear angle (strain) and various displacements is given below:

$$\begin{aligned}\varepsilon_1 &= \frac{\partial u_1}{\partial x} = \frac{\partial u_{1m}}{\partial x} - z_1 \frac{\partial^2 w}{\partial x^2} \\ \varepsilon_2 &= \frac{\partial u_2}{\partial x} = \frac{\partial u_{2m}}{\partial x} - z_2 \frac{\partial^2 w}{\partial x^2} \\ \varepsilon_3 &= \frac{\partial u_3}{\partial x} = \frac{\partial u_{3m}}{\partial x} - z_3 \frac{\partial^2 w}{\partial x^2} \\ \varepsilon_4 &= \frac{\partial u_4}{\partial x} = \frac{\partial u_{4m}}{\partial x} - z_4 \frac{\partial^2 w}{\partial x^2}\end{aligned}\quad \left.\right\} \quad (6.1) \{a, b, c, d\}$$

$$\gamma_2 = \frac{u_{1m} - u_{3m}}{h_2} + \frac{h}{h_2} \theta \quad (6.2)$$

Where $h = h_2 + \frac{(h_1+h_3)}{2}$ and θ denotes the slope. u and w denote the longitudinal and transverse displacements respectively. h_1, h_2, h_3 and h_4 denote the thickness of constraining layer, PVC layer, base beam and sensor layer respectively. ε 's are corresponding strains. The shear stress developed in PVC layers is denoted by τ_2 . The shear strain of the PVC layer is represented by γ_2 . u_1, u_2, u_3 and u_4 are the longitudinal displacement of the constraining layer, PVC layer, the base beam and sensor layer respectively and w is the transverse displacement of all the layers. The shear stress in PVC layers is given as:

$$\tau_2 = G_2 \gamma_2 \quad (6.3)$$

The PVC layers are initially stressed (tensile or compressive) to a magnitude of β_2 to cause stress in the base beam.

6.1.2 The Shape Functions

Nodal displacements are given as:

$$\{U\}_e = \{w_i \ \theta_i \ u_{bi} \ u_{ci} \ w_j \ \theta_j \ u_{bj} \ u_{cj}\}^T \quad (6.4)$$

The transverse displacement w , the rotation θ and the axial displacements of the respective layers are expressed in terms of nodal displacements by finite element shape functions as:

$$\begin{aligned}w &= [N_w] \{U\}_e, \theta = [N_\theta] \{U\}_e, u_1 = [N_{u1}] \{U\}_e, u_2 = [N_{u2}] \{U\}_e, u_3 = [N_{u3}] \{U\}_e \\ u_4 &= [N_{u4}] \{U\}_e \quad \gamma_2 = [N_{\gamma2}] \{U\}_e\end{aligned}\quad (6.5) \{a, b, c, d, e, f, g\}$$

Where the shape functions are given as:

$$[N_w] = \begin{bmatrix} 1 - 3\left(\frac{x}{L_e}\right)^2 + 2\left(\frac{x}{L_e}\right)^3 \\ x - 2\left(\frac{x^2}{L_e}\right) + \left(\frac{x^3}{L_e^2}\right) \\ 0 \\ 0 \\ 3\left(\frac{x}{L_e}\right)^2 - 2\left(\frac{x}{L_e}\right)^3 \\ -\left(\frac{x^2}{L_e}\right) + \left(\frac{x^3}{L_e^2}\right) \\ 0 \\ 0 \end{bmatrix}^T, \quad [N_\theta] = \begin{bmatrix} -6\left(\frac{x}{L_e^2}\right) + 6\left(\frac{x^2}{L_e^3}\right) \\ 1 - 4\left(\frac{x}{L_e}\right) + 3\left(\frac{x}{L_e}\right)^2 \\ 0 \\ 0 \\ 6\left(\frac{x}{L_e^2}\right) - 6\left(\frac{x^2}{L_e^3}\right) \\ -2\left(\frac{x}{L_e}\right) + 3\left(\frac{x}{L_e}\right)^2 \\ 0 \\ 0 \end{bmatrix}$$

$$[N_{u3}] = \begin{bmatrix} 0 & 0 & 1 - \frac{x}{L_e} & 0 & 0 & 0 & \frac{x}{L_e} & 0 \end{bmatrix}$$

$$[N_{u1}] = \begin{bmatrix} 0 & 0 & 0 & 1 - \frac{x}{L_e} & 0 & 0 & 0 & \frac{x}{L_e} \end{bmatrix}$$

$$[N_{u4}] = [N_{u1}]$$

$$[N_{u2}] = [N_{u3}] - \left(\frac{h_1 + h_3}{2}\right) [N_\theta]$$

$$[N_{\gamma 2}] = \left[\frac{1}{h_2}([N_{u1}] - [N_{u3}]) + \frac{h}{h_2}[N_\theta]\right]$$

6.1.3 Energies of the ACLD Treatment Combined with SLD Treatment

For simplicity, all the energies are given for a single element. The total energy can be obtained by the combination of all the elements. Kinetic energy (T_e), strain energy (V_e) and as well as the work done (W_e) by external transverse load, piezoelectric forces and moments are discussed in the following sub-sections.

6.1.3.1 Kinetic Energies

The position vector p_k of a special point in the k^{th} layer at a distance x from the origin of the beam given is as follows:

$$p_k = (x + u_k) i + w j \quad (6.6)$$

$$\dot{p}_k = (\dot{u}_k - w \dot{\theta}) i + (x \dot{\theta} + u_k \dot{\theta} + \dot{w}) j \quad (6.7)$$

Where the dot denotes differentiation with respect to time t . The total kinetic energy of the complete system comprises the kinetic energies of constraining layer, base beam and PVC layer and sensor layer.

$$T_e = \frac{1}{2} \int_0^{L_e} b \sum_{k=1}^4 \vartheta_k \rho_k h_k (\dot{p}_k^T \dot{p}_k) dx \quad \text{with } \vartheta_k = \begin{cases} 1, & \text{for } k = 1, 3, 4 \\ 2, & \text{for } k = 2 \end{cases}$$

$$T_e = \frac{1}{2} \int_0^{L_e} b \sum_{k=1}^4 \vartheta_k \rho_k h_k \left[\frac{\dot{u}_k^2 + \dot{w}^2 + (x + u_k)^2 \dot{\theta}^2 +}{w^2 \dot{\theta}^2 + 2(x + u_k) \dot{w} \dot{\theta} - 2\dot{u}_k w \dot{\theta}} \right] dx \quad (6.8)\{a, b\}$$

6.1.3.2 Potential Energies

The total potential energy of the complete system comprises the strain energies of constraining layer, base beam, PVC layer and sensor layer. For each individual part it is given below:

6.1.3.2.1 Constraining layer

The potential energy of the constraining layer due to axial displacement is:

$$V_{e1} = \frac{1}{2} E_1 h_1 b \int_0^{L_e} \left(\frac{\partial u_1}{\partial x} \right)^2 dx = \frac{1}{2} \{U\}_e^T [K_{1u}] \{U\}_e \quad (6.9)\{a,b\}$$

$$\text{Where } [K_{1u}] = E_1 h_1 b \int_0^{L_e} \left[\frac{\partial N_{u1}}{\partial x} \right]^T \left[\frac{\partial N_{u1}}{\partial x} \right] dx$$

The potential energy of the constraining layer due to transverse displacement is:

$$V_{e2} = \frac{1}{2} E_1 I_1 \int_0^{L_e} \left(\frac{\partial^2 w}{\partial x^2} \right)^2 dx = \frac{1}{2} \{U\}_e^T [K_{1w}] \{U\}_e \quad (6.10)\{a,b\}$$

$$\text{Where } [K_{1w}] = E_1 I_1 \int_0^{L_e} \left[\frac{\partial^2 N_w}{\partial x^2} \right]^T \left[\frac{\partial^2 N_w}{\partial x^2} \right] dx$$

6.1.3.2.2 PVC layer

The potential energy of the PVC layer due to axial displacement is:

$$V_{e3} = \frac{1}{2} E_2 (2h_2) b \int_0^{L_e} \left(\frac{\partial u_2}{\partial x} \right)^2 dx = \frac{1}{2} \{U\}_e^T [K_{2u}] \{U\}_e \quad (6.11)\{a,b\}$$

$$\text{Where } [K_{2u}] = E_2 (2h_2) b \int_0^{L_e} \left[\frac{\partial N_{u2}}{\partial x} \right]^T \left[\frac{\partial N_{u2}}{\partial x} \right] dx$$

The potential energy of the PVC layer due to transverse displacement is:

$$V_{e4} = \frac{1}{2} E_2 (2I_2) \int_0^{L_e} \left(\frac{\partial^2 w}{\partial x^2} \right)^2 dx = \frac{1}{2} \{U\}_e^T [K_{2w}] \{U\}_e \quad (6.12)\{a,b\}$$

$$\text{Where } [K_{2w}] = E_2 (2I_2) \int_0^{L_e} \left[\frac{\partial^2 N_w}{\partial x^2} \right]^T \left[\frac{\partial^2 N_w}{\partial x^2} \right] dx$$

The potential energy of the PVC layer due to shearing:

$$V_{e5} = \frac{1}{2} G_2 (2h_2) b \int_0^{L_e} \gamma_2^2 dx = \frac{1}{2} \{U\}_e^T [K_{2\gamma}] \{U\}_e \quad (6.13)\{a,b\}$$

$$\text{Where } [K_{2\gamma}] = G_2 (2h_2) b \int_0^{L_e} [N_{\gamma2}]^T [N_{\gamma2}] dx$$

In the above three equations h_2 and I_2 are multiplied by 2 to consider the contribution of both the PVC layers attached to both the sides of the base beam.

6.1.3.2.3 Base beam

The potential energy of the base beam due to axial displacement is:

$$V_{e6} = \frac{1}{2} E_3 h_3 b \int_0^{L_e} \left(\frac{\partial u_3}{\partial x} \right)^2 dx = \frac{1}{2} \{U\}_e^T [K_{3u}] \{U\}_e \quad (6.14)\{a,b\}$$

$$\text{Where } [K_{3u}] = E_3 h_3 b \int_0^{L_e} \left[\frac{\partial N_{u3}}{\partial x} \right]^T \left[\frac{\partial N_{u3}}{\partial x} \right] dx$$

The potential energy of the base beam due to transverse displacement is:

$$V_{e7} = \frac{1}{2} E_3 I_3 \int_0^{L_e} \left(\frac{\partial^2 w}{\partial x^2} \right)^2 dx = \frac{1}{2} \{U\}_e^T [K_{3w}] \{U\}_e \quad (6.15)\{a,b\}$$

$$\text{Where } [K_{3w}] = E_3 h_3 b \int_0^{L_e} \left[\frac{\partial^2 N_w}{\partial x^2} \right]^T \left[\frac{\partial^2 N_w}{\partial x^2} \right] dx$$

6.1.3.2.4 Sensor layer

The potential energy of the sensor layer due to axial displacement is:

$$V_{e8} = \frac{1}{2} E_4 h_4 b \int_0^{L_e} \left(\frac{\partial u_4}{\partial x} \right)^2 dx = \frac{1}{2} \{U\}_e^T [K_{4u}] \{U\}_e \quad (6.16)\{a,b\}$$

$$\text{Where } [K_{4u}] = E_4 h_4 b \int_0^{L_e} \left[\frac{\partial N_{u4}}{\partial x} \right]^T \left[\frac{\partial N_{u4}}{\partial x} \right] dx$$

The potential energy of the sensor layer due to transverse displacement is:

$$V_{e9} = \frac{1}{2} E_4 I_4 \int_0^{L_e} \left(\frac{\partial^2 w}{\partial x^2} \right)^2 dx = \frac{1}{2} \{U\}_e^T [K_{4w}] \{U\}_e \quad (6.17)\{a,b\}$$

$$\text{Where } [K_{4w}] = E_4 h_4 b \int_0^{L_e} \left[\frac{\partial^2 N_w}{\partial x^2} \right]^T \left[\frac{\partial^2 N_w}{\partial x^2} \right] dx$$

6.1.3.2.5 Centrifugal stiffening effect

The potential energy due to centrifugal stiffening:

$$V_{e10} = \frac{1}{2} \int_0^{L_e} P(x, t) \left(\frac{\partial w}{\partial x} \right)^2 dx \quad (6.18)$$

where

$$\begin{aligned} P(x, t) &= \int_x^L (\rho_1 h_1 + (2\rho_2 h_2) + \rho_3 h_3 + \rho_4 h_4) b \dot{\theta}^2 dx \\ &= \frac{1}{2} (\rho_1 h_1 + (2\rho_2 h_2) + \rho_3 h_3 + \rho_4 h_4) b \dot{\theta}^2 (L^2 - \theta^2) \end{aligned}$$

6.1.3.2.6 Effect of initial stress in PVC layers

The potential energy due to initial stresses (i.e. compressive or tensile):

$$V_{e11} = \pm \frac{1}{2} \int_0^{L_e} Q(x, t) \left(\frac{\partial y}{\partial x} \right)^2 dx \quad (6.19)$$

Where $Q(x, t) = 2 \int_0^{L_e} \beta_2 b h_2 dx$

The positive sign is for tensile stress and negative sign for compressive stress in the base beam. This corresponds to Compressed Layer Damping (CoLD) and Tensed Layer Damping (TeLD) Treatments respectively.

6.1.4 Work Done

For one dimensional structure with uni-axial loading, the constitutive equations of PZT material can be written as given below:

$$\begin{bmatrix} \varepsilon \\ D \end{bmatrix} = \begin{bmatrix} S^E_{11} & d_{31} \\ d_{31} & \varepsilon^\tau_{33} \end{bmatrix} \begin{bmatrix} \sigma \\ E \end{bmatrix} \quad (6.20, 6.21)$$

Where D is the electrical displacement, E is the electric field, ε is the mechanical strain in x direction, and σ is the mechanical stress in x direction. S^E_{11} is the elastic compliance constant, ε^τ_{33} is the dielectric constant and d_{31} is the piezoelectric constant. Forces exerted on the system are:

a) The externally applied mechanical force.

b) The piezoelectric force developed by the PZT patch.

The work done W_1 by the external transverse load “f” acting on the beam/ACLD system is given as:

$$W_{e1} = \int_0^{L_e} f w(x, t) dx = \{U\}_e^T \{F_d\}_e \quad (6.22)$$

Where $\{F_d\}_e = f \int_0^{L_e} \left[\frac{\partial^2 N_w}{\partial x^2} \right]^T dx$

The work done W_2 by the piezoelectric control forces and moments are given as:

$$W_{e2} = E_1 A_1 \int_0^{L_e} \left[\varepsilon_{piezo} \left(\frac{\partial u_1}{\partial x} \right) + h \varepsilon_{piezo} \left(\frac{\partial^2 w}{\partial x^2} \right) \right] dx \quad (6.23)$$

Where ε_{piezo} denotes the strain introduced by the piezoelectric effect and is given as

$$\varepsilon_{piezo} = \frac{d_{31} v_a \|_e}{h_1}$$

Here v_a is the applied voltage to the piezoelectric actuator. However $v_a \|_e$ represents corresponding elemental voltage although both are same in magnitude. This representation has significance in closed loop conditions. The work done can now be written as:

$$\begin{aligned} W_{e2} &= E_1 d_{31} b v_a \|_e \int_0^{L_e} \left(\frac{\partial u_1}{\partial x} \right) dx + h E_1 d_{31} b v_a \|_e \int_0^{L_e} \left(\frac{\partial^2 w}{\partial x^2} \right) dx \\ &= E_1 d_{31} b v_a \|_e \int_0^{L_e} \left[\frac{\partial N_{u1}}{\partial x} \right]^T dx + h E_1 d_{31} b v_a \|_e \int_0^{L_e} \left[\frac{\partial^2 N_w}{\partial x^2} \right]^T dx \end{aligned}$$

$$\{U\}_e^T (\{F_{c1}\}_e + \{F_{c2}\}_e) \quad (6.24)$$

Where

$$\{F_{c1}\}_e = E_1 d_{31} b v_a \|_e \int_0^{L_e} \left[\frac{\partial N_{u1}}{\partial x} \right]^T dx = E_1 d_{31} b v_a \|_e [0 \ 0 \ 0 \ -1 \ 0 \ 0 \ 0 \ 1]^T$$

and

$$\{F_{c2}\}_e = h E_1 d_{31} b v_a \|_e \int_0^{L_e} \left[\frac{\partial^2 N_w}{\partial x^2} \right]^T dx = h E_1 d_{31} b v_a \|_e [0 \ -1 \ 0 \ 0 \ 0 \ 1 \ 0 \ 0]^T$$

The work done W_3 by the applied hub torque τ is given by:

$$W_{e3} = \tau \theta \quad (6.25)$$

6.1.5 Pure Beam Elements

The stiffness and mass matrices of pure beam elements have dimensions of 6x6, and are similar to those given by Eqn. 6.7.

6.1.6 Equations of Motion

Using Hamilton's principle, the equations of motion for an ACLD element can be written as:

$$\int_{t_1}^{t_2} \delta(T - \sum_{j=1}^{11} v_j) dt + \int_{t_1}^{t_2} \delta(\sum_{j=1}^3 w_j) dt = 0 \quad (6.26)$$

For a single i^{th} element, defining the element coefficients and matrices as follows:

$$J_i = \int_0^{L_e} [\rho_1 h_1 + (2\rho_2 h_2) + \rho_3 h_3 + \rho_4 h_4] b (x_i + x)^2 dx \quad (6.27)$$

$$[M_i] = \int_0^{L_e} \sum_{k=1}^4 \rho_k h_k b (N_k^T N_k + N_w^T N_w) dx \quad (6.28)$$

Where $\rho_k h_k = 2 \rho_k h_k$ for $k = 2$

$$[K_i] = \int_0^{L_e} \sum_{k=1}^4 \left[E_k h_k b \left\{ \left(\frac{\partial N_k}{\partial x} \right)^T \left(\frac{\partial N_k}{\partial x} \right) \right\} + E_k I_k \left\{ \left(\frac{\partial^2 N_w}{\partial x^2} \right)^T \left(\frac{\partial^2 N_w}{\partial x^2} \right) \right\} \right] dx \quad (6.29)$$

Where $E_k h_k = 2 E_k h_k$ for $k = 2$

$$\{V_i\} = \int_0^{L_e} [\rho_1 h_1 + (2\rho_2 h_2) + \rho_3 h_3 + \rho_4 h_4] [b(x_i + x)] N_k dx \quad (6.30)$$

$$\{V_{2i}\} = \int_0^{L_e} [\rho_1 h_1 + (2\rho_2 h_2) + \rho_3 h_3 + \rho_4 h_4] [b(x_e + x)] N_w dx \quad (6.31)$$

$$\{V_{3i}\} = \frac{1}{2} \int_0^{L_e} (\rho_1 h_1 + 2\rho_2 h_2 + \rho_3 h_3 + \rho_4 h_4) b [L^2 - (x_i + x)] \left\{ \left(\frac{\partial N_w}{\partial x} \right)^T \left(\frac{\partial N_w}{\partial x} \right) \right\} dx \quad (6.32)$$

$$\{V_{4i}\} = \int_0^{L_e} G_2 h_2 b N_{y2}^T N_{y2} dx \quad (6.33)$$

$$\{R_i\} = \int_0^{L_e} \sum_{k=1}^4 \rho_k h_k b (N_k^T N_w) dx \quad \text{Where } \rho_k h_k = 2 \rho_k h_k \text{ for } k = 2 \quad (6.34)$$

$$[G_i] = [R_i]^T - [R_i] \quad (6.35)$$

$$\{F_{ci}\} = \{F_{c1}\}_e + \{F_{c2}\}_e \quad (6.36)$$

$$\{F_{di}\} = \{F_d\}_e \quad (6.37)$$

Where x is the distance from the clamped end to the left node of the element under consideration. J_i is the moment of inertia of the i^{th} element about the clamped end. $[M_i]$ and $[K_i]$ are the mass and stiffness matrices respectively. $\{V_{3i}\}$ and $\{V_{4i}\}$ are due to centrifugal force and shear deformation of the PVC layer respectively. The matrices $[R_i]$ and $[G_i]$ are due to the gyroscopic effects. The matrices $\{F_{ci}\}$ and $\{F_{di}\}$ are the control force and the external load respectively.

After using Hamilton's Principle, the equations of motion at the element level can be written as:

$$\begin{bmatrix} M_{\theta\theta i} & \{M_{\theta q i}\} \\ \{M_{q\theta i}\} & [M_{qq i}] \end{bmatrix} \begin{Bmatrix} \ddot{\theta} \\ \{\ddot{U}\}_i \end{Bmatrix} + 2\dot{\theta} \begin{bmatrix} 0 & \{0\} \\ \{0\} & [G_i] \end{bmatrix} \begin{Bmatrix} \dot{\theta} \\ \{\dot{U}\}_i \end{Bmatrix} + \begin{bmatrix} 0 & \{0\} \\ \{0\} & [K_{qq i}] \end{bmatrix} \begin{Bmatrix} \theta \\ \{U\}_i \end{Bmatrix} = \begin{bmatrix} Q_{\theta i} \\ Q_{qi} \end{Bmatrix} + \begin{bmatrix} F_{\theta i} \\ F_{qi} \end{bmatrix} \quad (6.38)$$

Where

$$M_{\theta\theta i} = J_i + \{q_i^T\}[M_i]\{q_i\} + 2\{V_{1i}\}\{q_i\} - \{q_i^T\}[V_{3i}]\{q_i\}$$

$$\{M_{\theta q i}\} = \{M_{q\theta i}\}^T = \{V_{2i}\} - \{q_i^T\}[G_i]$$

$$[M_{qq i}] = [M_i]$$

$$[K_{qq i}] = [K_i] - \dot{\theta}^2[M_i] + \dot{\theta}^2[V_{3i}] + [V_{4i}]$$

$$Q_{\theta i} = -2\dot{\theta}[\{q_i^T\}[M_i]\{\dot{q}_i\} + \{V_{1i}\}\{\dot{q}_i\} - \{q_i^T\}[V_{3i}]\{\dot{q}_i\}]$$

$$\{Q_{qi}\} = \dot{\theta}^2\{V_{1i}\}^T$$

$$F_{\theta i} = \tau$$

$$\{F_{qi}\} = \{F_{ci}\} + \{F_{di}\}$$

in which $M_{\theta\theta i}$ is the rotational inertia of the system, $[M_{qq i}]$ is the generalized mass matrix, $\{M_{\theta q i}\}$ is the non-linear inertia coupling between rigid body and the elastic deformations, $[K_{qq i}]$ is the generalized stiffness matrix and $[G_i]$ is the gyroscopic matrix. $Q_{\theta i}$ and Q_{qi} represent the non-linear pseudo loads. F_{qi} represents the sum of control force and external load. Eqn. 6.38 represents a non-linear hybrid gyroscopic dynamic system which is inertia coupled between rigid body and elastic deformations. Mode superposition is not applicable to non-linear systems. For simplicity the angular velocity $\dot{\theta}$ is assumed to be constant as well as no external load is applied. After linearization and assembling the elemental equations the global system equations are obtained as follows:

$$[M_{qq}]\{\ddot{U}\} + 2\dot{\theta}[G]\{\dot{U}\} + [K_{qq}]\{U\} = \{F_{qq}\} \quad (6.39)$$

Where $[M_{qq}]$ real symmetric positive is definite, $[G]$ is real skew symmetric and $[K_{qq}]$ is symmetric. $[K_{qq}]$ is complex due to complex shear modulus G_2 of the PVC layer. The above equation without subscript i denotes the global form of corresponding elemental co-efficient matrices.

6.1.6.1 Open Loop Conditions

The voltage developed v_s for a uniform sensor of length L_e (i.e. length of one element) is obtained from the following formula:

$$V_s \parallel_e = -\frac{k_{31}^2 D_d b}{g_{31} C} \int_0^{L_e} \frac{\partial^2 w}{\partial x^2} dx \quad (6.40)$$

Where k_{31} is the electromechanical coupling factor, D_d is the distance from the neutral axis to sensor surface. g_{31} is piezoelectric voltage constant. The capacitance C of the sensor is given by:

$$C = \frac{8.854 \times 10^{-12} A_s k_{3t}}{h_b} \quad (6.41)$$

Where A_s is the sensor area and k_{31} is the dielectric constant. Thus the voltage developed is given as:

$$v_s \parallel_e = [K_{sensor}]_e^T \{U\}_e \quad (6.42)$$

Where

$$[K_{sensor}]_e = -\frac{k^2_{31} D_d b}{g_{31} C} \int_0^{L_e} \frac{\partial^2 N_w}{\partial x^2} dx$$

6.1.6.2 Closed Loop Conditions

With Proportional Derivative controller, the relationship between actuator voltage $v_a \parallel_e$ and sensor voltage $v_s \parallel_e$ is given as:

$$v_a \parallel_e = -K_p v_s \parallel_e - K_d \frac{d v_s \parallel_e}{dt} \quad (6.43)$$

Where K_p and K_d are proportional and derivative control gains, respectively.

By considering the proportional gain K_p only and using Eqns. (6.24, 6.42 and 6.43) we get:

$$\{f_{c1}\}_e = k_p [0 \ 0 \ 0 \ -1 \ 0 \ 0 \ 0 \ 1]^T \begin{bmatrix} 0 & -\frac{g}{2} & 0 & 0 & 0 & \frac{g}{2} & 0 & 0 \end{bmatrix} \{U\}_e \quad (6.44)\{a\}$$

$$\{f_{c2}\}_e = k_p [0 \ -1 \ 0 \ 0 \ 0 \ 1 \ 0 \ 0]^T \begin{bmatrix} 0 & -\frac{gh}{2} & 0 & 0 & 0 & \frac{gh}{2} & 0 & 0 \end{bmatrix} \{U\}_e \quad (6.44)\{b\}$$

Where g is defined as:

$$g = \frac{E_c b^2 d_{31} k^2_{31} D_d}{g_{31} C}$$

Expressing $\{f_{c1}\}_e$ and $\{f_{c2}\}_e$ in terms of displacement feedback gain matrix $[G_p]_e$ yields:

$$\{f_{c1}\}_e + \{f_{c2}\}_e = -[G_p]_e \{U\}_e \quad (6.45)$$

Where $[G_p]_e = -K_p(C_1 + C_2)$

The constants C_1 and C_2 are given by following relations:

$$C_1 = [0 \ 0 \ 0 \ -1 \ 0 \ 0 \ 0 \ 1]^T \begin{bmatrix} 0 & -\frac{g}{2} & 0 & 0 & 0 & \frac{g}{2} & 0 & 0 \end{bmatrix}$$

and

$$C_2 = [0 \ -1 \ 0 \ 0 \ 0 \ 1 \ 0 \ 0]^T \begin{bmatrix} 0 & -\frac{gh}{2} & 0 & 0 & 0 & \frac{gh}{2} & 0 & 0 \end{bmatrix} \quad (6.46)\{a,b\}$$

Substituting the global form of Eqn. 6.34 into Eqn. 6.28, the closed loop equation of motion for the system with single element is given as:

$$[M_{qq}]_e \{\ddot{U}\}_e + 2 \dot{\theta} [G]_e \{\dot{U}\}_e + [[K_{qq}]_e + [G_p]_e] \{U\}_e = \{0\}_e \quad (6.47)$$

Collecting all the elements to form the global equations of motion

$$[M_{qq}] \{\ddot{U}\} + 2 \dot{\theta} [G] \{\dot{U}\} + [[K_{qq}] + [G_p]] \{U\} = \{0\} \quad (6.48)$$

The eigen value problem associated with Eqn. 6.65 is second order, so it does not permit a readymade solution. The difficulty can be overcome by converting into state space form:

$$[A]\dot{z} + [B]z = \{0\} \quad (6.49)$$

$$\text{Where } z = [[\dot{U}]^T \ [U]^T]^T \text{ and}$$

$$[A] = \begin{bmatrix} [M_{qq}] & [0] \\ [0] & [I] \end{bmatrix}, \quad [B] = \begin{bmatrix} 2\dot{\theta}[G] & [K_{qq} + G_{qq}] \\ [-I] & [0] \end{bmatrix},$$

The eigen value problem associated with Eqn. 6.49 becomes:

$$(\lambda_j A + B)Z_j = 0 \quad (6.50)$$

Where λ_j and Z_j are the j^{th} closed loop complex eigen value and eigenvector, respectively. Representing the complex eigen value by:

$$\lambda_j = \sigma_j + i \omega_j \quad (6.51)$$

Where the real part σ_j represents the vibration exponential decay while the imaginary part ω_j is the damped frequency. The damping ratio is given by:

$$\xi_j = \frac{\sigma_j}{\sqrt{\sigma_j^2 + \omega_j^2}} \quad (6.52)$$

However, the damped natural frequencies and damping ratios can be easily calculated using the DAMP command of MATLAB.

6.2 RESULTS AND DISCUSSION

6.2.1 Comparisons with Results from former studies

First of all to check the accuracy of the developed mathematical model, the comparison was done with results from former researchers. Table 6.1 shows the parameters of the PCLD system:

Table 6.1: Geometrical parameters and mechanical properties

Parameter	Base beam	VEM layer	Constraining Layer
Length (mm)	300	300	300
Width (mm)	12.7	12.7	12.7
Thickness (mm)	2.286	0.25	0.762
Young's Modulus (N/m ²)	7.1×10^{10}	2.98×10^7	6.49×10^{10}
Density (Kg/m ³)	2700	1250	7600
Loss factor	-	0.38	-
Shear Modulus (N/m ²)	-	2.61×10^5	-

For the full length treatment the results are shown in Table 6.2 under first boundary conditions (BC- I).

Table 6.2: Natural frequencies of the PCLD beam under different boundary conditions at 1000 RPM

Property/ Reference	Mode 1		Mode 2		Mode 3		
	Freq. (Hz)	Damp. ratio	Freq. (Hz)	Damp. ratio	Freq. (Hz)	Damp. ratio	
BC -I	Previous Studies	21.1	0.034	110.5	0.02	285.1	0.0116
	Present	21	0.034	110.3	0.0198	284	0.0115
BC -II	Previous Studies	17.6	0.0146	111.2	0.0215	285.2	0.0114
	Present	17.9	0.0144	113.1	0.0211	288	0.0112

Under these boundary conditions, the constrained layer was fixed against **radial motion** at the fixed end. The results obtained show the excellent match. For other boundary conditions (BC-II), the constraining layer was free for radial motion at both the ends. The results with these boundary conditions were matching properly. The reason for choosing these boundary conditions was that in case of partial treatment, same types of conditions exist. The results confirmed that mathematical modeling developed for partial treatment is correct.

6.2.2 Performance with SLD Treatment

Two PVC patches, one for each side of the base beam were attached to the base beam. The length of the PVC patches was chosen to be 100mm each. The thickness of the PVC patches was comparable to the base beam as shown in Table 6.3.

Table 6.3: Geometrical parameters and mechanical properties of structure used under analysis

Parameter/Property	Base beam	VEM/PVC layer	Constraining Layer
Length (mm)	300	100	100
Width (mm)	14	14	14
Thickness (mm)	1	1.5	0.5
Young's Modulus	3.21×10^{10}	2×10^7	70.37×10^9
Density (Kg/m ³)	4972	1390	7500
Loss factor	0.008	0.5	0
Shear Modulus (N/m ²)	-	7.69×10^6	-

To consider the inherent damping of the base beam, a loss factor of 0.008 was chosen by a researcher named Mostafa in 2006. Depending upon the type of (SLD) treatment (i.e. CoLD or TeLD), initial strain was given to either base beam or to the PVC layers. For the Compressed Layer Damping (CoLD) treatment, the base beam was initially strained (i.e. tensile strain) and afterwards PVC patches were attached, so that after removing the external force on the base beam, the PVC layers get compressed and the base beam itself comes under tension. However, for the Tensed Layer Damping (TeLD) treatment, the PVC patches were given initial tensile strain and were then attached to the base beam, so that after the removal of tensile external force on the PVC layers, base beam comes under compressive stress and the PVC patches (i.e. layers) itself come under tensile stress. Since the thickness of the base beam is less and is comparable to PVC layers, it can be assumed without loss of accuracy that only that much portion of the base beam comes under pressure on which the treatment was applied i.e. the PVC layers were attached. The PVC layers of 100 mm (i.e. 33% coverage) were first of all applied at a distance of 20 mm from the fixed end of the beam. The base beam was tensed to various levels of strain. Figure 6.3 shows the damping ratios of the overall system as a function of strain developed in the PVC layers at different values of loss factor of the PVC layers.

It is obvious (Figure 6.3) that damping ratios actually decrease with the strain in PVC layer if the loss factor of PVC layer is zero. But, damping ratios are enhanced with increasing values

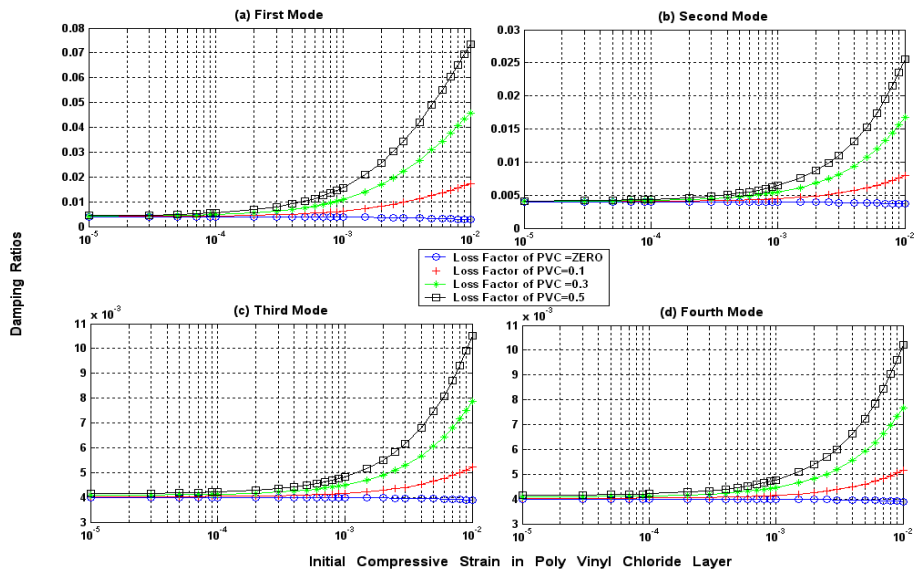


Fig. 6.3: Effect of initial compressive strain and loss factor of Poly Vinyl Chloride (PVC) layer on the damping ratios.

of loss factor. For a loss factor of 0.5 which is actually for these materials (i.e. PVC) under stationary conditions (i.e. zero RPM), damping ratios at 1% strain are 16.5, 6.34, 2.56 and 2.48 times the value at no strain for first, second, third and fourth mode respectively. One can appreciate the improvement. There is almost no change in the frequencies as the loss factor increases as shown in the next Figure 6.4.

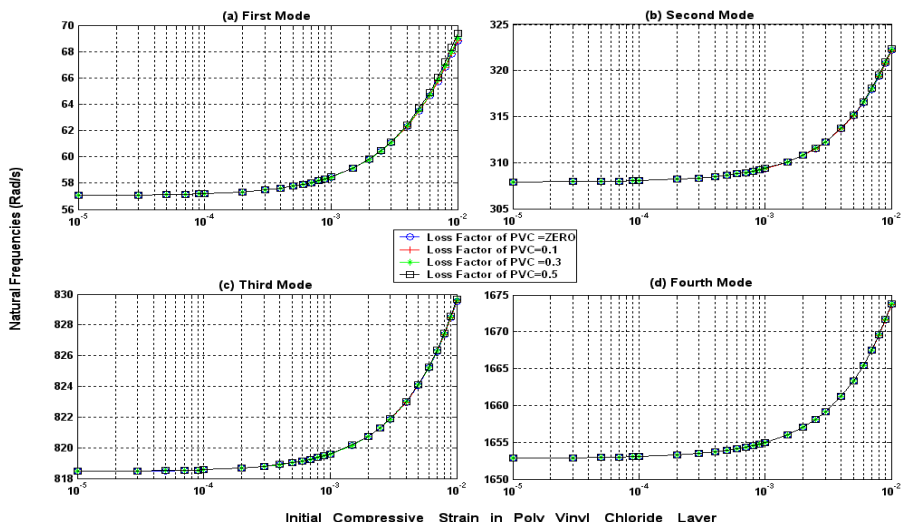


Fig. 6.4: Effect of initial compressive strain and loss factor of PVC layer on the natural Frequencies

However, the frequencies are increased due to stiffening of the base beam by centrifugal force. For the comparison of the CoLD and TeLD treatment, Figure 6.5 is constructed. It is observed that CoLD treatment is more effective as compared to TeLD

treatment except for the first mode. Another problem with TeLD treatment is that for the higher modes, even a small decrease in strain in PVC layer can significantly reduce the damping ratios. This problem is more prevalent for higher modes (i.e. third and fourth mode). However, CoLD treatment is free from this problem. As shown in this Figure, for rotating beams at high RPM, the improvement in damping performance by the application of SLD treatment is comparatively less. Centrifugal force developed due to rotation, stiffens the beam and hence raises the natural frequencies. In the TeLD treatment, due to compressive forces in the base beam, the natural frequencies tend to be lower.

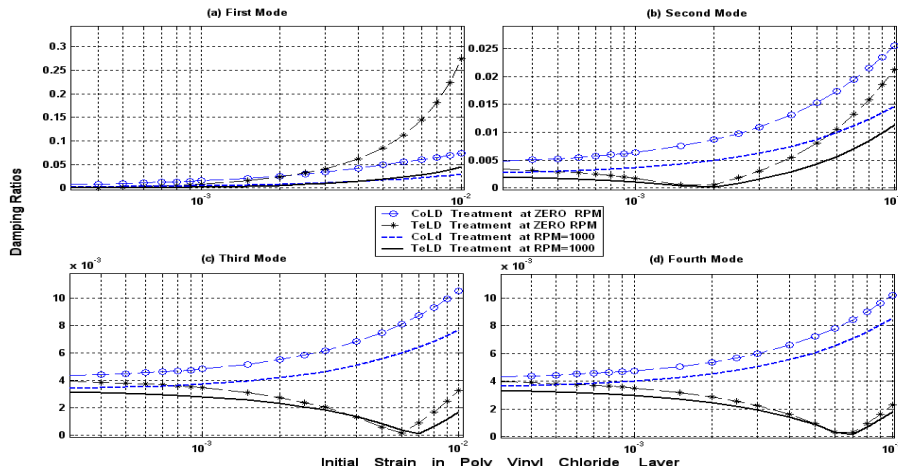


Fig. 6.5: Effect of initial strain on the damping ratios using SLD Treatment at different RPM of the beam with PVC patch located at a distance of 20 mm from the fixed end

6.2.3 Performance Combined with PCLD and SLD Treatment

The effort of applying a passive constraining layer on both the PVC layers is analyzed in this section. Constraining layer is made up of piezoelectric material. When the voltage is applied, it acts as an active constraining layer otherwise as a passive constraining layer. With the application of passive constrained layer, the damping ratios of all the modes except the first mode are enhanced. For the first mode, the performance with the use of constraining layers is degraded as compared to SLD treatment alone (Figure 6.6). The results are for a rotational speed of 1000 RPM. However, for the rest of the modes, damping performance of the PCLD + SLD treatment is much better than the SLD treatment.

With the initial strain of 1% in PVC layers, a damping improvement of 222% and 186% was achieved for first and second mode respectively. For the third and fourth mode, the damping improvement was not a function of initial strain in PVC layers. However, PCLD treatment which uses constraining layers over the PVC layers enhances the performance of CoLD treatment by 700% and 2100% for third and fourth mode respectively. Unfortunately, performance of the PCLD + TeLD treatment is inferior as compared to PCLD + CoLD for the first two modes.

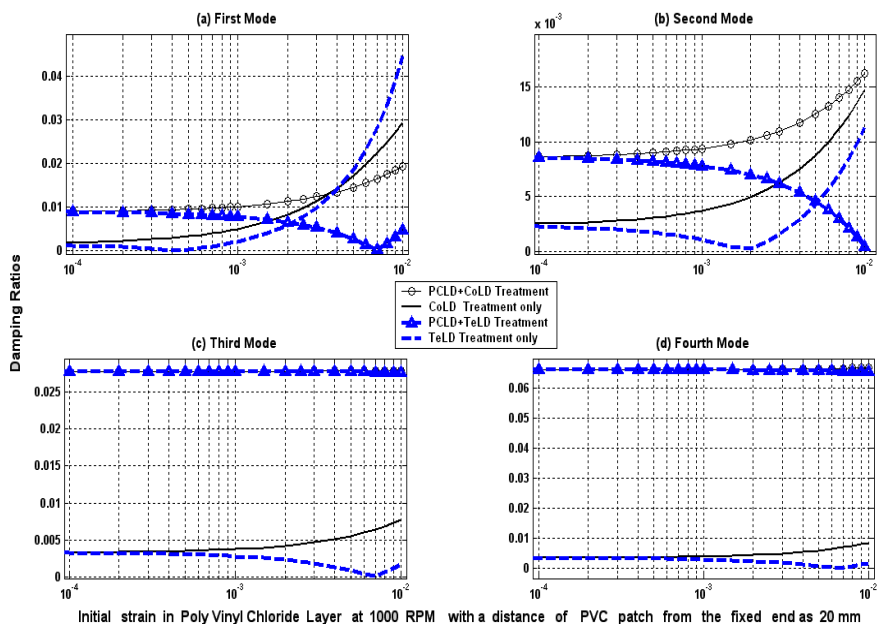


Fig. 6.6: Effect of initial strain on the damping ratios using PCLD + SLD treatment at 1000 RPM of the beam with PVC patch located at a distance of 20 mm from the fixed end.

However, constant performance is obtained for higher modes using both the techniques. With PCLD treatment combined with SLD treatment, the natural frequencies of the beam increase as compared to SLD treatment for all the modes except the second mode. However, when compared with the natural frequencies of the bare beam, PCLD+SLD treatment tries to make the natural frequencies close to the natural frequencies of the bare beam for all the modes except for the first mode. As initial strain increases the gap between natural frequencies of the bare and treated beam decreases for PCLD combined with CoLD treatment and increases with PCLD combined with TeLD treatment (for the purpose of brevity these graphs are not shown).

To analyze the effect of rotational speed on the damping performance, Figure 6.7 is constructed as above. As the RPM of the beam increases, damping provided by CoLD as well as TeLD treatment decreases. Only for the first mode the damping performance for the TeLD treatment is better and it too losses its superiority as RPM of the rotating beam increases. There is a marginal performance difference at 1000 RPM between the two strategies for the first mode of vibration; however, for the rest of the modes there is a vast difference even at higher RPMs. CoLD treatment is definitely a better alternative and for thin walled structures it is not difficult to employ the CoLD treatment practically. The natural frequencies are higher with CoLD treatment as compared to TeLD treatment for all the modes due to the additional tensile strain in base beam with CoLD treatment.

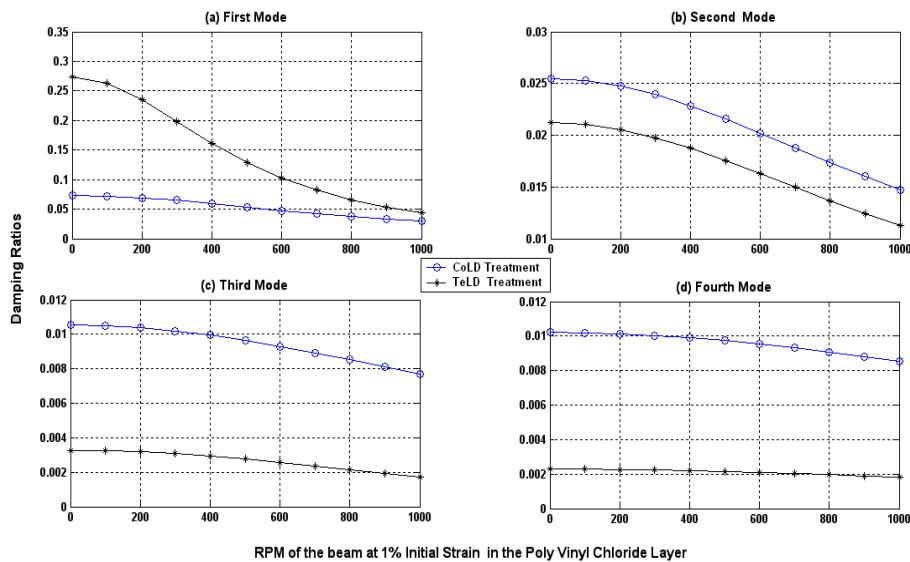


Fig. 6.7: Effect of RPM of the beam on the damping ratios at 1% strain in PVC layer with SLD Treatment

To compare the effectiveness of the proposed technique over conventional PCLD treatment, Figure 6.8 is constructed. Results show that PVC layers without initial strain are not as efficient as VEM layers with similar thicknesses. The damping performance at various thicknesses of the VEM layers is shown in Figure 6.8. A combination of PCLD and CoLD is better for first and second mode as compared to PCLD + TeLD system. However, for third and fourth mode there is no significant difference in performance by both the techniques. Various modal frequencies depend differently on the type of treatment.

First and fourth natural frequencies are highest with PCLD + CoLD treatment. However, second and third natural frequencies are highest with PCLD treatment with zero initial strain in PVC layer. To visualize the effect of location of PVC layers on the damping performance, Figures 6.9-6.10 are generated. Different locations of the treatment affect the different modes in a different way.

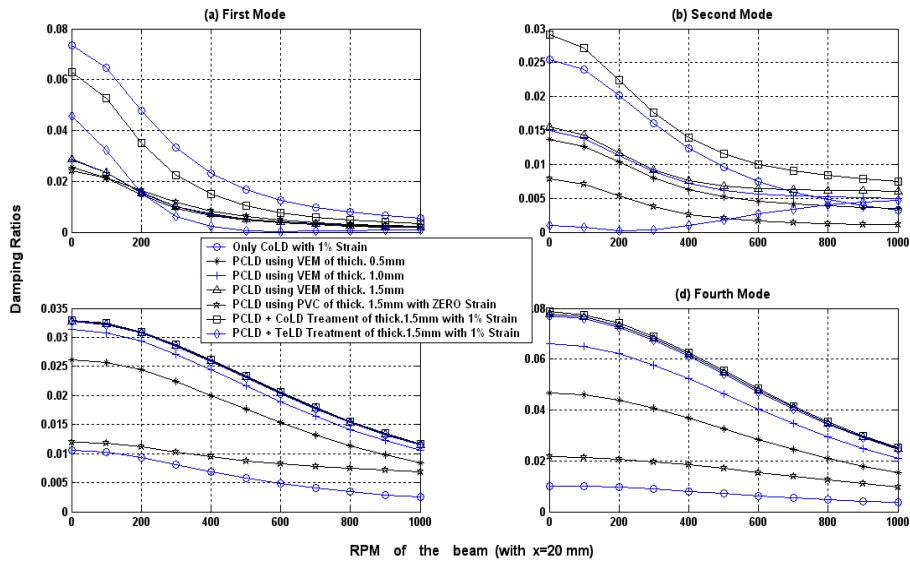


Fig. 6.8: Comparison of damping ratios of PCD Treatment with PCLD + SLD treatment with 1% strain in PVC layer at different RPM's of the beam.

6.2.4 Performance Combined with ACLD and SLD Treatment

Figure 6.11 shows the comparison of ACLD system to its counterpart PCLD System. For the ACLD treatment, upper constraining layer was made actuator, while the lower layer was made sensor. In this manner, the upper layer system becomes ACLD system and lower layer system becomes PCLD system. Table 6.4 on page no. 135 shows the electrical parameters of the piezoelectric materials. The feedback proportion gain was set at 20 (i.e. $K_p = 20$). Almost for all the modes, ACLD treatment combined with

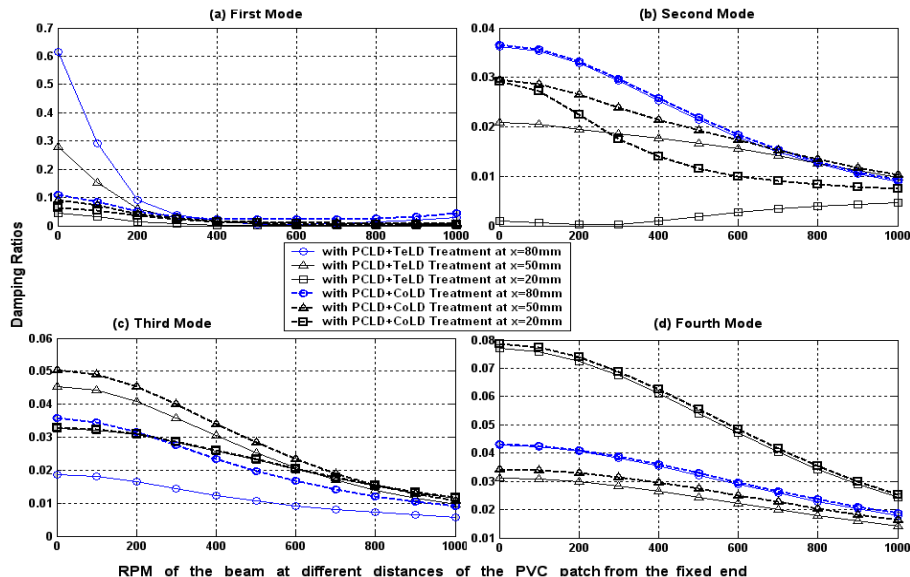


Fig. 6.9: Effect of RPM on damping ratios at different Locations of PVC patch by using PCLD+SLD Treatment

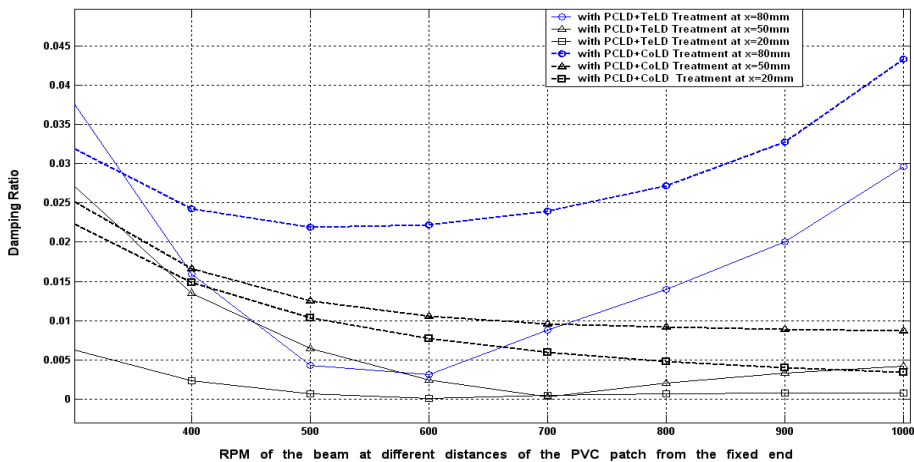


Fig. 6.10: Effect of RPM on damping ratios of the first mode at different Locations of PVC patch by using PCLD+SLD Treatment.

CoLD treatment gives better results as compared to the ACLD system with TeLD treatment. For higher modes the effect of ACLD treatment is more dominant, although this dominance was slightly diluted at very higher rotational speeds of the beam. In this figure the results are obtained for the ACLD patch attached at a distance of 20 mm from the fixed end. To see the effect of location, results were taken for different locations of the treatment in Figure 6.12. Except for the fourth mode, patch location of 80 mm gives the best results. At higher rotational speed the damping performance at the first mode started increasing instead of decreasing. This is due to the fact that at a larger distance of the patch (i.e. treatment) from the origin, due to high centrifugal forces, large magnitude shear stress is developed which causes enhancement of damping characteristics. But, centrifugal force developed acts at origin which causes other types of problems. Hence it is not always desirable. Each location of the treatment influences a certain mode number. Figure 6.13 shows the corresponding natural frequencies.

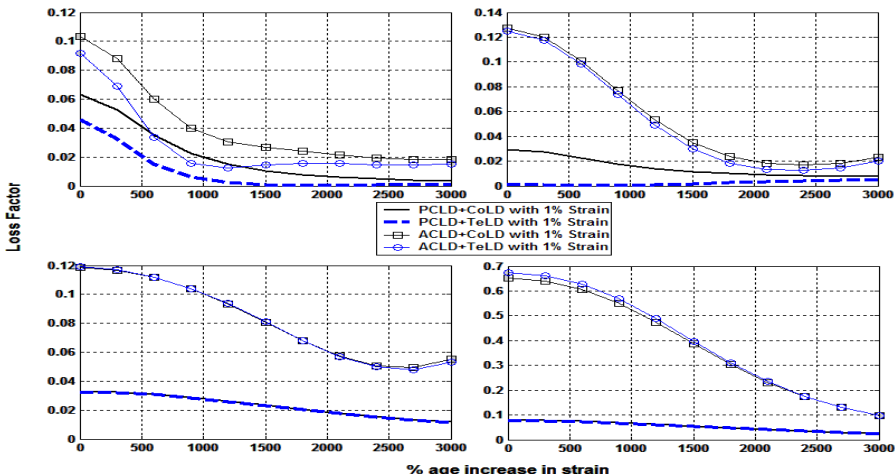
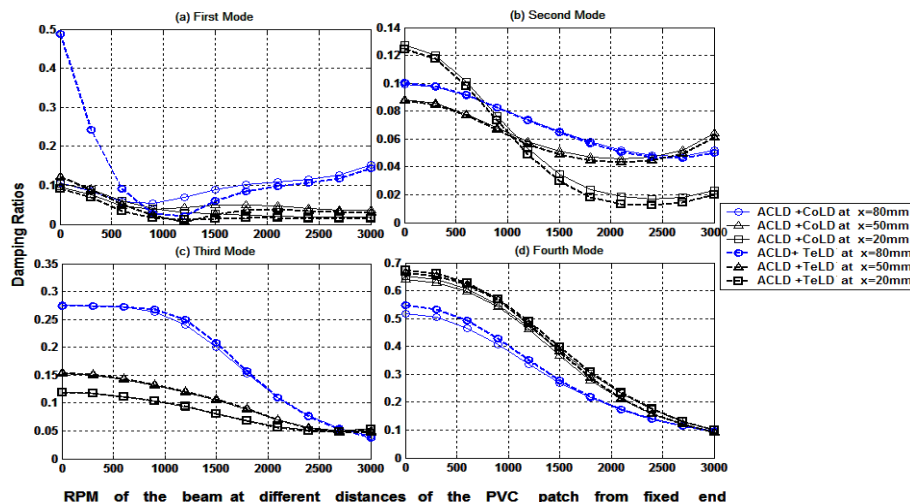


Fig. 6.11: Comparison of ACLD and PCLD treatment combined with SLD treatment at various RPM's of the beam

Table 6.4: Electrical properties of the piezoelectric materials

Property	Symbol	Value
Piezoelectric charge constant (m V^{-1})	d_{31}	171×10^{-12}
Electromechanical Coupling factor	k_{31}	0.12
Piezoelectric voltage constant (VmN^{-1})	g_{31}	216×10^{-3}
Dielectric constant	k_{3t}	12

**Fig. 6.12:** Effect of RPM on the damping ratios of the ACLD+SLD Treatment at different locations of the PVC patch at $k_p = 20$

In general, the natural frequencies of the ACLD system combined with CoLD treatment gives higher closed loop frequencies. To confirm the perception that damping performance is also related to centrifugal force, the thickness of the constraining layers is varied. Accordingly, the centrifugal force and hence the shear stress developed are also varied in Figure 6.14. Part (a) and (c) of this figure represent the first and second mode of the PCLD + CoLD system. Part (b) and (d) of this figure represent the first and second mode of the ACLD + CoLD system. The patches at the base beam were attached at a distance of 80mm from the fixed end (i.e. center of rotation). With the decrease in thickness of the constraining layers, fewer centrifugal forces were developed and hence the shear stress in PVC layers.

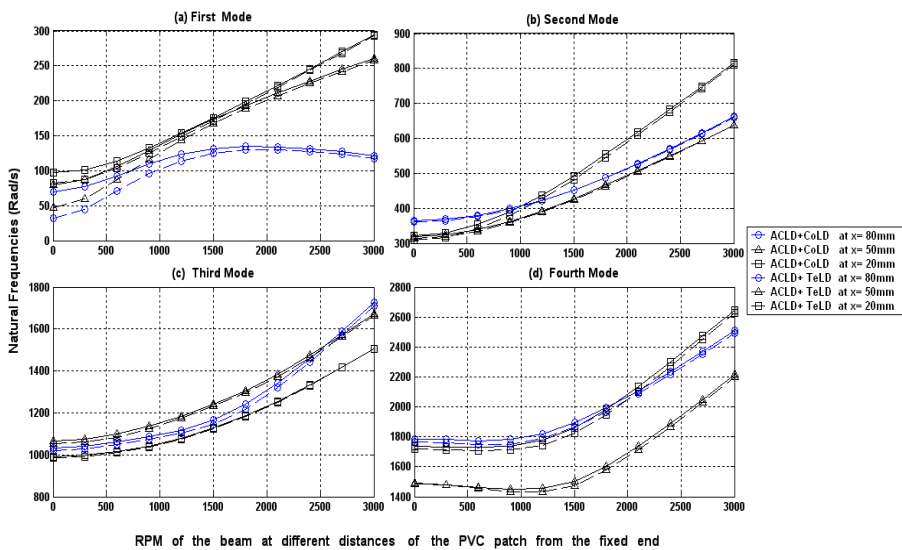


Fig. 6.13: Effect of RPM on the natural frequencies of the ACLD+SLD Treatment at different locations of the PVC patch at $k_p=20$

Due to this, the damping performance was observed to decrease as thickness of constraining layers decreased. As the RPM of the beam increases, effect of centrifugal force on damping performance is more prevalent for ACLD system as compared to PCLD. Initial strain in the PVC layers also plays an important role in damping performance. The effect of initial strain on the damping performance at a constant rotational speed is shown in Figure 6.15.

The RPM of the beam was fixed at 1000. Damping performance (with 1% initial strain in PVC layer) was found to increase by 117% for ACLD + CoLD treatment and by 40% for PCLD + CoLD treatment for the first mode. The performance improvement of 89% for the PCLD+SLD treatment for the second mode was observed as compared to the situation when no initial strain was there in the PVC layers. The damping enhancement for this mode by ACLD+SLD system was not appreciable. For the third and fourth mode, the effect of strain damping performance was negligible by both the techniques. Although damping performance improvement due to strain observed for lower modes with ACLD+SLD system, the pure active action slightly decreases with strain in the base beam. The pure active action means the performance obtained by subtracting the performance of PCLD+SLD system from ACLD+SLD system. The initial strain in CoLD treatment increases the natural frequencies of all the modes. ACLD treatment makes the gap between the frequencies of the treated and bare beam smaller. The effectiveness of ACLD treatment with both types of SLD techniques is compared in Figure 6.16.

A rotational speed of 1000 RPM was taken for the results of this Figure. ACLD + CoLD system outperform ACLD + TeLD system for the first two modes. For the third and fourth mode, ACLD + TeLD treatment gives better performance although percentage improvement was very less. Though the pure active action of ACLD + CoLD treatment decreases with initial strain, the cumulative effect (i.e. sum of active and passive performance) of this treatment was better.

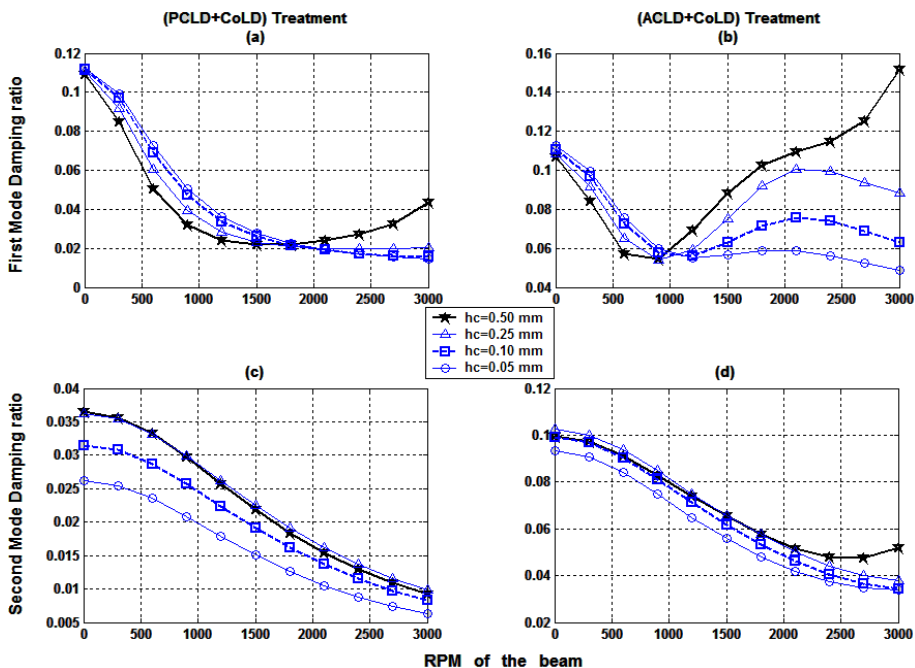


Fig. 6.14: Damping effectiveness of the PCLD and ACLD treatments combined with CoLD treatment at different thickness of the constraining layer.

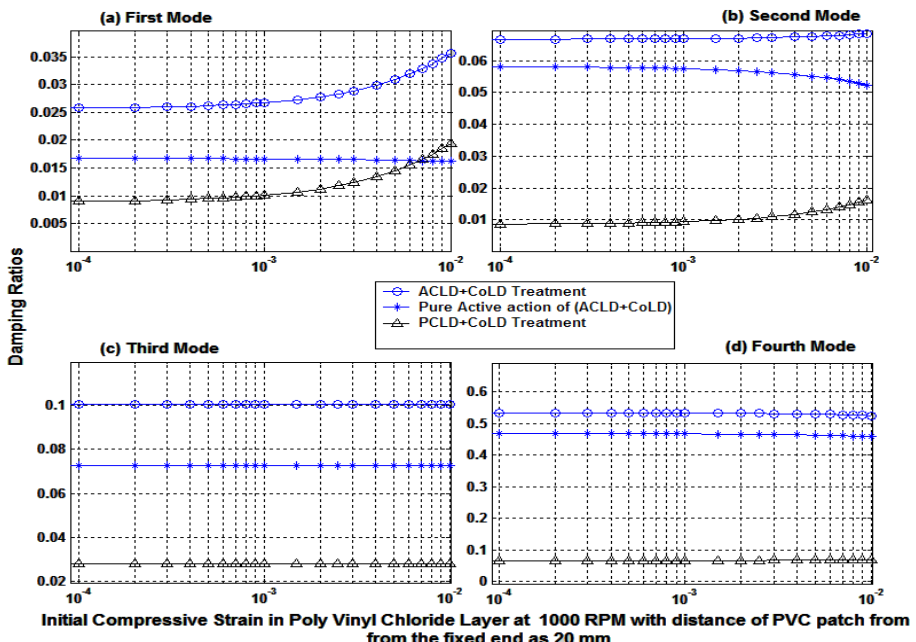


Fig. 6.15: Comparison of damping ratios by different techniques as a function of initial strain in PVC patch lying at a distance of 20 mm from the fixed end at 1000 RPM.

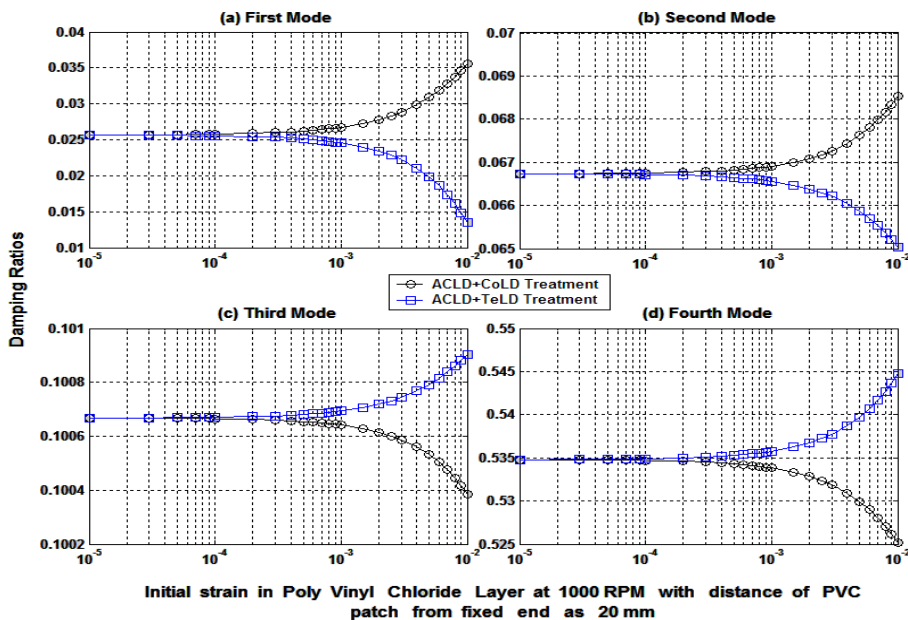
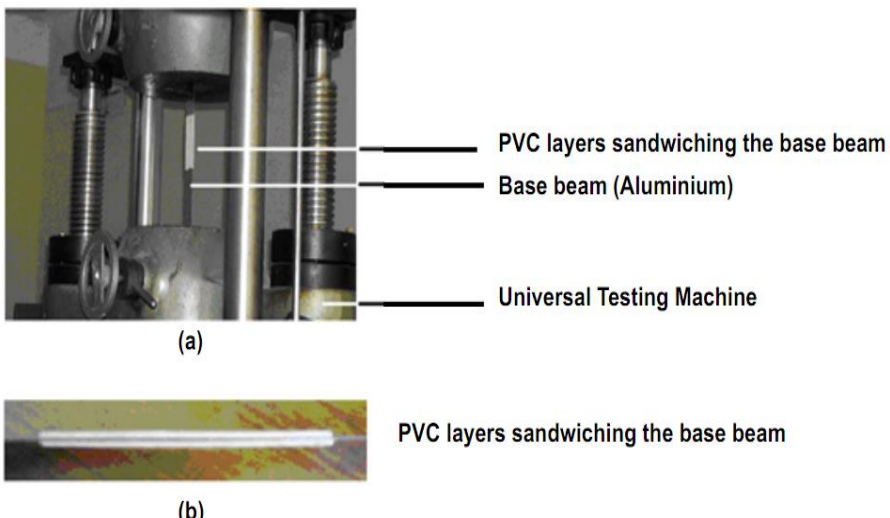


Fig. 6.16: Comparison of damping ratios using CoLD and TeLD treatment as a function of initial strain in the PVC patch lying at a distance of 20 mm from the fixed end at 1000 RPM

6.3 EXPERIMENTAL VALIDATION

6.3.1 Experimental Setup

To check the authenticity of the theoretical results experimental setup was generated, which is shown in Photograph 6.1, 6.2 and Figure 6.17.



Photograph 6.1: Apparatus for PTLD treatment (a) Tensioning of the base beam at Universal Testing Machine (b) PVC layers attached to base beam

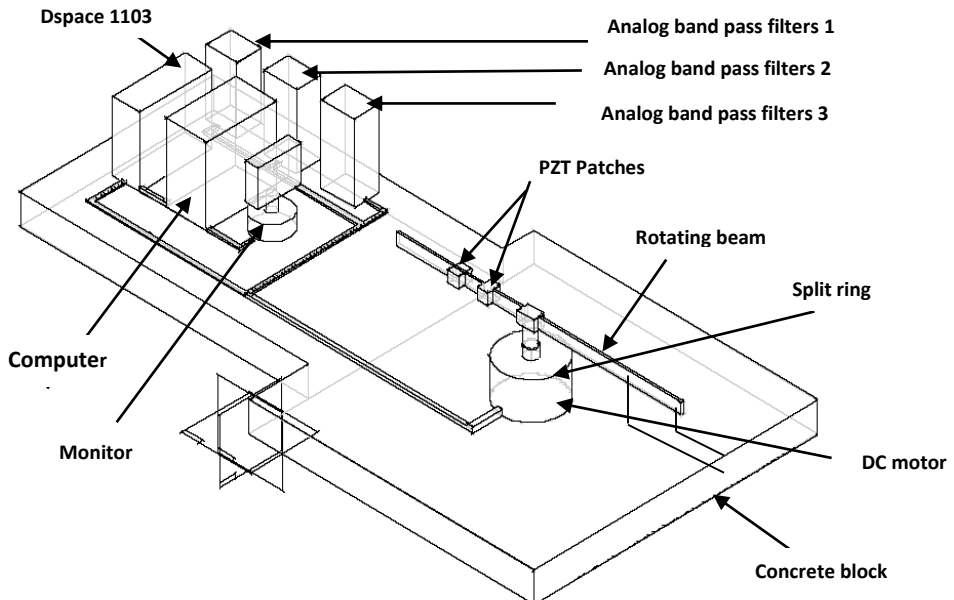


Fig. 6.17: Schematic experimental setup of the rotating beam



Photograph 6.2: Closer view of the beam treated with (ACLD + PTLD + CoLD) Treatment

The length of the treatment is chosen as 50 mm with 20 % coverage. Correspondingly 250 mm long base beam was selected for equivalent coverage. Steel is the material of the base beam (density and modulus of elasticity specified in Table 6.3. The thickness of the base beam is 1.0 mm. The thickness of the PVC layers is 1.5 mm each. The first edge of the treatment is at a distance of 20 mm from the fixed edge of the rotating beam. Thickness of the constraining layer is 0.5 mm. The thickness and length of the PZT patches is 1 mm and 20 mm respectively. Feedback gain of 10 is applied for all the readings. To provide pre-compression in PVC layers indirect method was

employed. The base beam was tensed on the ‘Universal Testing Machine’ and the PVC layers were attached. Afterwards the tension on the base beam was removed so that base is under tension and PVC layers under compression. Now two PZT layers were glued on the PVC layers, one forming the actuator and one forming the sensor.

A low pass filter was also used to remove the effect of out of range modes. The voltage from sensor PZT patch was passed to a high voltage amplifier MA-17. After inversion and amplification from the first channel of the amplifier, the voltage was directed to the actuator PZT patch. The experimental results are closely related to theoretical results. Table 6.5 shows the comparison between theoretical and experimental vibration characteristics. The variation between the results is attributed to the reasons that the strain developed in the base beam varies due to lose adhesive bond of the gluing adhesives and the variation in the properties of the PVC and PZT material parameters.

Table 6.5: Comparison of experimental and theoretical frequency response of the beam using ACLD + CoLD treatment at $k_p=10$

Vibration characteristics		Theoretical			Practical		
		RPM= 0	RPM= 500	RPM= 1000	RPM= 0	RPM= 500	RPM= 1000
Frequencies (Hz)	Mode 1	12.91	13.55	15.1	12.1	12.9	14.3
	Mode 2	81.93	84.57	92.0	76.4	79.2	87.4
	Mode 3	219.11	222.06	230.5	207.0	212.7	214.4
Damping ratios	Mode 1	0.049	0.045	0.036	0.040	0.038	0.032
	Mode 2	0.012	0.011	0.0091	0.010	0.009	0.007
	Mode 3	0.0106	0.0102	0.0092	0.008	0.008	0.007

CHAPTER – 7

VIBRATION CONTROL OF ROTATING STRUCTURES USING A UNIQUE LAYER

Although active constrained layer damping (ACLD) treatment increases the efficiency of passive constrained layer damping (PCLD) treatment, it suffers from the disadvantage of reduced transmissibility of active forces. In case of circuit failure, only the decreased efficiency of PCLD treatment is available. By using edge anchors and hybrid constraining layer this problem can be solved up to certain extent. However, by adding the standoff layer (SOL) between the viscoelastic layer and the base beam, not only the efficiency of PCLD treatment can be improved dramatically but also the effect of active forces and moments can be enhanced even without using edge anchors. Theoretical results are verified experimentally. The study will be useful for rotating structures like rotorcraft blades, helicopter wings and robotic systems. Documented literature in this field shows the gap in implementing the ACLD treatment with SOL layer to the rotating as well as stationary beams.

This chapter presents the vibration behavior and control of axial deformation and chord wise bending of a clamped-free rotating flexible beam with partially covered ACLD treatment with a very unique and special layer called **SOL(Stand-off layer)**. Since the beam taken is rotating in horizontal plane, gravitational effect and rotary inertia are neglected. The stress strain relationship for the VEM layer is described by complex modulus. Hamilton principle in conjunction with Finite Element Method (FEM) is used to derive the equation of motion. The effect of centrifugal stiffening due to rotation is also considered. PD controllers are designed for piezo sensor and actuator. The closed loop equation of motion for the system is derived and complex eigen value problem is solved numerically. The effects of different rotating speed, thickness of VEM layer, loss factor of VEM layer, thickness of SOL layer and shear modulus of SOL layer are studied. The effect of each parameter on the damping ratios and damped natural frequencies is investigated.

The main contribution of the present work is divided into following parts:

- a) *A Finite Element Method is employed in the present work, so that partial treatment can also be accommodated easily.*
- b) *Effect of SOL layer is investigated for rotating beams with ACLD treatment which is never considered earlier in literature for even stationary beams.*

7.1 SYSTEM DESCRIPTION AND MODELING

7.1.1 Basic Relationships

Figure 7.1 shows the cross-section of the beam with ACLD+ SOL system. One side of host structure or the base beam is attached with a VEM layer and SOL layer. The VEM

layer in turn is constrained by an active piezoelectric material PZT (Lead Zirconated Titrate).

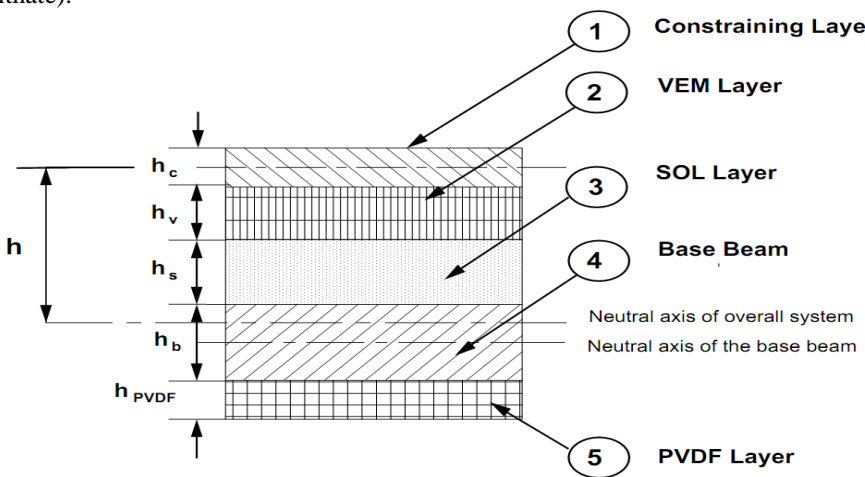


Fig. 7.1: Schematics of structure with ACLD + CoLD/TeLD treatment

It acts as a constraining layer and an actuator. The Poly Vinylene Di-Fluoride (PVDF) layer acts as sensor and is attached on the other side of the base beam. For simplicity, the constrained layer (i.e. PZT patch) is numbered as 1, VEM layer as no. 2, SOL layer as no. 3, the base beam as no. 4 and sensor layer (i.e. PVDF layer) as no. 5. The base beam and constraining layer can be modeled as Euler-Bernoulli beams using first two conditions. For the continuity of displacements at the interface between the layers the relation between shear angle (strain) and various displacements given as under:

$$\begin{aligned}\varepsilon_1 &= \frac{\partial u_1}{\partial x} = \frac{\partial u_{1m}}{\partial x} - z_1 \frac{\partial^2 w}{\partial x^2} \\ \varepsilon_2 &= \frac{\partial u_2}{\partial x} = \frac{\partial u_{2m}}{\partial x} - z_2 \frac{\partial^2 w}{\partial x^2} \\ \varepsilon_3 &= \frac{\partial u_3}{\partial x} = \frac{\partial u_{3m}}{\partial x} - z_3 \frac{\partial^2 w}{\partial x^2} \\ \varepsilon_4 &= \frac{\partial u_4}{\partial x} = \frac{\partial u_{4m}}{\partial x} - z_4 \frac{\partial^2 w}{\partial x^2} \\ \varepsilon_5 &= \frac{\partial u_5}{\partial x} = \frac{\partial u_{5m}}{\partial x} - z_5 \frac{\partial^2 w}{\partial x^2}\end{aligned}\quad (7.1)\{a, b, c, d, e\}$$

$$u_2 = \frac{(u_4+u_1)}{2} + \frac{(h_1-2h_3-h_4)}{4} \theta \quad (7.2)\{a\}$$

For the continuity of displacements at the interface between the layers the relation between shear angle (strain) and various displacements is as under:

$$u_3 = u_4 - \frac{(h_1+h_4)}{2} \theta \quad (7.2)\{b\}$$

$$\begin{aligned}\gamma_3 &= \left[\frac{u_1-u_4}{h_3} + \frac{1}{2} \left(1 + \frac{h_1+2h_2+2y_b}{2h_3} \right) \theta \right] - \left(\frac{h_2}{h_3} \right) \gamma_2 \\ &= \left[\frac{u_1-u_4}{h_3} + \frac{1}{2} \frac{h}{h_3} \theta \right] - \left(\frac{h_2}{h_3} \right) \gamma_2\end{aligned}\quad (7.3)$$

Where $h = y_b + h_2 + h_3 + \frac{h_1}{2}$ and θ denotes the slope. u and w denote the longitudinal and transverse displacements respectively. h_1 , h_4 , h_2 and h_3 denote the thickness of constraining layer, base beam, viscoelastic layer and standoff layer respectively. The distance between the top surface of the base beam and the neutral axis of the overall system is denoted by y_b . The shear stress developed in VEM layer is denoted by τ_2 . The shear strain of the VEM layer is represented by γ_2 . Similarly shear stress developed in SOL layer is denoted by τ_3 . The shear strain of the SOL layer is represented by γ_3 . u_1 and u_4 are the longitudinal displacement of the constraining layer and the base beam respectively and w is the transverse displacement of the constraining layer as well as of the base beam. The shear stress in both the layers is given as:

$$\tau_3 = G_3 \gamma_3 \quad \text{and} \quad \tau_2 = G_2 \gamma_2 \quad (7.4)\{a,b\}$$

Since equal stress is developed in both the layers, hence

$$\tau_3 = \tau_2 \quad (7.4)\{c\}$$

Relation (7.4) shows that:

$$\gamma_3 = \left(\frac{G_2}{G_3} \right) \gamma_2 \quad (7.5)$$

Solving equations (7.1- 7.3) and (7.5), we get:

$$\gamma_2 = \left[\frac{u_1 - u_4}{h_3} + \left(1 + \frac{h_1 + 2h_2 + 2y_b}{2h_3} \right) \frac{\partial w}{\partial x} \right] / \left(\frac{h_2}{h_3} + \frac{G_2}{G_3} \right) \quad (7.6)$$

and θ denotes the slope.

7.1.2 The Shape Functions

Nodal displacements are given as:

$$\{U\}_e = \{w_i \ \theta_i \ u_{bi} \ u_{ci} \ w_j \ \theta_j \ u_{bj} \ u_{cj}\}^T \quad (7.7)$$

The transverse displacement w , the rotation θ and the axial displacements of the respective layers are expressed in the nodal displacements by finite element shape functions:

$$\begin{aligned} w &= [N_w] \{U\}_e, \theta = [N_\theta] \{U\}_e, u_1 = [N_{u1}] \{U\}_e, u_2 = [N_{u2}] \{U\}_e, u_3 = [N_{u3}] \{U\}_e \\ u_4 &= [N_{u4}] \{U\}_e, u_5 = [N_{u5}] \{U\}_e \end{aligned} \quad \gamma_2 = [N_{\gamma_2}] \{U\}_e \text{ and } \gamma_3 = [N_{\gamma_3}] \{U\}_e \quad (7.8) \{a, b, c, d, e, f, g, h, i\}$$

7.1.3 Energies of ACLD System with SOL Treatment

For simplicity, all the energies are given for a single element. The total energy can be obtained by the combination of all the elements. Kinetic energy (T_e), strain energy (V_e) and as well as the work done (W_e) by external transverse load, piezoelectric forces and moments are discussed as below:

7.1.3.1 Kinetic Energies

The position vector p_k of a special point in the k^{th} layer at a distance x from the origin of the beam is given by:

$$p_k = (x + u_k)i + w j \quad (7.9)$$

where the dot denotes differentiation with respect to time t . The total kinetic energy of the complete system comprises the kinetic energies of constraining layer, base beam, SOL layer, sensor layer and VEM layer and is given as:

$$\begin{aligned} T_e &= \frac{1}{2} \int_0^{L_e} b \sum_{k=1}^5 \rho_k h_k (\dot{p}_k^T \dot{p}_k) dx \\ T_e &= \frac{1}{2} \int_0^{L_e} b \sum_{k=1}^5 \rho_k h_k \left[\dot{u}_k^2 + \dot{w}^2 + (x + u_k)^2 \dot{\theta}^2 + w^2 \dot{\theta}^2 + 2(x + u_k) \dot{w} \dot{\theta} - 2\dot{u}_k w \dot{\theta} \right] dx \end{aligned} \quad (7.10)$$

7.1.3.2 Potential Energies

The total potential energy of the complete system comprises the strain energies of constraining layer, base beam, VEM layer, SOL layer and Sensor layer. For each individual part it is given below:

7.1.3.2.1 Constraining layer

The potential energy of the constraining layer due to axial displacement is:

$$V_{e1} = \frac{1}{2} E_1 h_1 b \int_0^{L_e} \left(\frac{\partial u_1}{\partial x} \right)^2 dx = \frac{1}{2} \{U\}_e^T [K_{1u}] \{U\}_e \quad (7.11)\{a, b\}$$

$$\text{Where } [K_{1u}] = E_1 h_1 b \int_0^{L_e} \left[\frac{\partial N_{u1}}{\partial x} \right]^T \left[\frac{\partial N_{u1}}{\partial x} \right] dx$$

The potential energy of the constraining layer due to transverse displacement is:

$$V_{e2} = \frac{1}{2} E_1 I_1 \int_0^{L_e} \left(\frac{\partial^2 w}{\partial x^2} \right)^2 dx = \frac{1}{2} \{U\}_e^T [K_{1w}] \{U\}_e \quad (7.11)\{c, d\}$$

$$\text{Where } [K_{1w}] = E_1 I_1 \int_0^{L_e} \left[\frac{\partial^2 N_w}{\partial x^2} \right]^T \left[\frac{\partial^2 N_w}{\partial x^2} \right] dx$$

7.1.3.2.2 VEM layer

The potential energy of the VEM layer due to axial displacement is:

$$V_{e3} = \frac{1}{2} E_2 (h_2) b \int_0^{L_e} \left(\frac{\partial u_2}{\partial x} \right)^2 dx = \frac{1}{2} \{U\}_e^T [K_{2u}] \{U\}_e \quad (7.12)\{a,b\}$$

$$\text{Where } [K_{2u}] = E_2 (h_2) b \int_0^{L_e} \left[\frac{\partial N_{u2}}{\partial x} \right]^T \left[\frac{\partial N_{u2}}{\partial x} \right] dx$$

The potential energy of the VEM layer due to transverse displacement is:

$$V_{e4} = \frac{1}{2} E_2 (I_2) \int_0^{L_e} \left(\frac{\partial^2 w}{\partial x^2} \right)^2 dx = \frac{1}{2} \{U\}_e^T [K_{2w}] \{U\}_e \quad (7.12)\{c,d\}$$

$$\text{Where } [K_{2w}] = E_2 (I_2) \int_0^{L_e} \left[\frac{\partial^2 N_w}{\partial x^2} \right]^T \left[\frac{\partial^2 N_w}{\partial x^2} \right] dx$$

The potential energy of the VEM layer due to shearing:

$$V_{e5} = \frac{1}{2} G_2 (h_2) b \int_0^{L_e} \gamma_2^2 dx = \frac{1}{2} \{U\}_e^T [K_{2\gamma}] \{U\}_e \quad (7.13)\{a, b\}$$

$$\text{Where } [K_{2\gamma}] = G_2 (h_2) b \int_0^{L_e} [N_{\gamma 2}]^T [N_{\gamma 2}] dx$$

7.1.3.2.3 SOL layer

The potential energy of the SOL layer due to axial displacement is:

$$V_{e6} = \frac{1}{2} E_3 (h_3) b \int_0^{L_e} \left(\frac{\partial u_3}{\partial x} \right)^2 dx = \frac{1}{2} \{U\}_e^T [K_{3u}] \{U\}_e \quad (7.14)\{a, b\}$$

$$\text{Where } [K_{3u}] = E_3 (h_3) b \int_0^{L_e} \left[\frac{\partial N_{u3}}{\partial x} \right]^T \left[\frac{\partial N_{u3}}{\partial x} \right] dx$$

The potential energy of the SOL layer due to transverse displacement is:

$$V_{e7} = \frac{1}{2} E_3 I_3 \int_0^{L_e} \left(\frac{\partial^2 w}{\partial x^2} \right)^2 dx = \frac{1}{2} \{U\}_e^T [K_{3w}] \{U\}_e \quad (7.14)\{c, d\}$$

$$\text{Where } [K_{3w}] = E_3 I_3 \int_0^{L_e} \left[\frac{\partial^2 N_w}{\partial x^2} \right]^T \left[\frac{\partial^2 N_w}{\partial x^2} \right] dx$$

The potential energy of the SOL layer due to shearing:

$$V_{e8} = \frac{1}{2} G_3 (h_3) b \int_0^{L_e} \gamma_3^2 dx = \frac{1}{2} \{U\}_e^T [K_{3\gamma}] \{U\}_e \quad (7.14)\{e, f\}$$

$$\text{Where } [K_{3\gamma}] = G_3 (h_3) b \int_0^{L_e} [N_{\gamma 3}]^T [N_{\gamma 3}] dx$$

7.1.3.2.4 Base beam

The potential energy of the base beam due to axial displacement is:

$$V_{e9} = \frac{1}{2} E_4 h_4 b \int_0^{L_e} \left(\frac{\partial u_4}{\partial x} \right)^2 dx = \frac{1}{2} \{U\}_e^T [K_{4u}] \{U\}_e \quad (7.15)\{a, b\}$$

$$\text{Where } [K_{4u}] = E_4 h_4 b \int_0^{L_e} \left[\frac{\partial N_{u4}}{\partial x} \right]^T \left[\frac{\partial N_{u4}}{\partial x} \right] dx$$

The potential energy of the base beam due to transverse displacement is:

$$V_{e10} = \frac{1}{2} E_4 I_4 \int_0^{L_e} \left(\frac{\partial^2 w}{\partial x^2} \right)^2 dx = \frac{1}{2} \{U\}_e^T [K_{4w}] \{U\}_e \quad (7.15)\{c, d\}$$

$$\text{Where } [K_{4w}] = E_4 h_4 b \int_0^{L_e} \left[\frac{\partial^2 N_w}{\partial x^2} \right]^T \left[\frac{\partial^2 N_w}{\partial x^2} \right] dx$$

7.1.3.2.5 Sensor layer

The potential energy of the sensor layer due to axial displacement is:

$$V_{e11} = \frac{1}{2} E_5 h_5 b \int_0^{L_e} \left(\frac{\partial u_5}{\partial x} \right)^2 dx = \frac{1}{2} \{U\}_e^T [K_{5u}] \{U\}_e \quad (7.16)\{a, b\}$$

$$\text{Where } [K_{5u}] = E_5 h_5 b \int_0^{L_e} \left[\frac{\partial N_{u5}}{\partial x} \right]^T \left[\frac{\partial N_{u5}}{\partial x} \right] dx$$

The potential energy of the sensor layer due to transverse displacement is:

$$V_{e12} = \frac{1}{2} E_5 I_5 \int_0^{L_e} \left(\frac{\partial^2 w}{\partial x^2} \right)^2 dx = \frac{1}{2} \{U\}_e^T [K_{5w}] \{U\}_e \quad (7.16)\{c, d\}$$

$$\text{Where } [K_{5w}] = E_5 I_5 \int_0^{L_e} \left[\frac{\partial^2 N_w}{\partial x^2} \right]^T \left[\frac{\partial^2 N_w}{\partial x^2} \right] dx$$

7.1.3.2.6 Centrifugal stiffening effect

The potential energy due to centrifugal stiffening

$$V_{e13} = \frac{1}{2} \int_0^{L_e} P(x, t) \left(\frac{\partial w}{\partial x} \right)^2 dx \quad (7.17)$$

Where

$$\begin{aligned} P(x, t) &= \int_x^L (\rho_1 h_1 + \rho_2 h_2 + \rho_3 h_3 + \rho_4 h_4 + \rho_5 h_5) b \dot{\theta}^2 dx \\ &= \frac{1}{2} (\rho_1 h_1 + \rho_2 h_2 + \rho_3 h_3 + \rho_4 h_4 + \rho_5 h_5) b \dot{\theta}^2 (L^2 - \theta^2) \end{aligned}$$

7.1.4 Work Done

For one dimensional structure with uni-axial loading, the constitutive equations of PZT material can be written as given by:

$$[\mathbf{D}] = \begin{bmatrix} S^E_{11} & d_{31} \\ d_{31} & \epsilon^T_{33} \end{bmatrix} \begin{bmatrix} \sigma \\ E \end{bmatrix} \quad (7.18)$$

Where \mathbf{D} is the electrical displacement, \mathbf{E} is the electric field, $\boldsymbol{\epsilon}$ is the mechanical strain in x direction, and $\boldsymbol{\sigma}$ is the mechanical stress in x direction. S^E_{11} is the elastic compliance constant, ϵ^T_{33} is the dielectric constant, and d_{31} is the piezoelectric constant. Forces exerted on the system are:

- a) The externally applied mechanical force.
- b) The piezoelectric force developed by the PZT patch.

The work done W_1 by the external transverse load f acting on the beam/ACLD system is given as:

$$W_{e1} = \int_0^{L_e} f w(x, t) dx = \{U\}_e^T \{F_d\}_e \quad (7.19)$$

$$\text{Where } \{F_d\}_e = f \int_0^{L_e} \left[\frac{\partial^2 N_w}{\partial x^2} \right]^T dx$$

The work done W_2 by the piezoelectric control forces and moments are given as:

$$W_{e2} = E_1 A_1 \int_0^{L_e} \left[\varepsilon_{piezo} \left(\frac{\partial u_1}{\partial x} \right) + h \varepsilon_{piezo} \left(\frac{\partial^2 w}{\partial x^2} \right) \right] dx \quad (7.20)$$

Where ε_{piezo} denotes the strain introduced by the piezoelectric effect and is given as:

$$\varepsilon_{piezo} = \frac{d_{31} v_a \|_e}{h_1}$$

Here v_a is the applied voltage to the piezoelectric actuator. However, $v_a \|_e$ represents corresponding elemental voltage although both are same. This representation has significance in closed loop conditions. The work done can now be written as:

$$\begin{aligned} W_{e2} &= E_1 d_{31} b v_a \|_e \int_0^{L_e} \left(\frac{\partial u_1}{\partial x} \right) dx + h E_1 d_{31} b v_a \|_e \int_0^{L_e} \left(\frac{\partial^2 w}{\partial x^2} \right) dx \\ &= E_1 d_{31} b v_a \|_e \int_0^{L_e} \left[\frac{\partial N_{u1}}{\partial x} \right]^T dx + h E_1 d_{31} b v_a \|_e \int_0^{L_e} \left[\frac{\partial^2 N_w}{\partial x^2} \right]^T dx \\ \{U\}_e^T (\{F_{c1}\}_e + \{F_{c2}\}_e) \end{aligned} \quad (7.21)\{a\}$$

Where

$$\{F_{c1}\}_e = E_1 d_{31} b v_a \|_e \int_0^{L_e} \left[\frac{\partial N_{u1}}{\partial x} \right]^T dx$$

and

$$\{F_{c2}\}_e = h E_1 d_{31} b v_a \|_e \int_0^{L_e} \left[\frac{\partial^2 N_w}{\partial x^2} \right]^T dx$$

The work done W_3 by the applied hub torque τ is given by:

$$W_{e3} = \tau \theta \quad (7.21)\{b\}$$

7.1.5 Pure Beam Elements

The stiffness and mass matrices of pure beam elements have dimensions of 6x6, and are similar to those given by eq. (7.9).

7.1.6 Equations of Motion

Using Hamilton's principle, the equations of motion for an ACLD element can be written as:

$$\int_{t_1}^{t_2} \delta(T - \sum_{j=1}^{13} U_j) dt + \int_{t_1}^{t_2} \delta(\sum_{j=1}^3 w_j) dt = 0 \quad (7.22)\{a\}$$

For a single i^{th} element, defining the element coefficients and matrices as follows:

$$J_i = \int_0^{L_e} \sum_{k=1}^5 \rho_k h_k b (x_i + x)^2 dx \quad (7.22)\{b\}$$

$$[M_i] = \int_0^{L_e} \sum_{k=1}^5 \rho_k h_k b (N_k^T N_k + N_w^T N_w) dx \quad (7.22)\{c\}$$

$$[K_i] = \int_0^{L_e} \sum_{k=1}^5 \left[E_k h_k b \left\{ \left(\frac{\partial N_k}{\partial x} \right)^T \left(\frac{\partial N_k}{\partial x} \right) + E_k I_k \left\{ \left(\frac{\partial^2 N_w}{\partial x^2} \right)^T \left(\frac{\partial^2 N_w}{\partial x^2} \right) \right\} \right\} dx \quad (7.22)\{d\} \right]$$

$$\{V_{1i}\} = \int_0^{L_e} [\sum_{k=1}^5 \rho_k h_k b (x_i + x)] N_k dx \quad (7.22)\{e\}$$

$$\{V_{2i}\} = \int_0^{L_e} [\sum_{k=1}^5 \rho_k h_k b (x_i + x)] N_w dx \quad (7.22)\{f\}$$

$$\{V_{3i}\} = \frac{1}{2} \int_0^{L_e} \sum_{k=1}^5 \rho_k h_k b [L^2 - (x_i + x)] \left\{ \left(\frac{\partial N_w}{\partial x} \right)^T \left(\frac{\partial N_w}{\partial x} \right) \right\} dx \quad (7.22)\{g\}$$

$$\{V_{4i}\} = G_2 h_2 b \int_0^{L_e} [N_{\gamma 2}]^T [N_{\gamma 2}] dx + G_2 h_2 b \int_0^{L_e} [N_{\gamma 3}]^T [N_{\gamma 3}] dx \quad (7.22)\{h\}$$

$$\{R_i\} = \int_0^{L_e} \sum_{k=1}^5 \rho_k h_k b (N_k^T N_w) dx \quad \text{Where } \rho_k h_k = 2 \rho_k h_k \text{ for } k = 2 \quad (7.22)\{i\}$$

$$[G_i] = [R_i]^T - [R_i]$$

$$\{F_{ci}\} = \{F_{c1}\}_e + \{F_{c2}\}_e \quad (7.22)\{j\}$$

$$\{F_{di}\} = \{F_d\}_e \quad (7.22)\{k\}$$

Where x is the distance from the clamped end to the left node of the element under consideration. J_i is the moment of inertia of the i^{th} element about the clamped end. $[M_i]$ and $[K_i]$ are the elemental mass and stiffness matrices respectively. $[V_{3i}]$ and $[V_{4i}]$ are due to centrifugal force and shear deformation of the VEM layer and SOL layer respectively. The matrices R_i and G_i are due to the gyroscopic effects. The matrices $\{F_{ci}\}$ and $\{F_{di}\}$ are the control force and the external load respectively.

After using Hamilton's Principle, the equations of motion at the element level can be written as:

$$\begin{bmatrix} M_{\theta\theta i} & M_{\theta q i} \\ M_{q\theta i} & M_{qq i} \end{bmatrix} \begin{Bmatrix} \ddot{\theta} \\ \{\dot{U}\}_i \end{Bmatrix} + 2\dot{\theta} \begin{bmatrix} 0 & \{0\} \\ \{0\} & [G_i] \end{bmatrix} \begin{Bmatrix} \dot{\theta} \\ \{\dot{U}\}_i \end{Bmatrix} + \begin{bmatrix} 0 & \{0\} \\ \{0\} & [K_{qq i}] \end{bmatrix} \begin{Bmatrix} \theta \\ \{U\}_i \end{Bmatrix} = \begin{bmatrix} Q_{\theta i} \\ Q_{qi} \end{bmatrix} + \begin{bmatrix} F_{\theta i} \\ F_{qi} \end{bmatrix} \quad (7.23)$$

Where

$$M_{\theta\theta i} = J_i + \{q_i^T\}[M_i]\{q_i\} + 2\{V_{1i}\}\{q_i\} - \{q_i^T\}[V_{3i}]\{q_i\}$$

$$\{M_{\theta q i}\} = \{M_{q\theta i}\}^T = \{V_{2i}\} - \{q_i^T\}[G_i]$$

$$[M_{qq i}] = [M_i]$$

$$[K_{qq i}] = [K_i] - \dot{\theta}^2[M_i] + \dot{\theta}^2[V_{3i}] + [V_{4i}]$$

$$\{Q_{\theta i}\} = -2\dot{\theta}[\{q_i^T\}[M_i]\{\dot{q}_i\} + \{V_{1i}\}\{\dot{q}_i\} - \{q_i^T\}[V_{3i}]\{\dot{q}_i\}]$$

$$\{Q_{qi}\} = \dot{\theta}^2\{V_{1i}\}^T$$

$$F_{\theta i} = \tau$$

$$\{F_{qi}\} = \{F_{ci}\} + \{F_{di}\}$$

in which $M_{\theta\theta i}$ is the rotational inertia of the system, $[M_{qq i}]$ is the generalized mass matrix, $\{M_{\theta q i}\}$ is the non-linear inertia coupling between rigid body and the elastic deformations, $[K_{qq i}]$ is the generalized stiffness matrix and $[G_i]$ is the gyroscopic matrix. $\{Q_{\theta i}\}$ and $\{Q_{qi}\}$ represent the non-linear pseudo loads. $\{F_{qi}\}$ represents the sum of control force and external load. Eqn. 6.38 represents a non-linear hybrid gyroscopic dynamic system which is inertia coupled between rigid body and elastic deformations. Mode superposition is not applicable to non-linear systems. For simplicity the angular velocity $\dot{\theta}$ is assumed to be constant as well as no external load is applied. After linearization the elemental equations become:

$$[M_{qq i}]\{\ddot{U}_i\} + 2\dot{\theta}[G_i]\{\dot{U}_i\} + [K_{qq i}]\{U_i\} = \{F_{qq i}\} \quad (7.24)\{a\}$$

and assembling the elemental equations we obtain the global system equations are obtained as:

$$[M_{qq}]\{\ddot{U}\} + 2\dot{\theta}[G]\{\dot{U}\} + [K_{qq}]\{U\} = \{F_{qq}\} \quad (7.24)\{b\}$$

Where $[M_{qq}]$ real symmetric positive is definite, $[G]$ is real skew symmetric and $[K_{qq}]$ is symmetric. $[K_{qq}]$ is complex due to complex shear modulus G_2 of the VEM layer, and G_3 of the SOL layer respectively. The above equation without subscript i denotes the global form of corresponding elemental co-efficient matrices.

7.1.6.1 Open Loop Conditions

The voltage developed v_s for a uniform sensor of length L_e (i.e. length of one element) is obtained from the following formula:

$$V_s \parallel e = -\frac{k^2 g_{31} D_d b}{g_{31} C} \int_0^{L_e} \frac{\partial^2 w}{\partial x^2} dx \quad (7.25)\{a\}$$

Where k_{31} is the electromechanical coupling factor, D_d is the distance from the neutral axis to sensor surface. g_{31} is piezoelectric voltage constant. The capacitance C of the sensor is given by:

$$C = \frac{8.854 \times 10^{-12} A_s k_{3t}}{h_b} \quad (7.25)\{b\}$$

Where A_s is the sensor area and k_{3t} is the dielectric constant. Thus the voltage developed is given as:

$$v_s \parallel e = [K_{sensor}]_e^T \{U\}_e \quad (7.25)\{c\}$$

Where

$$[K_{sensor}]_e = -\frac{k^2 g_{31} D_d b}{g_{31} C} \int_0^{L_e} \frac{\partial^2 N_w}{\partial x^2} dx$$

7.1.6.2 Closed Loop Conditions

With Proportional Derivative controller, the relationship between actuator voltage $v_a \parallel e$ and sensor voltage $v_s \parallel e$ is given as:

$$v_a \parallel e = -K_p v_s \parallel e - K_d \frac{d v_s \parallel e}{dt} \quad (7.26)$$

Where K_p and K_d are proportional and derivative control gains, respectively. Substituting Eqn. (7.26) into Eqn. (7.24), the closed loop equation of motion for the system with single i^{th} element is given as:

$$[M_{qq}]_i \{\ddot{U}\}_i + 2 \dot{\theta} [G]_i \{\dot{U}\}_i + [[K_{qq}]_i + [G_p]_i] \{U\}_i = \{0\}_i \quad (7.27)\{a\}$$

Collecting all the elements to form the global equations of motion we get:

$$[M_{qq}] \{\ddot{U}\} + 2 \dot{\theta} [G] \{\dot{U}\} + [[K_{qq}] + [G_p]] \{U\} = \{0\} \quad (7.27)\{b\}$$

The eigen value problem associated with eq. (7.27b) is second order, so it does not permit a ready solution. The difficulty can be overcome by converting into state space form:

$$[A]\dot{z} + [B]z = \{0\} \quad (7.28)$$

Where $z = [[\dot{U}]^T \ [U]^T]^T$ and

$$[A] = \begin{bmatrix} [M_{qq}] & [0] \\ [0] & [I] \end{bmatrix}, \quad [B] = \begin{bmatrix} 2\dot{\theta}[G] & [K_{qq} + G_{qq}] \\ [-I] & [0] \end{bmatrix},$$

The eigen value problem associated with eq. (7.28) is:

$$(\lambda_j A + B)Z_j = 0 \quad (7.29)\{a\}$$

Where λ_j and Z_j are the j^{th} closed loop complex eigen value and eigenvector, respectively. Representing the complex eigen value by:

$$\lambda_j = \sigma_j + i \omega_j \quad (7.29)\{b\}$$

Where the real part σ_j represents the vibration exponential decay while the imaginary part ω_j is the damped frequency. The damping ratio is given by:

$$\xi_j = \frac{\sigma_j}{\sqrt{\sigma_j^2 + \omega_j^2}} \quad (7.29)\{c\}$$

However, the damped natural frequencies and damping ratios can be easily calculated using the DAMP command of MATLAB.

7.2 RESULTS AND DISCUSSION

7.2.1 Comparisons with Results from Previous Researches

In order to check the accuracy of the developed mathematical model, the comparison was done with the work done earlier in the history. With these boundary conditions, results were found to match properly. Which confirmed that mathematical modeling developed for partial treatment is also correct.

7.2.2 Performance with Full PCLD Treatment using SOL Layer

By applying a SOL layer on the base beam and afterwards attaching VEM layer between the constraining layer and SOL layer, the damping performance is enhanced. The damping ratios also tend to increase as the thickness of SOL layer increases. With a SOL layer of 2.286 mm (i.e. equal to base beam), the damping ratios increase by a factor of 3.5 times, 4 times, 5.6 times and 6.10 times for the first, second, third and fourth mode respectively Figure 7.2 and Figure 7.3 show the damping ratios and natural frequencies as a function of RPM of the beam respectively. With the addition of SOL layer, the natural frequencies are enhanced as compared to simple PCLD treatment. As the thickness of the SOL layer increases, natural frequencies tend to increase for all the modes.

Further, a comparison of ACLD (without SOL) treatment with PCLD using SOL layer is given in Figure 7.4. Normal ACLD treatment with a feedback gain of 20 lags behind in damping ratios than PCLD with SOL layer treatment. It is a surprising performance as reliability of passive techniques is much more than active techniques. Thus, PCLD with SOL layer is an efficient technique. At very high feedback gain (i.e. $k_p=30$), although damping performance of

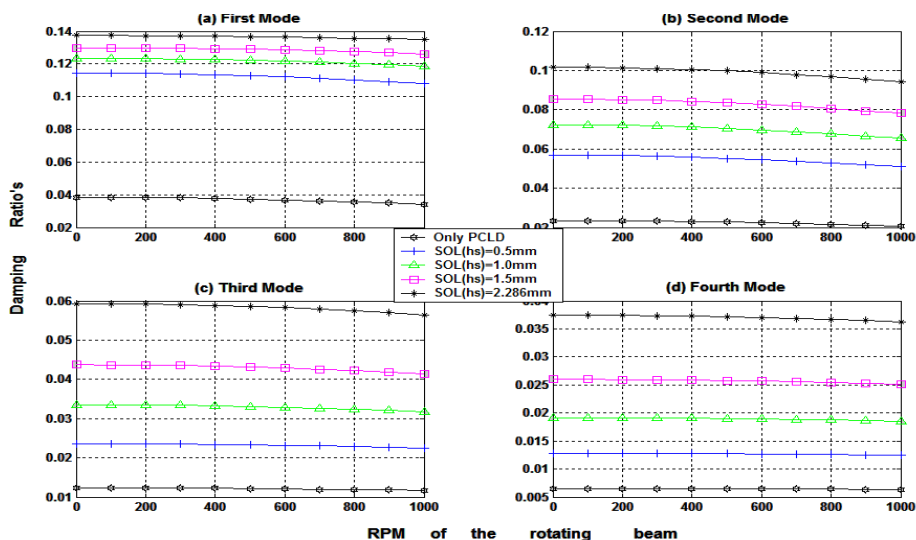


Fig. 7.2: Damping ratios of the rotating PCLD beam system (with SOL layer) as a function of RPM at different thickness's of SOL layer [thickness of VEM layer = 0.25 mm, $G_s = (0.2615 e9) \times (1+0.38 \times i)$]

normal ACLD treatment is better than PCLD with SOL treatment for rest of modes except the first mode, the later technique surpasses the former for the first mode. The most important results of this work are demonstrated in this paragraph. Any random combination of shear modulus of the SOL layer and VEM layer will not serve the purpose. Surprisingly, if the shear modulus of the SOL layer is same as VEM layer, damping performance will be degraded instead of improving.

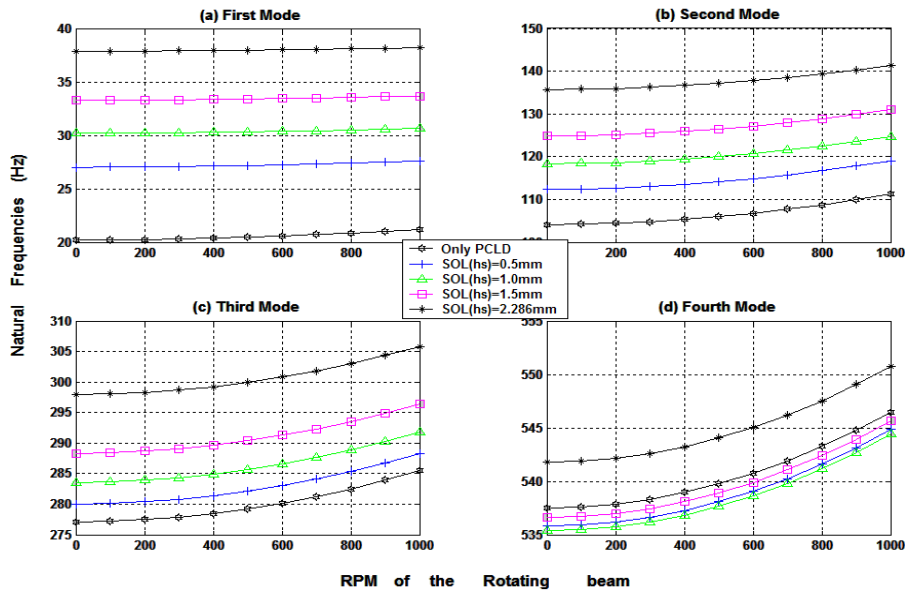


Fig. 7.3: Natural frequencies of the rotating PCLD beam system (with SOL layer) as a function of RPM at different thicknesses of SOL layer [thickness of VEM layer = 0.25 mm, $G_s = (0.2615e9) \times (1+0.38 \times i)$]

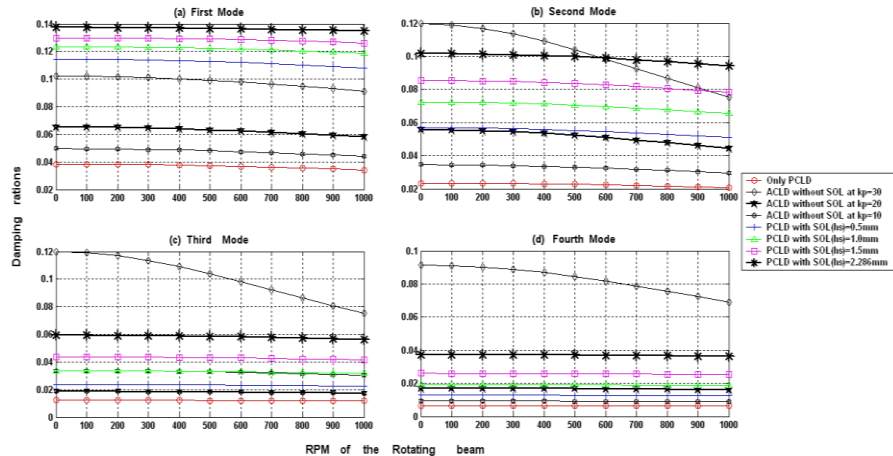


Fig. 7.4: Comparison of damping ratios of the rotating PCLD beam system (with SOL layer) and ACLD (without SOL) as a function of RPM at different thickness's of SOL layer [thickness of VEM layer = 0.25 mm, $G_s = (0.2615e9) \times (1+0.38 \times i)$]

The damping performance is at its peak when the shear modulus of SOL is in the range 1×10^8 - 1.3×10^8 N/m 2 . The VEM layer has a shear modulus of 2.6×10^5 N/m 2 . The maximum performance is achieved when the shear factor of the SOL layer is 10^3 times that of VEM layer.

7.2.3 Performance with ACLD Treatment using SOL Layer

7.2.3.1 Full Treatment

The relative contribution of passive action and active control action is shown in Figure 7.5.

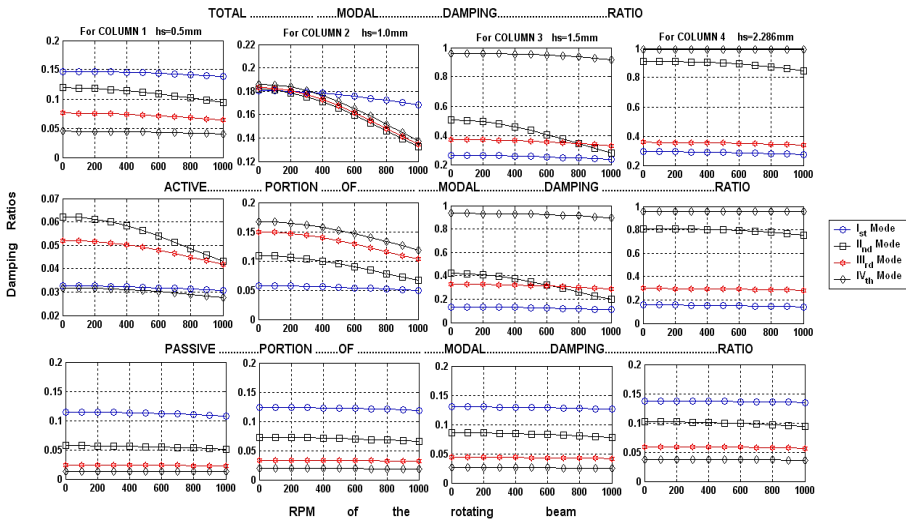


Fig. 7.5: Comparison of active and passive portion of damping ratios of the rotating ACLD beam system (with SOL layer) as a function of RPM at different thickness's of SOL layer [thickness of VEM layer = 0.25 mm, $G_s = (0.2615e9) \times (1+0.38 \times i)$] with $k_p=20$

Each column of this figure represents the results for a particular thickness of the SOL layer (i.e. 0.5mm, 1.0 mm, 1.5 mm, and 2.286 mm). All the first four modal damping ratios are shown as a function of RPM of the rotating beam. Lowermost row represents the contribution due to PCLD treatments with SOL layer. Middle row represents contribution due to the active portion of the ACLD treatment with SOL layer. This is obtained by subtracting the contribution of PCLD system from the total contribution of ACLD system. The feedback gain of 20 is taken for this set of readings. With increase in thickness of the SOL, total damping factor of each mode increases. The increase in the performance due to passive portion with SOL thickness is very small (lowermost row). However, the increase in the performance due to the active portion is very high as the thickness of SOL increases (middle row). The rise in the damping performance for the first mode is by a factor of 2, 4.6 and 5.3 as the thickness of SOL changes from 0.5 mm to 1.0 mm, 1.5 mm and 2.286 mm respectively. This factor has the corresponding values as 3, 6.6 and 13.3 for the second mode. Thus, the effect of SOL layer thickness on the damping performance is magical. This is probably due to the reason that with the increase in thickness of SOL layer, the distance between the neutral axis of the constraining layer and the base beam increases which increases the bending moment applied by the active constraining layer. One thing worth observing is that as the thickness of SOL increases, the plot of damping ratios as a function of RPM of the

rotating beam becomes flat (fourth column of the Figure) i.e. reducing the negative effect of RPM of the beam to decrease all the modal damping ratios. This is the major problem in simple ACLD or PCLD treatment without SOL layer.

7.2.3.2 Partial Treatment

Partial treatment is preferred instead of full treatment due to weight and ease of attachment considerations. In the present work, a partial treatment of 33% was considered. The length of the treatment was 100 mm. For various locations of the treatment, different results were obtained. First of all PCLD treatment with SOL layer was investigated. Figure 7.6 shows that the treatment at a distance of 100 mm from the fixed end gave maximum damping performance for all the modes except the second mode.

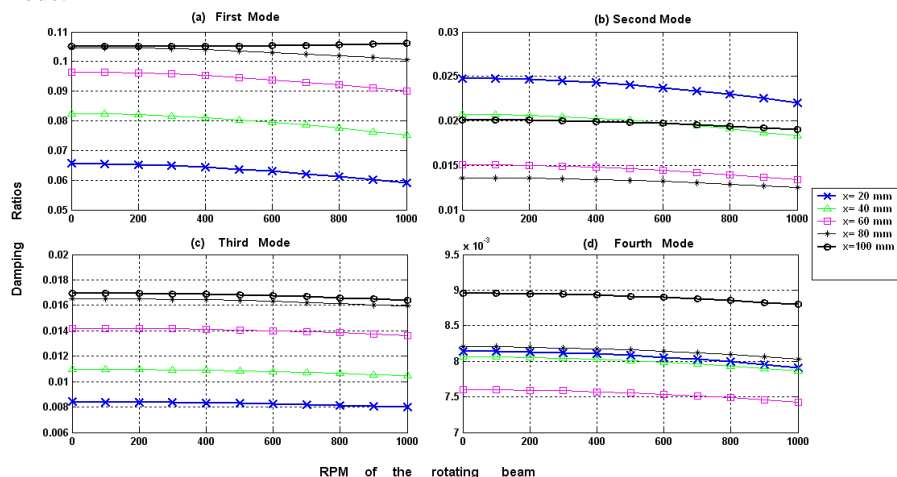


Fig. 7.6: Damping ratios of the rotating PCLD beam system as a function of RPM at different location of patch [SOL layer thickness = 1.5 mm, VEM layer thickness = 0.25mm, $G_s = (0.2615e9) \times (1+0.38 \times i)$] ACLD

The damping performance increased as the distance of the patch location from the fixed end was increased. The natural frequencies increased with the RPM of the beam for lower distances of the treatment from the fixed end. However, for higher distances of the treatment from the center of rotation, first natural frequency decreased as RPM of the beam was increased. For the ACLD treatment with SOL layer, the same pattern was not followed as shown in Figure 7.7. The damping performance of the second mode was best when the treatment was at a distance of 20 mm from the fixed end of the rotating beam. First mode damping performance was best when the treatment was at a distance of 80mm from the center of rotation. Third and fourth mode damping performance was best when the treatment was done at a distance of 100 mm and 40 mm respectively from the center of rotation. It has been observed that for pure ACLD treatment without SOL layer, the damping ratios are maximum when the center of the treatment lies on the point where the modal amplitude is maximum. At nodal points where modal amplitude is zero damping ratios are minimum. However, using SOL layer in the ACLD or PCLD treatment, this behavior of damping ratios was not there.

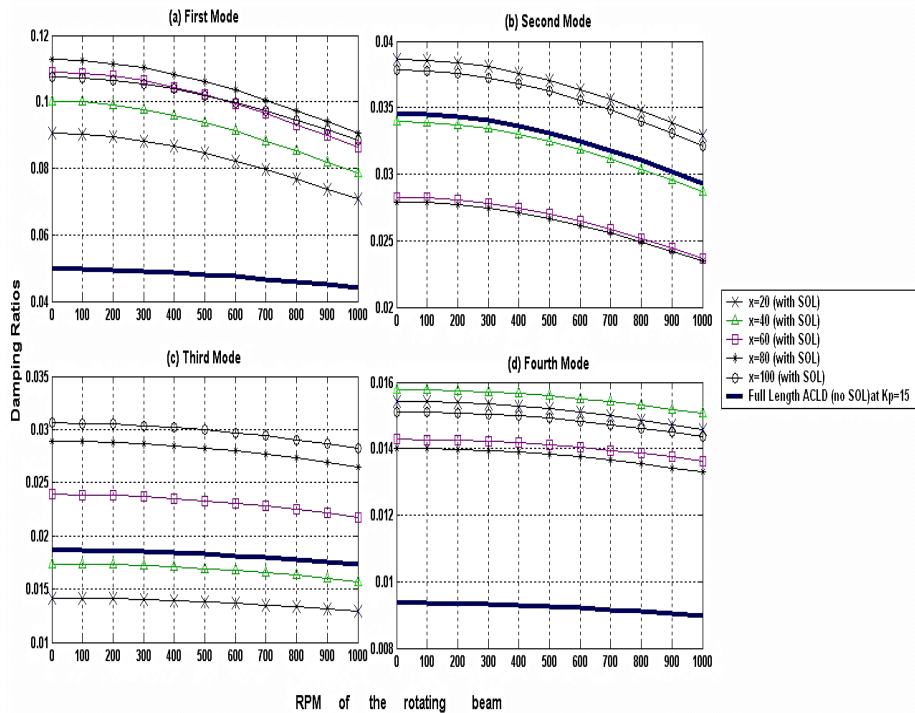
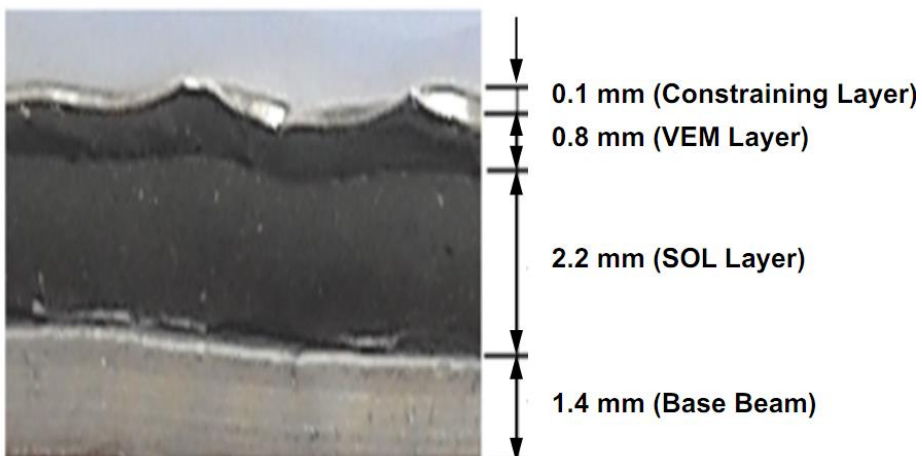


Fig. 7.7: Damping ratios of the rotating beam system as a function of RPM at different location of patch [SOL layer thickness = 1.5mm, VEM layer thickness = 0.25 mm, $K_p=15$, $G_s= (0.2615e9) \times (1+0.38 \times i)$]

7.3 EXPERIMENTAL VALIDATION

7.3.1 Experimental Setup

To check the validity of the theoretical results, an experimental setup was made. Photograph 7.1 shows the PCLD treated beam with SOL layer.



Photograph 7.1: Beam treated with PCLD (with SOL layer) treatment

Photograph (7.2) as below shows the picture of experimentally treated rotating beam. Length of the beam is 250 mm.



Photograph 7.2: Experimental setup of the rotating beam mounted on milling m/c bed

Figure 7.8 shows the schematics of the experimental setup with the associated hardware involved.

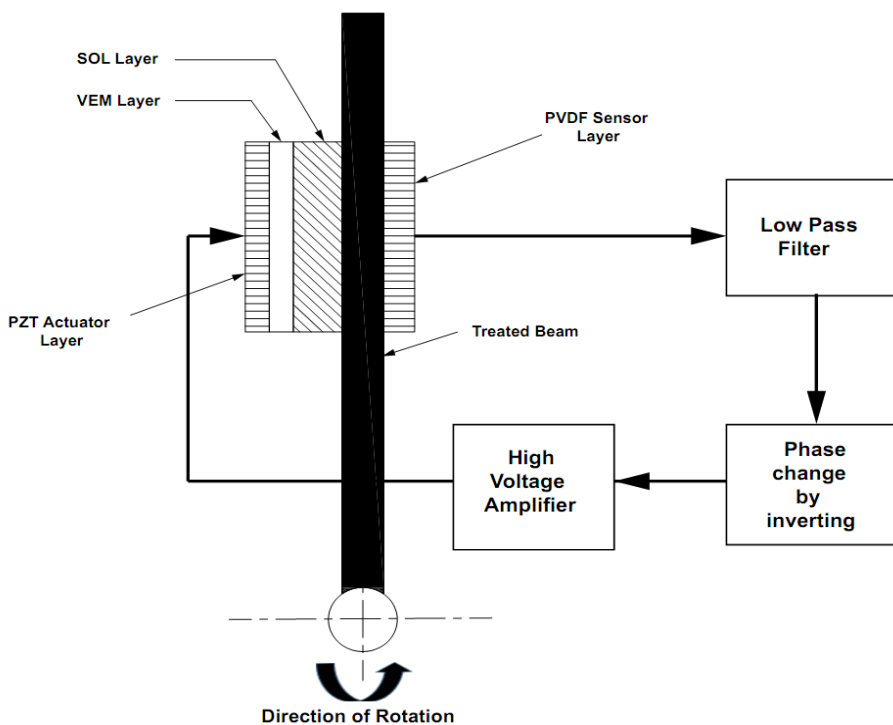


Fig. 7.8: Schematic of the rotating beam along with control hardware

The PVDF and PZT layers are shown in the Figure 7.8. A passive constraining layer of aluminium of 0.1mm is shown in the Photograph 7.1. Length of the treated portion is 50 mm and the treatment is done at a distance of 20 mm from the free end (i.e. starting point of PCLD treatment is at a distance of 20 mm from the fixed end). DYAD 606 and ISD 112 are the professional material names for SOL and VEM layer respectively. For ACLD treatment, a PZT patch of appropriate dimensions was attached on the aluminium constraining layer and a PVDF layer of 0.08 mm was attached on the other side of the base beam. The thickness of the VEM layer is 0.8 mm and SOL layer is 2.2 mm.

The base beam is made of steel and is of the thickness 1.4mm. The length of the PZT patch is 20 mm only and is attached at the mid of the constraining layer. The voltage from sensor

PZT patch was passed to a high voltage amplifier MA-17. A low pass filter with cut-off frequency equal to just above the fourth resonance frequency of the vibrating structure was applied to remove the influence of higher modes. After inversion and amplification from the first channel of the amplifier, the voltage was directed to the actuator PZT patch. A spectrum analyzer was used to create signals of various frequencies. The modulus of rigidity and density of the base beam for this material is $70 \times 10^9 \text{ N/m}^2$ and 2710 Kg/m^3 respectively. Practically the shear modulus of DYAD 606 (SOL layer material) is 100-300 times that of ISD 112 (VEM layer). Experimental and theoretical frequency response comparison of the beam is shown in the Table 7.1.

Table 7.1: Comparison of experimental and theoretical frequency response of the beam

Vibration Characteristics		Theoretical			Practical		
		Kp= 0	Kp= 5	Kp= 10	RPM= 0	RPM= 500	RPM= 1000
Frequencies(Hz)	Mode 1	19.9	19.0	17.9	19.3	18.5	17.2
	Mode 2	119.0	118.2	117.1	117.1	116.4	115.3
	Mode 3	320.1	315.3	308.3	310.2	304.2	295.3
Damping ratios	Mode 1	0.020	0.023	0.028	0.015	0.020	0.022
	Mode 2	0.0081	0.0086	0.0094	0.0070	0.0074	0.0082
	Mode 3	0.0028	0.0034	0.0041	0.0020	0.0028	0.0031

The experimental results are sufficiently close to theoretical results. The variation between the results is attributed to the reasons that the strain developed in the base beam varies due to lose adhesive bond of the gluing adhesives and the variation in the properties of the PZT, aluminium, VEM, SOL layer material parameters and compression damping factor which needs addition of separate transverse displacement for the constraining layer. For calculations, the loss factor and shear modulus of the VEM and SOL layer were taken to be constant for small frequency range covering first three modes. This can cause certain deviation of theoretical results from experimental data.

@Seismicisolation

CHAPTER – 8

CONTROLLING VIBRATIONS BY VARIOUS CONTROLLERS

Due to the distributed nature of flexible structures, these structures contain large number of modes and their transfer functions contain many poles close to the imaginary axis. These systems are generally difficult to control. In most cases, only first few modes need to be controlled. However, the presence of these uncontrolled modes can lead to the problem of spillover i.e. the some of the control energy is utilized to excite the higher order modes that causes the system destabilization. It is very difficult to model the higher modes exactly, by using present modeling techniques. The widely used smart materials for vibration control in structures are piezoelectric materials since they have desirable characteristics. Based on these characteristics, piezoelectric materials are used as sensors and actuators and up to certain extent this problem can be solved by using collocated sensors and actuators.

For collocated sensor/actuator system, a large number of control techniques are available with guaranteed and unconditional system stability. Velocity feedback and resonant controllers are the two examples of such controllers as explained. However, positive position feedback (PPF) controllers are insensitive to spillover effect. These have the additional property that it rolls off quickly at higher frequencies. However, these don't guarantee the unconditional closed loop stability. One of the issues with resonant controllers is their limited performance (in terms of the damping provided to the flexible structure). On the other hand, with velocity feedback controllers, high control effort is required. Also, all the modes can't be controlled uniformly.

Recently optimal control was combined with PPF controller. PPF controllers have also been combined with delayed-feedback controllers to design a more robust control system. Adaptive control was used for the multimode control of frequency varying structures.

The simple PPF has been modified for reducing the vibration amplitude caused by simultaneous impulsive and periodic disturbances. Adaptive PPF controllers have been used for actively absorbing the energy in acoustic cavities. The above said controllers have been successively used to reduce the tip vibrations of flexible manipulators.

However, very limited study is available for the systematic design of PPF controllers. Only recently a man called Moheimani used Linear Matrix Inequality based techniques for the systematic design of Multi-Input, Multi-Output PPF controller in 2006. Linear Matrix Inequality approach (LMI) was used to design the PPF system with pole optimization. Resonant controllers are somewhat similar to PPF controllers. A Lagrange multiplier approach was used to find the optimal parameters of the above said resonant controller by Moheimani and his co-worker Halim in 2001. For Single-Input and Single-Output application, the work reported by some scientists in the same year

2001 is also quite helpful. It uses on-line pole-zero identification method for autonomous vibration suppression. However, the above references don't give any systematic method to design the PPF controllers in the presence of phase lead/lag problems caused by instrumentations. Improvements can be made by eliminating the smoothing filters from the control transfer function by utilizing more sophisticated sensing techniques such as self-sensing. However, the problem of system delay remained as such.

Real time engines provided by National Instruments and controller boards provided by dSPACE Corporation are dedicated processors with real time software support. These can work at very high sampling rates without any delay in the application of control input. However, the ordinary data acquisition card working with an ordinary computer, suffer from time delay in the applied input. A lot of time is used in control calculations. Hence, low sampling rates has to be maintained. The digital controllers obtained by digitizing the continuous time controllers suffer from certain problems if low sampling frequency is used for continuous to discrete time conversion. Thus, these problems of phase lead/lag and system delay are unavoidable with low cost instrumentation.

Present research is directed with the aim of designing an efficient PPF controller with a systematic design process which works efficiently even in the presence of problems mentioned above. Direct search based optimization technique like pattern search has been applied to reduce the H_2 norm or H_∞ norm of the closed loop systems with actually considering the hardware present in the loop. MATLAB based Pattern search tool box has been used for corresponding optimization..

The contribution of the present work can be divided in to the following:

- A systematic design methodology has been suggested to design the PPF controllers. The controllers are designed in such a way that uniform damping can be provided to all the modes. Since the controller has been designed by considering the instrumentation and time delay actually present in the control loop, phase lead and lag problem caused by instrumentation can be completely eliminated.*
- The objective function of the optimization is H_2 or H_∞ norm of the closed loop system. With this method the use of other complicated frequency domain techniques and root locus techniques can be avoided. Also, the controllers designed based on the reduction of H_∞ norm of the closed loop system are robust in nature.*
- PPF controllers are of low order and avoid the problem of spillover so are easy to implement in practice.*

8.1 MODELING OF THE FLEXIBLE BEAM

Lagrange's Equations of motion for linear systems are given as below:

$$\sum_{s=1}^n [m_{js} \ddot{y}_s(t) + c_{js} \dot{y}_s + k_{js} y_s(t)] = Q_j(t) \quad j = 1, 2, 3, \dots, n \quad (8.1)$$

where $y(t)$ is the physical displacement, $\dot{y}(t)$ is physical velocity and $\ddot{y}(t)$ is the acceleration at time instant 't' for the particular degree of freedom. Also m, c and k are the elements of mass, damping and stiffness respectively. Equation 8.1 represents a set of n simultaneous second-order ordinary differential equations in generalized coordinates. By this relation, the infinitely many-degree-of-freedom distributed system is approximated by a n-degree of freedom system. This relation can be written in matrix form as given by:

$$M \ddot{y}(t) + C \dot{y}(t) + K y(t) = Q(t) \quad (8.2)$$

where M , C and K are the global mass, damping and stiffness matrices respectively, and $Q(t)$ is the vector of physical applied forces at various degrees of freedom on instant of time t . The column vector x is the nodal (also called physical) displacements at time t . Using these global mass and stiffness matrices the frequencies and mode shapes of the system can be obtained. Damping ratios can be obtained from experiments. By using natural frequencies, damping ratio's and mode shapes, the system can be represented in the following state space form as:

$$\begin{aligned}\dot{x}(t) &= A x(t) + B u(t) \\ y(t) &= C x(t)\end{aligned}\quad (8.3)$$

Normally first few modes are used to represent the flexible structures. The matrices A , B and C are calculated by using multiple modes into consideration. In the transfer function form it can be written as:

$$G^n(s) = \sum_{i=1}^n \frac{\phi_i \phi'_i}{s^2 + 2 \omega_i \eta_i s + \omega_i^2} \quad (8.4)$$

Where ω_i , η_i and $\phi_i \phi'_i$ represent the modal frequency, modal damping factor and product of mode shapes at the sensor and actuator location respectively for the i^{th} mode. To consider the effect of high frequency un-modeled modes, the existence of feed through term D is necessary and hence the system can be represented as:

$$G^n(s) = \sum_{i=1}^n \frac{\phi_i \phi'_i}{s^2 + 2 \omega_i \eta_i s + \omega_i^2} + D \quad (8.5)$$

Figure 8.19 (a, b, c) gives the complete picture of the flexible structure. Part (a) describes the geometry of the flexible beam with PZT actuator and PVDF sensor. Part (b) shows the frequency response function (FRF) of the flexible beam from the distributed piezoelectric actuator to the distributed sensor. Part (c) shows the frequency response function (FRF) of the flexible beam from the distributed piezoelectric actuator to the distributed sensor. The effect of feed-through term is clearly visible in this Figure.

In the present case a steel beam of 600 mm length is fixed at one end and is kept free at the other end. The width and thickness of the beam is 20 mm and 3 mm respectively. The thickness of the PZT patches applied on both the ends is 1 mm. Both the patches are 50 mm long and 20 mm wide. These are attached to the beam at a distance of 40 mm from the fixed end.

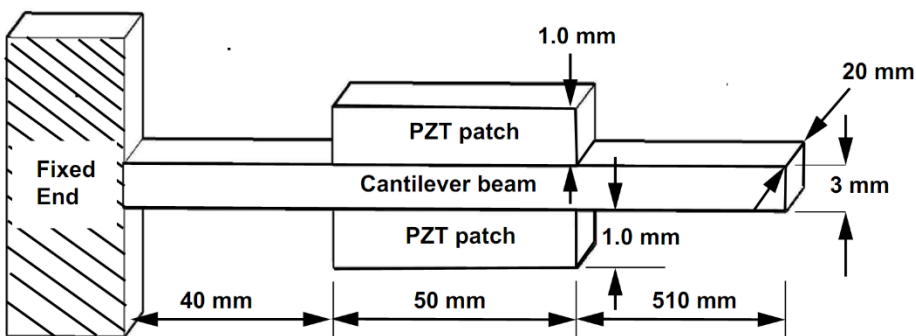


Fig. 8.1 (a): Geometry of the flexible beam with PZT actuator and PVDF sensor

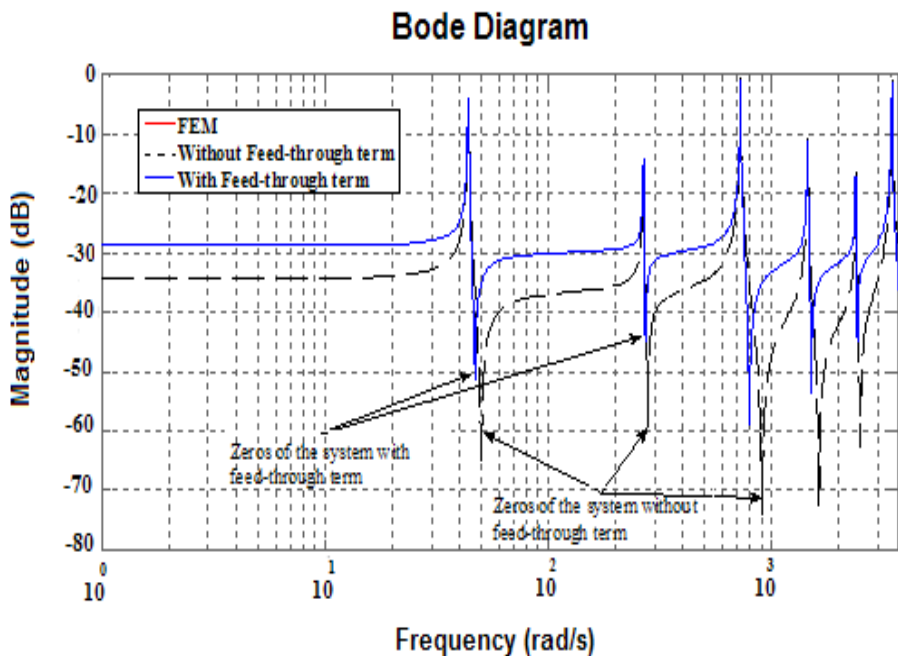


Fig. 8.1 (b): Effect of feed through term on the FRF of the flexible beam

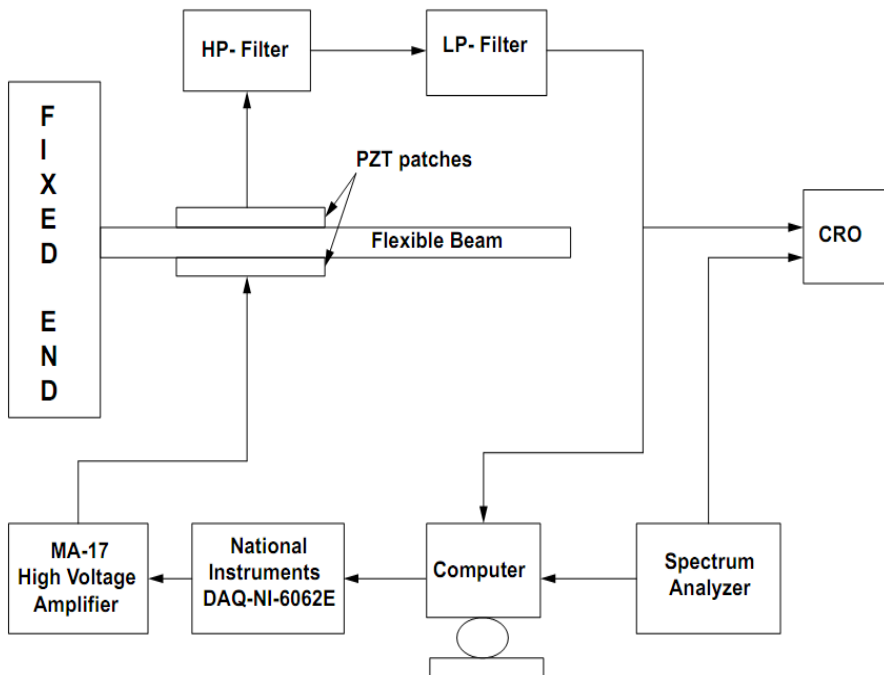


Fig. 8.1 (c): Schematic for experimental setup for system identification

The electrical properties of the PZT patches are shown in Table 8.1 below:

Table 8.1: Electrical properties of PZT

Property	Symbol	Value
Piezoelectric charge constant (m V^{-1})	d_{31}	171×10^{-12}
Electromechanical Coupling factor	k_{31}	0.12
Piezoelectric voltage constant (VmN^{-1})	g_{31}	216×10^{-3}
Dielectric constant	k_{3t}	12

The total beam is divided into 20 segments for FEM analysis. If the feed-through term D is considered, the response obtained from FEM data (i.e. with Eqn. 8.2) matches well with that obtained using Eqn. 8.5. Without this term, the zeros of the open loop system can't be identified accurately, hence reducing the efficiency of the optimally designed controller.

8.2 GREYBOX SUBSPACE SYSTEM IDENTIFICATION

The matrix \mathbf{K} can be real or complex. It is easy to construct the frequency response function (FRF) from the input -to- output data using \mathbf{M} and \mathbf{K} matrices with the help of standard MATLAB tools. Reduced order system transfer function can be identified from FRF data using standard system identification methods. Another advantage of this technique is that experimentally obtained FRF can be clubbed with FEM results to construct more realistic models of the dynamic system. In the present study experimental setup as shown in Figure 8.1 (c) is used for system identification purpose. A spectrum analyzer was used to generate the optimal excitation signal. For the identification of linear systems, there are three basic fundamentals for the excitation signal:

- a) The asymptotic properties of the estimate (bias and variance) depend only on the input spectrum and not the actual waveform of the input.
- b) The input must have limited amplitude.
- c) Periodic inputs may have certain advantages. Based on several other factors, the classification of the input signal can be done into various categories viz. Filtered Gaussian White Noise, Random Binary Signal, Pseudo-Random Binary Signal, Multi Sines and Chirp Signals or Swept Sinusoids.

The magnitude of the excitation signal was 20 volt. The duration of the excitation signal was chosen to be 8 secs. The frequency content of the signal was 0–400 Hz. To minimize the measurement noise the experiment was repeated several times. 400 spectral lines were used for the identification. In the first stage, natural frequencies and damping ratios are identified. Afterwards the mode shape product and feed through term are calculated. For the purpose of brevity detailed procedure is not mentioned here.

It has been observed that sub-space based models are more useful in designing the controller as compared to polynomial based models. The sub-space (state space) model has certain physically meaningful parameters like natural frequencies, damping ratios and mode shapes. These would be helpful in the construction of a system with real parametric uncertainties given by. The system can be written in the form written as below:

$$\dot{x}(t) = A x(t) + B u(t)$$

$$= \begin{pmatrix} 0 & I \\ -\Omega & -\Lambda \end{pmatrix} x(t) + \begin{pmatrix} 0 \\ B_2 \end{pmatrix} u(t) \quad (8.6) \{a\}$$

$$y(t) = C x(t) = (B_2^T \quad 0) x(t) \quad (8.6) \{b\}$$

Where Ω and $\Lambda \in R^{n \times n}$ and $B_2 \in R^{n \times m}$ has to be estimated if inputs and outputs are collocated, which is there in our present work. Here m represents the number of inputs of the system and n is related with number of modes considered for modeling. For a single input single output (SISO) system, with single mode consideration, the above model can be written as:

$$\begin{aligned} \dot{x}(t) &= \begin{pmatrix} 0 & 1 \\ -\omega^2 & -2\eta\omega \end{pmatrix} x(t) + \begin{pmatrix} 0 \\ \phi\phi' \end{pmatrix} u(t) \\ y(t) &= (1 \quad 0) x(t) \end{aligned} \quad (8.7)$$

where ω , η and $\phi\phi'$ are the natural frequency, damping ratio and mode shape (of the considered mode) respectively of the structure at the location where actuator and sensor are attached. $\phi\phi'$ is obtained by multiplying the mass normalized mode shapes at the sensor and actuator location. By considering the various modes of interest, the model above can be extended to multi-mode case easily. The frequencies and mode shapes are available by solving the eigenvalue problem from global mass and stiffness matrices using standard methods. Damping ratios can be identified experimentally. Now, by using these parameters, $\phi\phi'$ for each mode will be calculated. Let $G(j\omega)$ represents the FRF of the continuous time system obtained from FEM data which can then be written as:

$$G(j\omega) = \sum_{i=1}^n \psi_i(j\omega)^i \phi_{12} = \sum_{i=1}^n \psi_i(j\omega) R_i \quad (8.8)$$

Where $R_i = i_{\phi_{12}}$ is the residue matrix corresponding to i^{th} mode. It can be calculated using the following equation:

$$\Xi R = \Upsilon \quad (8.9)$$

Where

$$\Xi = \begin{pmatrix} \psi_1(j\omega_1)I_p & \psi_2(j\omega_1)I_p & \dots & \psi_n(j\omega_1)I_p \\ \psi_1(j\omega_2)I_p & \psi_2(j\omega_2)I_p & \dots & \psi_n(j\omega_2)I_p \\ \vdots & \vdots & \ddots & \vdots \\ \psi_1(j\omega_M)I_p & \psi_2(j\omega_M)I_p & \dots & \psi_n(j\omega_M)I_p \end{pmatrix} \quad (8.10)$$

I_p is a unity matrix with appropriate dimensions considering the number of inputs and outputs.

$$R = \begin{pmatrix} R_1 \\ R_2 \\ \vdots \\ R_n \end{pmatrix} \in R^{m \times m} \quad (8.11)$$

$$\Upsilon = \begin{pmatrix} \mathbf{G}(\omega_1) \\ \mathbf{G}(\omega_2) \\ \vdots \\ \mathbf{G}(\omega_M) \end{pmatrix} \in C^{p \times m} \quad (8.12)$$

Since

$$\mathbf{R} = \mathbf{X}^T \begin{pmatrix} \operatorname{Re} \Psi \\ \operatorname{Im} \Psi \end{pmatrix}, \text{ where } \mathbf{X} = \begin{pmatrix} \operatorname{Re} \Xi \\ \operatorname{Im} \Xi \end{pmatrix} \quad (8.13)$$

Using the above approach, system can be modeled in state space form given by Eqn. 8.2 as is shown in Figure 8.2.

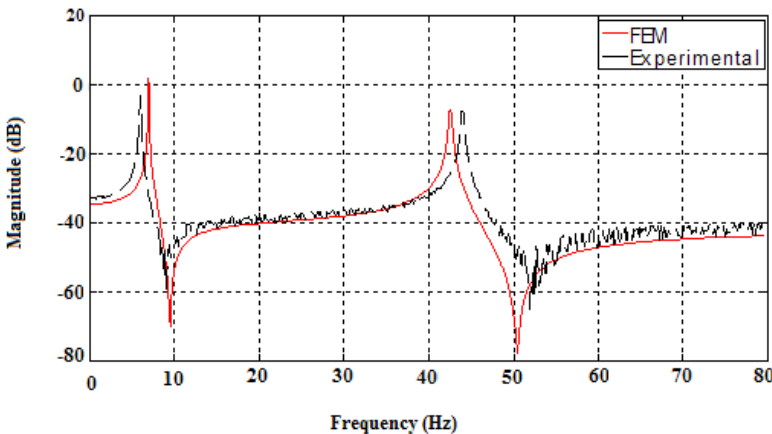


Fig. 8.2: Comparison of ‘FEM’ and ‘EXPERIMENTAL’ results

The Figure shows the zeros of a system using feed through term can be accurately identified. By correcting the model shown in Eqn. 8.2 (b), the following equation can be written:

$$y(t) = C x(t) + D u(t) = (B_2^T \ 0) x(t) + D \quad (8.14)$$

Actual value of this term can be obtained by iteratively varying the value of ‘D’ from zero to certain positive constant until the FRF of the identified model matches with the one obtained from FEM analysis. Main advantage of this type of modeling technique is that the effect of higher modes on the low order model can easily be considered. This eliminates the need to consider the un-modeled dynamics in controller design.

8.3 DESIGN OF EFFICIENT POSITIVE POSITION FEEDBACK CONTROLLER

For a system represented by Eqn. 8.5, a PPF controller is given as:

$$K^n(s) = \sum_{i=1}^n \frac{-\alpha_i \alpha'_i}{s^2 + 2 \delta_i \psi_i s + \psi_i^2} \quad (8.15)$$

The existence of negative term in Eqn.8.15, the overall system resembles as PPF controller. The important property of the PPF controller is that its structure resembles with the flexible system shown. A second order controller is required for a single vibration mode of the flexible structure. Simple PPF control has a second order compensator which acts as a positive feedback controller as shown in Figure 8.3(a, b).

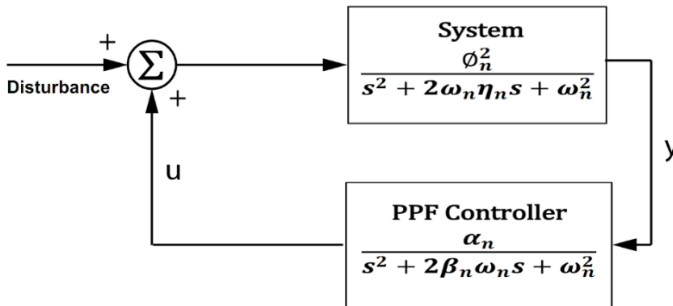


Fig. 8.3 (a): Block diagram of simple PPF control

Based on the number of modes to be controlled, the number of such compensators can be increased with connection parallel to each other. The compensator frequency ω_n is taken as the same as of the flexible structure i.e. ω_n . The Damping ratio β_n of the compensator is different from the damping factor η_n of the flexible structure mode.

8.3.1 Standard Stability Criterion

For explaining the stability of the CL system with PPF control, following theorems are necessary:

Theorem1: Considering the following multivariable system:

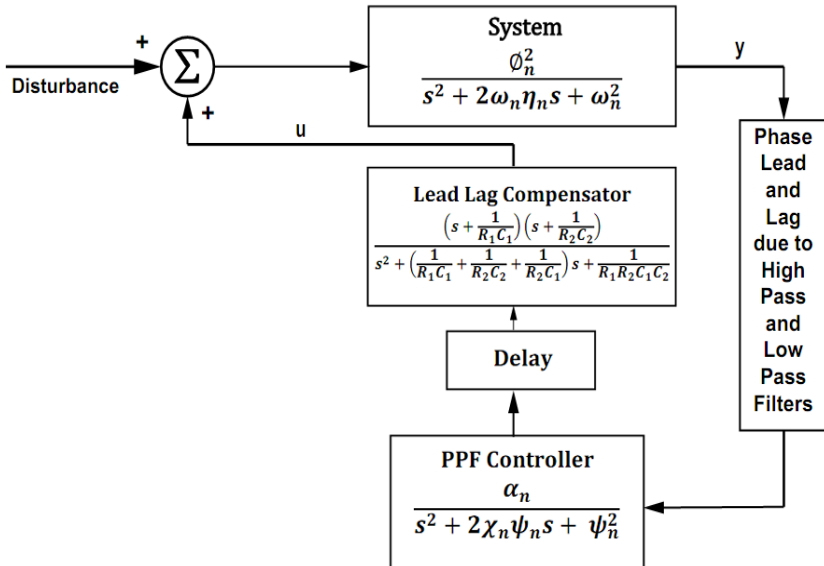


Fig. 8.3 (b): Block diagram of Efficient PPF control

$$\ddot{q}(t) + D \dot{q}(t) + K q(t) = 0 \quad (8.16)$$

The system represented by Eqn. 8.7 is exponentially stable if and only if:

$K = K' > 0$ by assuming $D = D' > 0$.

Theorem2: By making the following definitions

$$\mathbf{N} = \begin{bmatrix} \eta_1 & & & \\ & \eta_2 & & \\ & & \ddots & \\ & & & \eta_n \end{bmatrix}, \quad \boldsymbol{\Omega} = \begin{bmatrix} \omega_1 & & & \\ & \omega_2 & & \\ & & \ddots & \\ & & & \omega_n \end{bmatrix}, \quad (8.17)\{a, b\}$$

$$\Delta = \begin{bmatrix} \delta_1 & & & \\ & \delta_2 & & \\ & & \ddots & \\ & & & \delta_n \end{bmatrix}, \quad \boldsymbol{\Psi} = \begin{bmatrix} \psi_1 & & & \\ & \psi_1 & & \\ & & \ddots & \\ & & & \psi_1 \end{bmatrix}, \quad (8.17)\{c, d\}$$

$$\phi = [\phi_1 \quad \phi_2 \quad \dots \quad \phi_n] \quad (8.17)\{e\}$$

and

$$\Lambda = [\alpha_1 \quad \alpha_2 \quad \dots \quad \alpha_n] \quad (8.17)\{f\}$$

It is also assumed that:

$$\Delta > 0 \quad (8.18)$$

The theorem says that:

The negative feedback connection of (8.5) and (8.6) with (8.9) is exponentially stable if and only if:

$$\psi^2 - \Lambda' D \Lambda > 0 \quad (8.19)\{a\}$$

and

$$\Omega^2 - \Phi' \Lambda (\Psi^2 - \Lambda' D \Lambda)^{-1} \Lambda' \Phi > 0 \quad (8.19)\{b\}$$

8.3.2 Stability Considerations using H₂ Norm or H_∞ Norm Calculations

The H₂ norm of the flexible structure represented by transfer function G(s) can be used as a performance measure. In mathematical form it can be represented as:

$$\|G\|_2^2 = \frac{1}{2\pi} \int_{-\infty}^{\infty} \text{tr}\{G(j\omega)^* G(j\omega)\} d\omega \quad (8.20)\{a\}$$

and can be calculated using standard software. The purpose of the controller is to reduce the effect disturbances acting on the system and can be obtained by moving the poles of the closed loop system towards the farthest point in the negative direction in the left hand side of the imaginary plane. By doing so necessary damping can be provided to the structure. The simplest way to do this is to reduce the closed loop system's H₂ norm as small as possible. *The problem of stability will be automatically solved by this method. The H₂ norm of an unstable closed loop system doesn't make any sense; hence minimum value of this norm can only be obtained when the closed loop system is stable.* The CL performance of the control system is also dependent on loop zeros of the system. These zeros are accurately identified by using the feed through term. Currently available techniques of designing optimal PPF controller don't allow for a feed through term in the model of the flexible structure. Using the proposed method of PPF controller design, system can be represented in the form shown in Eqn. 8.5. It is difficult to find the H₂ norm in this form using standard software.

Similarly H_∞ norm of the flexible structure represented by transfer function G(s) can be used as a performance measure. In mathematical form it can be represented as:

$$\|G\|_{\infty} = \sup_{\omega} \sigma \{G(j\omega)\} \quad (8.20) \{b\}$$

A control engineering interpretation of the infinity norm of a scalar transfer function G is the distance in the complex plane from the origin to the farthest point on the Nyquist plot of G, and it also appears as the peak value on the Bode magnitude plot of $G(j\omega)$. Normally H_{∞} norm of G(s) can be regarded as the largest possible amplification factor of the system's steady state response to sinusoidal excitation. For example, the steady-state response of the system with respect to sinusoidal input $u(t) = U \sin(\omega_0 t + \phi)$ is:

$$y(t) = U|G(j\omega_0)| \sin(\omega_0 t + \phi + \angle G(j\omega_0))$$

and thus the maximum possible amplification factor $\sup_{\omega_0} |G(j\omega_0)|$, is precisely the H_{∞} norm of the transfer function.

8.3.3 Efficient Positive Position Feedback Controller Design Using Pattern Search Algorithm

8.3.3.1 Terminology and Working of Pattern Search Algorithm

A pattern search algorithm computes a sequence of points that get closer and closer to the optimal point. At each step, the algorithm searches a set of points, called a *mesh*, around the *current point* — the point computed at the previous step of the algorithm. The algorithm forms the mesh by adding the current point to a scalar multiple of a fixed set of vectors called a *pattern*. If the algorithm finds a point in the mesh that improves the objective function at the current point, the new point becomes the current point at the next step of the algorithm. The terminology and how the pattern search technique works is discussed in brief below:

Patterns: A *pattern* is a collection of vectors that the algorithm uses to determine which points to search at each iteration.

Meshes: At each step, the pattern search algorithm searches a set of points, called a *mesh*, for a point that improves the objective function. The algorithm forms the mesh by:

- a) Multiplying the pattern vectors by a scalar, called the mesh size
- b) Adding the resulting vectors to the *current point* — the point with the best objective function value found at the previous step

Polling: At each step, the algorithm polls the points in the current mesh by computing their objective function values. When option complete poll has the default setting off, the algorithm stops polling the mesh points as soon as it finds a point whose objective function value is less than that of the current point. If this occurs, the poll is called *successful* and the point it finds becomes the current point at the next iteration. The algorithm only computes the mesh points and their objective function values up to the point at which it stops the poll. If the algorithm fails to find a point that improves the objective function, the poll is called *unsuccessful* and the current point stays the same at the next iteration. If one sets complete poll to on, the algorithm computes the objective function values at all mesh points. The algorithm then compares the mesh point with the smallest objective function value to the current point. If that mesh point has a smaller value than the current point, the poll is successful.

Generally speaking, pattern search methods generate a sequence of iterates $\{x^{(k)}\}$ without using any information of the derivatives, including gradient and second-order derivative, of the objective function. They only depend on function values. In fact,

ordinal information about function values is enough. At each iteration, the objective function is evaluated at a finite number of trial points (defined below) and the purpose is to look for one point which can yield a lower function value than the current iterate. If such a point is found, it is set to be the new iterate, and the iteration is called successful; otherwise, it is declared as unsuccessful and the trial points are updated. Torczon generalizes this kind of methods and presents a global convergence theory for them. In Torczon's generalized pattern search method, two components are needed, one is a pattern $P^{(k)}$, and the other one is a real scale factor $\Delta^{(k)} > 0$.

The pattern $P^{(k)}$ consists of a basis matrix A and a generating matrix $C^{(k)}$. Among them, any nonsingular matrix in $R^{n \times n}$ could be chosen as A and $C^{(k)} I Z^{n \times p}$ ($p > 2n$) could be partitioned into three parts:

$$C^{(k)} = [M^{(k)} - M^{(k)} D^{(k)}] \quad (8.21)$$

Where $M^{(k)} \in M \subset Z^{n \times n}$, M is a finite set of nonsingular matrices, $D^{(k)} \in Z^{n \times (p-2n)}$ contains at least one column, the column of zeros.

Then $P^{(k)}$ could be written as:

$$P^{(k)} = AC^{(k)} = [AM^{(k)} - AM^{(k)} AD^{(k)}]. \quad (8.22)$$

It is noted that because both the basis matrix A and the generating matrix $C^{(k)}$ have rank n , the columns of $P^{(k)}$ can span R^n .

The real scale factor $\Delta^{(k)}$ works as a step length parameter. Let $C^{(k)} = [c_1^{(k)}, c_2^{(k)}, \dots, c_p^{(k)}]$, then a

trial step $s_i^{(k)}$ is defined as any vector of the form:

$$s_i^{(k)} = \Delta^{(k)} A c_i^{(k)} \quad (8.23)$$

In fact, $Ac_i^{(k)}$ determines the direction of the step and at iteration k , all the trial points possess the form of:

$$x_i^{(k)} = x^{(k)} + s_i^{(k)} \quad (8.24)$$

where $x^{(k)}$ is the current iterate.

Then a generalized pattern search method could be outlined as follows:

Let initial iterate $x^{(0)} \in R^n$, $A \in R^{n \times n}$, $C^{(0)} \in Z^{n \times p}$, $\Delta^{(0)} > 0$, $k = 0$.

While (Stopping conditions do not hold) do

Step 1. Find a step $s(k)$ using Exploratory Moves($\Delta^{(k)}$, $AC^{(k)}$).

Step 2. If $f(x^{(k)} + s^{(k)}) < f(x^{(k)})$, then $x^{(k+1)} = x^{(k)} + s^{(k)}$. Otherwise, $x^{(k+1)} = x^{(k)}$.

Step 3. Update $C^{(k)}$ and $\Delta^{(k)}$ to $C^{(k+1)}$ and $\Delta^{(k+1)}$, $k = k + 1$.

8.3.3.2 Controller Design Based on Pattern Search Algorithm

Due to the phase lead/ lag produced by the filters and the system delay, the CL system with simple PPF controller loses efficiency and sometimes gets unstable. To get optimal results, the LP and HP filters and system Delay should be considered while designing the efficient PPF controller. Figure 8.3 (b) shows the block diagram of the proposed efficient PPF control. To avoid the decreased efficiency of the closed loop system (with simple PPF controller) with phase change caused by filters and inherent time delay (due

to control signal calculations), lead-lag compensator should be added in series with the PPF controller. Figure 8.4 shows the block diagram of the lead / lag compensator circuit as:

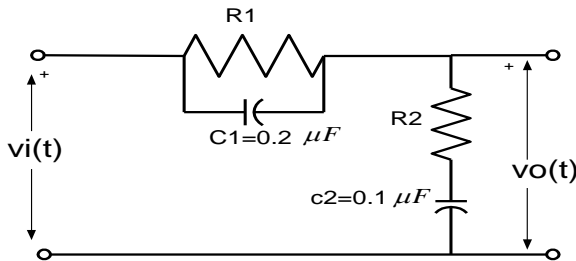


Fig. 8.4: Block diagram of Lead / Lag Compensator circuit

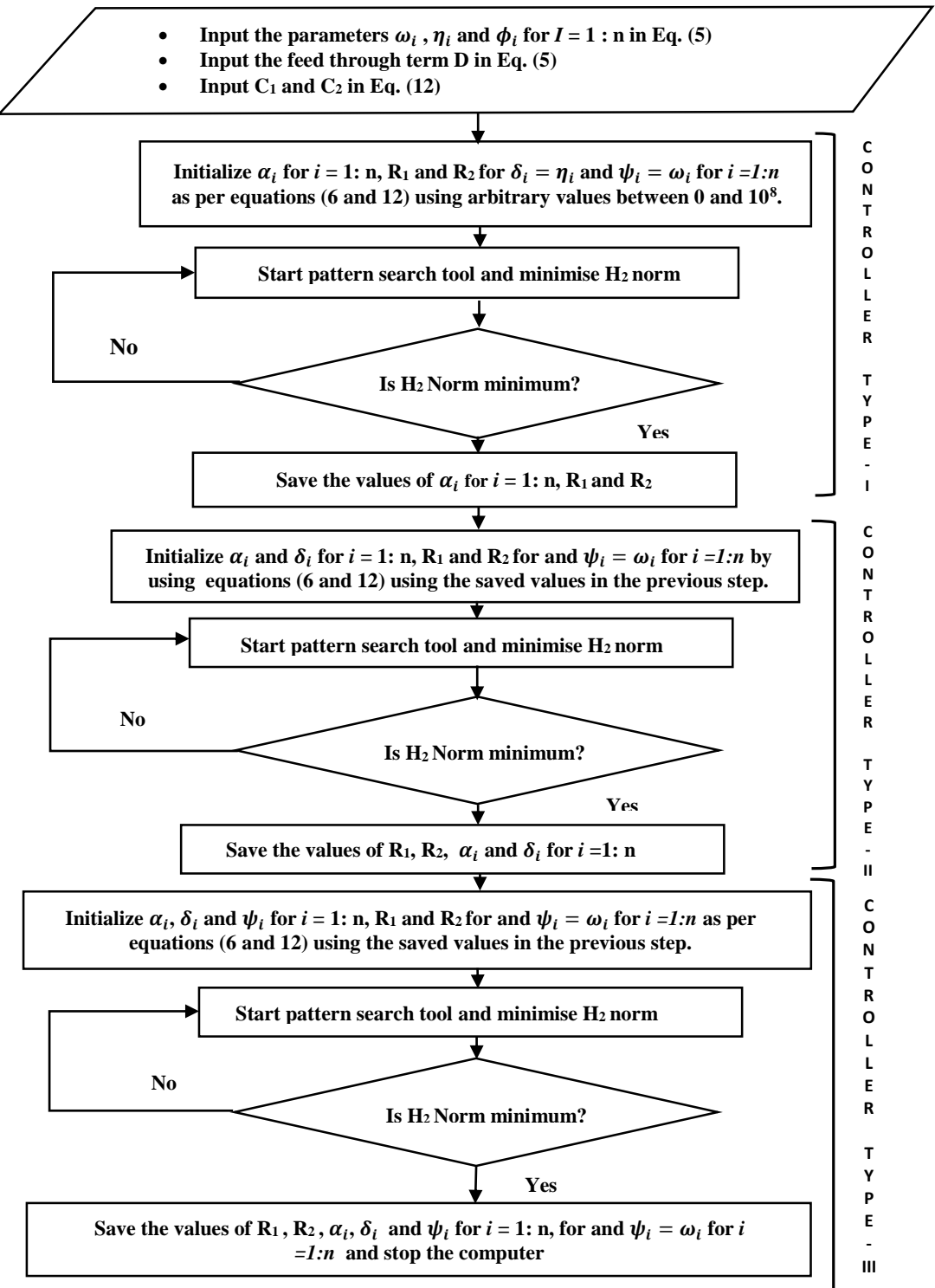
The capacitance values are fixed as in this Figure. However, the resistance values are designed simultaneously with the PPF controller. The transfer function of the compensator is given as

$$TF = \frac{\left(s + \frac{1}{R_1 C_1}\right) \left(s + \frac{1}{R_2 C_2}\right)}{s^2 + \left(\frac{1}{R_1 C_1} + \frac{1}{R_2 C_2} + \frac{1}{R_1 R_2 C_1 C_2}\right)s + \frac{1}{R_1 R_2 C_1 C_2}} \quad (8.25)$$

Figure 8.5 (a) shows the flow chart for the design of efficient PPF controller. Here the parameters $\alpha_i, \delta_i, R_1, R_2$ and ψ_i are obtained by using the mentioned flowchart. If the frequencies of the compensator are kept equal to the natural frequencies of the flexible structure and the damping factors are fixed at the start of the design process, the resultant controller is termed as PPF controller of type-I. However, if the damping factors are not fixed at the start but are calculated during the design process, the resultant controller is termed as PPF controller of type-II. For PPF controller of type-III, all the parameters α_i, δ_i and ψ_i along with R_1 and R_2 are calculated during the design process. Suppose it is desired that Type-III PPF controller is to be designed, algorithm as shown in Figure 8.5(b) will be used.

First of all the system is constructed using grey box identification technique so that the parameters ω_i, η_i and ϕ_i for $i=1:n$ are available for controller design. Afterwards, a LP filter and HP filter is constructed based on the required specifications. Certain amount of time delay is specified and is constructed into transfer function form using Pade's approximation method. Initial parameters for the PPF controller like $\alpha_i, \delta_i, R_1, R_2$ and ψ_i for $i=1:n$ are chosen arbitrarily for optimization.

The LP filter, HP filter, time delay, compensation circuit in transfer function form and the open loop (OL) system is connected in series to form a Modified OL system. The PPF controller is connected in feedback with this Modified OL system to form a CL system. The next step is to calculate the H_2 norm or H_∞ norm of the CL system. Then the mesh size of the Pattern search algorithm is further reduced to minimize the H_2 norm or H_∞ norm of the CL system. If further improvement is there the control is shifted back to the step where new parameters of the PPF controller are fed. In this manner the loop continues to search for a PPF controller along with the parameters of the compensation circuit to find the lowest H_2 norm or H_∞ norm of the CL system. Figure 8.6 shows the frequency response function of the system with Pattern Search based optimal PPF controller (type-I and type-II).

**Fig. 8.5 (a):** Flow chart for efficient PPF controller design (compact)

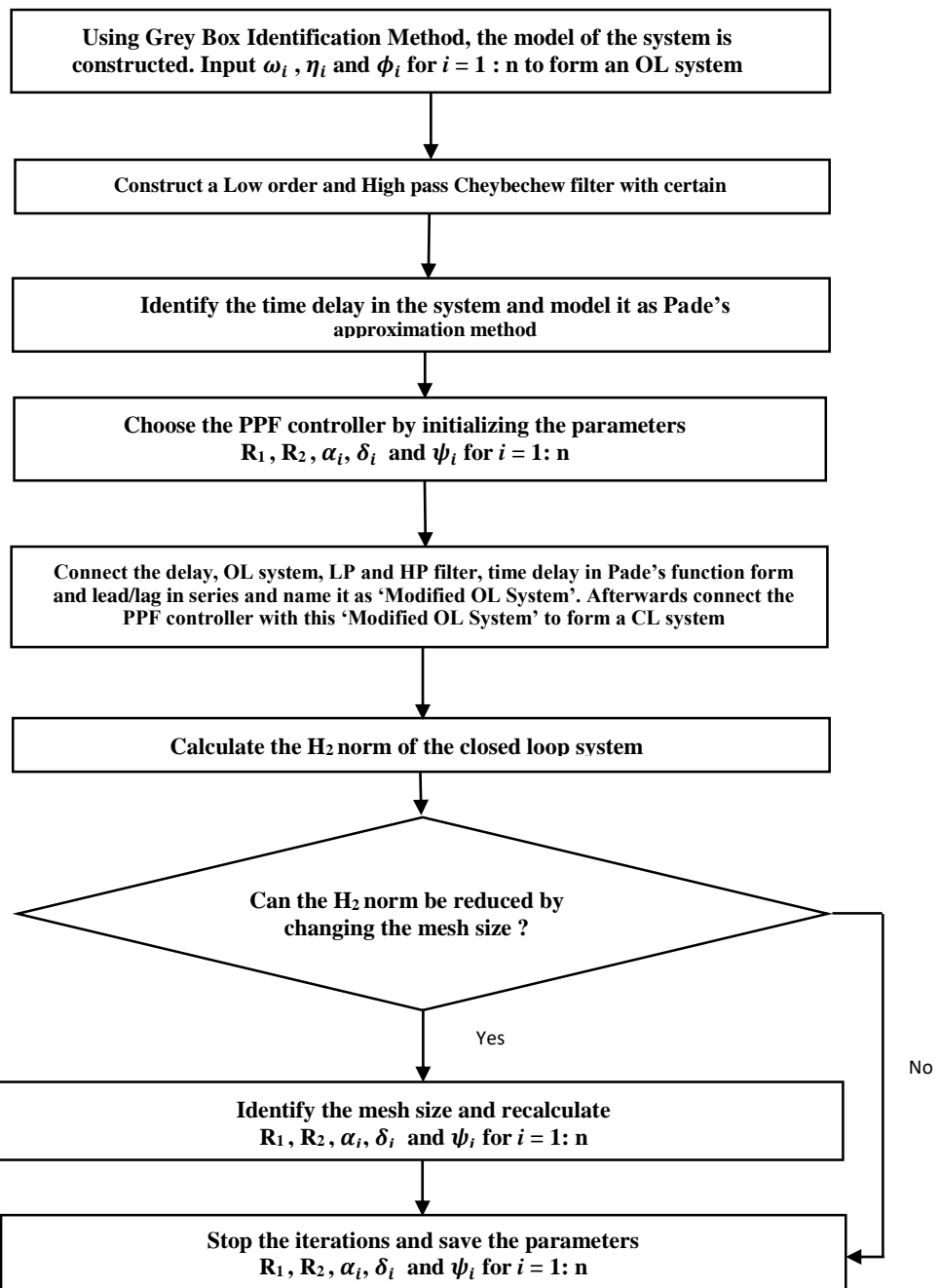


Fig. 8.5 (b): Flow chart for efficient PPP controller design (detailed)

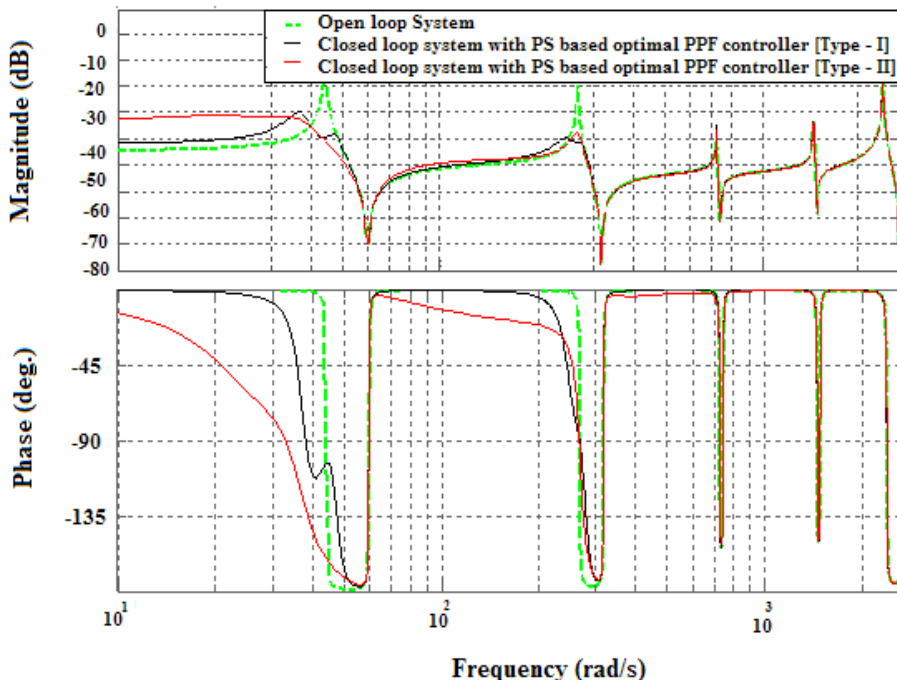


Fig. 8.6: Frequency response function of the system with GA based optimal PPF controller (type-I and type-II)

It is assumed for the time being that no filters have been used and no time delay is present in the system. The system performance is nearly same with both types of PPF controllers except in low frequency region. The effect becomes significant in the presence of hardware filters and time delay. The H_2 norm of the OL system is 2.57.

8.4 RESULTS WITH POSITIVE POSITION FEEDBACK CONTROL

8.4.1 Frequency Domain Results using Efficient Positive Position Feedback Control

8.4.1.1 Effect of phase lead (Effect of high pass filter)

To remove the DC offset from the signal and effect of un-modeled dynamics, high pass and Low pass filters have to be used. Figure 8.7 shows the effect of use of these filters on amplitude and phase. High pass filter has a cut-off frequency of nearly 2Hz and Low pass filter has a cut-off frequency of nearly 70 Hz. This frequency is chosen so as to pass only first two modes of vibration. First natural frequency of the flexible structure is near the cut-off frequency of the HP filter, which causes a phase change near the first mode as shown in Figure 8.8.

Due to this phase change (i.e. phase lead) problem, the effectiveness of the PPF controller reduces as shown in Figure 8.9. The efficiency of both type -I and type-II, PPF

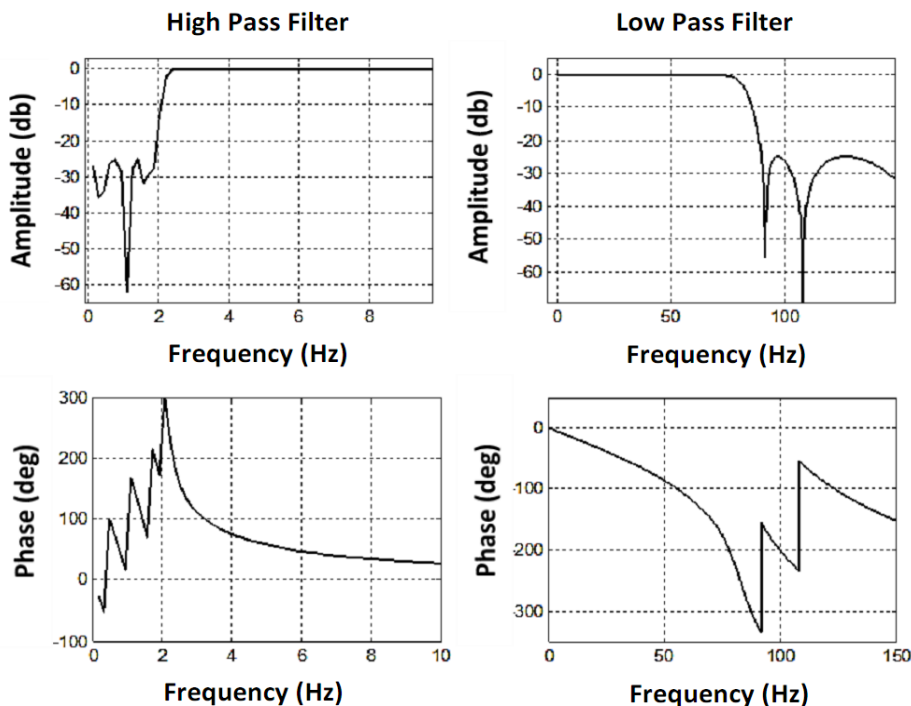


Fig. 8.7: Frequency response functions of the implemented Low Pass and High Pass filters

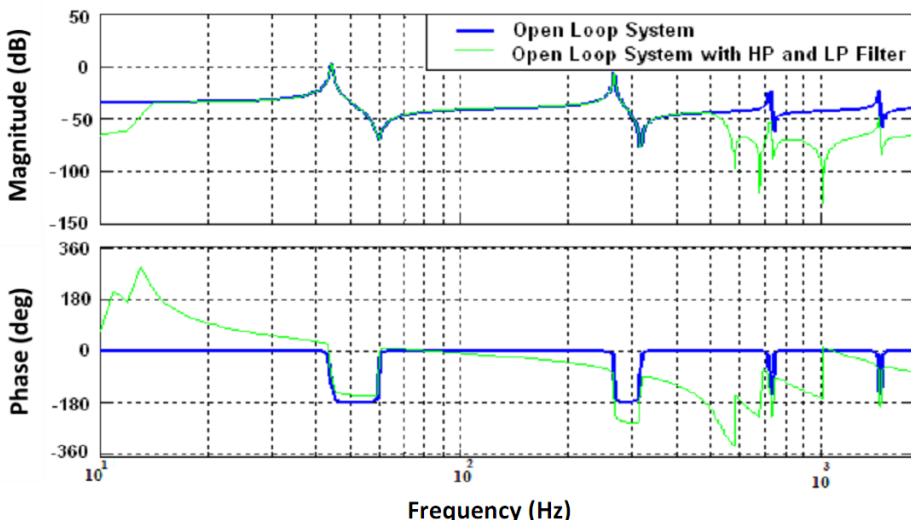


Fig. 8.8: Frequency response function of the open loop system with filters

Controllers reduce. In the presence of filters, the amplitude reduction at the first mode reduces to nearly 16 dB instead of 21 dB in the ideal case with no hardware filters Figure 8.6. By observing minutely it is clear that the reduction in efficiency of the CL system with type-I PPF controller is more severe than type-II PPF controller. This fact

is clearer near the second mode. The closed loop H_2 norm of the system is 2.47 with type-II PPF controller.

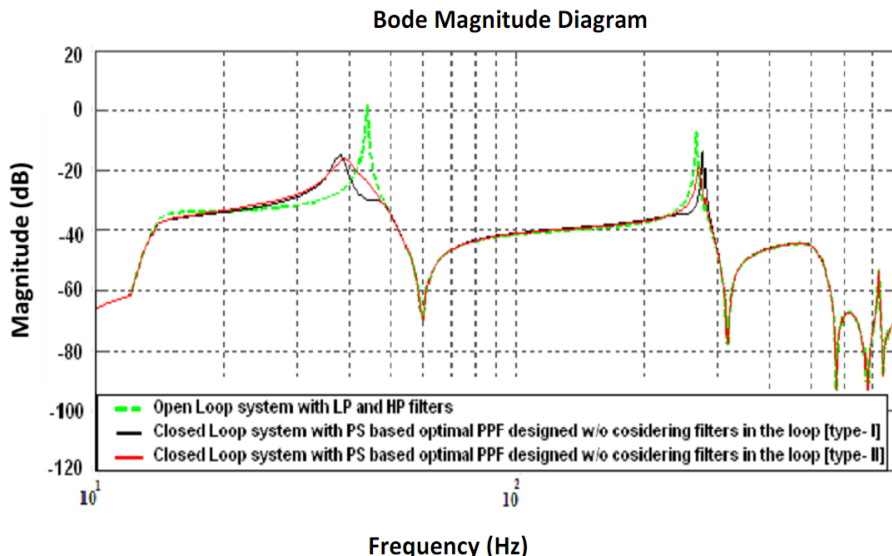


Fig. 8.9: Frequency response function of the system (with LP and HP filters) using PS based optimal PPF controllers designed without considering the filters in the loop (type-I and type-II).

8.4.1.2 Effect of Phase Lag (Effect of Time Delay)

To study the effect of delay present in the system, Figure 8.10 is constructed. It is seen that as delay changes from 1×10^{-3} second to 10×10^{-3} second, phase change increases. The pure time delay can be modeled as Pade's approximation and is shown in Figure 8.11. If the type -I PPF controller designed for ideal system is applied to the system where hardware filters are provided and a time delay of 5×10^{-3} second is applied, the CL system will be as shown in Figure 8.12.

Only 10 dB amplitude reduction is obtained for the first mode. However, when type-II PPF controller is applied (compensator was not added in the circuit), 20 dB amplitude reductions is obtained. In order to compensate for the effect of filters and time delay, PPF controller of type-II is redesigned by considering the effect of phase change from hardware filters and time delay in the system. Now, the **hardware compensator is simultaneously designed with the PPF controller to reduce the H_2 norm of the CL system.**

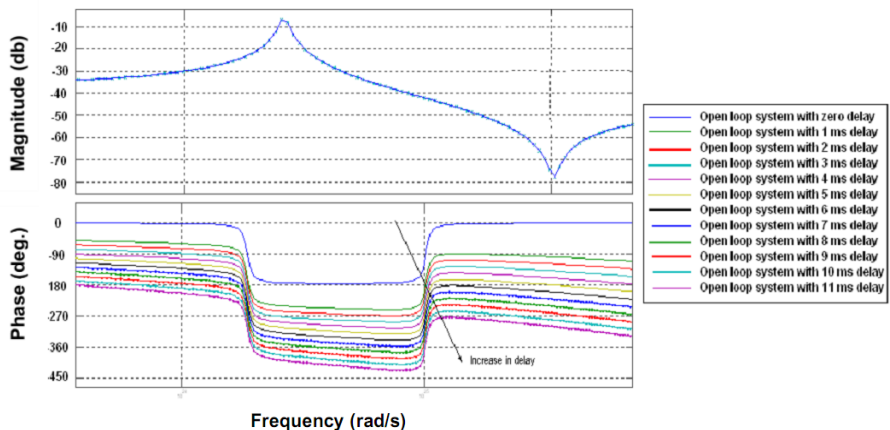


Fig. 8.10: Effect of system delay on the open loop system (with filters)

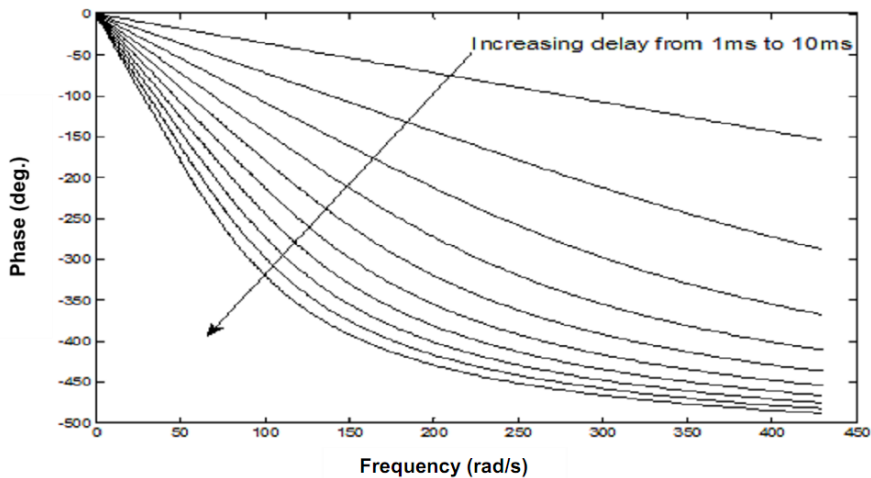


Fig. 8.11: Quantification of system delay using Pade's approximation

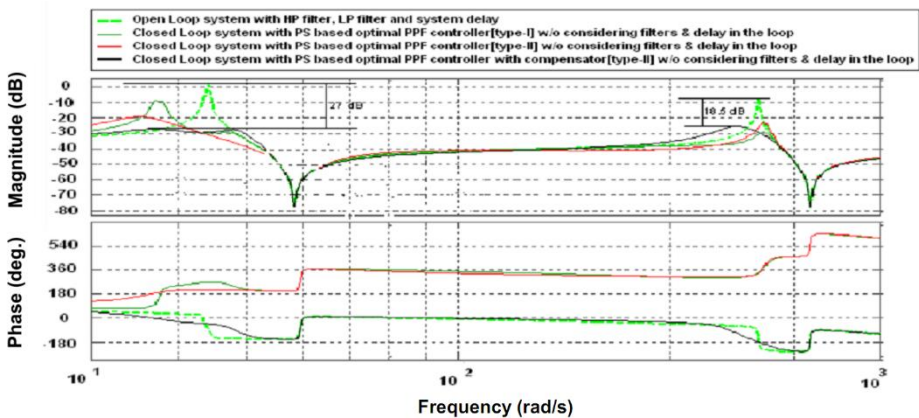


Fig. 8.12: Effect of considering the filters and system delay in the design of PS based optimal PPF controllers

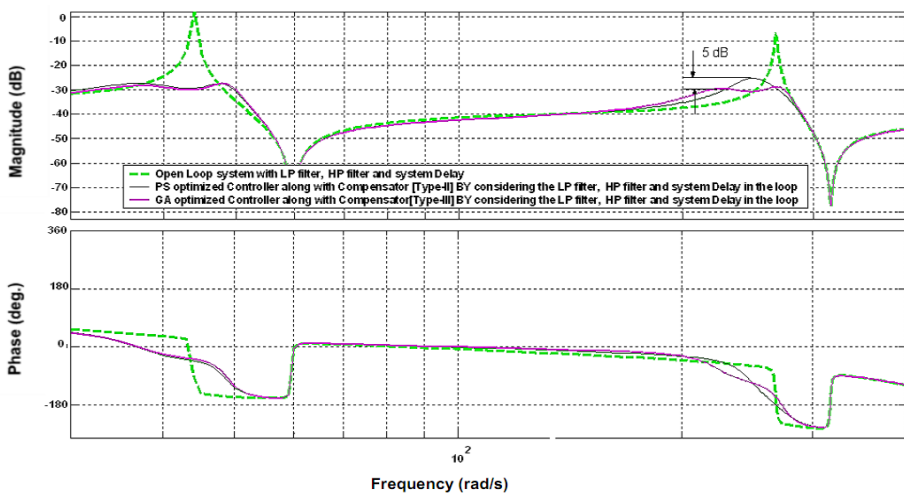


Fig. 8.13: Frequency response function of the open and closed loop system using various types of PS based optimal PPF controllers along with compensator (with filters and system delay in the system)

By applying this controller along with compensator, the amplitude reduction of 27 dB for the first mode is obtained. The corresponding amplitude reduction for the second mode is 18.5 dB.

With type-III PPF controller further improvement is possible. The frequency of the PPF controller is allowed to deviate from the OL system frequency. *A further amplitude reduction of 5 dB is obtained for the second mode with this type-III controller (Figure (8.13)).* In this particular case the second natural frequency of the PPF controller differs from that of the OL system. *When the second natural frequency of the controller is 38.19 Hz, best results are obtained as compared to the situation when the natural frequency of the PPF controller lies at 42.56 Hz (second OL natural frequency of the system).* The optimal first and second damping ratios of the PPF controllers are at 0.194 and 0.227 respectively. The effect of time delay on the amplitude reduction of the second mode is shown in Figure 8.14.

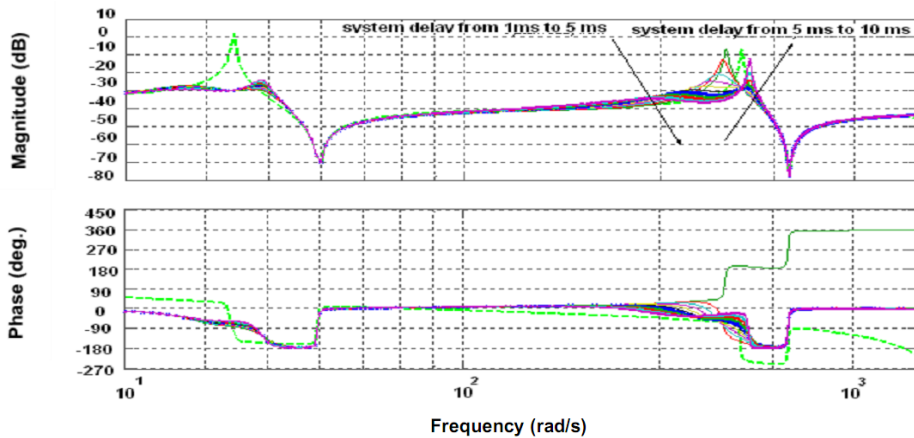


Fig. 8.14: Effect of system delay from 1 ms to 10 ms on the closed loop system with

PS based optimal controller [Type-II]

The PPF controller is designed based on Pattern search technique in such a way that it assumes a natural time delay of 5×10^{-3} second present in the circuit. If the time delay present in the system was made to decrease or increase beyond this value, the amplitude reduction capacity of the CL system is badly affected. The affect is prevalent at second mode. It has a marginal effect on the efficiency of the first mode. Figure 8.15 shows the close up of the Figure 8.14 for the second mode.

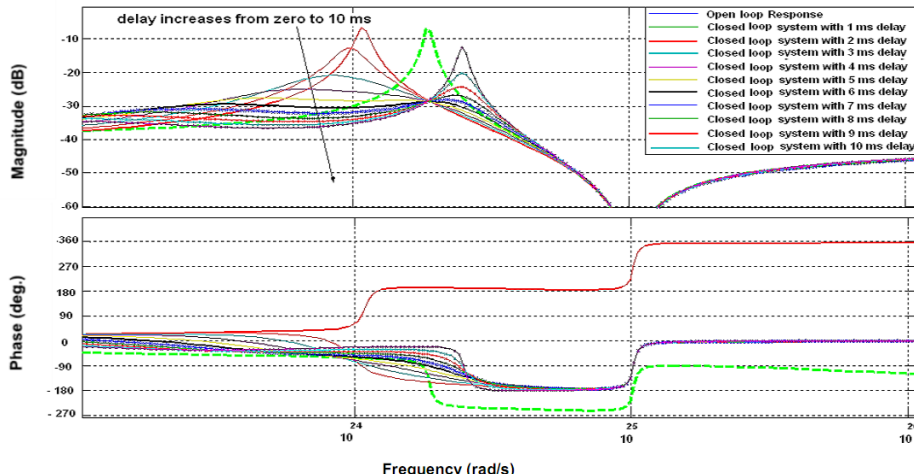


Fig. 8.15: Effect of system delay from 1 ms to 10 ms on the closed loop system with PS based optimal controller [Type-II] (close up for the second mode)

8.4.2 Time Domain Results using Efficient Positive Position Feedback Control

A ball from certain height is made to fall on the tip of the cantilever beam. Due to the inherent damping present in the system, the OL amplitude decreases with time. After that a type-II PPF controller is used without hardware compensator in the circuit. The amplitude reduces much quickly with time. The lower part of the Figure shows the time history of applied voltage at the PZT actuator. It is seen that with the application of the compensation circuit, the applied voltage reduces to a lower value. ***Lower control effort can do the same reduction in CL amplitude with compensation circuit.*** Output response remains almost unaffected. Figure 8.16 shows the transfer function of the compensation circuit for type I, II and II PPF controller required to nullify the effect of hardware filters and time delay present in the system.

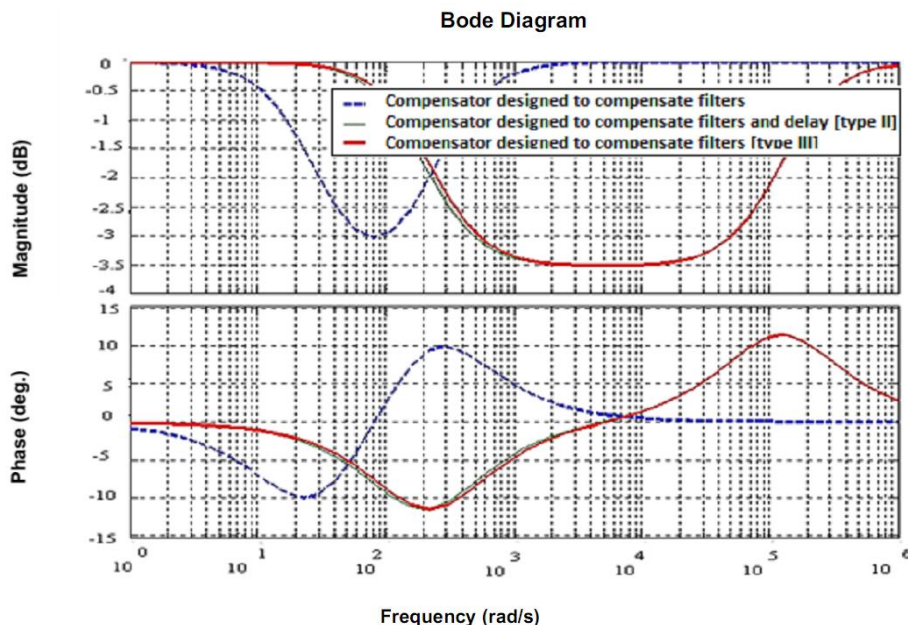


Fig. 8.16: Transfer function for compensation circuits for various types PPF controllers

8.5 EXPERIMENTAL VALIDATION AND RESULTS

After H_2 optimization, H_∞ optimization is investigated and the results are as follows: The H_∞ norm of the OL system is 1.4946. After the application of the type-III PPF controller the H_∞ norm of the CL system reduces to 0.0418. The OL vs. CL response in frequency domain is given in Figure 8.17. This shows that for the first mode the amplitude reduction is 32 dB, however, for the second mode the corresponding reduction is 22 dB.

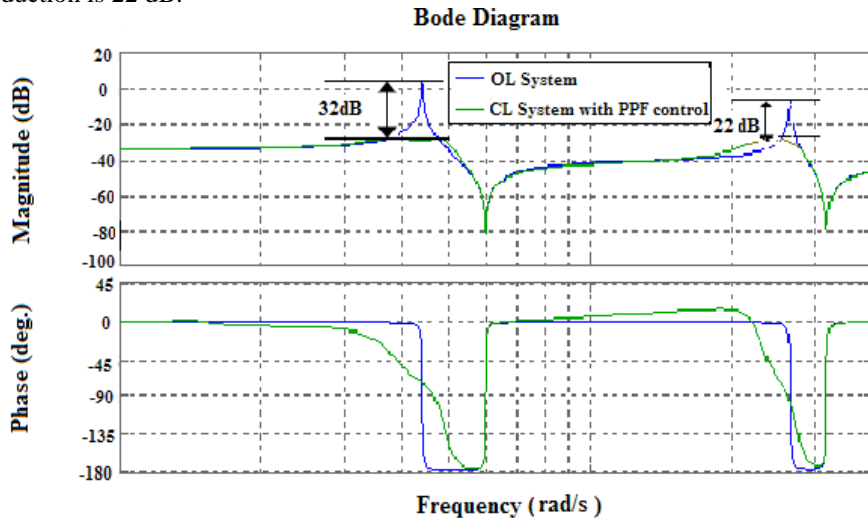


Fig. 8.17: Open and Closed Loop response using PPF control with H_∞ norm minimization

8.5.1 Experimental Setup

The experiments' setup is shown in Figure 8.18. The characteristics of different equipments/components used in the set up are:

8.5.1.1 Software 'Lab VIEW'

The National Instruments 'Lab VIEW' is a highly productive graphical development environment for building data acquisition, instrumentation and control systems. With 'Lab VIEW' it is easy to create interfaces that give interactive control of software system. The tight integration of 'Lab View' with measurement hardware facilities, rapid development of data acquisition and control is possible. This software contains powerful built-in measurement analysis and a graphical compiler for optimum performance.

8.5.1.2 Simultaneous I/O Data acquisition card (DAQ 6062 E)

National Instruments 'E-Series' technology is a complete data acquisition (DAQ) hardware architecture that takes advantage of the latest in electronics and technological innovations and advances the capabilities of PC – based DAQ solutions. 'E-Series' is a standard

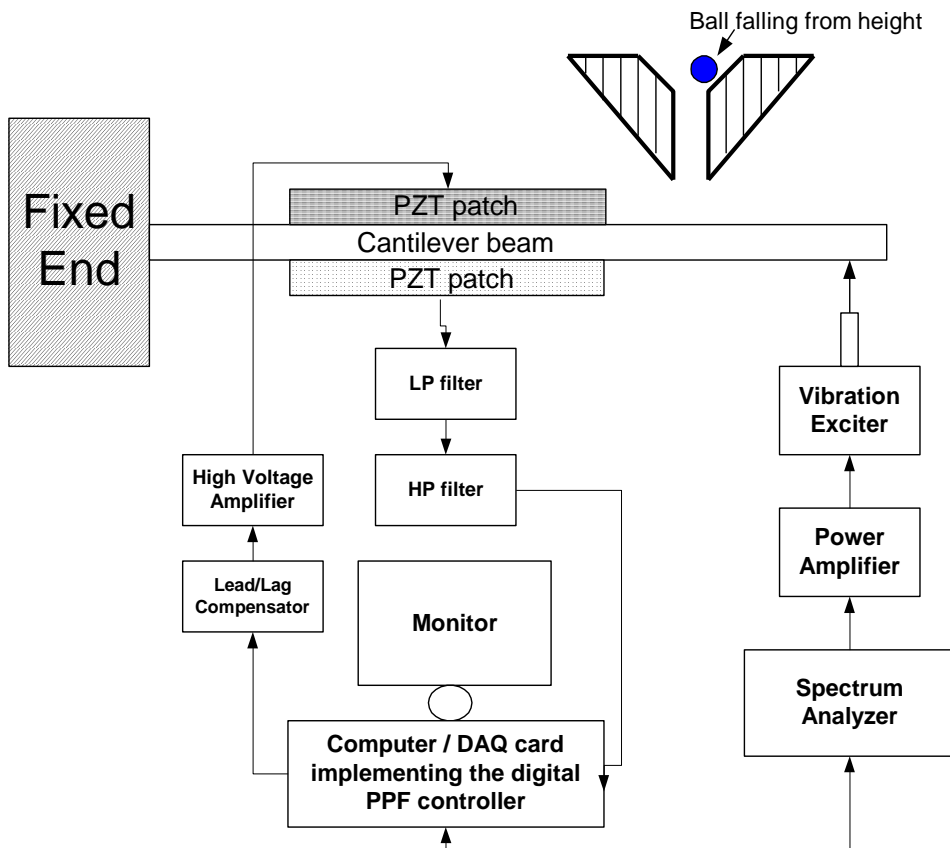


Fig. 8.18: Schematic of experimental setup

architecture in instrumentation class, for multichannel data acquisition. This architecture includes the followings:

- NI – PGIA gain independent, fast settling time amplifier
- RTSI multiboard/multifunction synchronization bus
- DAQ – STC counter/timer
- MITE PCI bus master interface
- Shielded, latching metal connectors

Following are some of the important features of the E series data acquisition system:

8.5.1.2.1 Analog input FIFO

The ‘E series’ devices perform both single and multiple Analog – to – Digital (A/D) conversion of a dynamic signal made of infinite number of samples. A large FIFO buffer holds the data during the A/D conversion so that no data is lost. Multiple A/D conversions can be handled with programmed input-output, interrupts, or direct memory access (DMA). Total 16 no. of channels can be handled. The maximum input voltage range is –10 Volts to +10 Volts. 12-bit resolution is there, which means that full-scale accuracy is 1.443 mV.

8.5.1.2.2 Analog output

The ‘E series’ devices also perform both single and multiple ‘Digital-to-Analog (D/A) conversion’ from a fixed number of data points to infinite number of samples. Multiple D/A conversions can be handled with programmed input-output, interrupts, or direct memory access (DMA). Total 2 numbers of channels can be handled. The maximum input voltage range is –10 Volts to +10 Volts. A 12 bit resolution is there, which means that full scale accuracy is 1.443 mV. Large FIFO DAC buffers for high-speed analog output updates are available to accommodate varying bus latencies and to ensure no data loss.

8.5.1.2.3 DAQ-STC system

The ‘E Series’ devices use the National Instruments DAQ – STC for counting and timing related functions. The DAQ STC is specially designed with functions for A/D and D/A timing with random logic associated with routing timing I/O signals between I/O connector and the RTSI bus. The DAQ – STC derives its internal timing from a 20 MHz source. External clocking options are available for all counter / timing sections. Each group can be configured independently with timing resolution down to 50 ‘ns’. The general-purpose counter/timers are capable of DMA data transfers and fast processing. This capability is important for relative time stamping of signals with varying frequency, synchronization with analog conversions. The DAQ – STC provides a flexible timing I/O interconnection that consists of 10 programmable inputs (PFI). Any PFI can be programmatically connected as an external source or an output for a given timing signal.

8.5.1.2.4 Multifunction DAQ software NI-DAQ

‘NI – DAQ driver software’ bundled with ‘E-series’ multifunction DAQ device, provides access to the features of the DAQ hardware.

8.5.1.2.5 Sampling rate

Sampling rates up to several kHz can be handled. But even with real time engine there is limit to computational speed. Each computation requires some computational effort. So there is a limit to sampling frequency, which can be handled using the real time engine. Control signals must be calculated from input – output data, in a time interval,

less than the sampling period. Hence, based on the capability of the processor, we cannot go beyond a certain sampling rate.

8.5.1.3 Amplifiers

The control signals generated from the computer via data acquisition card, are in the range -10 volt to +10 volt. Since for getting lesser and lesser settling times, the control voltage has to be increased. This job is done by the amplifiers. A High Voltage Amplifier MA-17 from Apex Technologies was used to amplify the voltage generated by the computer. These amplifiers are capable of increasing the control signal voltage up to 150 volt, without any phase change.

8.5.1.4 High-Pass and Low-Pass filters

Any vibrating flexible structure, contains infinite number of modes of vibration. Although for practical purposes only few modes are of importance. The dynamics of these structures can be modelled mathematically, using finite number of modes using modal analysis. For better sensing the signal obtained from these vibrating structures, higher modes need to be eliminated. This work is done by higher order low pass filters. They pre-filter the input signal, to remove the high frequency signals. Hence, sometimes these low pass filters are also called ‘pre-filters’ or Low Pass Filters. On the other hand to remove the DC component from the sensor signal, High Pass filter with appropriate specifications is applied.

8.5.1.5 Host PC (Core 2 Duo)

For control applications, the real time processor is being used. But for offline identification and other offline purposes Core 2 Duo is being used as computational machine. The RAM is 2 GB. Clock speed of 1.2 G Hz etc.

8.5.1.6 Cathode ray Oscilloscope

Agilent 56020 Cathode Ray Oscilloscopes (CRO) was used. Forgetting the instant value of the dynamic signals CRO are quite helpful, even in the presence of data acquisition card, since it affects the efficiency of control to get every state back on the host PC.

8.5.1.7 PZT patches as Sensors/Actuators

“Piezoelectric (PE)” materials are those materials which when subjected to electric field get deformed and vice – versa. This change in configuration may be used to nullify the effect of vibrations induced by external disturbances. These are made by the combination of three elements i.e. lead, zirconium and titanium.

8.5.2 Experimental Results

The PPF controller is digitized at 1.3 kHz sampling frequency. A ball from certain height is made to fall on the free end of the cantilever beam to excite it. Response of the system is as shown in Figure 8.19.

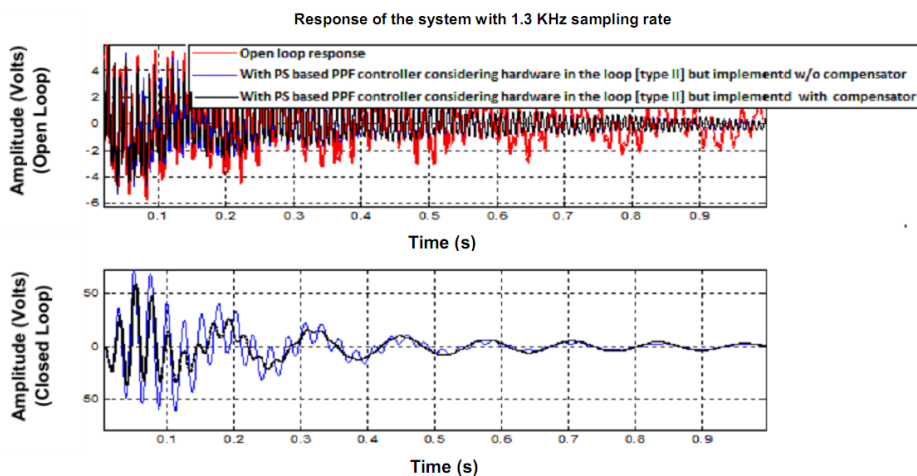


Fig. 8.19: Experimental time domain response of the open and closed loop system with digitized PS based optimal PPF controller [Type –II], digitized at 1.3 kHz (with and without compensator).

The same PPF controller is used with and without compensator circuit. Using compensator circuit much less voltage and control effort are required for almost similar closed loop response. Figure 8.20 considers the forced vibration control. A random signal is constructed with the help of spectrum analyzer. It is made to pass through the LP filter so that it has a spectrum such that only first two modes are excited. The controller (PPF – III) is applied to reduce the amplitude of the vibrations. Much better amplitude reduction is possible with the help of the controller. This time domain response was converted into frequency domain using PSD (power spectral density) function of the MATLAB.

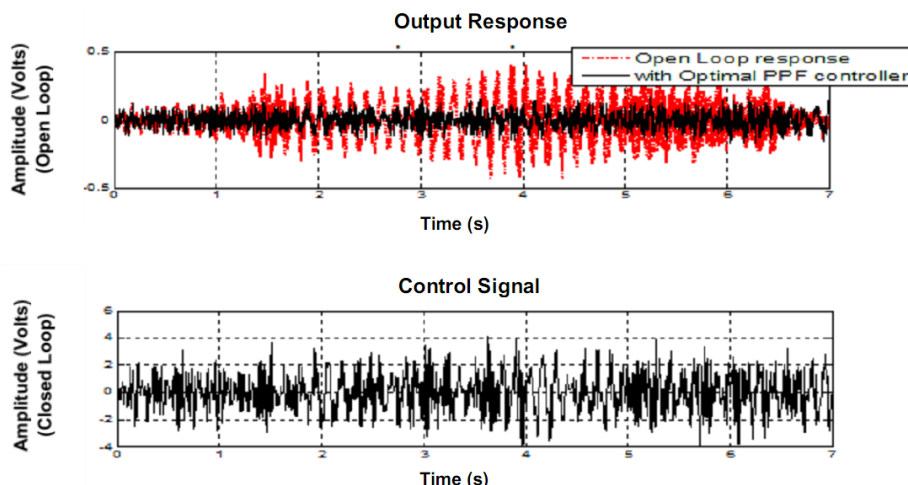


Fig. 8.20: Experimental time domain response of the open and closed loop system with digitized PS based optimal PPF controller [Type –II], digitized at 1.3 kHz for a random force applied at the free end (with and without compensator)

Open loop (OL) amplitude of the vibrations at first and second mode is 0.7 dB and 0.5 dB as shown in Figure 8.21. After the application of the controller, amplitude at both the modes becomes less than 0.05 dB.

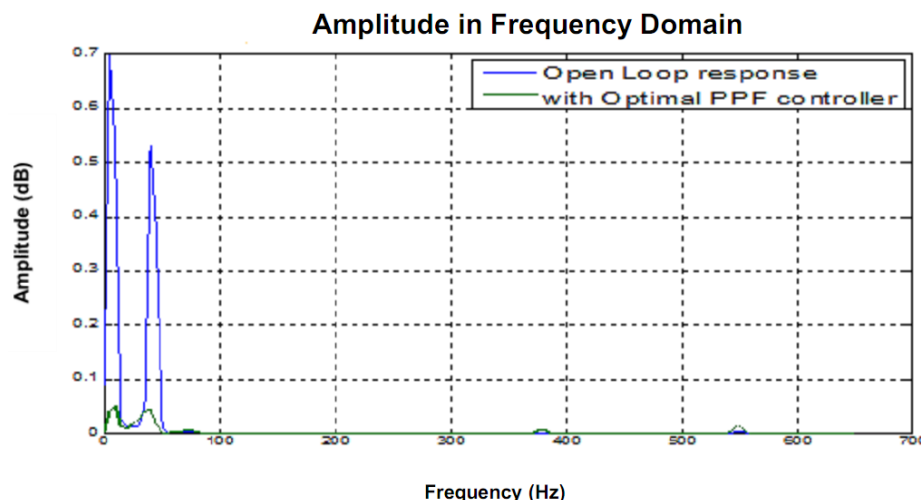


Fig. 8.21: Experimental frequency domain response of the open and closed loop system with digitized PS based optimal PPF controller [Type –II], digitized at 1.3 kHz for a random force applied at the free end (with and without compensator)

Glossary of Terms

The terminology frequently used in the field of vibration analysis and in this book is compiled here from various books and other sources like internet and including the document prepared by a company Metrix Instrument Co. Ltd., New York.

Accelerometer: A transducer that converts mechanical acceleration into an electronic signal. It is a seismic sensor made from a piezoelectric material which produces a charge output proportional to acceleration (pC/g). When housed together with an electronic charge amplifier and charge-to-voltage converter (mV/g), it is referred to as an "internally amplified" accelerometer. If, due to temperature, only the sensor is machine mounted, the remote electronics are referred to as a "charge amplifier" (although it usually also contains a charge-to-voltage convertor).

Accelerometer Frequency Response: Accelerometer frequency response is a specification of the accelerometer sensitivity as a function of frequency.

Accelerometer Sensitivity: Accelerometer sensitivity is a specification of the ratio of the accelerometer's mechanical input to electrical output typically specified at a 100-Hz reference frequency or, as in the case of Accelerometer Frequency Response, as a function of a range of frequencies.

Active Constrained Layer Damping (ACLD): When the constraining layer in PCLD techniques is replaced by or enhanced with actuators it is called ACLD. There has been much research in the field of ACLD in the past years. ACLD is described as a smart, failsafe and efficient vibration control method over a large frequency band.

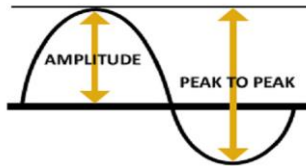
Active Vibration Control: Active vibration control is the active application of force in an equal and opposite fashion to the forces imposed by external vibration. With this application, a precision industrial process can be maintained on a platform essentially vibration-free.

Adaptive Control System: An adaptive control system is one that contains a controller which can use the information it gathers online to change itself and improve its performance; in a sense it "adapts" to the feedback loop it is inside, and develops into a better controller over time. This is unlike the usual (non-adaptive) controller, the parameters of which are constant and which thus relies on the control design conducted prior to closed-loop operation.

Amplifier: An amplifier is an electronic device that increases the *voltage, current, or power of a signal*. Amplifiers are used in *wireless* communications and broadcasting, and in audio equipment of all kinds. They can be categorized as either *weak-signal amplifiers* or *power amplifiers*.

Amplitude: Amplitude is a measure of the change of a signal value as a function of time. "Peak-to-peak amplitude" refers to the change between minimum and maximum

values of a signal. "RMS Amplitude" refers to Root Mean Square amplitude which is the square root of the mean of a signal.



Glossary of Terms

Analytical modeling: Analytical modeling is a mathematical modeling technique used for simulating, explaining, and making predictions about the mechanisms involved in complex physical processes.

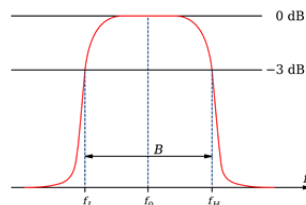
A/D Converters: An A/D converter is a device that converts analog signals (usually voltage) obtained from environmental (physical) phenomena into digital format. Conversion involves a series of steps, including sampling, quantization, and coding.

Axial (Thrust) Position: Change in (or average) position of a rotor in the axial direction with respect to a thrust bearing support structure or nearby fixed point. A proximity probe observes the shaft, its thrust collar or other nearby integral axial shaft surface. Measurement is made by a known probe gap distance (voltage) representing a known position of the thrust collar relative to the thrust bearing clearance.

Balance-of-Plant Machines: Those that are not critical to the overall plant process. They often operate in tandem or spared installations.

Balancing: Procedure for adjusting the radial mass distribution of a rotor so that the mass centerline (principal inertia axis) approaches the rotor rotational axis. This reduces the radial vibration of the rotor due to unbalanced inertia forces and the forces on the bearings at the once-per-revolution frequency.

Band-Pass Filter (BPF): A band-pass filter (also band pass filter, BPF) is a device that passes frequencies within a certain range and rejects (attenuates) frequencies outside that range.



Beam Element: A beam element is one of the most capable and versatile elements in the finite element library. It is very commonly used in the aerospace stress analysis industry and also in many other industries such as marine, automotive, civil engineering structures etc. In aircraft cabin interiors however, in most cases a bar element is sufficient to get you the loads you need.

Bode Plot: In control theory, a **Bode plot** is a **graph** of the frequency response of a system. It is usually a combination of a *Bode magnitude plot*, expressing the

magnitude (usually in decibels) of the frequency response, and a *Bode phase plot*, expressing the phase shift. A *Bode Plot* is a useful tool that shows the gain and phase response of a given LTI system for different frequencies. *Bode Plots* are generally used with the Fourier Transform of a given system. An example of a *Bode* magnitude and phase plot set.

Calibration: Test where known values of the measured variable are applied to a sensor, signal conditioner, monitor or the entire channel output readings to verify or adjust as necessary.

Cantilever Beams: A cantilever is a rigid structural element, such as a beam or a plate, anchored at one end to a (usually vertical) support from which it protrudes; this connection could also be perpendicular to a flat, vertical surface such as a wall. Cantilevers can also be constructed with trusses or slabs.

Channel: A sensor with the associated signal conditioner and monitor hardware required to display its output signal.

Closed Loop Control Systems: A closed loop system is also referred as a feedback control system. These systems record the output instead of input and modify it according to the need. It generates preferred condition of the output as compared to the original one. It doesn't encounter any external or internal disturbances.

Condition Monitoring: A broad field of measurement and analysis of machine parameters to determine machinery health. Modern condition monitoring programs supplement real-time catastrophic vibration, temperature and process "protection monitoring" with more complex often computer based "predictive" maintenance analysis tools. Their aim is to predict the potential timing of machinery failures relative to scheduled production rather than potentially unnecessary time interval-based "preventative" maintenance. Supplemental tools may include performing vibration analysis, oil analysis, laser alignments and automated balancing. The use of thermography for undesirable heat transfer due to coupling misalignment, process or electrical connection problems, and the monitoring of acoustic changes in certain valves and rolling element bearings are also employed.

Crest factor: Crest factor is defined as the ratio of peak value to rms value of a current waveform: The crest factor for a sinusoidal current waveform, such as that which a pure resistive load would draw, is 1.414 since the peak of a true sinusoid is 1.414 times the rms value.

Critical Machines: Critical machines are those required for a major part of the plant. When they go down, that part of the process cannot operate. They are usually unspared and monitored continuously.

Cross Axis (Transverse) Sensitivity: Ratio of the change in signal output of a seismic sensor to an incremental change to a stimulus along any axis perpendicular to the sensitive axis.

Cross Talk: Interference or noise in a sensor or channel which has its origin in another sensor or channel. It may occur when two (or more) proximity probe tips are too close

together, resulting in the interaction of their electro-magnetic fields. The result is to have one signal component on each sensor's output signal. The frequency of the noise is the difference (beat frequency) of the two probe driver oscillation frequencies.

Damped Vibration: If any energy is lost during oscillations, however, it is called damped vibration.

Data acquisition (DAQ): Data acquisition is the process of measuring an electrical or physical phenomenon such as voltage, current, temperature, pressure, or sound with a computer. A DAQ system consists of sensors, DAQ measurement hardware, and a computer with programmable software. Compared to traditional measurement systems, PC-based DAQ systems exploit the processing power, productivity, display, and connectivity capabilities of industry-standard computers providing a more powerful, flexible, and cost-effective measurement solution.

Deterministic Vibrations: If the value or magnitude of the excitation (force or motion) acting on a vibratory system is known at any given time, the excitation is called deterministic. The resulting vibrations are known as deterministic vibrations.

Digital Proximity System: The DPS consists of a proximity probe, an extension cable, and a signal conditioner. Two models are available for the signal conditioner depending on the required signal output format: the MX2033 3-Wire Driver and the MX2034 4-20 mA Transmitter. You can reconfigure these flexible devices to handle a variety of probe and cable combinations from Metrix as well as Bentley Nevada and other competitor companies.

Digital to Analog Converter (DAC): Digital to Analog Converter (DAC) is a device that transforms digital data into an analog signal. According to the Nyquist-Shannon sampling theorem, any sampled data can be reconstructed perfectly with bandwidth and Nyquist criteria. A DAC can reconstruct sampled data into an analog signal with precision. The digital data may be produced from a microprocessor, Application Specific Integrated Circuit (ASIC), or *Field Programmable Gate Array (FPGA)*, but ultimately the data requires the conversion to an analog signal in order to interact with the real world.

Digital Controller: A digital controller is a small digital unit that acts as a system controller. Depending on the controlling requirement, a digital controller can take the form of a desktop computer or it can be as small as a micro controller. The Laplace transform is replaced by Z-transform in the digital controller wherein a discrete time signal in the form of a sequence of complex or real numbers is converted into a complex frequency domain representation.

Direct Search Optimization Techniques: Direct search is a method for solving optimization problems that does not require any information about the gradient of the objective function. Unlike more traditional optimization methods that use information about the gradient or higher derivatives to search for an optimal point, a direct search algorithm searches a set of points around the current point, looking for one where the value of the objective function is lower than the value at the current point. You can

use direct search to solve problems for which the objective function is not differentiable, or is not even continuous.

Pattern Search Algorithms: These are same as direct search algorithms. All are *pattern search* algorithms that compute a sequence of points that approach an optimal point. At each step, the algorithm searches a set of points, called a *mesh*, around the *current point*—the point computed at the previous step of the algorithm. The mesh is formed by adding the current point to a scalar multiple of a set of vectors called a *pattern*. If the pattern search algorithm finds a point in the mesh that improves the objective function at the current point, the new point becomes the current point at the next step of the algorithm.

Displacement: The change in distance, or position, of an object. It is usually a peak-to-peak measurement of vibration with units of mils or microns. In proximity monitoring, eddy current proximity probes measure shaft displacement directly. In seismic monitoring, integration of a velocity sensor signal is necessary to obtain displacement. An acceleration signal requires double (two stage) integration to yield a displacement measurement.

Dual Path: Technique used in signal conditioners and/or monitors whereby a single sensor input is processed through two separate paths; each has its' own measurement units (e.g., velocity and displacement), optional filtering, set points and readout displays.

Dual Voting: A concept requiring that two independent inputs agree before action is taken. This function may be incorporated in a monitor, whereby two (vs. only one) sensor input signals must both measure an amplitude value which exceeds a set point (usually the Danger set point only) before an alarm condition is indicated.

Eddy Current: Electrical current generated (and dissipated) in a conductive material (usually a rotor shaft) when it intercepts the electro-magnetic field of a proximity probe.

Electrical Run Out: A source of signal error from a proximity sensor system which repeats with each shaft revolution; A probe driver output signal change not resulting from a probe gap change (dynamic motion or change in position); Often caused by varying conductivity of the shaft material or the presence of localized magnetic fields at a point(s) on a shaft surface.

Electronic Vibration Switch: Utilization of an accelerometer, signal conditioner and monitor (i.e. single seismic monitoring channel). Offers set point time delay(s) for false trip avoidance and more sensitive velocity (or displacement) measurement. Most have an optional second set point.



Enhanced ACLD Treatment: This is the active constrained layer damping technique in which edge anchors have been installed at both ends of the constraining layer to directly connect the basic beam to the constraining layer to increase the transmissibility of the system.

Enhanced ACLD Stand-off Layer (EACLDSOL) Damping Treatment: It is the enhanced ACLD treatment used in conjunction with stand-off layer damping treatment to compensate the reduced effectiveness of PCLD system which was resulted by implementing edge anchors. Stand-off layer increased the effect of active forces and moments because of its higher range of shear modulus i.e. $10^8\text{-}10^9 \text{ N/m}^2$.

Error: Difference between the indicated and true values of the measured variable. Typically expressed as relative error which is a percentage of the output reading of the sensor.

Essential Machinery: Then one critical to part of the plant. When down, the overall plant cannot operate to full capacity. They can be spared or unspared and are usually monitored continuously.

Equations of Motion: The equations of motion of kinematics describe the most fundamental concepts of motion of an object. These equations govern the motion of an object in 1D, 2D and 3D. They can easily be used to calculate expressions such as the position, velocity, or acceleration of an object at various times.

Extension Cable: A coaxial cable used to connect a proximity probe's cable to a probe driver. It serves to

1. extend the distance to a suitable location for a probe driver
2. provide a disconnect point for easier installation and removal of standard mount style, threaded proximity probes.

Filter: Implementable digitally in software or with analog circuitry, filters are elements that pass or rejects a frequency band usually to isolate a particular machinery mechanical condition(s). “High pass” filters allow only frequencies higher than their design frequency to pass (i.e. be detected). “Low pass” filters permit only lower ones. “Band pass filters” are both low and high pass to narrow both ends of a standard frequency response range. At a filter’s design frequency, amplitude signal attenuation is usually -3 dB and then slopes off (attenuates further) beyond at the design “roll off rate”.

Finite Element Methods (FEMs): The Finite Element Method (FEM) is arguably the most powerful method known for the numerical solution of boundary- and initial-value problems characterized by *partial differential equations*. Consequently, it has had a monumental impact on virtually all areas of engineering and applied science.

Forced Vibration: Forced vibration is the oscillation of a system under the action of a forcing function usually occurring at the frequency of the excitation force.

Free Vibration: Vibration of a mechanical system following an initial perturbation (change of position or velocity). Depending on the kind of perturbation, the system responds by free vibration at one or more of its natural frequencies.

Free-Free Beams: Chladni Patterns are created by the sand that moves to the nodes or nodal lines of the vibrating beam as it is excited at his resonant frequencies. Free Free conditions are simulated suspending the beam with springs giving an extra low frequency mode that does not affect too much the bending behavior.

Fixed-Fixed Beams: Fixed-Fixed beams are common in the interior section of a building (not around the edges). Since both sides of the beam is capable of retaining a moment, this beam is significantly stronger than the *Simply Supported Beams* you've seen earlier.

Frequency: Repetition rate of a periodic vibration within a unit time. Normally expressed in units of cycles per minute (cpm), or cycles per second (cps or Hz) and may be expressed relative to shaft RPM. For rotating machinery vibrations, there are two types of frequencies of interest: 1) the shaft rotational frequency (RPM) and 2) the various vibration frequencies as measured by vibration sensors. Vibration frequencies are usually expressed as a fraction or percentage of the shaft RPM: 1X means one times RPM, 2X means two times, 1/2X, means 50%, etc.

Frequency Response: It is the measured amplitude and phase characteristics of a mechanical or electronic system with respect to frequency. "Small" g is the value of acceleration yielded by the force of Earth's gravity, which varies somewhat with the latitude and elevation of the point of observation. A value of $9.81 \text{ m/s}^2 = 386 \text{ in/s}^2 = 32.2 \text{ ft/s}^2$ is used for the acceleration due to gravity at sea level.

Gear Mesh Frequency: Potential vibration frequency on any machine employing gears. It is calculated by multiplying the number of gear teeth times the RPM of that gear shaft. For a given set of gears, all contacting gears have the same gear mesh frequency for normal operation or else they would not mesh and soon fail.

Grey Box Identification Technique: Grey box modeling is an intermediate identification technique when the uncertainties of internal laws are not entirely known, so it is based on both insight into the system and on experimental data analysis. Grey-box modelling deals with models which are able to integrate the following two kinds of information: qualitative (expert) knowledge and quantitative (data) knowledge, with equal importance.

Golla-Hughes-McTavish (GHM) Method: The Golla-Hughes-McTavish (GHM) method is one technique developed during 1980s to 1990s for the modeling of damping in complex structures. This method adds non-spatial degrees of freedom to a finite element model in order to account for a viscoelastic material's ability to dissipate energy. In the GHM method, a material modulus function is used to characterize the frequency-dependent complex modulus.

H₂ norm: The H_2 norm of a stable system H is the root-mean-square of the impulse response of the system. The H_2 norm measures the steady-state covariance (or power) of the output response $y = H w$ to unit white noise inputs w .

H_∞ norm: H_∞ (i.e. "**H-infinity**") methods are used in *control theory* to synthesize controllers to achieve stabilization with guaranteed performance. To use H_∞ methods,

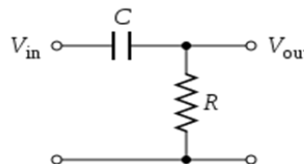
a control designer expresses the control problem as a *mathematical optimization or mathematical programming* problem and then finds the controller that solves this optimization. H_∞ techniques have the advantage over classical control techniques in that they are readily applicable to problems involving multivariate systems with cross-coupling between channels

Hamilton's Principle: It states that the *dynamics* of a physical system is determined by a *variational problem* for a *functional* based on a single function, the *Lagrangian*, which contains all physical information concerning the system and the forces acting on it.

Harmonics: Sinusoidal quantities at frequencies that are an integer multiple of the fundamental frequency.

Hertz (Hz): Unit of frequency in cycles/second. Divide shaft RPM by 60 for getting frequency in Hz.

High-Pass Filter (HP Filter): A high-pass filter is an electronic filter that passes signals with a frequency higher than a certain cutoff frequency and attenuates signals with frequencies lower than the cutoff frequency. The amount of attenuation for each frequency depends on the filter design.



Hysteresis (Dead band): Non-uniqueness between two variables as a parameter increases or decreases. In particular, the maximum difference in output at any given value of the measured variable within the specified range, when the value is first approached with an increasing signal and then a decreasing one. Also called dead band, or that portion of a system's response where a change in input does not produce a change in output.

Inertially Referenced: Inertially referenced motion is referenced to free space or to a fixed point in space; a sensor which measures such motion.

Integrator: Circuitry used in a seismic signal conditioner and/or monitor which performs mathematical integration. It converts a velocity signal to displacement or an acceleration signal to velocity. A double integrator converts an acceleration signal to displacement.

Kalman Filtering: Kalman Filtering, also known as linear quadratic estimation (LQE), is an *algorithm* that uses a series of measurements observed over time, containing *statistical noise* and other inaccuracies, and produces estimates of unknown variables that tend to be more accurate than those based on a single measurement alone, by estimating a *joint probability distribution* over the variables for each timeframe. The filter is named after *Rudolf E. Kálmán*, one of the primary developers of its theory.

Kinetic Energy: In this case the kinetic energy of all the elements is combined to get the total kinetic energy of the system assuming uniform properties. The total kinetic energy (T_e) of the complete system comprises the kinetic energies of the constraining layer (T_1+T_2), base beam (T_3+T_4) and VEM layers (T_5+T_6) i.e. $T_e = T_1 + T_2 + T_3 + T_4 + T_5 + T_6$.

Lagrange's Equation: Elegant and powerful methods have also been devised for solving dynamic problems with constraints. One of the best known is called Lagrange's equations. The *Lagrangian L* is defined as $L = T - V$, where T is the *kinetic energy* and V the *potential energy* of the system in question. Generally speaking, the potential energy of a system depends on the coordinates of all its particles; this may be written as $V = V(x_1, y_1, z_1, x_2, y_2, z_2 \dots)$. The kinetic energy generally depends on the velocities, which, using the notation $v_x = dx/dt = \dot{x}$, may be written $T = T(\dot{x}_1, \dot{y}_1, \dot{z}_1, \dot{x}_2, \dot{y}_2, \dot{z}_2\dots)$. Thus, a dynamic problem has six *dynamic variables* for each particle—that is, x, y, z and $\dot{x}, \dot{y}, \dot{z}$ —and the Lagrangian depends on all $6N$ variables if there are N particles.

Lead Zirconated Titnate (PZT) Layer or Actuator Layer: It is a form of piezoelectric materials. These are the materials that change their configuration by the application of an electric field and vice versa. It is also known as the actuator layer as this layer provides necessary controlling action to the base beam after getting feedback from the sensor layer i.e. PVDF layer

Learning Vector Quantization Neural Networks (LVQNN): The Learning Vector Quantization algorithm (or LVQ for short) is an artificial neural network algorithm that lets you choose how many training instances to hang onto and learns exactly what those instances should look like.

Linearity: Closeness of a calibration curve to a specific straight line, expressed as the maximum deviation of any calibration point to that line during any one calibration increment.

Linear Matrix Inequalities: Linear Matrix Inequalities (LMIs) and LMI techniques have emerged as powerful design tools in areas ranging from control engineering to system identification and structural design. Three factors make LMI techniques appealing:

- A variety of design specifications and constraints can be expressed as LMIs.
- Once formulated in terms of LMIs, a problem can be solved *exactly* by efficient convex optimization algorithms.
- While most problems with multiple constraints or objectives lack analytical solutions in terms of matrix equations, they often remain tractable in the LMI framework. This makes LMI-based design a valuable alternative to classical “analytical” methods.

Linear Vibrations: If all the basic components of a vibratory system the spring, the mass, and the damper behave linearly, the resulting vibration is known as linear vibrations.

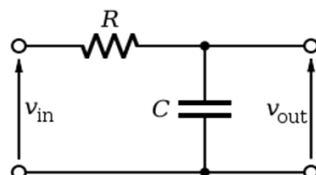
Linear time-invariant systems (LTI systems): These are a class of systems used in *signals and systems* that are both linear and time-invariant. Linear systems are systems whose outputs for a linear combination of inputs are the same as a linear combination of individual responses to those inputs. Time-invariant systems are systems where the output does not depend on *when* an input was applied. These properties make LTI systems easy to represent and understand graphically.

Linear Quadratic Gaussian Controller (LQGC): When we use the combination of an optimal estimator and an optimal regulator to design the controller, the compensator is called Linear Quadratic Gaussian (LQG). Great news about an LQG design is that stability of the closed-loop system is guaranteed.

Linear Quadratic Regulator (LQR): The Linear Quadratic Regulator (LQR) is a well-known method that provides optimally controlled feedback gains to enable the closed-loop stable and high performance design of systems. The LQR algorithm reduces the amount of work done by the control systems engineer to optimize the controller. The LQR algorithm is essentially an automated way of finding an appropriate state-feedback controller. As such, it is not uncommon for control engineers to prefer alternative methods, like full state feedback, also known as pole placement, in which there is a clearer relationship between controller parameters and controller behavior. Difficulty in finding the right weighting factors limits the application of the LQR based controller synthesis.

Linear Variable Differential Transformer (LVDT): An LVDT (linear variable differential transformer) is an electromechanical sensor used to convert mechanical motion or vibrations, specifically rectilinear motion, into a variable electrical current, voltage or electric signals, and the reverse. Actuating mechanisms used primarily for automatic control systems or as mechanical motion sensors in measurement technologies. The classification of electromechanical transducers includes *conversion principles or types of output signals*.

Low-Pass Filter: A low-pass filter (LPF) is a filter that passes signals with a frequency lower than a certain cutoff frequency and attenuates signals with frequencies higher than the cutoff frequency.



Mathematical Modeling: Mathematical modeling is the process of taking a phenomenon which you only have a *qualitative* description of (whether that means a verbal description, a video recording or any other possibility) and attempting a *quantitative* description (which one should then test against measurements of the phenomenon).

Mass Matrix: One of the three methods to construct an element mass matrix can be distinguished as Direct Mass Lumping (DML). The total mass of the element is distributed to the nodes so that a diagonally lumped mass matrix (DLMM) is produced.

Mechanical Run out: Source of error on the output of signal of a proximity sensor system; a probe gap change not resulting from a shaft center position change or dynamic motion. Common sources include out-of-round shafts, scratches, chain marks, dents, rust, stencil marks, at spots, and engravings.

Mechanical Vibration Switch: Resettable device which, after observance of a forced vibration greater than its set point, accelerates a mass (e.g. a lever) to initiate closure or opening of a set of internal field contacts.

Micron (Micrometer): Length or displacement equal to 10^{-6} meters. One micron is equal to 0.04 mil.

Modulus of Rigidity: Shear Modulus or Modulus of Rigidity is the elasticity coefficient for shearing or torsion force. Sponsored Links. Modulus of Rigidity - G - (Shear Modulus) is the coefficient of elasticity for a shearing force. It is defined as. "The ratio of shear stress to the displacement per unit sample length (shear strain)"

Monitor: A loosely used instrumentation term. For machinery, a “protection” monitor may accept inputs from a variety of sensors including temperature, vibration, RPM and 4- 20 mA output types. As a minimum, the monitor compares real-time measured values (after any signal conditioning) to an alarm set point(s), various input sensor/wiring integrity and provides for relay output for machinery ALERT and/or DANGER warning. When the accepted monitor inputs include traditional vibration sensors with dynamic output that require the monitor to also have internal signal conditioning, it is referred to as a “vibration input” monitor. When a monitor accepts only 4-20 mA inputs from vibration transmitters (such as a PLC, DCS or certain Matrix products) it is often referred to as a “4-20 mA input” monitor.

Neural Network: A type of *artificial intelligence* that attempts to imitate the way a human brain works. Rather than using a *digital* model, in which all computations manipulate zeros and ones, a neural network works by creating connections between *processing elements*, the *computer* equivalent of neurons. The organization and weights of the connections determine the *output*.

Nyquist Plots: Nyquist plots are the continuation of polar plots for finding the stability of the closed loop control systems by varying ω from $-\infty$ to ∞ . That means, Nyquist plots are used to draw the complete frequency response of the open loop transfer function

Noise: Any component of a sensor output signal that does not represent the variable intended to be measured.

Non-Linear Vibrations: If, however, any of the basic components behave nonlinearly, the vibration is called nonlinear vibration.

Open Loop Control Systems: An open-loop control system takes input under the consideration and doesn't react on the feedback to obtain the output. This is why it is

also called a non-feedback control system. There are no disturbances or variations in this system and works on fix conditions.

Passive Constrained Layer Damping (PCLD): *PCLD* is a surface damping treatment that consists of one or more viscoelastic layers and one or more non-actuated CL. These *PCLD* treatments are mounted to a base layer, the layer that exhibits the unwanted vibration or resonance. If the base layer is subject to bending, the *VEM* layer is constrained by the base layer and the CL, which causes the *VEM* layer to shear. This shear deformation causes the energy dissipation.

Peak-to-Peak Value: The difference between positive and negative extreme values of a signal or dynamic motion.

Periodic Vibration: Oscillatory motion whose amplitude pattern repeats in time.

Phase: A measurement of the timing relationship between two signals, or between a specific vibration signal and a once-per shaft revolution event (phase angle).

Phase Reference Probe: A probe is used for:

1. determining the unbalance location (phase angle) relative to a measure once-per shaft revolution event location (e.g. a keyway or reflective tape)
2. for complex vibration vector addition or subtraction measurements. The sensor used in phase reference measurements with installed “protection” monitors is usually a proximity sensor system over a keyway. Unprotected machines, or those without a permanent phase reference probe, may have reflective tape temporarily added to be observed by an optical sensor.

Piezoelectric: Any material which provides a conversion from mechanical to electrical energy. For a piezoelectric crystal, if mechanical stresses are applied on two opposite faces, electrical charges appear on another pair of faces.

Polyvinyl Chloride (PVC) Layer: It is an additional layer which is initially stressed (either tensed or compressed) and attached to the base beam to increase the damping performance of the system and the material of this layer is poly vinyl chloride (PVC).

Poles and Zeros: *Poles* and *Zeros* of a transfer function are the frequencies for which the value of the denominator and numerator of transfer function becomes zero respectively. The values of the poles and the zeros of a system determine whether the system is stable, and how well the system performs. Control systems, in the simplest sense, can be designed simply by assigning specific values to the poles and zeros of the system. Physically realizable control systems must have a number of poles greater than or equal to the number of zeros. Systems that satisfy this relationship are called *Proper*.

Pole Zero Identification Method: A recent method based on pole zero identification is shown to be rigorous and simple to use. However, this method requires a special additional software STability Analysis (STAN) to identify poles and zeros of power amplifiers

Potential Energy: The total potential energy V_e of the complete system comprises the strain energies of constraining layer (V_1, V_2), VEM layer (V_3-V_5) and base beam (V_6, V_7) and i.e. $V_e = V_1 + V_2 + V_3 + V_4 + V_5 + V_6 + V_7$.

Power Spectral Density (PSD): The *power spectral density* (PSD) of a signal describes the *power* present in the signal as a function of frequency in Hz or per unit frequency (Hz). Power spectral density is commonly expressed in *watts per hertz* (W/Hz).

Prefilter: these are basically high pass filters installed on the sensors detecting vibrations of flexible structures. Generally, there are infinite number of modes of vibration signals out of which only a few modes, normally first four are of actual importance. To avoid higher modes we take help of HP filters which only allows to pass only predefined cut-off frequency signals and attenuates signals higher than this cut-off frequency signals and due to this they act as prefilters.

Probe: Loosely used term for any machine mounted instrument including a vibration sensor.

Proximity Monitoring: One or more channels of monitoring each consisting of:

1. Proximity sensor system
2. Signal conditioner
3. Monitor.

For a given application, these monitoring components may be partially combined (e.g. a probe driver and a signal conditioner to form a unitized vibration transmitter) or entirely into a proximity switch with relay output.

Proximity Probe: A non-contacting device which measures the displacement motion and position of an observed surface relative to the probe mounting location. Proximity probes used for rotating machinery measurements usually operate on the eddy current principle and measure shaft displacement motion and position relative to the machine bearing(s) or housing.

Proximity Probe Driver (Oscillator-Demodulator): A device which sends a radio frequency signal to an eddy current proximity probe usually through an extension cable, demodulates the probe output, and provides output signals proportional to both the average and dynamic probe gap distances.

Proximity Probe Gap: The physical distance in micrometers or mils between a target (e.g. a machinery shaft or proximity sensor calibrator target) and a proximity probe tip. The measurement is made either mechanically with a “feeler” or thickness gauge or, more commonly due to machinery case access constraints, electrically by a DC output voltage signal reading from a powered proximity sensor system. Setting the probe gap refers to static (i.e. machine off) positioning of the probe to a distance from the shaft in the center of the sensor system’s linear range.

Proximity Probe Orientation: The angular location of a proximity probe with respect to a polar coordinate system when viewed from the driver end of a machine. Usually,

zero degrees is at top dead center (vertical) or at the horizontal right (3 o'clock) position on the coordinate system.

Proximity Sensor Calibrator: A mechanical device which generates dynamic motion of an observed surface at a known amplitude and frequency. The surface is observed by a proximity probe for the purpose of calibrating only the proximity sensor system or, with its monitor, an entire proximity channel.

Proximity Sensor System: An electrically matched (tuned) sensor system comprised of a proximity probe, usually an extension cable and a probe driver.

Positive Position Feedback (PPF) Control: The terminology *positive position* is derived from the fact that the *position* measurement is positively fed into the compensator and the *position signal* from the compensator is positively fed back to the structure. This property makes the *PPF controller* very suitable for collocated actuator/sensor pairs.

Polyvinilidene Di Fluoride (PVDF) layer or Sensor Layer: It is also a form of piezoelectric material. This is called a sensor layer in our case as it analyses any disturbance of the base structure in the form of shape change and gives necessary signal to the actuator in the form of voltage.

Radial: A direction of a machine which is perpendicular to the shaft centerline; in the XY plane; usually refers to direction of shaft or casing motion or measurement.

Radial (Centerline) Position: The average position of the shaft centerline within the bearing. This can be measured by noting the change in VDC output of two XY probes from a known position with the shaft at rest. The XY probes should be attached to the bearing or its' housing to eliminate thermal growth errors.

Radial (Lateral) Position: Shaft dynamic motion or casing vibration which is measured at 90° to the shaft centerline.

Random Vibrations: In some cases, the excitation is nondeterministic or random; the value of the excitation at a given time cannot be predicted. In these cases, random vibrations are produced.

Relative Motion Vibration: measured relative to a chosen reference. Proximity probes measure shaft dynamic motion and position relative to the probe mounting, usually the bearing or bearing housing.

Relative Probe: A proximity probe observing shaft motion relative to a stationary reference such as a bearing housing.

Repeatability: The ability of a sensor or monitor to reproduce output readings when the same value is applied to it repeatedly, under the same conditions, and in the same direction. Also the maximum deviation from the mean of corresponding data points taken from repeated tests under identical conditions.

Resistance Temperature Detector (RTD): A sensor which measures temperature or temperature change as a function of resistance.

Resolution: The smallest change in applied stimulus that will produce a detectable change in the instrument output. Resolution differs from precision in that it is a psycho-physical term referring to the smallest increment of humanly perceptible output (rated in terms of the corresponding increment of input).

Resonant Controllers: Resonant controllers includes primary controllers for double-ended (half-bridge) topologies, designed to provide high efficiency under any load conditions, as well as high noise immunity (zero voltage switching operation).

The L6598, the 1st generation resonant controllers, implement an HV half bridge driver that directly drives two power *Metal Oxide Semiconductor Field Effect Transistors (MOSFETs)* and has a dedicated timing section to set soft start duration and minimum operating frequency.

These controllers are widely used in LCD TVs, all-in-one PCs, high-power LED lighting and AC-DC adapters (>90 W).

Resonance: The condition where a forcing frequency coincides with a natural frequency of the system. A resonant condition usually causes a substantial amplitude increase.

RMS (ROOT MEAN SQUARE): Square root of the arithmetic average of a set of squared instantaneous values. In rolling element bearings, certain bearing problems may be indicated by increased RMS vibration levels of the outer race motion.

Rolling Element Bearing: A bearing which uses rolling elements (rollers or balls) to support the load of a rotating shaft with minimum friction.

Ryton: A highly chemical and abrasion resistant polymer (poly phenylene sulfide resin) made by Chevron Phillips Petroleum Company used to fabricate proximity probe tips.

Sampling Rate: Sampling Rate is the number of samples of audio carried per second, measured in Hz or kHz (one kHz being 1 000 Hz). For example, 44 100 samples per second can be expressed as either 44 100 Hz, or 44.1 kHz. Bandwidth is the difference between the highest and lowest frequencies carried in an audio stream

Seismic Monitoring: One or more channels of monitoring each consisting of:

1. seismic (casing) accelerometer or velocity sensor
2. signal conditioner
3. monitor

For a given application, these monitoring components may be partially combined (e.g. an accelerometer and a signal conditioner to form a unitized vibration transmitter) or entirely into an electronic vibration switch with relay output.

Sensor: A device for translating the magnitude of one quantity to another. The second quantity often has different units of measure and serves to provide a more useful signal. Vibration sensors convert mechanical motion into an electronic (typically a voltage proportional) signal.

Set Point (Trip) Multiplier: A function provided in a monitor system to temporarily increase the alarm (Alert and Danger) set point values by a specific multiple (usually

two or three). This function may be applied by manual or control relay action during start-up to allow a machine to pass through high vibration speed ranges without excessive monitor alarm indications. Such speed ranges may include system resonances and other normal transient vibrations.

Set point: An adjustable threshold above which a measured value will initiate relay output indicating a machine or process Alert and/or Danger warning condition.

Shape Functions: The shape functions are the functions which interpolate the solution between the discrete values obtained at the mesh nodes. Therefore, appropriate functions have to be used and, as already mentioned, low order polynomials are typically chosen as shape functions. In this work linear shape functions are used.

Signal Attenuation: The reduction in magnitude of a signal without changing the basic characteristics of the signal. Also, the amount of voltage reduction utilized to reduce large electronic signals down to full scale deviation on instruments such as tape recorders. This non-dimensional number is usually in even steps of 0.5, 0.2 and 0.1. Signal attenuation may also result from reduced mechanical transmission of vibration from one machine part to another (e.g., shaft to bearing housing) and also from signal conditioner circuits in some applications.

Signal Conditioner: A device placed between a signal source (sensor) and a monitor to change the signal. Examples: attenuators, amplifiers, signal converters (for changing one electrical quantity into another such as volts to amps, analog to digital, integrators) and filters.

Signal Gain: The change in magnitude of a signal. Also, the voltage amplification utilized to enlarge small electronic signals up to full scale deviation on instruments. Often expressed in steps of 2, 5, and 10.

Simply Supported Beam: A simply supported beam is a type of beam that has pinned support at one end and roller support at the other end. Depending on the load applied, it undergoes shearing and bending. It is the one of the simplest structural elements in existence.

Ski-Slope: An elevated noise floor that decreases with increasing frequency, often overwhelming the peaks at discrete frequencies that are present in normal measurements.

Smart Materials: Smart materials are those materials which have one or more properties that changes significantly by reacting to the environment all by itself. The reaction may exhibit itself as a change in *volume, color or viscosity* and this may occur in response to a change in *temperature, stress, electrical current, pH or magnetic field*.

Spall: A flake or chip of metal removed from one of the races from a rolling element of a bearing. Spalling is evidence of serious bearing degradation and may be detected by relatively small increases in signal amplitude at the bearing frequencies during operation.

Spillover: When a ROM (Read-only memory) based controller is applied to the full order system, actuator forces for reducing the *vibration* of the lower modes will also influence the residual modes of the structure and produce undesirable *vibration* due to the un-modeled dynamics. This phenomenon is known as control *spillover*.

Stand-off Layer (SOL): This is an additional constraining layer which is sandwiched between the base beam and the viscoelastic material layer to increase the effectiveness of conventional passive constraining layer damping treatment which was decreased using edge anchors because these anchors only increase the transmissivity at very higher feedback gain levels. At these gain levels the efficiency of PCLD technique was deferred. With the addition of this layer viscoelastic strains were enhanced allowing more dissipation of energy also the active forces and moments were enhanced to very high level as shear modulus of the system was $10^8\text{-}10^9 \text{ N/m}^2$.

Stiffness Matrix: In the finite element method for the numerical solution of elliptic partial differential equations, the stiffness matrix represents the system of linear equations that must be solved in order to ascertain an approximate solution to the differential equation.

Stressed Layer Damping (SLD) Treatment: It is the treatment which is combined with ACLD treatment to increase damping performance of the system. In this technique a poly vinyl chloride (PVC) layer will be attached to the base beam which is first stressed either by stretching it on UTM resulting the base beam in tension or by compressing it leaving the base beam in compression. In the first case, the attached PVC layer will be under compressive stresses and in the second case PVC layer will under tensile stresses.

System Classification: Systems are classified into the following categories:

1. Liner and Non-liner Systems
2. Time Variant and Time Invariant Systems
3. Liner Time variant and Liner Time invariant systems
4. Static and Dynamic Systems
5. Causal and Non-causal Systems
6. Invertible and Non-Invertible Systems
7. Stable and Unstable Systems

System Delays: A system can be built with an inherent delay. Delays are units that cause a time-shift in the input signal, but that don't affect the signal characteristics. An ideal delay is a delay system that doesn't affect the signal characteristics at all, and that delays the signal for an exact amount of time. Some delays, like processing delays or transmission delays, are unintentional. Other delays however, such as synchronization delays, are an integral part of a system.

System Length: A feature of proximity sensor systems equal in magnitude to the combined electrical lengths of a proximity probe and (usually) an extension cable are matched (tuned) to the proximity probe driver electronics for proper function (linearity). Newer proximity sensor systems generally have 5 or 9 m system lengths that are normally within $\pm 5\%$ of their dimensional length. Some older systems have

15 or 20 feet system lengths and, for small diameter probes, have up to -15% shorter dimensional lengths.

Thermistor: An electrical device used for temperature measurement. Their coefficients of resistance are either positive or negative (i.e., with increasing temperature, the resistance may increase or decrease for a given type).

Thermocouple: A temperature sensing device comprised of two dissimilar metal wires which when thermally affected (heated or cooled) produce a proportional change in electrical potential at the point where they join.

Threshold: The smallest change in the measured variable that will result in a measurable change in an output signal.

Time Delay: Electronic vibration protection systems usually offer two types of time delay to avoid false alarms for transient conditions:

1. machine start up time delay (or set point multiplication)
2. monitor (running) time delay.

They may be of fixed or adjustable time duration.

Total Run out: Equal in magnitude to the electrical plus the mechanical run out.

Transient Vibrations: Temporary vibrations of a mechanical system. These may consist of forced or free vibration or both. Transient vibrations are typically associated with changes in machine operating condition such as speed, load, etc. and are pure function of time.

Turbine Supervisory Instrumentation (TSI): A TSI system is a continuous monitoring system generally used on turbo generator sets. It can include such measurements as shaft radial vibration, shaft absolute vibration, axial thrust position, differential expansion case expansion, valve position, eccentricity peak-to-peak, zero speed, and shaft RPM. Metrix does not currently offer this type of instrumentation.

Unbalance (Imbalance): Unequal radial weight distribution on a rotor system; a shaft condition where the mass centerline (principal inertial axis) does not coincide with the geometric centerline. Also, the amount of mass causing the unbalance.

Undamped Vibrations: If no energy is lost or dissipated in friction or other resistance during oscillation, the vibration is known as undamped vibration

Velocity: Time rate of change of displacement. Velocity leads displacement by 90 degrees in time. Units for velocity are inches/second or millimeters/second, zero-to-peak or RMS. Velocity measurements are obtained by:

1. electronic integration of an acceleration signal from an accelerometer or
2. directly from a velocity sensor. Velocity is a widely used measurement for evaluating machine casing and other structural response characteristics.

Velocity Sensor: A seismic sensor which converts velocity motion into a proportional electrical signal.

Velocity Transmitter: A velocity transmitter produces a 4-20 mA signal proportional to axial velocity.

Vibration: Dynamic motion resulting from an applied stimulus. Out-of-tolerance measurements for excessive vibration are useful to protect from:

1. personnel injury
2. costly machinery downtime
3. avoidable extensive repairs
4. higher insurance rates.

Vibration Analysis and Data Collection: Process involving the collection, manipulation, display and more specifically the interpretation of machine casing and/or shaft vibration waveform as it relates to machine condition. Except for the very largest machines, data collection is commonly done by walk around operators who are properly trained in collecting scheduled measurement points. Permanently mounted proximity or seismic sensors that are of part of an excessive vibration “protection” monitor are accessed when possible, or an accelerometer is temporarily attached for casing measurements.

Vibration Meter: A portable one or two part (remote sensor) instrument used to measure seismic (casing) vibration amplitude.

Vibration Transmitter: An instrument combining a seismic accelerometer or a proximity probe driver vibration sensor together with a voltage-to-current signal conditioner to provide proportional 4-20 mA output. This output represents the zero to full scale nameplate vibration and provides an input to a user’s PLC or DCS wherein a set point(s), time delay(s) and input integrity check(s) may be programmed as part of the monitor function.

Velocity Feedback Controller: The closed-loop action is obtained by comparing the angular position of the motor shaft with the input signal by the interfaced circuit. A tacho-generator is used to measure the angular velocity, which can be used as a feedback signal to the input of the servo valve drive amplifier and is called a Velocity Feedback Controller.

Viscoelastic Materials: Viscoelasticity is the property of materials that exhibit both viscous and elastic characteristics when undergoing deformation. Viscous materials, like honey, resist shear flow and strain linearly with time when a stress is applied.

Waveform: A presentation or display of the instantaneous amplitude of a signal as a function of time. A vibration waveform can be viewed on an oscilloscope in the time base mode.

XY: Perpendicular axes in a Cartesian coordinate system. Usually used as a reference for orthogonal mutually perpendicular dual vibration sensors.

Zero-to-Peak Value: One half of the peak-to-peak value.

4-20 mA Signal (4-20 mA Current Loop): A 4-20 mA current loop is an analog electronic signaling approach in which a two-wire transmitter device sets current in a range of 4 to 20 mA to a value that is proportional to a signal of interest. Widely used in industrial control applications, the approach offers an advantage that accuracy is not affected by a voltage drop due to electrical resistance in the wiring. Additionally, it can provide operating power to the connected transmitter.

Glossary of Symbols

a	Number of actuators
ak	Maximum amplitude of kth sinusoid.
A	Area of cross-section of general section
Ap	Area of cross section of PZT patch
As	Area of cross section of the steel structure
Ac	Equivalent state coupling matrix for the closed loop system
A	State-coupling matrix in canonical form
A0	Auto regressive coefficients matrices of ARMA form at time t
A1	Auto regressive coefficients matrices of ARMA form at time (t-1)
A2	Auto regressive coefficients matrices of ARMA form at time (t-2)
A1	Output of LVQ neural network
A2.	Output of LVQ neural network
b	Width of the 2D beam element
B	Input coupling matrix in canonical form
B1	Moving average coefficients matrices of ARMA form at time (t-1)
B2	Moving average coefficients matrices of ARMA form at time (t-2)
B'	Transformation matrix
cji	Element of damping matrix
Cr	Crest factor of the excitation signal
C	Global damping matrix
C~	Symmetric damping matrix
C	Output coupling matrix in canonical form
d31	Dielectric constant of PZT material (m/v),

d32 Dielectric constant of PZT material (**m/v**),

D Dynamical matrix of the system

E Young's modulus of elasticity for general material

Es Young's modulus of elasticity for steel

Ep Young's modulus of elasticity for the total structure

E otal modal energy of the system

Er Cumulative Error

F State coupling matrix in coupled control form (DISCRETE)

F State coupling matrix in coupled control form (CONTINUOUS)

$F_{x_1}(t)$ Horizontal Force acting at node 1 of the 2D beam element at the instant of time t.

$F_{x_2}(t)$ Horizontal Force acting at node 2 of the 2D beam element at the instant of time t.

$F_{y_1}(t)$ Vertical Force acting at node 1 of the 2D beam element at the instant of time t.

$F_{y_2}(t)$ Vertical Force acting at node 2 of the 2D beam element at the instant of time t.

G Input coupling matrix in coupled control form (DISCRETE)

G Input coupling matrix in coupled control form (CONTINUOUS)

h Length of 2D beam element

H Output coupling matrix in coupled control form (DISCRETE)

H Output coupling matrix in coupled control form (CONTINUOUS)

I Moment of inertia of 2D beam element about the bending axis

Is Moment of inertia of 2D beam element made of STEEL about the bending axis

Ip Moment of inertia of 2D beam element made of PZT about the bending axis

Glossary of Abbreviations

A/D	Analog to Digital
AC	Active Control
ACLD	Active Constrained Layer Damping
AVC	Active Vibration Control
CL	Closed Loop
CLD	Constrained Layer Damping
CoLD	Compressed Layer Damping
CRO	Cathode Ray Oscilloscope
D/A	Digital to Analog
DAQ	Data Acquisition
DAQ-STC	Data Acquisition System Time Controller
DAQ-STC	Data Acquisition-System Time Counter
DMA	Direct Memory Access
DYAD	/Soundcoat
EACLDSOL	Enhanced Active Constrained Layer Damping with SOL Layer
EBAM	Energy Based Analytical Methods
ER FLUIDS	Electro-Rheological Fluids
FEM	Finite Element Method
FEA	Finite Element Analysis
FRF	Frequency Response Function
GHM	Golla-Hughes-McTavish
HP FILTER	High Pass Filter
LMI	Linear Matrix Inequality

LQG	Linear Quadratic Gaussian
LP FILTER	Low Pass Filter
LQR	Linear Quadratic Regulator
LTI	Linearly Time Invariant
LVDT	Linear Variable Differential Transformer
LVQNN	Learning Vector Quantization Neural Networks
MIMO	Multiple Input Multiple Output
MISO	Multiple Input Single Output
MR FLUIDS	Magneto-Rheological Fluids
OL	Open Loop
PC	Passive Control
PCLD	Passive Constrained Layer Damping
PID	Proportional-Integral-Derivative
PD	Proportional Derivative
PE	Piezo-Electric
PFI	Programmable Free Interface
PGIA	Programmable Gain Instrumentation Amplifier
PPF	Positive Position Feedback
PSD	Power Spectral Density
PS	Power System
PVC	Poly Vinyl Chloride
PVDF	Poly Vinylene Di-Fluoride
PZT	Lead Zirconium Titnate
RMS	Root Mean Square

RTSI	Real time System Integration
S/N RATIO	Signal-to-Noise Ratio
SIMO	Single Input Multiple Output
SISO	Single Input Single Output
SLD	Stressed Layer Damping
SOL	Stand-Off Layer
TeLD	Tensed Layer Damping
VEM	Visco-elastic Material

BIBLIOGRAPHY

A plenty of outstanding text and reference books on vibration analysis and numerical methods are available for the readers who wish to pursue their topics further. Also there are several publications devoted to presenting research results and in-depth case studies in vibration analysis. The following list is a representative sample of many excellent references that includes journals and periodicals on vibration analysis and numerical methods.

Araujo, A. L., Martins, P., Mota, Soares, C. M., Mota, Soares, C. A., and Herskovits, J., 2009, “Damping optimization of viscoelastic laminated sandwich composite structures”, Structural and Multidisciplinary Optimization, vol. 39, pp. 569–579.

Araujo, A. L., Mota, Soares, C. M., Mota, Soares, C.A., and Herskovits, J., 2010a, “Optimal design and parameter estimation of frequency dependent viscoelastic laminated sandwich composite plates.” Composite Structures, vol. 92, pp. 2321–2327.

Araujo, A. L., Mota, Soares, C. M., Mota, Soares, C.A., and Herskovits, J., 2010b, “Damping optimization of hybrid active–passive sandwich composite structures”, Advances in Engineering Software, vol. 46, pp. 69-74.

Azvine, B., Tomlinson, G.R., and Wynne, R.J., 1995, “Use of Active constrained layer damping for controlling resonant vibrations”, Smart Materials and Structures, vol. 4, pp. 1-6.

Balas, M.J., 1978, “Active control of flexible systems”, Journal of Optimization Theory and Applications, vol. 25, pp.415-436.

Baz, A., and Tempia, A., 2004, “Active piezoelectric damping composites”, Sensors and Actuators A: Physical, vol. 112, pp. 340-350.

Baz, A., and Chen, T., 2000, “Control of axi-symmetric vibrations of cylindrical shells using Active constrained layer damping”, Thin-Walled Structures, vol. 36, pp. 1-20.

Baz, A., and Park, C. H., 1999, “Vibration control of bending modes of plates using active constrained layer damping”, Journal of Sound and Vibration, vol. 227, pp. 711-734.

Baz, A., and Poh, S., 1988, “Performance of active control system with piezoelectric crystals”, Journal of Sound and Vibration, vol. 126(2), pp. 327-343.

Baz, A., and Ro, J., 1995, “Optimum design and control of active constrained layer damping”, Journal of Dynamic Systems Measurement and Control Transactions of the ASME, vol. 117, pp. 135-144.

Baz, A., and Ro, J., 2001, “Vibration control of rotating beams with active constrained layer damping”, Smart Materials and Structures, vol. 10, pp. 112-120.

- Baz, A.**, 1997, "Dynamic boundary control of beams using active constrained layer damping", Mechanical Systems and Signal Processing, vol. 11, pp. 811-825.
- Baz A.**, 1998, "Robust control of active constrained layer damping", Journal of Sound and Vibration, vol. 211, pp. 467-480.
- Bernzen, Werner.** 1999, "Active vibration control of flexible robots using virtual spring-damper systems", Journal of Intelligent and Robotic Systems, vol. 24, pp. 69-88.
- Birman, V., Griffin, S., and Knowles, G.**, 2000, "Axisymmetric dynamics of composite spherical shells with Active piezoelectric/composite stiffeners", Acta Mechanica, vol. 141, pp. 71-83.
- Blais, Jean-Francois., Cimmino, Massimo., Ross, Annie., and Granger, Daniel.**, 2009, "Suppression of time aliasing in the solution of the equations of motion of an impacted beam with partial constrained layer damping", Journal of Sound and Vibration, vol. 326, pp. 870–882.
- Boudaoud, Hakim., Belouettar, Salim., Daya, E.M., and Potier-Ferry, Michel.**, 2009a, "A numerical method for nonlinear complex modes with application to Active-passive damped sandwich structures", Engineering Structures, vol. 31, pp. 284-291.
- Boudaoud, Hakim., Daya, E.M., Belouettar, Salim., Duigou, L., and Potier-Ferry, Michel.**, 2009b, "Damping analysis of beams submitted to passive and active control", Engineering Structures, vol. 31, pp. 322-331.
- Brenann, M.J., Elliott, S.J., and Pinnington, R.J.**, 1995, "Strategies for the active control of flexural vibration on a beam", Journal of Sound and Vibration, vol. 186(4), pp. 657-688.
- Brennan, M.J., Anantha, gneshan, K.A., Elliot, S.J..**, 2007, "Instabilities due to instrumentation phase-lead and phase-lag in the feedback control of a simple vibrating system.", Journal of Sound and Vibration, vol. 304, pp. 466-478.
- Burdisso, R.A., and Fuller, C.R..**, 1991, "Eigen properties of feed-forward controlled flexible structures", Journal of intelligent Material Systems and structures, vol. 2(4), pp. 494-507.
- C.W., Chang., and A.A., Shabana..**, 1987, "Hybrid control of flexible multi-body systems", Computers & Structures, vol. 25(6), pp. 831–844.
- Cai, C., Zheng, H., and Liu, G.R..**, 2004, "Vibration analysis of a beam with PCLD Patch", Applied Acoustics, vol. 65, pp. 1057-1076.
- Cai, Guoping., Teng, Youyou., and Lim, C.W..**, 2010, "Active control and experiment study of a flexible hub-beam system", Acta Mechanica Sinica, vol. 26, pp. 289–298.

- Carneal, James, P., Giovanardi, Marco., Fuller, Chris, R., and Palumbo, Dan.,** 2008, “Re-active passive devices for control of noise transmission through a panel”, Journal of Sound and Vibration, vol. 309, pp. 495–506.
- Choi, S.B.,** 1995, “Alleviation of chattering in flexible beam control via piezofilm actuator/sensors”, AIAA Journal, vol. 33(3), pp. 564-567.
- Clark, R.L.,** 1997, “Accounting for out-of-bandwidth modes in the assumed model approach: Implications on collocated output feedback control”, Journal of Dynamic Systems, Measurement, and Control, vol. 119, pp.390-395.
- Cole, D.G., and Clark, R.L.,** “Adaptive compensation of piezoelectric sensor actuators”, Smart Materials and Structures, vol. 5, pp. 665-672.
- Crawley, E.F., and Luis, Javier De.,** 1987, “Use of piezoelectric actuators as Elements of intelligent structures”, AIAA Journal, vol. 25(10), pp. 1373-1385.
- Creasy, M.A., Leo, D.J., and Farinholt, K.M.,** 2008, “Adaptive positive position feedback for actively absorbing energy in acoustic cavities”, Journal of Sound and Vibration, vol. 311, pp. 461-472.
- Damle, R., Lashlee, R., Rao, V., and Kern, F.,** 1994, “Identification and robust control of smart structures using artificial neural networks,” Smart Materials and Structures, vol. 3, pp. 35-46.
- D. Butler, Nigel. and Oyadiji, S.Olutunde.,** 2008, “Transmissibility characteristics of stiffened profiles for designed-in viscoelastic damping pockets in beams” Computers & Structures, vol. 86, pp. 437–446.
- Deng, Xueying., And Wang, Yankui.,** 2004, “Asymmetric vortices flow over slender body and its active control at high angle of attack”, Acta Mechanica Sinica, vol. 20(6), pp. 567–579.
- Denoyer, K.K., and Kwak, M.K.,** 1996, “Dynamic modeling and vibration suppression of a slewing structure utilizing piezoelectric sensors/actuators”, Journal of Sound and Vibration, vol. 189 (1), pp. 13-31.
- Deu, J.F., Larbi, W., and Ohayon, R.,** 2008, “Piezoelectric structural acoustic problems: Symmetric variational formulations and finite element results”, Computer Methods in Applied Mechanics and Engineering, vol. 197, pp. 1715–1724.
- Deu, Jean-Francois., and Benjeddou, Ayech.,** 2005, “Free-vibration analysis of laminated plates with embedded shear-mode piezoceramic layers”, International Journal of Solids and Structures, vol. 42, pp. 2059–2088.
- Dhuri, K.D., and Seshu, P.,** 2009, “Multi-objective optimization of piezo actuator placement and sizing using genetic algorithm”, Journal of Sound and Vibration, vol. 323, pp. 495–514.

Di, Taranto R.A., 1965, "Theory of vibratory bending for elastic and Viscoelastic finite length beams", Journal of Applied Mechanics Transactions of the ASME, vol. 32, pp. 881-886.

Dongchang, Sun., and Liyong, Tong., 2002, "Modelling and vibration control of beams with partially debonded active constrained layer damping patch", Journal of Sound and Vibration, vol. 252, pp. 493-507.

Dongchang, Sun., and Liyong, Tong., 2003, "Effect of debonding in Active constrained layer damping patches on hybrid control of smart beams", International Journal of Solids and Structures, vol. 40, pp. 1633-1651.

Dongchang, Sun., and Liyong, Tong., 2004, "A compressional-shear model for vibration control of beams with Active constrained layer damping", International Journal of Mechanical Sciences, vol. 46, pp. 1307-1325.

Dosch, J., Inman, D.J., and Garcia, E., 1992, "A self-sensing piezoelectric actuator for collocated control", Journal of Intelligent Material Systems and Structures, Vol. 3, pp.166-185.

Drozdov, A. D., and Dorfmann, A., 2002, "The effect of temperature on the viscoelastic response of rubbery polymers at finite strains", Acta Mechanica, vol. 154, pp. 189- 214.

Eissa, M., Bauomy, H.S., and Amer, Y. A., 2007, "Active control of an aircraft tail subjected to harmonic excitation", Acta Mechanica Sinica, vol. 23, pp. 451–462.

Falugi, M., 1991, "Analysis of a five layer viscoelastic constrained layer beam", Proceedings of Damping 91, vol. II, Paper No. CCB.

Falugi, M., Moon, Y., and Arnold, R., 1989, "Investigation of a four layer Viscoelastic constrained layer damping system", USAF/WL/FIBA/ASIAC, Report No. 189.1 A.

Fan, Rongping., Meng, Guang., Yang, Jun., and He, Caichun., 2009, "Experimental study of the effect of viscoelastic damping materials on noise and vibration reduction within railway vehicles", Journal of Sound and Vibration, vol. 319, pp. 58–76.

Fasana, A., and Marchesiello, S., 2001, "Rayleigh–Ritz analysis of sandwich beams", Journal of Sound and Vibration, vol. 241(4), pp. 643-652.

Fung, E. H. K., and Yau, D. T. W., 2004, "Vibration characteristics of a rotating flexible arm with ACLD treatment", Journal of Sound and Vibration, vol. 269, pp. 165-182.

Gao, J., and Shen, Y., 1999, "Dynamic characteristic of a cantilever beam with partial self-sensing Active constrained layer damping treatment", Acta Mechanica Solida Sinica, vol. 12(4), pp. 316-327.

Index

A

Active control 1.1, 1.3, 1.10, 2.2, 2.3, 2.6, 4.1, 5.1, 5.2, 5.14
Active-passive treatment 1.9
Active vibration control 1.3, 1.11, 2.1, 2.2, 6.2
ACLD treatment 1.9, 1.10, 1.12, 2.3, 4.1-4.3, 4.6, 4.12, 4.14-4.16, 5.1, 5.2, 5.5, 5.14, 5.17, 5.19, 5.20, 5.23, 6.2, 6.3, 6.5, 6.17, 6.18, 6.20, 6.21, 7.1, 7.9-7.13, 7.15
Actuators 1.3, 1.7, 1.8, 1.10, 2.1-2.3, 2.5, 2.6, 4.1, 8.1, 8.25
Adaptive control 1.1, 1.2, 1.7, 1.8, 8.1
A/D conversion 2.3, 2.4, 8.24
ACLD+SLD 6.19, 6.20
Algorithm 1.2, 1.8, 8.10-8.13
Amplitude 1.1-1.3, 4.14, 4.16, 4.17, 4.22, 4.23, 5.16, 5.17, 5.23, 7.13
Analytical modeling 1.10, 3.13
Analysis 1.2, 1.3, 1.10-1.12, 2.1, 2.4, 2.5, 4.2, 4.10, 4.11, 6.2, 6.4, 8.5, 8.7, 8.23, 8.25
Appropriate boundary conditions 3.12, 4.9, 5.9
Approximation 1.3, 2.5, 8.12, 8.15, 8.18, 8.19
Axial displacement 3.8-3.11, 4.4-4.7, 5.4, 5.6-5.8, 6.4, 6.6, 6.7, 7.3-7.5, 8.1, 8.5, 8.16-818, 8.20-8.22, 8.26, 8.27

B

Bare beam 6.15, 6.20
Base beam 3.1, 3.11, 3.13, 3.14, 3.16-3.18, 2.1, 4.1-4.7, 4.10-4.12, 4.14, 4.16, 4.19, 4.21, 5.1, 5.3, 5.4, 5.6, 5.7, 5.12, 5.14-5.16, 5.18-5.23, 6.1-6.7, 6.11-6.14, 6.16, 6.19, 6.20, 6.22-6.24, 7.1-7.5, 7.9, 7.12, 7.15, 7.16

Beams 1.9-1.12, 3.1, 3.7, 3.15, 3.17, 3.19, 3.20, 4.3, 5.20, 6.1, 6.4, 6.14, 7.1
Beam element 3.2, 3.4, 3.8, 3.12, 4.5, 4.7, 5.4, 5.9, 6.8, 7.6
Boundary conditions 1.3, 2.5, 3.1, 3.3, 3.12, 3.14-3.17, 3.20, 4.9, 5.9, 5.11, 6.12, 7.9.

Bending moment 3.3, 5.19, 5.20, 7.12

C

Cantilever beam 1.9, 3.20-3.22, 6.1, 8.21, 8.23, 8.25
Characteristics 1.1, 1.8, 2.3, 4.1, 4.21, 4.22, 5.1, 5.23, 6.1, 6.24, 7.16, 8.1, 8.23
Clamped 4.21, 5.11, 5.22, 6.2, 6.9, 7.1, 7.7
Closed loop conditions 4.9, 5.9, 6.8, 6.10, 7.6, 7.8
Closed loop systems 8.2, 8.9, 8.12, 8.15, 8.20, 5.21, 5.26, 8.27
Configurations 1.3, 1.6, 1.9, 2.1, 2.2, 2.5
Constraining layers 3.14, 4.2, 4.12, 4.14, 6.2, 6.3, 6.15, 6.19, 6.20
Continuous 1.4, 1.5, 8.2, 8.6
Control signals 1.1, 1.7, 2.1, 2.3, 2.5, 8.25
Crest factor 4.17
Control theory 1.2, 1.4-1.6
Cut-off frequency 7.15

D

D/A conversion 1.7, 2.3, 2.4, 8.23
Damping ratios 4.1, 4.2, 5.23, 6.1, 6.2, 6.11, 6.13-6.19, 6.21, 6.22, 6.24, 7.1, 7.9-7.13, 7.16, 8.3, 8.5, 8.6, 8.14
Damping techniques 1.9, 4.1, 5.20
Data acquisition 2.4, 2.5, 8.2, 8.23-

8.25
 Difference equation form 1.5, 1.7
 Differential equations 1.6, 4.1, 6.1,
 8.2
 Discrete 1.4, 1.5, 8.2
 Discrete systems 1.4
 Dielectric constant 2.2, 4.8, 4.9,
 4.11, 5.6, 5.10, 5.14, 6.7, 6.10,
 6.19, 7.5, 7.8, 8.5
 Displacements 4.15, 4.18, 4.21,
 5.1, 5.3-5.8, 5.10, 5.22, 5.23, 6.4,
 6.6, 6.7, 6.10, 7.3-7.5, 7.16
 Dynamics 2.2, 2.5, 4.21, 8.7, 8.17,
 8.25

E

Eigenvalue problems 3.15, 4.2,
 4.10, 8.6
 Eigenvectors 6.11, 7.8
 Elasticity 4.18, 4.19, 5.11, 6.4,
 6.23
 Electromechanical coupling factor
 2.2, 4.9, 4.10, 5.9, 5.14, 6.10,
 6.19, 7.8, 8.5
 Electro-rheological fluids 1.8
 Element stiffness 3.6
 Energy based analytical methods
 (EBAM) 1.11, 1.12, 3.1, 3.16,
 3.20, 3.22
 Energy losses 6.1
 Enhanced ACLD treatment
 1.12, 5.2, 5.5,
 Equations of motion 3.12, 3.15,
 4.1, 4.2, 4.8, 4.19, 5.1, 5.9, 5.19,
 6.1, 6.8, 6.9, 6.11, 7.6-7.8, 8.1

F

Fast Fourier Transfer (FFT) 2.3,
 4.18-4.21, 8.3, 8.5-8.7
 FEM 1.3, 1.9, 2.2, 2.5, 3.1, 3.8,
 3.12, 3.16-3.19, 3.22, 4.2, 4.9,
 4.11, 4.20, 4.21, 5.1, 5.9, 5.10,
 6.2, 7.1, 8.5-8.7
 Finite element methods 1.3, 1.11,
 1.12, 2.5, 3.1, 3.8, 4.1, 4.2, 4.5,
 4.18, 5.2, 5.4, 6.1, 6.2, 6.4, 7.1, 7.3

Fiber optic devices 1.2
 First natural frequency 5.20, 7.13,
 8.16
 Fixed-fixed beam 3.15, 3.18, 3.20
 Flexible beam 4.1, 4.17, 4.19, 6.2,
 7.1, 8.3, 8.4
 Flexible structures 1.3, 1.6, 1.8, 2.1,
 3.1, 4.1, 6.1, 8.1, 8.3
 Flexural rigidity 1.1
 Forced vibration control 8.26
 Free-free beam 3.14, 3.15, 3.17,
 3.18
 Free-free boundary conditions 3.17
 Frequency response 5.23, 6.24,
 7.15, 7.16, 8.3, 8.5, 8.13, 8.16-
 8.18, 8.20

G

Gaussian controller 1.7, 4.1, 4.2,
 4.17, 4.21
 General configurations 1.3, 2.5
 Generalized co-ordinates 3.1, 3.13,
 3.15, 8.2
 Generalized forces 4.8
 Generalized pattern search method
 8.11
 Geometrical parameters 2.1, 2.2,
 3.15, 4.10, 6.11, 6.12
 Global equations of motion 6.11,
 7.8
 Global mass 8.3, 8.6
 Global system 6.9, 7.7
 Graphical compiler 2.4, 3.3
 Grey box identification technique
 8.12, 8.14

H

Hamilton's principle 3.1, 3.12, 4.1,
 4.2, 4.8, 5.1, 5.9, 6.1, 6.2, 6.8,
 6.9, 7.1, 7.6, 7.7
 H₂ norm 8.2, 8.9, 8.10, 8.12-8.16,
 8.18
 H_∞ norm 8.2, 8.9-8.13, 8.22
 Helicopters 1.3
 HP filter 8.11, 8.12, 8.14, 8.15,
 8.17, 8.22
 High frequency signals

High pass filter 2.3, 8.15, 8.16,
8.24

High sampling rate 2.1, 8.2

I

Instrumentation 1.1, 2.3, 2.4, 8.2,

8.23, 8.24

Instruments 1.7, 2.4, 8.2, 8.23,
8.24

Intelligent structures 1.2, 1.3, 2.5

Internal variables 4.18

Iteration 8.10, 8.11, 8.15

Implementation 1.5, 1.8, 1.12, 2.5,
4.17, 4.20

K

Kinetic energies 3.9, 3.13, 4.6, 5.6,
6.5, 7.3

L

LabVIEW 1.7, 2.6, 8.23

Lagrange's equation 3.1, 3.2, 3.4,
3.15, 8.1, 8.2

Laplace complex number 1.5

Laplace domain 4.18

Laplace operator 4.18

Laplace transformation 1.6

Linear systems 1.2, 1.4, 4.17, 6.9,
7.7, 8.2, 8.5

Linear variable differential
transformer 1.7

Linear quadratic gaussian control
1.7

Loss factor 1.1, 1.10, 2.1, 2.2, 3.1,
3.12, 3.15-3.21, 4.2, 4.10-4.16,
4.18-4.20, 5.10-5.16, 5.17-5.21,
5.23, 6.1, 6.2, 6.11-6.14, 7.1,
7.16

Low pass filter 2.3, 2.5, 4.14, 4.21,
5.22, 6.24, 7.15, 8.16, 8.24

LP filter 8.12, 8.23, 8.25

LTI systems 1.2, 1.8

LVDT 1.2, 1.4, 1.5, 1.8

M

Machines 2.1

Machine tools 2.1

Magneto-rheological fluids 1.8

Mass matrix 3.4-3.6

Mass matrices 3.2, 3.5, 3.11, 5.9,
6.8, 7.6

MIMO 1.4, 1.5, 1.7, 1.9

Mathematical models 3.1, 6.11,
7.9

Mathematical modeling 1.1, 1.3,
1.10, 6.12, 7.9

Modal analysis 2.5, 8.24

Modal frequencies 3.12, 3.15,
4.10, 4.14, 5.10-5.13, 5.20, 6.16

Modal parameters 2.1, 3.1

Mode shapes 3.13, 3.14, 4.14,
4.16, 4.20, 8.3, 8.5, 8.6

Modulus of rigidity 5.12-5.14,
5.19, 5.22, 7.15

Modulus of elasticity 4.18, 4.19,
5.11, 6.23

Multiple modes 8.3

N

Natural frequency 4.20, 5.20, 7.13,
8.6, 8.16, 8.20

Neural network 1.6

Nodes 3.3, 5.16

Non-adaptive vibration control 1.8

Non-collocated sensors 2.2

Non-isotropy 1.3, 2.5

Non-linear Pseudo loads 6.9, 7.7

Non-linear systems 6.9, 7.7

Non-linearity 1.3, 2.5

Non-zero eigenvalues 4.18, 4.20

Normal ACLD treatment 7.9, 7.10

Normalized modes 4.20, 8.6

Numerical calculations 5.20, 5.21

O

Objectives 1.9, 1.10

Online identification 1.1, 1.6

Open loop conditions 4.9, 5.9,
6.10, 7.8

Open loop systems 8.5, 8.17, 8.19

Ordinary differential equations 8.2

Ordinary FEA techniques 1.3, 2.5

Ordinary PCLD treatment 4.1,
5.13, 6.1, 6.2

P

- Parameters 1.1-1.7, 2.1, 2.2, 2.5, 3.1, 3.13, 3.15, 3.20, 4.1, 4.10, 4.18-4.20, 5.20, 5.23, 6.1, 6.11, 6.12, 6.17, 6.24, 7.15, 8.1, 8.5, 8.6, 8.12-8.14
 Partial derivatives 3.15
 Partial treatment 3.14, 4.2, 4.11, 4.12, 5.2, 5.15, 6.2, 6.12, 7.1, 7.9, 7.12
 Passive control 1.2, 1.2, 5.14
 Passive constraining layer 3.10, 3.11, 3.14, 4.6, 4.7, 4.12, 5.11, 5.20, 5.21, 6.15, 7.15
 Passive damping 4.1, 5.19, 6.1
 PCLD + SLD 6.15, 6.17, 6.18, 6.20
 Phase lead/lag 1.11, 8.2
 Phase change 2.5, 8.11, 8.15, 8.17, 8.24
 Piezoceramic materials 1.1, 1.3
 Piezoceramic sensors 1.7
 Piezoelectric charge constant 2.2, 4.10, 5.14, 6.19, 8.5
 Piezoelectric voltage constant 2.2, 4.9, 4.10, 5.9, 5.14, 6.10, 6.19, 7.8, 8.5
 Piezopolymers 1.3
 Poisson's ratio 6.4
 Potential energies 3.10, 3.13, 3.15, 4.6, 5.7, 6.6, 7.4
 Power spectral density (PSD) 8.25
 PPF controller 1.11, 8.1, 8.2, 8.7-8.9, 8.11-8.15, 8.17, 8.19-8.21, 8.24-8.26
 Proportional feedback controller 4.1, 4.2, 6.1, 6.2
 Proportional feedback gain 5.23
 Proportional derivative (PD) controller 4.9, 5.9, 6.10, 7.8
 PVC layers 1.10, 2.1, 3.11, 4.1-4.12, 4.14, 4.18, 4.19, 4.21, 6.1-6.7, 6.9, 6.12-6.18, 6.20, 6.22-6.24
 PVDF 1.2, 1.3, 5.2, 5.14, 5.21, 7.2, 7.15, 8.3
 PZT 1.3, 2.1-2.3, 2.6, 4.3, 4.8, 4.10, 4.12, 4.16, 4.18, 4.21, 5.2, 5.6,

5.14-5.16, 5.19-5.23, 6.3, 6.4, 6.7, 6.23, 6.24

- PZT patches 2.1, 2.3, 2.6, 6.2, 6.3, 8.3, 8.4, 8.25
 PZT material 2.2, 4.8, 4.10, 4.21, 5.6, 5.14, 6.7, 6.24, 7.5
 Polynomial matrix form 1.17

Q

- Quadratic form 3.6
 Quartz 1.3
 Quantification 8.18

R

- Random binary signal 4.17, 8.5
 Random force 8.25, 8.26
 Random logic 2.4, 8.23
 Random signal 8.25
 Real time engine 2.1, 2.3, 2.5, 2.6, 8.2, 8.23
 Real time operating system 2.5, 2.6
 Real time performance 2.4
 Real time processor 2.6, 8.24
 Resonance frequency 5.22, 7.15
 Resonant controllers 8.1
 Rigid body 6.9, 7.7
 Rod element 3.5, 3.6
 Rotating beam 1.9-1.12, 2.1-2.3, 6.1, 6.2, 6.14, 6.16, 6.23, 7.1, 7.11-7.14
 Rotating structures 4.1, 6.1, 7.1

S

- Samples 1.7, 2.4, 8.23
 Sensors 1.2-1.3, 1.7, 1.8, 1.10, 2.1-2.3, 2.6, 2.6, 4.1, 8.1, 8.25
 Shape functions 3.3, 3.8, 3.14, 4.5, 5.4, 6.4, 6.5, 7.3
 Shape memory alloys 1.2, 1.8
 Shear modulus 2.1, 2.2, 3.12, 3.15, 4.9, 4.10, 4.18-4.21, 5.1, 5.10-5.13, 5.15, 5.23, 6.9, 6.11, 6.12, 7.1, 7.7, 7.10, 7.11, 7.15, 7.16
 SISO 1.4, 4.20, 8.6
 Simply supported beam 3.16, 3.17, 4.2, 4.9, 4.14, 4.15, 5.21, 5.9
 Simulink 2.3, 2.4, 3.15, 4.17

Smart materials 1.2, 1.3, 4.1, 5.1, 6.1, 8.1
 Smart structures 1.2, 1.8, 1.11
 Smart sensors 1.2
 SOL layer 1.9-1.11, 5.1-5.3, 5.6-5.8, 5.10, 5.12-5.14, 5.16-5.21, 5.23, 7.1-7.4, 7.7-7.14
 Strain 1.2, 1.3, 2.2, 2.3, 3.4, 3.7, 3.8-3.10, 3.13, 4.1-4.6, 4.8, 4.10, 4.11-4.15, 4.21, 5.3, 5.5-5.9, 5.19, 5.23, 6.1, 6.2, 6.4, 6.5, 6.7-6.8, 6.12, 6.13-6.17, 6.20-6.22, 6.24, 7.1-7.6, 7.16
 Structural mechanics 1.2

T

Tension 4.11, 4.21, 6.24
 Time varying systems 1.4
 Transfer function 1.4-1.8, 8.1-8.3, 8.5, 8.9, 8.10, 8.12, 8.20, 8.21
 Transmissibility 5.1, 5.2, 5.19, 7.1
 Transverse displacements 3.8-3.11, 4.5-4.7, 5.3, 5.4, 5.6-5.8, 5.23, 6.4, 6.6, 6.7, 7.3-7.5, 7.15
 Transverse load 4.6, 4.8, 5.5, 5.8, 6.5, 6.7, 7.3, 7.5
 Transverse vibrations 4.18

U

Unconditional system stability 8.1
 Unconditional closed loop stability 8.1
 Uncontrolled modes 8.1
 Uniform properties 3.6
 Uniform sensor 4.9, 5.9, 6.9, 7.8
 Unstable mode 1.1

V

Vibration analysis 1.12
 Vibration control 1.2, 1.3, 1.8, 1.11, 1.12, 2.1, 3.1, 4.1, 5.1, 6.1, 7.1, 8.1, 8.25
 VEM 1.1, 1.2, 1.9, 1.10, 2.1, 3.1, 3.6-3.8
 Viscoelastic layers 1.9, 5.19

W

Waveform 4.17, 4.18, 8.5

@Seismicisolation